Sede Amministrativa: Università degli Studi di Padova

Dipartimento di Biologia

SCUOLA DI DOTTORATO DI RICERCA IN: BIOSCIENZE E BIOTECNOLOGIE
INDIRIZZO: BIOCHIMICA E BIOFISICA
CICLO XXVII

Functional and structural analysis of [NiFe]- and [FeFe]-hydrogenases, the key enzymes for biohydrogen production

Direttore della Scuola: Ch.mo Prof. Giuseppe Zanotti
Coordinatore d'indirizzo: Ch.mo Prof. Fabio Di Lisa
Supervisore: Dott.ssa Paola Costantini

Dottorando : Edith De Rosa

CONTENTS

RIASSUNTO

Negli ultimi anni il problema della crisi energetica ha assunto un'importanza tale da spingere la ricerca verso fonti di energia diverse dai combustibili fossili. In questo ambito l'idrogeno molecolare rappresenta una valida alternativa in quanto è una risorsa di energia rinnovabile e pulita dal momento che l'acqua è l'unico sottoprodotto della sua combustione. Le attuali tecniche di produzione dell'idrogeno, tuttavia, necessitano di miglioramenti in termini di rendimento e di costo. Una via promettente è quella biologica, che sfrutta microorganismi fotosintetici dai quali, in opportune condizioni, producono idrogeno solo con acqua e luce solare. Esistono due principali classi di enzimi coinvolti nel metabolismo dell'idrogeno: le [FeFe]- e le [NiFe]-idrogenasi, entrambe catalizzano la reazione reversibile $2H^+ + 2e^- \leftrightarrow H_2$, ma le [FeFe]-idrogenasi risultano più interessanti perchè presentano un'attività specifica superiore a quella delle [NiFe]-idrogenasi. Nonostante queste due idrogenasi abbiano sia strutture tridimensionali che sequenze differenti, e siano filogeneticamente distinte, rappresentano un chiaro esempio di evoluzione convergente in quanto, oltre a catalizzare la stessa reazione, hanno un sito attivo molto simile. L'assemblaggio di quest'ultimo è in entrambi i casi un processo complesso: nel caso delle [NiFe]-idrogenasi è regolato da sei proteine (HypA-F) ed è stato ampiamente studiato e caratterizzato. Il meccanismo di maturazione delle [FeFe]-idrogenasi, invece, coinvolge tre maturasi, HydE, HydF, HydG e non è ancora stato chiarito completamente. In particolare HydF, la cui struttura 3D è stata risolta nel nostro laboratorio (Cendron L. et al., 2011), è una proteina ad attività GTPasica e svolge un ruolo centrale in questo processo. Tuttavia, molti dettagli mancano ancora per definire con precisione la sua funzione, anche a causa del fatto che la sua struttura è stata risolta in forma apo, completamente priva di cofattori. Questa lacuna rappresenta un limite per lo sviluppo di biotecnologie che permetterebbero di esprimere *in vitro* [FeFe]-idrogenasi ricombinanti in forma cataliticamente attiva. Un altro tema irrisolto riguarda il ruolo biologico delle idrogenasi, dal momento che questi enzimi vengono inibiti dall'ossigeno, ma curiosamente sono espressi da microrganismi che vivono prevalentemente in

condizioni aerobiche. Nel corso del Dottorato ho concentrato il mio lavoro sperimentale principalmente su due argomenti: il ruolo fisiologico della [NiFe]-idrogenasi nel cianobatterio *Synechocystis* sp. PCC 6803; la caratterizzazione biochimica del dominio GTPasico di HydF.

Synechocystis sp PCC 6803, diversamente da altri ceppi di cianobatteri, possiede solamente una [NiFe]-idrogenasi bidirezionale. Questo enzima è composto da cinque subunità combinate in due unità funzionali: la porzione idrogenasica, chiamata HoxYH, che ospita il sito attivo, e la porzione diaforasica, chiamata HoxEFU, che probabilmente agisce come partner redox per il subcomplesso catalitico. La funzione fisiologica di questo enzima è ancora oggetto di discussione: il consenso generale è che può giocare un ruolo soltanto in condizioni di crescita specifiche e/o transitorie. È interessante notare che, pur essendo completamente inattiva in presenza di ossigeno, la proteina Hox è costitutivamente espressa in *Synechocystis* sia in anaerobiosi che in aerobiosi, suggerendo una sua funzione aggiuntiva, oltre al coinvolgimento nel metabolismo dell'idrogeno, perlomeno in condizioni selettive. Ho generato diversi ceppi mutanti di *Synechocystis*, eliminando singoli geni *hox* e *hyp* o combinazioni di essi, codificanti rispettivamente per la subunità idrogenasica e per le proteine coinvolte nell'assemblaggio del sito attivo, e ho analizzato il loro fenotipo in condizioni di crescita al buio completo e prolungato in aerobiosi e anaerobiosi, alle quali i cianobatteri sono spesso esposti in natura. Abbiamo riscontrato che il ceppo mutante *knock out* ΔHoxEFUYH, privo dell'intero operone *hox*, ha una notevole riduzione della crescita se confrontato con il ceppo *wild type*. Poiché la funzione idrogenasica della proteina Hox è immediatamente inattivata dall'ossigeno, abbiamo supposto che il fenotipo osservato non fosse collegato alla sua porzione YH. Questa ipotesi è stata esplorata eliminando i geni codificanti i) per le proteine HypA e HypB, coinvolte nell'ultima fase della maturazione idrogenasi e ii) per la porzione HoxYH, e valutando il loro comportamento in queste condizioni di stress ambientale. Abbiamo evidenziato che un sito attivo funzionale e correttamente assemblato non è indispensabile per conferire a *Synechocystis* la capacità di affrontare l'oscurità prolungata. Per caratterizzare ulteriormente il ceppo *wild type* e il mutante ΔHoxEFUYH cresciuti in queste condizioni abbiamo effettuato un'analisi proteomica quantitativa. L'esame delle

proteine identificate ha dimostrato che quasi tutte le subunità idrofiliche del complesso I della catena respiratoria hanno ridotti livelli di espressione. Questi risultati sono coerenti con precedenti studi indipendenti in cui la [NiFe]-idrogenasi è stata funzionalmente associata al complesso I (Cournac L. et al., 2004) e indicherebbero che l'intero flusso di elettroni è alterato quando *Synechocystis* cresce in buio prolungato, una condizione in cui sia la fotosintesi che la respirazione risultano compromesse. Pertanto, l'esito delle nostre ricerche potrebbe fornire una prova molecolare a supporto dell'ipotesi che la [NiFe]-idrogenasi sia funzionalmente correlata alla catena respiratoria, e più in generale far luce sull'espressione e sulla funzione dell'enzima in condizioni aerobiche.

La proteina HydF possiede tre diversi domini: uno coinvolto nel legame e idrolisi del GTP, uno di dimerizzazione e uno per il legame del centro FeS. Nella seconda parte del mio progetto abbiamo studiato le possibili variazioni conformazionali indotte dal legame del GTP, esprimendo in *Escherichia coli* il solo dominio di legame del GTP della proteina ricombinante HydF di *Thermotoga neapolitana*. In questo dominio abbiamo mutato dei siti ritenuti interessanti per la nostra analisi inserendo delle cisteine, che successivamente sono state marcate con lo *spin-label* MTSSL nitrossido, selettivo per i tioli. Questa sonda, ampiamente utilizzata in spettroscopia EPR, ci ha permesso in primo luogo di studiare la mobilità locale dei nitrossidi in ogni singolo sito mutato; in seguito, mediante spettroscopia PELDOR, abbiamo analizzato delle coppie di residui marcati con la stessa tecnica. Abbiamo scoperto che il legame del nucleotide non induce grandi effetti conformazionali all'interno del dominio isolato. Tuttavia, sono state osservate piccole variazioni nelle distanze tra i doppi residui marcati che potrebbero avere effetti diffusi e riflettersi nella conformazione di HydF. I risultati ottenuti potrebbero far chiarezza sul ruolo del legame del GTP a HydF e sulle sue implicazioni nelle interazioni di questa proteina con le altre due maturasi.

Con questo studio abbiamo cercato di ampliare le conoscenze sulla struttura e sulla funzione delle idrogenasi per acquisire una maggiore comprensione dei meccanismi alla base della loro attività catalitica e dare un contributo per la messa a punto di sistemi biomimetici basati su questi enzimi, in cui massimizzare la produzione di H_2.

SUMMARY

In recent years the problem of energy crisis has assumed such importance to promote research into sources of energy different from fossil fuels. In this context, molecular hydrogen represents a valid alternative because it is a renewable and clean energy resource since water is the only by-product of its combustion. The hydrogen production techniques currently used, however, require improvement in terms of performance and costs. A promising approach is to exploit biological photosynthetic microorganisms which, under suitable conditions, provide hydrogen from water and sunlight only. There are two main classes of enzymes involved in the metabolism of hydrogen: the [FeFe]- and [NiFe]-hydrogenases, both catalyze the reversible reaction $2H^+ + 2e^- \leftrightarrow H_2$, however [FeFe]-hydrogenases are more interesting for hydrogen bioproduction since they have a specific activity greater than [NiFe]-hydrogenases. Despite these two classes have different three-dimensional structures, different sequences and are phylogenetically distinct, they represent a clear example of convergent evolution since they catalyze the same reaction and have a similar catalytic site. In both cases, the assembly of the latter is a complex process: in the case of the [NiFe]-hydrogenases is driven by six proteins (HypA-F) and has been extensively studied and characterized. The maturation mechanism of [FeFe]-hydrogenases, instead, involves three maturases, HydE, HydF, HydG, and is less known. In particular, HydF, whose 3D structure has been solved in our laboratory (Cendron L. et al., 2011), is a GTPase protein and plays a central role in the maturation process. However, many functional details remain to be clarified, mainly due to the fact that its structure has been obtained in the apo form, completely lacking the cofactors. This gap is a limit for the development of biotechnologies that allow to express *in vitro* recombinant catalytically active [FeFe]-hydrogenases. Another unsolved issue concerns the biological role of hydrogenases, since these enzymes are inhibited by oxygen, but curiously they are expressed by microorganisms that live mainly in aerobic conditions.

During the PhD I focused my experimental work mainly on two topics: first, the physiological role of the [NiFe]-hydrogenase in the cyanobacterium

Synechocystis sp. PCC 6803; secondly, the biochemical characterization of the GTPase domain of HydF.

Synechocystis sp PCC 6803, unlike other cyanobacteria strains, holds only a bidirectional [NiFe]-hydrogenase. This enzyme has five subunits combined into two functional units: the hydrogenase portion, called HoxYH, that harbours the active site, and the diaphorase portion, called HoxEFU, which probably acts as a redox partner for the catalytic subcomplex. The physiological function of this enzyme is still under discussion: the general consensus is that it can play a role only under transient and/or specific growth conditions. It is interesting to note that, while being completely inactive in the presence of oxygen, the Hox protein is constitutively expressed in *Synechocystis* both in anaerobiosis and in aerobiosis, suggesting an additional function, besides hydrogen metabolism, at least in selected conditions. I generated several *Synechocystis* mutant strains, deleting individual or combinations of *hox* and *hyp* genes, encoding respectively for the hydrogenase subunits and for the proteins involved in the assembly of the active site, and analyzed their phenotype during prolonged, complete darkness in aerobiosis, a growth condition to which cyanobacteria are frequently exposed in nature. I found that the ΔHoxEFUYH knock out mutant strain, lacking the entire *hox* operon, has a notable reduction of growth when compared to the wild type strain. Since the hydrogenase function of the Hox protein is promptly inactivated by oxygen, we have assumed that the observed phenotype is not associated to its YH portion. This hypothesis has been explored by deleting genes coding for i) the HypA and HypB proteins, involved in the last steps of the hydrogenase maturation and for ii) the HoxYH portion, and evaluated their behavior under this environmental stress condition. We found that a correctly folded, functional [NiFe]-hydrogenase active site is indeed not essential to confer to *Synechocystis* the capability to face a prolonged darkness. To further characterize the wild type and the ΔHoxEFUYH mutant strain grown under these conditions we performed a quantitative proteomic analysis. The examination of the identified proteins showed that almost all the hydrophilic subunits of the respiratory chain complex I are downregulated in their expression. These results are consistent with previous independent studies in which [NiFe]-hydrogenase has been proposed to be functionally associated with the complex I (Cournac L. et al., 2004), and indicate

that the entire electrons flow is altered when *Synechocystis* is grown under prolonged darkness, a condition in which both photosynthesis and respiration are affected. Therefore, the outcome of our research could provide a molecular evidence in support of the hypothesis that the [NiFe]-hydrogenase is functionally linked to respiratory chain, and more generally shed light on the expression and function of this enzyme under aerobic conditions.

HydF is composed of three domains: the first is involved in the binding and hydrolysis of GTP, the second is the dimerization domain and the third is the FeS center binding domain. In the second part of this work, we have investigated the possible conformational changes induced by the binding of GTP, by expressing in *Escherichia coli* only the GTP binding domain of a recombinant HydF protein from *Thermotoga neapolitana*. In this domain we inserted, by site-specific mutagenesis, cysteine residues in positions useful for spectroscopic analysis. These residues were subsequently labeled with the thiol-selective spin-label MTSSL nitroxide. This probe, largely used in EPR spectroscopy, has allowed us first to study the local mobility of nitroxides at each mutated site, and then, by PELDOR spectroscopy, to analyze couple of residues labeled with the same technique. We found that the binding of the nucleotide does not induce large conformational effects within the isolated GTP domain. However, small variations were observed in the distances between the couple of labeled residues that could have diffused effect reflecting in the conformation of HydF. The results may add new insights into the role of GTP binding to HydF and its implications in the interaction of this protein with the other two maturases.

With these studies we wanted to broaden the knowledge on the structure and function of hydrogenases, to gain a greater understanding of the mechanisms underlying their catalytic activity. This could in turn contribute to the development of biomimetic systems wherein optimize hydrogen production exploiting this class of enzymes.

INTRODUCTION

Hydrogen: a promising energy carrier

Global warming caused by human activities has become unmistakably a serious problem with widespread melting of ice, noticeable climate changes and rising of sea levels, demanding strong remedial action as soon as possible. This predicament has many causes, but predominant among them is the nearly 20-fold increase in world energy use due to industrial development and population growth, which resulted in the emission of greenhouse gases, mainly carbon dioxide, produced by burning fossil fuels (such as petroleum, coal, and natural gas). The state of the art is that this scenario is not going to improve (figure 1 shows the forecasts of energy demand for 2035).

Figure 1. Primary energy demand for 2035: values are expressed in million tons of oil equivalent (adapted from annual report of IEA, 2013).

The cumulative depletion of the most convenient oil and gas deposits that this growth has entailed, resulting in increasing resort to costlier and/or environmentally more disruptive energy sources, have lead to the current energy crisis. Coping with global energy problems will require great efforts aimed at reducing the environmental impact of contemporary energy technologies and improving the efficiency of energy use to fulfill the request of the world population which, currently, is 10 billions people with an estimated energy

consumption of about 30 terawatts per year (compared to 13.2 terawatts in 1990). An immediate response to this situation is necessary both for ethical reasons, to preserve the Earth for future generations, and for economic reasons and world security by allowing all countries to be independent from the petroleum producers and, therefore, less involved with events in the Middle East.

All these reasons have led in recent years to search for energy sources alternative to fossil fuels. In 2007 the European Parliament has taken an official position on the future lines of energy development of the member countries, establishing that, among the key factors for energy independence, the development of a technology based on hydrogen as energy carrier of the future stands out, to store renewable energies and create smart power grids to distribute energy itself.

Apart from those initiatives adopted in Europe, many developing nations, the entire scientific community and some industries share a common interest and have invested in hydrogen as a viable replacement to the current economy principally based on non-renewable energy sources. Hydrogen-based economy is a system assumed for the future in which various forms of energy are stored in the form of hydrogen (gaseous and liquid hydrogen, or compounds such as metal hydrides) to be used both in applications in motion and to provide additional energy to the national grid and to the world in times of excessive energy load. In particular, at the end of the twentieth century, the project of a hydrogen car has quickly developed, which uses hydrogen as a fuel in special cells or batteries, generating energy in the form of electricity with minimal or no emissions. This has opened new horizons for a more widespread use of hydrogen to the point that, in terms of global convenience, it is thought that fuel cells (figure 2) will be the equivalent future of the steam engine in the nineteenth century or the internal combustion engine of the twentieth century.

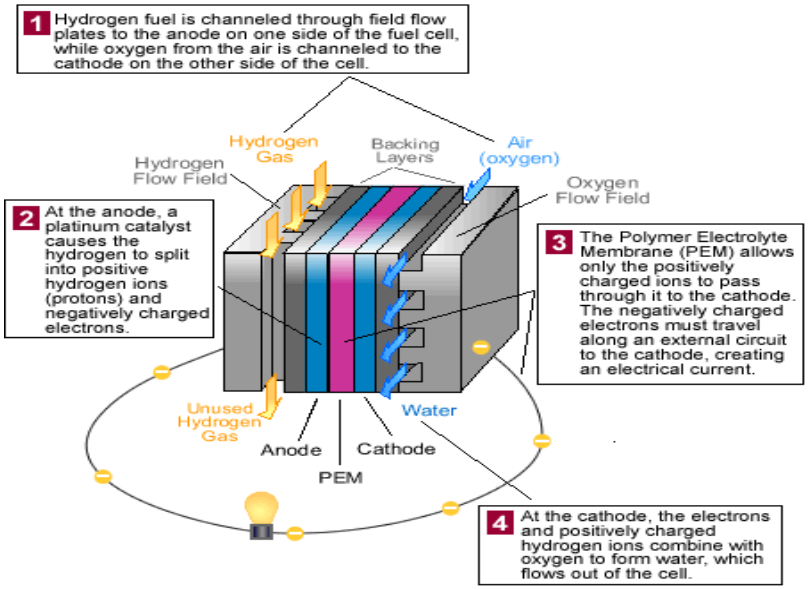

Figure 2. Functioning of a fuel cell: a device that converts the chemical energy from a fuel into electricity through a chemical reaction with oxygen or another oxidizing agent.

The advantage of using hydrogen as an energy carrier are numerous:

- when it combines with oxygen the only by-products are water and heat, no greenhouse gases or other particulates are produced;
- its high-efficiency transformation leads less waste of resources, reduces pollution and improves air quality;
- the ability to get it from many sources allows to reduce the dependence on oil and promotes the necessary diversification of energy sources.

The hydrogen gas (H_2) is considered very promising, especially in relation to the possible and the final take-off of renewable energy sources (solar radiation and wind above all), as it may be the best answer to the their difficult storage. As stated above, an advantage of hydrogen is that it can be produced with different processes and energy sources. Consequently, hydrogen can also be produced in remote parts of the world, regardless of the economic development level and of local infrastructure quality. Indeed, vast quantities of hydrogen as an industrial gas are nowadays produced around the world (total annual production amounts to 500 billions normal cubic meters per year and the estimated growth rate is 10% per year). Nevertheless, almost all of this hydrogen is produced by using fossil

fuels and, since hydrogen storage and transport are very onerous, only 5% of this production is commercially used and distributed, whereas most of it is normally produced and used locally by the same industries that produce it, typically oil refineries or chemical plants. The US space program has been the only case where hydrogen was used as a fuel: until now, indeed, this technology has not entirely replaced gasoline and diesel fuel.

Hydrogen on earth is mostly combined with other elements, such as oxygen to form water molecules or carbon to form organic compounds; therefore, it is not properly a source of energy (but an energy carrier) since it must be "manufactured". Most of the hydrogen is extracted from other substances with chemical and electrolytic procedures, or may be produced by other fuels using substances with a high energy content, as fossil fuels. Such an hydrogen economy needs a new infrastructure for production, storage and transportation of this new fuel, requiring the overcoming of several problems associated with it. Today, the major technological "crucial points" that hinder the development of hydrogen energy include:

• the issue of thermodynamics convenience, *i.e.* there is a net energy gain in the production and use of hydrogen from other sources of energy;

• the economic advantage or the fact that the set of technologies and infrastructures that are resting on hydrogen are overall less expensive than using conventional fossil fuels. Its use, in fact, requires many changes to industry and transportation on a very large scale. Anyway, economic incentives, the expected increase in oil prices for the inevitable increase in its production cost and deficient alternatives, make this transition economically viable in the future;

• the problem of storage/transport: since it is a small molecule, the diatomic hydrogen tends to diffuse through each coating material that is used for its containment. Hydrogen has a low density (0.0708 g /cm^3 at -253 °C); this means that a reservoir large enough is necessary to store it, also using additional energy to compress it, which causes safety problems for the high-pressure gas.

Consequently, many hydrogen technologies still need to be improved in terms of performance and cost reduction in order to be considered best available

options. The four fundamental technological and technical challenges related to hydrogen production are:

1. develop and introduce economic, durable, safe, and environmentally acceptable fuel cells and hydrogen storage systems;
2. develop the infrastructure to provide hydrogen for the light-duty vehicle user;
3. reduce the costs of hydrogen production from renewables over the next few decades;
4. if politically feasible and acceptable, capture and store the CO_2 by products of hydrogen production from coal.

Currently, the production of hydrogen is carried out for the 48% from natural gas, 30% from oil (by-product of the distillation and reforming of diesel oil), 18% from coal; the electrolysis of water is used to produce only 4% of H_2 (figure 3).

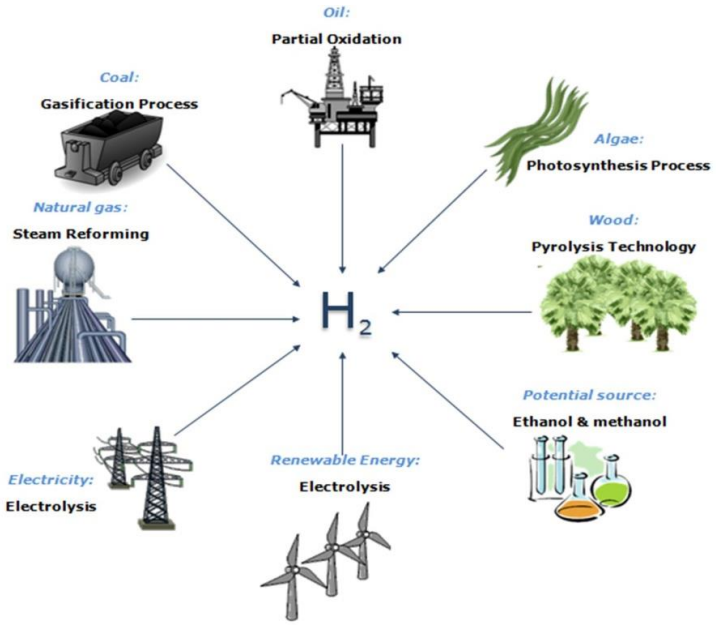

Figure 3. Hydrogen sources and production processes.

- Reforming of methane, oil and coal, in addition to deplete non-renewable resources, generate CO_2 (9 kg CO_2 per kg of H_2 obtained) in larger amounts than the conventional engines, exacerbating the greenhouse effect if used in motor vehicles. However, to date, this appears to be the only system of

hydrogen production economically viable, with an energy efficiency of about 80%;

- hydrogen can also be processed from gasoline or methanol, though again CO_2 is an unwanted by-product;
- the pyrolysis, or dry distillation, consists in the thermal (400 - 800 °C), not oxidative (*i.e.* without addition of oxygen) decomposition of organic materials; the molecules are transformed into simpler elements such as hydrogen, carbon monoxide, carbon dioxide, light hydrocarbons;
- hydrogen could be produced by the electrolysis of water using large amounts of electricity. This production has efficiencies ranging from 50 to 70% (depending on the power density, temperature and catalyst employed). Since electrolysis uses electricity as an input, it offers the advantage of having no geographical restrictions that alternative ways have. Therefore, it allows flexible and remote siting of hydrogen generators, providing distributed generation of this energy carrier, without requiring physical transport and large scale storage. On the other hand, this process requires a lot of electricity, which, currently in the world, is mostly generated by fossil fuels such as natural gas or fuel oil or with nuclear energy;
- hydrogen produced from renewable energy sources is a way to bring zero-emission clean energy. In this case hydrogen is commonly produced by a device called an electrolyzer, which uses electricity to separate water into hydrogen and oxygen. Conversion of renewable energy into hydrogen would allow to store it in a fuel cell for long periods and to use it at any time of day or night.

The energy balance of hydrogen, however, is still unfavorable compared to other energy technologies that already exist, also considering the best available methods. The research has focused on finding alternative and clean methods to produce hydrogen and, in this respect, a promising way exploits the biological processes.

Biohydrogen

The term biohydrogen indicates the molecular hydrogen produced biologically exploiting metabolic processes of some microorganisms (such as green algae, cyanobacteria, photosynthetic and fermentative bacteria) capable of producing H_2 using heat as an energy source and an organic medium (thermophilic bacteria), light and an organic medium (photosynthetic bacteria) or light and water (microalgae). These microorganisms are able to produce hydrogen thanks to particular enzymes, the hydrogenases (H_2ases). Although some observations of hydrogen production by microalgae and bacteria extend back over 100 years (Jackson D.D. et al., 1896), basic research in this field started only in the late 1920s with bacterial H_2 production (Strickland L.H., 1929) and in the 1940s with microalgal hydrogen production (Gaffron H. et al., 1942). Hereinafter, algae have started to become promising candidates for hydrogen production when Melis, along with other researchers, found that, when deprived of sulfur and oxygen, the green alga *Chlamydomonas reinhardtii* was able to evolve hydrogen (Melis A. et al., 2000).

One of the major advantages of the biological production of hydrogen is to use processes that exist in nature to convert a primary energy source, such as solar energy, in the hydrogen carrier thus lowering the rate of the pollutant waste accumulation. The main biological hydrogen production processes are represented in figure 4, and can be classified as follows:

1. direct and indirect biophotolysis of water by green algae and cyanobacteria;
2. photodecomposition of organic compounds by photosynthetic bacteria;
3. dark fermentation of organic compounds;
4. hybrid systems using fermentative and photosynthetic bacteria.

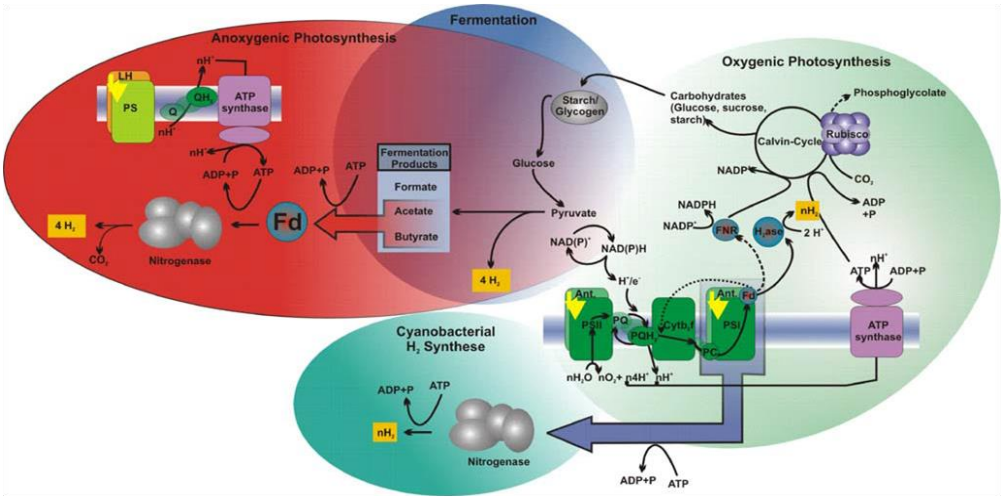

Figure 4. Representation of the solar H_2 production biochemistry. The yellow arrows indicate systems that can capture solar energy. Photofermentation is represented in red, fermentation in blue, biophotolysis in green (Rupprecht J. et al., 2006).

1. **Biophotolysis**, or photoautotrophic biohydrogen production, is the production of molecular oxygen and hydrogen from water using energy from absorbed light. Biophotolysis proceeds in two distinctive ways, directly and indirectly.

1.1 *Direct biophotolysis* is generally performed by green algae (in particular it has been extensively studied in the unicellular green alga *C. reinhardtii*) under anaerobic conditions and may be represented by the following general reaction:

$$2H_2O + \text{light energy} \rightarrow 2H_2 + O_2$$

This process involves photosynthetic reaction where light energy is absorbed by photosystems I (PSI) and photosystems II (PSII) of microalgae (figure 5).

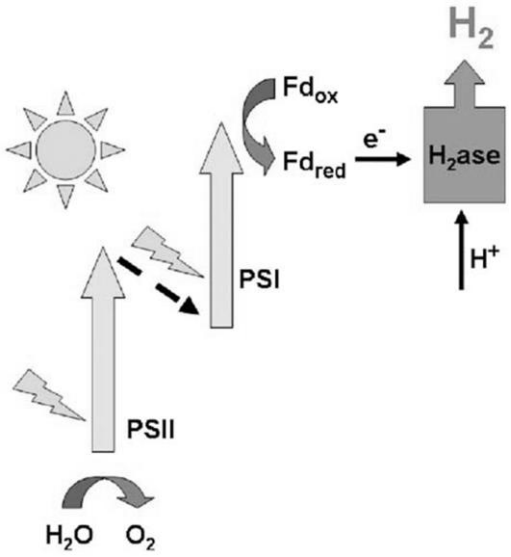

Figure 5. Biophotolysis (Hallenbeck P.C. et al., 2009).

The excited reaction centers transfer energy through an electron transport chain, ultimately reducing ferredoxin (Fd), which provides electrons to the enzyme hydrogenase that catalyzes the conversion of hydrogen ion into hydrogen gas. Despite this route seems to be very attractive as it uses solely water and solar energy for hydrogen production, it presents a significant limit, *i.e.* oxygen as by-product, which inhibits hydrogenases. As a consequence, this leads to a photochemical efficiency of only about 1-2% (Hallenbeck P.C. and Benemann J.R., 2002), much lower than that theoretically possible of about 10 %. Several process variants have been developed to prevent the inhibition of hydrogenases, by separating the oxygen production phase from that of hydrogen: this occurs in the indirect biophotolysis.

1.2 In the *indirect* process carbohydrate energy stores from previous photosynthetic activities are used to provide the energy needed to generate hydrogen from water, according to the following reactions:

$$12H_2O + 6CO_2 + \text{light energy} \rightarrow C_6H_{12}O_6 + 6O_2$$

$$C_6H_{12}O_6 + 12H_2O + \text{light energy} \rightarrow 12H_2 + 6CO_2$$

Generally, this is a mechanism employed by cyanobacteria (also known as blue-green algae), a large and diverse group of photoautotrophic microorganisms that contain photosynthetic pigments (see more below). They are divided in two major classes: nitrogen and non nitrogen fixing and both use ATP to synthesize hydrogen gas by means of nitrogenase enzyme. In this system, photosynthesis (O_2 evolution and CO_2 fixation) and N_2 fixation (with H_2 production) are either spatially or temporally separated from each other. Filamentous cyanobacteria, such as those in the genus *Anabaena*, spatially separate the two processes by forming heterocysts, specialized cells for nitrogen fixation that are fed by neighboring photosynthetic cells, so they do not need their own photosynthetic machinery, which would prevent the function of the O_2-sensitive nitrogenase enzyme (figure 6)

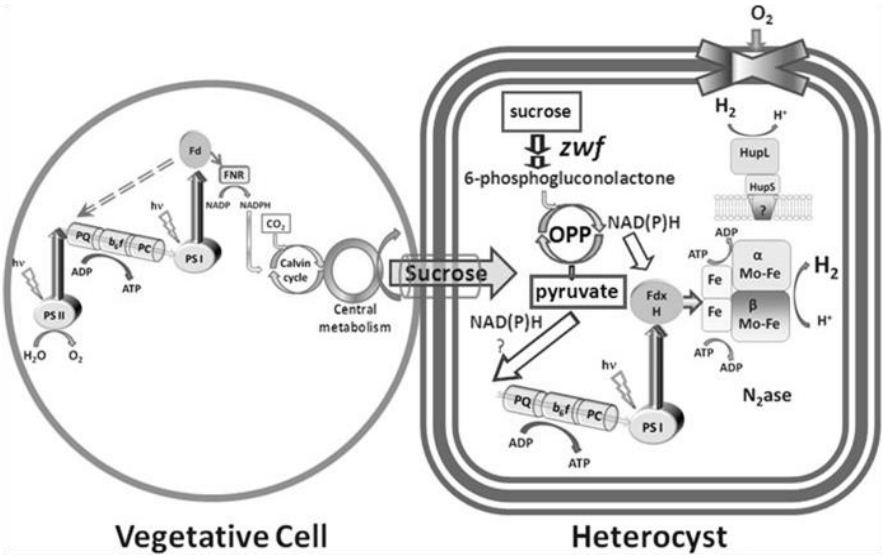

Figure 6. Metabolic interactions during biophotolysis by heterocystous cyanobacterial cultures. Water splitting photosynthesis and consequent ferredoxin reduction are used to fix CO_2 and the resulting reduced carbon compound can be used to drive hydrogen evolution in a separate reaction, overcoming the production of oxygen and the inhibition of hydrogenase activity (Hallenbeck P.C., 2012).

Indeed, nitrogenase is protected from O_2 by a heavy cell wall that reduces O_2 diffusion, and by high rates of respiration, absorbing any residual oxygen (Weare N.M. et al., 1974). In other cyanobacterial genera, such as *Gleocapsia alpicola* or *Synechocystis* sp., photosynthesis and H_2 production stages are temporally separated. Cells are grown photoautotrophically to accumulate stores of glycogen that is then fermented under dark incubation to drive production of H_2.

Indirect biophotolysis shares the advantages of direct biophotolysis because water is still the electron donor and inorganic carbon is the carbon source in this process. Although this path is able to mitigate some of the O_2 sensitivity issues of direct biophotolysis, it still needs metabolic engineering efforts to increase its efficiency and to lead to hydrogen competitive production rates.

2. **Photoheterotrophic H_2 production** (or photofermentation) differs from biophotolysis sincet it utilizes energy from sunlight to oxidize organic compounds and generate the electron potential needed to drive H_2 production under anaerobic conditions, through the action of the nitrogenase (Harwood C.S., 2008) (figure 7).

$$CH_3COOH + 2H_2O + \text{light energy} \rightarrow 4H_2 + 2CO_2$$

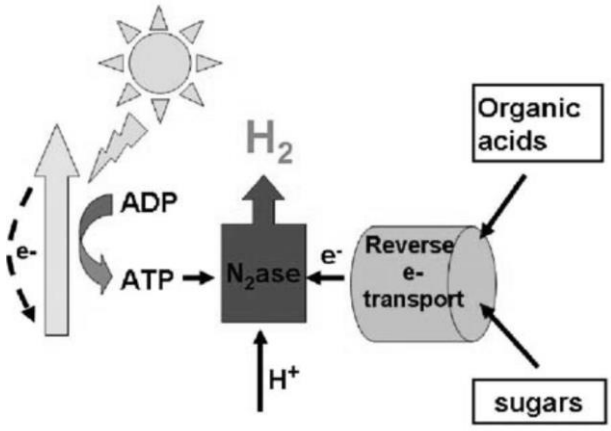

Figure 7. Photofermentation by photosynthetic bacteria (Hallenbeck P.C. et al., 2008).

This pathway has been found among a diverse group of photosynthetic bacteria and well-characterized in purple non sulfur bacteria (PNSB) (Hallenbeck P.C. and Benemann J.R., 2002). Under anaerobic conditions, the electrons scavenged from organic acids are transferred to oxidized ferredoxin (Fd_{ox}). Then, the electrons in reduced ferredoxin (Fd_{rd}) are primarily used to reduce molecular dinitrogen (N_2) to ammonia (NH_3) by the action of nitrogenase (N_2ase). However, in the absence of N_2, nitrogenase catalyses the reduction of protons to produce H_2 (Harwood C.S., 2008). The advantage of their use, compared to cyanobacteria and algae, is in the versatile metabolic capabilities and in the lack of photosystem II (PSII), which automatically eliminates the difficulties associated with O_2 inhibition of H_2 production. On the other hand, the nitrogenase enzyme has high-energy demand and the solar energy conversion efficiencies are low. The photosystem of the photosynthetic bacteria is, like that of microalgae and cyanobacteria, optimized for low-light conditions. Thus, cyclic light process operation (*i.e.* light-dark cycles) has been shown to increase the amount of hydrogen evolved when compared to continuous illumination (Koku H. et al., 2003). In addition, photofermentation would require elaborate anaerobic photobioreactors covering large areas (Fedorov A.S., 1998). Due to these several drawbacks, this process is not regarded as a very competitive method for hydrogen production.

3. In **dark fermentation**, microorganisms anaerobically break down carbohydrate-rich substrates into organic acids and alcohols, releasing H_2 and CO_2 in the process (figure 8).

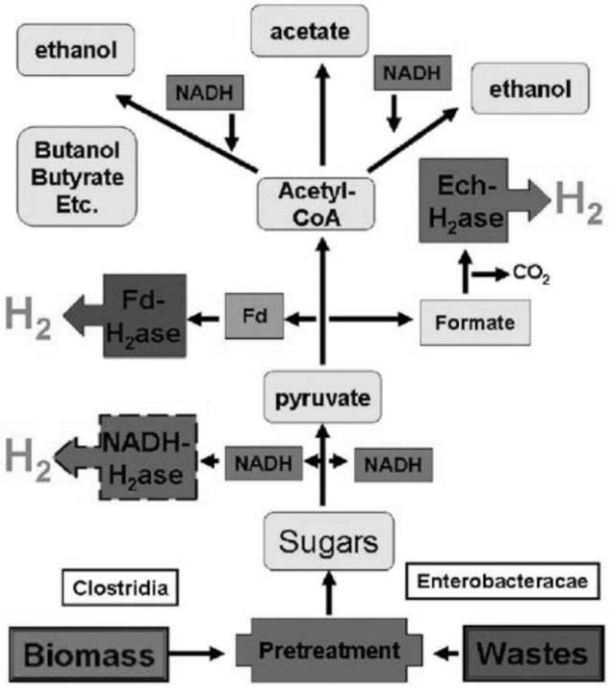

Figure 8. Dark fermentation (Hallenbeck P.C. et al., 2008)

When bacteria grow on organic substrates (heterotrophic growth), these substrates are degraded by oxidation to provide building blocks and metabolic energy for growth. This oxidation generates electrons which need to be disposed to maintain electrical neutrality. In the hydrogen fermentation process, glucose is initially converted to pyruvate by the glycolytic pathways. This is oxidized to acetyl-CoA, which can be converted to acetyl phosphate and results in the generation of ATP and the excretion of acetate. Pyruvate oxidation to acetyl-CoA requires reduced ferredoxin (Fd_{rd}), that is oxidized by hydrogenase which generates Fd_{ox} and releases electrons to produce molecular hydrogen (Nath K. and Das D., 2004). Fermentative processes can use either biomass or, perhaps more attractively, various waste streams. Compared to photofermentation and photolysis, dark fermentation exhibits a markedly high H_2 production rate. However, it presents low H_2 yield (only 33% of the stoichiometric maximum) on organic substrates, caused by the excessive formation of various by-products, such as alcohols and acids that beyond a certain threshold inhibits cell growth, which further decreases the H_2 yield. This drawback hinders this method to be economically viable as an

alternative to existing chemical or electrochemical processes of hydrogen generation (Hallenbeck P.C. and Ghosh D., 2009).

4. **Hybrid systems** represent a new approach in hydrogen production from biological wastes, where a combination of dark fermentation and photofermentation is used. It is considered as the most promising process because others fail to achieve complete conversion. Hybrid systems comprise of non-photosynthetic and photosynthetic bacteria: for example, in a dark anaerobic reactor, *Clostridium butyricum* produces hydrogen with the degradation of carbohydrates. Because this anaerobic digestion occurs only with negative free energy, the formed organic acids could not be decomposed to hydrogen any more but, in a photofermentation bioreactor, they could be sources for photosynthetic bacteria to produce hydrogen. The combination of the both kinds of bacteria seems to be promising and productive not only because it reduces the light energy demand of photosynthetic bacteria but also because it increases hydrogen production.

In conclusion, several different ways exists by which microorganisms can produce hydrogen, each one with seeming advantages, as well as problematic issues (Hallenbeck P.C. and Benemann J.R., 2002). Relevant advances have been made in biohydrogen production; however, these biotechnologies have yet to be utilized on a large scale to be considered as valid alternatives to the technologies currently in use for hydrogen production. It is necessary to maximize hydrogen production potential and, in this perspective, in recent years researchers have made considerable efforts to improve the biochemical and structural knowledge of the hydrogenases, as enzymes involved in the production of hydrogen.

The hydrogenases

Hydrogenase is a family of enzymes that catalyze the reversible oxidation of hydrogen into its elementary particle constituents, two protons (H^+) and two electrons: $H_2 \leftrightarrow 2H^+ + 2e^-$. They work to either couple H_2 oxidation to energy-yielding processes or reduce protons as a mechanism to recycle reduced electron carriers that accumulate during fermentation (Vignais P.M. and Billoud B., 2007). Hydrogen metabolism is probably one of the most fundamental and ancient processes of living systems. Transfer of electrons to hydrogenase, with subsequent production of hydrogen, is intimately related to the primary energy metabolism in different microorganisms. Following their initial discovery in colon bacteria by Stephenson and Stickland in 1931, hydrogenases have been identified in all kingdoms of life (Vignais P.M. et al., 2001; Meyer J., 2007; Vignais P.M. and Billoud B., 2007; Posewitz M.C. et al., 2008). The first descriptions of hydrogen production, by photosynthetic eukaryotic algae, were published more than 70 years ago (Gaffron H. and Rubin J., 1942) and were soon followed by reports of hydrogen production by non-photosynthetic protozoa (Suzuoki Z. and Suzuoki T., 1951); while the first eukaryotic hydrogenase gene was cloned from *Trichomonas vaginalis* about twenty years ago (Bui E.T. and Johnson P.J., 1996). These enzymes have been shown to play a central role in the hydrogen metabolism of many microorganisms of great biotechnological interest, such as methanogenic, acetogenic, nitrogen-fixing, photosynthetic and sulfate-reducing bacteria.

The two main types of hydrogenases are classified by the nature of the metal clusters at their catalytic sites and are termed [FeFe]- and [NiFe]-hydrogenases. A subgroup of the last class comprises the [NiFeSe]-hydrogenases, in which one of the cysteine ligands of the nickel atom is replaced by a selenocysteine (Garcin E. et al., 1999). The [FeFe]-hydrogenases are typically associated with proton reduction and [NiFe]-hydrogenases with hydrogen oxidation. [FeFe]-hydrogenases are found in anaerobic bacteria and are especially prevalent among the fermentative organisms. They are also found in a number of eukarya including algae and protists but, surprisingly, they have yet to be found in cyanobacteria or in the archaeal domain. In contrast, [NiFe]-hydrogenases are frequently associated

to cyanobacteria and archaea, in addition to their common occurrence in a large number of bacteria. As can be noted in figure 8, the active sites of these three classes have structural characteristics in common, including the presence of carbon monoxide (CO) and cyanide (CN^-) groups which were first detected by FTIR spectroscopy (Happe R.P. et al., 1997, Pierik A.J. et al., 1998), bound to the iron ions.

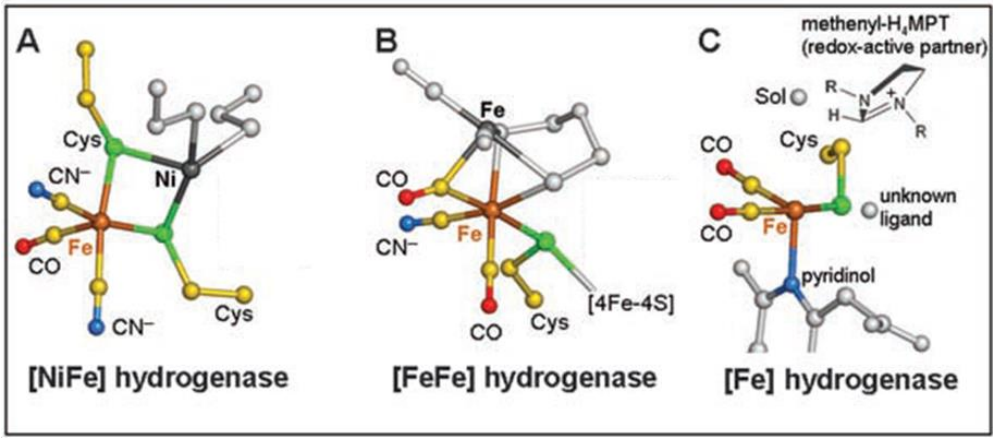

Figure 8. Active-site structures of the three phylogenetically unrelated hydrogenases. (A) [NiFe]-hydrogensase from *Desulfovibrio gigas*. (B) [FeFe]-hydrogenase from *Clostridium pasteurianum* and *Desulfovibrio desulfuricans*. (C) [Fe]-hydrogenase from *Methanocaldococcus jannaschii* In [Fe]-hydrogenase, the fifth and sixth ligation sites are marked by gray spheres. All three hydrogenase types have in common a low-spin iron (brown) ligated by thiolate(s), CO, and cyanide or pyridinol which acts together with a redox-active partner (dark gray). The nichel atom, the distal iron, and methenyl-H4MPT+ (modeled), respectively. (Adapted from Shima S. et al., 2008).

The third type of hydrogenases, the [Fe]-hydrogenase, catalyzes CO_2 reduction with H_2 to methane (Vignais P.M. and Billoud B., 2007), contains a mononuclear iron center and is found only in some hydrogenotrophic methanogenic archaea. Despite sharing several features, the [FeFe]- and [NiFe]-hydrogenases are not evolutionarily related and show no sequence similarity (Vignais P.M. and Billoud B., 2007, Vignais P.M. et al., 2001). The two independent paths for their evolution represent perhaps one of the most profound cases of evolutive convergence and this is supported by differences in the taxonomic distribution, by the pathways required to synthesize active site co-factors and by their physiological roles.

A comparison of the active-site metal centers of the three hydrogenase types reveals unexpected common features. All three types contain a redox-inactive low-spin iron, presumably in the oxidation state II, that is asymmetrically connected to five or six ligands arranged as a distorted square pyramid or octahedron. Moreover, three π-accepting ligands comprising CO, cyanide, or pyridinol (considered as a cyanide functional analog) are oriented perpendicular to each other in a geometrically related manner, and a thiolate sulfur always coordinates the iron trans to a diatomic molecule. All three iron centers act together with a redox-active partner: methenyl-H_4MPT^+ in the case of [Fe]-hydrogenase, the distal iron in the case of [FeFe]-hydrogenase, and nickel in the case of [NiFe]-hydrogenase.

Hydrogenases are present in the periplasm or in the cytosol, either in soluble form or membrane bound. Generally, hydrogenases located in the cytoplasm are associated with hydrogen evolution, whereas those located in the periplasm or membrane are associated with hydrogen uptake (Vignais P.M. et al., 2001). In eukarya hydrogenases are often found in specialized cellular compartments (Vignais P.M. et al., 2001; Wu L.F. et al., 1993). The X-ray crystal structures of hydrogenases from all three classes have been determined and include the structure of [Fe]-hydrogenase from *Methanocaldococcus jannaschii* (Shima S. et al., 2008), [NiFe]-hydrogenase structures from sulfate-reducing bacteria as *Desulfovibrio gigas* (Volbeda A. et al., 1995, 1996), and *D. vulgaris* (Higuchi Y. et al., 1997, 1999), [FeFe]-hydrogenase structures from anaerobic soil bacterium *Clostridium pasteurianum* (CpI) (Peters J.W. et al., 1998) localized in the cytoplasm and sulfate reducing bacterium *D. desulfuricans* (DdH) (Nicolet Y. et al., 1999) found in the periplasm. Analysis of crystal structures from all three classes of hydrogenases revealed a network of hydrophobic cavities, that form pathways connecting the active site to the surface of the enzyme (Volbeda A. et al., 1995; Montet Y. et al., 1997; Nicolet Y. et al., 1999, 2000; Fontecilla-Camps J.C. et al., 2007; Hiromoto T. et al., 2009). These can facilitate diffusion of hydrogen between the bulk solvent and the active site (Montet Y. et al., 1997). In addition, the pathways make it possible for small gas molecules, such as CO and O_2, to access the active site, which, in the case of [FeFe]-hydrogenases, results in an inhibition, reversible by CO and irreversible by O_2 (Bennett B. et al., 2000; De

Lacey A.L. et al., 2007; Stripp S.T. et al., 2009a). Significant interest surrounds molecular engineering studies aimed at achieving hydrogenases with low levels of sensitivity to oxygen (Friedrich B. et al., 2011), and [FeFe]-hydrogenases are often the main target of these studies because they typically possess 100 times higher H_2-evolution rates than [NiFe]-hydrogenases (Adams M.W.W., 1990, Frey M., 2002). Improving oxygen tolerance of [FeFe]-hydrogenases could allow best biotechnological solutions for hydrogen production as an alternative source of energy.

The [Fe]-hydrogenases

In 1990 in *Methanothermobacter marburgensis* a third type of hydrogenase was discovered, the [Fe]-hydrogenase, formerly named H_2-forming methylenetetrahydromethanopterin (methylene-H_4MPT) dehydrogenase (Hmd) (Shima S., et al., 2007), which has a mononuclear iron active site and is devoid of iron–sulfur clusters. Hmd is composed of two identical subunits of 38 kDa molecular mass (Thauer R.K. et al., 1996) and is involved in CO_2 reduction to methane transferring a hydride derived from H_2 to methenyl-H_4MPT^+ to form methylene-H_4MPT (Lyon E.J. et al., 2004, Shima S. et al., 2007).

$$\text{methenyl-}H_4MPT^+ + H_2 \rightarrow \text{methylene-}H_4MPT + H^+$$

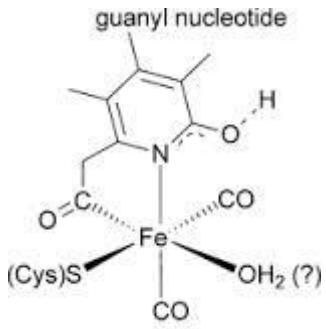

Figure 9. **Active-site structure of the [Fe]-hydrogenase from *Methanocaldococcus jannaschii*.** The catalytically center moiety consists of a mononuclear iron atom ligated to the pyridinol nitrogen and carbon atom of the guanylylpyridinol molecule. Further ligands are two CO molecules and a cysteine sulfur atom. The sixth position is probably occupied by a labile water molecule (Hu B. et al., 2014).

The cytoplasmic enzyme is only found in methanogenic archaea and, even in these, it is not ubiquitously present. A reason for this is that the reduction of methenyl-H_4MPT^+ with H_2 is also possible via two other enzymes and Hmd results essential only when methanogenic archaea grow under conditions of nickel limitation (Afting C. et al., 1998), when the other two enzymes do not work. Hmd contains only two iron per homodimer and no acid labile sulfur. Because iron was not found to be redox-active, the transition metal was long thought to have a structural rather than a catalytic role (Berkessel A., 2001). Subsequently, it has been shown that iron is essential for the activation of hydrogen and therefore that Hmd is not a "metal free" hydrogenase as previously proposed (Lyon E.J. et al., 2004). It was later renamed iron–sulfur cluster-free hydrogenase to highlight an important structural difference with the [FeFe]- and [NiFe]-hydrogenases, and with which Hmd is phylogenetically unrelated.

Despite the related low-spin iron centers, the enzymatic mechanism of [Fe]-hydrogenase differs fundamentally from that of the other two enzymes because of the different nature of the redox-active partner and the accompanying electron delivery mode.

The [FeFe]-hydrogenases and the H-cluster

[FeFe]- as well as [NiFe]-hydrogenases are highly modular proteins, consisting of a conserved structural core indispensable for stability and activity, complemented by variable numbers of accessory domains or subunits. The smallest [FeFe]-hydrogenases (~45 kDa), which are found in green algae (Florin L. et al., 2001), may be regarded as minimal forms of these enzymes, as they consist of barely more than the catalytic domain (M1). [FeFe]-hydrogenases also exist as trimers, as in *Thermotoga maritima* (Verhagen M.F. et al., 1999), or tetramers, as in *Desulfovibrio fructosovorans* (Malki S. et al., 1995) and *Thermoanaerobacter tengcongensis* (Soboh B. et al., 2004). The majority of [FeFe]-hydrogenases are soluble and cytoplasmic. Periplasmic [FeFe]-hydrogenases nevertheless do exist, mostly in sulfate-reducing bacteria. [FeFe]-hydrogenases were initially presumed to be present in a limited number of bacteria and anaerobic living protozoa (Horner D.S. et al., 2002). Subsequently,

it was revealed that their distribution in eukaryotes is also quite significant, whereas they do not occur in Archaea.

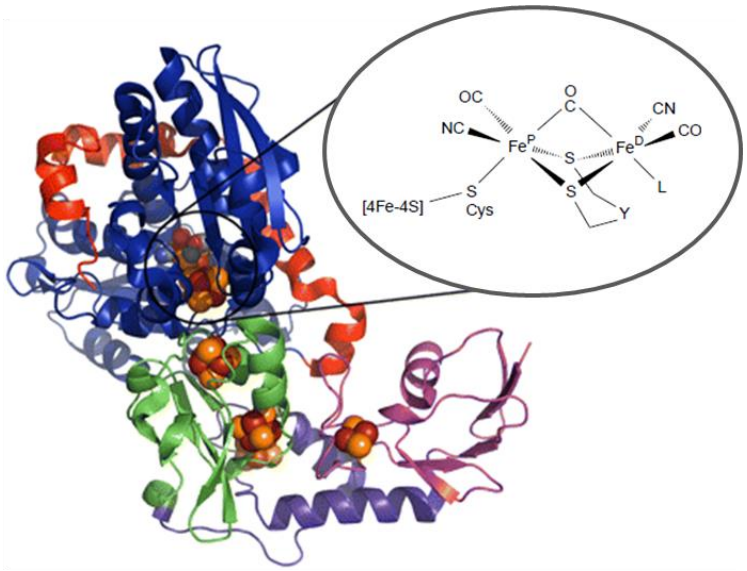

Figure 9. X-ray structure of [FeFe]-hydrogenase from *Clostridium pasteurianum* (CpI). The CpI domains are represented with different colors (C terminus: red, catalytic domain: blue, ferredoxin-like domains: green, purple, and magenta), inside the circle is schematized the active site named H-cluster: Fe^P and Fe^D are proximal and distal, respectively, in relation to the [4Fe-4S] cluster; L is an exchangeable ligand (H_2O) and Y may be an amino-N atom, as recently proposed (adapted from Shepard E.M. et al., 2010).

The core of [FeFe]-hydrogenases consists of about 40 kDa (350 amino acids) and exists as a pseudosymmetric structure in which two twisted β sheet regions come together to form a cleft in which the enzyme active site is located (see figure 9). This site is called H-cluster and consists of a bimetallic center with two Fe atoms, a proximal (Fe^P) and distal (Fe^D) Fe atom, with the distal Fe proposed as the site for hydrogen catalysis (Lemon B.J. and Peters J.W., 1999). A [4Fe-4S] subcluster is bridged to the Fe atoms through a bridging cysteine thiolate. The 2Fe subcluster is also coordinated by the non-protein ligands carbon monoxide, cyanide and a dithiolate ligand that was recently confirmed as an amine (Berggren G. et al., 2013; Esselborn J. et al., 2013). The CO and CN^- ligands, quite unexpected because of their toxicity as free entities, promote reversible heterolytic hydrogen cleavage and stabilize the low spin states of the two Fe atoms of the subcluster (Adams M.W.W., 1990).

The highly conserved H-cluster binding domain can be identified in primary sequences by three distinct binding motifs termed L1, L2 and L3 (Vignais P.M. et al., 2001). Each of these motifs contain conserved cysteine residues (from C_2 to C_5) involved in the coordination of the active site to the protein (Meyer J., 2007).

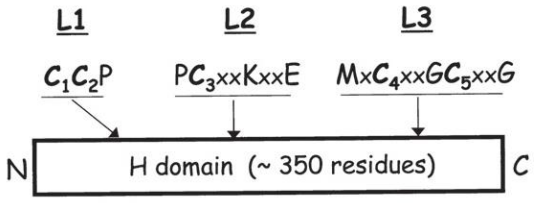

Figure 10. Schematic representation of the [FeFe]-hydrogenases H domain. Cys_2 to Cys_5 are ligands of the H-cluster, Cys_1 is believed to act as an acid/base near the active site.

The largest structural differences among [FeFe]-hydrogenases are related to their accessory FeS clusters (F-cluster), which putatively function to regulate electron transfer to and/or from the H-cluster active site. They are typically located at the N terminus of the H-cluster binding domain and are either [4Fe-4S] or [2Fe-2S] cluster.

The biochemical and spectroscopic characterization of [FeFe]-hydrogenases concerned the simplest form present in the chlorophycean algae, including *C. reinhardtii*, *Chlorella fusca*, and *Scenedesmus obliquus*, as they lack the additional FeS clusters present in most native [FeFe]-hydrogenases that can complicate the direct examination of the H-cluster (Kamp C. et al., 2008; Mulder D.W. et al., 2009, 2010).

1. [FeFe]-hydrogenase sensitivity to O_2

The catalytic activity of most hydrogenases is inhibited by oxygen, either temporarily or permanently, depending on the species they belong to. Differently from [NiFe]-hydrogenases, that are generally reversibly inhibited by oxygen, [FeFe]-hydrogenases are mostly irreversibly inhibited. Analysis of crystal structures and molecular dynamics simulations allowed to assume the existence of transient hydrophobic channels, formed by dynamic movement of the protein, involved in the gas exchange between the active site and the protein-solvent interface. In particular, studies conducted on [FeFe]-hydrogenase from *C.*

pasteurianum (CpI) showed two distinct pathways that depart from different positions of the protein surface and then converge, together, in the cavity of the active site (Cohen J. et al., 2005). Thanks to its small size, hydrogen finds a greater amount of accessible spaces and then spreads in a more extended way also in neighboring regions; instead, oxygen can spread more slowly and only through these channels. The mechanism of inhibition has not yet been clarified; it has been proposed that the exposure of the active site to oxygen impairs the enzyme activity occupying the vacant position of the distal iron atom of the active site, leading to the oxidation of this Fe, causing the loss of the CN^- and CO ligands, and resulting in breaking down of the H-cluster (Lubitz W. et al., 2007). It is interesting to note that not all hydrogenases are equally inhibited by oxygen. There are some microorganisms which possess an unusual capacity to produce hydrogen even under microaerobic conditions; this tolerance to O_2 is determined by the electronic structure of the active site and the surface charge of the protein. Bioinformatical analysis conducted on the [FeFe]-hydrogenase from *Thermotoga neapolitana*, capable of producing H_2 in the presence of small amounts of O_2 (6-12%) (Van Ooteghem S.A. et al., 2004), has highlighted the possibility that the increased oxygen tolerance is due to the more polar residues placed at the hydrophobic channel entrance (Tosatto S.C.E. et al., 2007). However, it remains to clarify the molecular details of the hydrogenases sensitivity to oxygen, which contributes to delay the development of biotechnological systems of hydrogen production by these enzymes. In addition to oxygen, CO has also an inhibitory action, even if reversible both for [NiFe]-hydrogenases and [FeFe]-hydrogenases, as it occupies the vacant coordination site in the bimetallic center that is supposed to be the first binding site of hydrogen, thereby blocking the catalytic cycle.

2. [FeFe]-hydrogenase maturation protein machinery

With respect to maturation, the knowledge of [FeFe]-hydrogenases has long had more gaps than that of [NiFe]-hydrogenases. To date, all genes committed to the assembly of [NiFe]-hydrogenases have been isolated, their products characterized, and most of their functions unraveled (Blokesch M., et al., 2002); on the other hand, less is known about their putative counterparts in [FeFe]-hydrogenases maturation. The identification and involvement of maturases in the

synthesis of the H-cluster were initially discovered by screening *C. reinhardtii* mutant strains incapable of producing hydrogen (Posewitz M.C. et al., 2004). The mutations were mapped to two genes, *hydEF* and *hydG*. It was demonstrated that an active [FeFe]-hydrogenase is obtained when they are coexpressed with the *C. reinhardtii* structural gene *hydA* in *E. coli*, which is otherwise unable to synthesize active [FeFe]-hydrogenases (Posewitz M. C. et al., 2004). Characterization of the expression products of the maturation genes from *T. maritima* in *E. coli* revealed that HydE is a radical-SAM protein containing two [4Fe-4S] clusters (Rubach J. K. et al., 2005), HydF is a GTPase containing a [4Fe-4S] cluster (Brazzolotto X. et al., 2006) and HydG is a radical-SAM protein containing a [4Fe-4S] cluster and an undefined FeS cluster (Rubach J. K. et al., 2005). Point mutations in the radical SAM motifs of HydE and HydG, as well as in the FeS cluster and GTPase regions of HydF, all proved to be deleterious to achieving activation of HydA lacking all maturation proteins ($HydA^{\Delta EFG}$), meaning that HydE, HydF, and HydG functionalities are indispensable for a proper H-cluster synthesis (King P.W. et al., 2006). Moreover, genes encoding for HydE, HydF, and HydG are present in all organisms capable of synthesizing an active HydA (Meyer J., 2007). In several green algae, *hydE* and *hydF* are fused (Böck A. et al., 2006), but in the majority of microorganisms and in all bacteria they exist as separately transcribed genes. Based on the available experimental data, two pathways of the [FeFe]-hydrogenase maturation mechanism, illustrated in figure 11, have been recently proposed. In (a), HydE modifies a [2Fe–2S] cluster on HydF by synthesis and insertion of the dithiomethylamine bridging ligand. Then, HydG catalyzes the formation of CO and CN^-, which are delivered to the 2Fe subcluster. The assembled 2Fe subcluster is then transferred to HydA. Direct interactions between the radical SAM maturases and HydF have been reported (McGlynn S.E. et al., 2008; Vallese F. et al., 2012), and may be important for efficient delivery of the products of HydE and HydG. An alternate pathway is shown in (b), involving iron-bound cyanide and carbon monoxide that are first synthesized on HydG, and then delivered to HydF as cyano-carbonyl-Fe units, where dithiomethylamine addition stitches the two mononuclear Fe species together. The synthesis of iron-bound diatomics on HydG is consistent with the recent FTIR spectroscopic studies (Kuchenreuther J.M. et al., 2014).

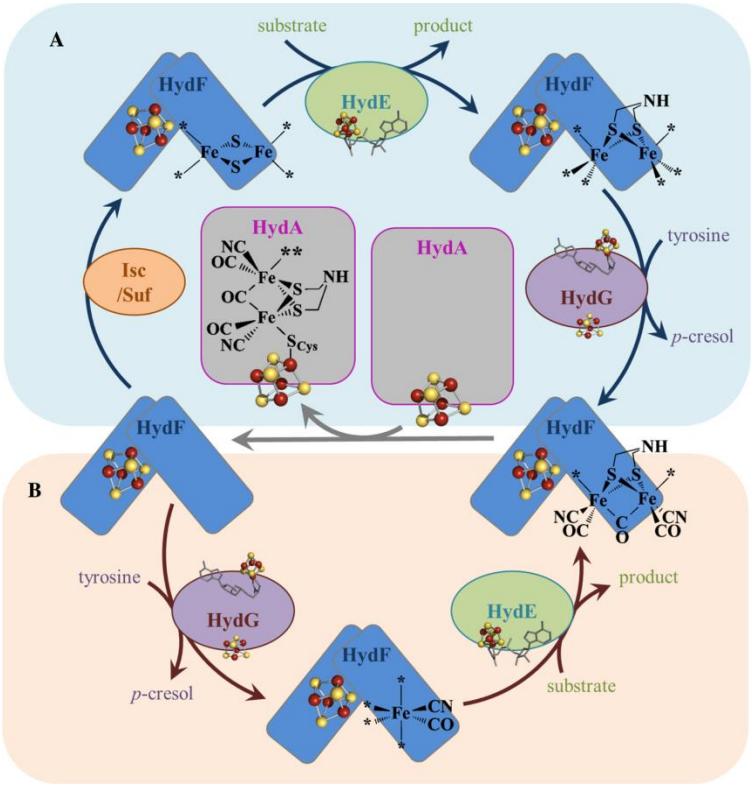

Figure 11. The two possible pathways proposed for the maturation of [FeFe]-hydrogenase. In both pathways, the maturation process involves synthesis and assembly of the 2Fe subcluster of the H-cluster, followed by insertion of this 2Fe subcluster to generate the active hydrogenase. Asterisks indicate unknown ligands (Broderick J.B.et al., 2014).

The crystal structure of $HydA^{\Delta EFG}$ from *C. reinhardtii* heterologously expressed in *E. coli* provided important clues into the maturation process and cluster insertion (Bethel R.D. et al., 2010; Mulder D.W. et al., 2010), indicating that the [4Fe-4S] subcluster is synthesized by the *E. coli* FeS cluster biosynthetic machinery (ISC and/or Suf) before the synthesis and insertion of the 2Fe subcluster by the specialized *hyd* encoded maturation machinery (Mulder D.W. et al., 2010; Shepard E.M. et al., 2011). Insertion of the 2Fe subcluster presumably occurs via a positively charged channel that closes following 2Fe subcluster incorporation by conformational changes in two conserved loop regions. Several details of this mechanism need to be clarified and, whereas the combination of HydE, HydF, and HydG appears to be competent for the assembly of [FeFe] active sites in most organisms, it cannot yet be excluded that additional maturation genes may be required in some cases (Böck A. et al., 2006).

3. Radical SAM Chemistry in H-cluster Biosynthesis

Radical-SAM (radical S-adenosyl methionine) enzymes generally catalyze complex chemical processes such as the biosynthesis of cofactors, methylations, isomerizations, insertion of S atoms, enzyme activation, formation of metal proteins clusters. Radical SAM enzymes catalyze the reduction of *S*-Adenosyl methionine by a reaction generating methionine and the high oxidizing 5'-deoxyadenosyl radical (5'-Ado). The structures of several radical-SAM enzymes have been determined, revealing a high similarity among the members of this superfamily.

3.1 HydG

This monomeric protein (55 kDa) is a member of the radical SAM superfamily enzymes (Posewitz M.C. et al., 2004; Broderick J.B. et al., 2014) as it contains a CX3CX2C N-terminal motif. Similarly to anaerobic tyrosine lyase enzyme (ThiH), it utilizes L-tyrosine as substrate and forms p-cresol. Unlike ThiH and uncommon to radical SAM enzymes in the C-terminal extension it contains a CX2CX22C motif that harbors an accessory [4Fe–4S] cluster which is essential for [FeFe]-hydrogenase maturation, and the formation of the diatomic products CO and CN^- (King P.W. et al., 2006; Driesener R.C. et al., 2010; Shepard E.M. et al., 2010). Recent mutagenesis experiments on HydG from *Clostridium acetobutylicum* suggests that CO production depends on the presence of the second FeS cluster, presumed to be [4Fe-4S] in nature, whereas CN^- production occurs independently of the C-terminal cluster (Nicolet Y. et al., 2010; Tron C. et al., 2011). Nicolet, in 2010, proposed that the homolytic tyrosine cleavage results in a glycyl radical that undergoes protonation and subsequent decarboxylation to yield $H_2C{=}NH$, an intermediate in HCN production, and $^{\bullet}CO_2^-$ that may be reduced to CO species at the site-differentiated Fe of the C-terminal $[4Fe\text{-}4S]^{2+}$ cluster (see figure 12). Further studies are required to shed light on the HydG mechanism by which the diatomic ligands are delivered to HydF.

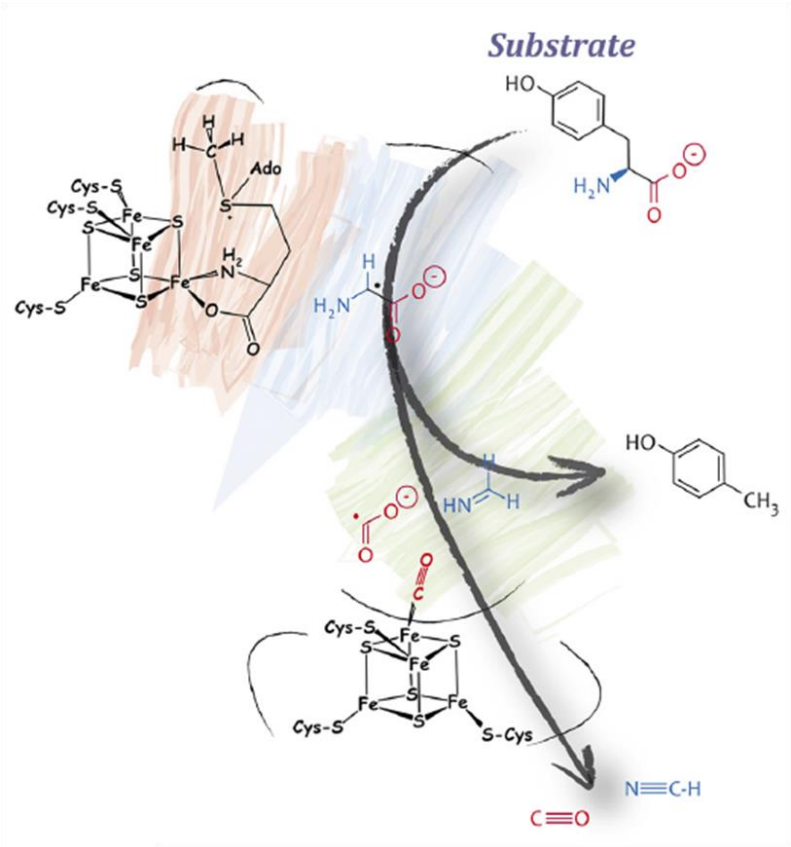

Figure 12. Depiction of the topology of the CO/ CN^- synthesis by HydG from tyrosine. *Shading* represent the SAM-binding region (*orange*), the substrate-binding region (*blue*), and the specificity region (*green*) (Nicolet Y. and Fontecilla-Camps J.C., 2012).

3.2 HydE

HydE is a 42 kDa monomer containing the canonical CX3CX2C sequence–N-terminal motif, like the other radical SAM enzymes (Posewitz M.C. et al., 2004; Broderick J.B. et al., 2014). The structure of HydE from *T. maritima*, depicted in figure 13, was determined by X-ray diffraction revealing an (a/b)8 triose-phosphate isomerase (TIM) barrel fold with a site-differentiated [4Fe-4S] cluster responsible for binding and cleaving SAM (Nicolet Y. et al., 2008, 2009), and an additional [2Fe-2S] cluster coordinated by three Cys residues.

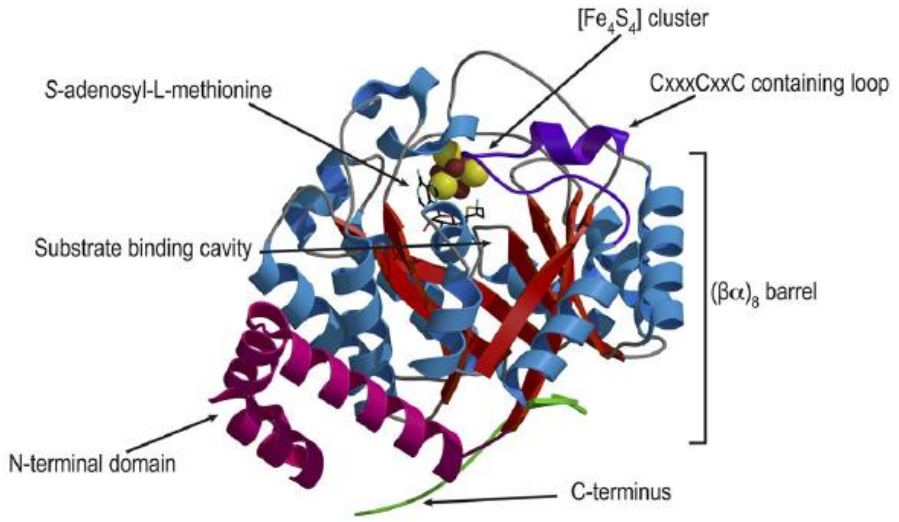

Figure 13. X-ray structure of HydE from *T. maritima*. (Protein Data Bank ID code: 3CIW). The TIM-barrel domain is depicted in red (strands) and blue (helices). The N-terminal domain is depicted in pink and the C-terminal extension in green. The substrate binding cavity extends from the top to the bottom of the barrel. Upon thiocyanate binding, slight movements of conserved hydrophobic residues, disposed as a crown, split the cavity to generate two separate pockets (Nicolet Y. et al., 2008).

HydE shows high sequence similarity to the methylornithine synthase PylB (Rubach J.K. et al., 2005), rather than to enzymes like biotin sinthase (BioB) that catalyzes a sulfur insertion reaction (Nicolet Y. et al., 2008). The role of this protein in H-cluster biosynthesis is still not clarified. It has been suggested that it functions as a chaperone assisting HydF during translocation of the 2Fe subcluster species (Kuchenreuther J.M. et al., 2011). More likely, however, HydE synthesizes the bridging dithiomethylamine ligand. The formation of a dithiolate-linked cluster intermediate could result from alkylation of the sulfides of a [2Fe-2S] cluster, thereby effectively protecting the sulfides against further reactivity and shifting the chemical reactivity toward the Fe sites, essentially priming them for addition of CO and CN^- (Peters J.W. et al., 2006).

Evidence in support of its essential role comes from the absolute requirement of HydE to achieve [FeFe]-hydrogenase activity in experiments using *E. coli* lysate (McGlynn S.E. et al., 2007). As assessed before, HydE and HydF exist as a fused gene product in some organisms (Posewitz M.C. et al., 2004) and surface plasmon resonance experiments, conducted in our laboratory, indicate that they

interacts with high affinity (Vallese F. et al., 2012). Up to date, however, the substrate and mechanism of HydE in H-cluster biosynthesis remain unresolved.

3.3 HydF: an iron sulfur cluster binding GTPase

HydF is that binds FeS clusters and hydrolyzes GTP to GDP (Brazzolotto X. et al., 2006; Shepard E.M. et al., 2010). It presents a N-terminal GTPase domain, including a Walker A P-loop and a Walker B Mg^{2+}-binding motifs, and a C-terminal domain with conserved Cys and His residues.

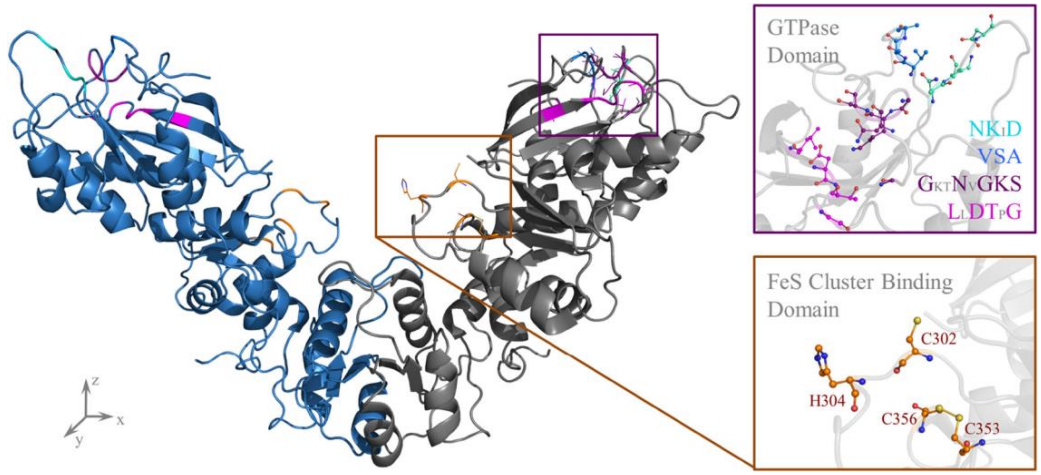

Figure 14. The maturase HydF has GTPase and FeS domains. Maturase HydF from *T. neapolitana* is depicted (left) in dimer form with residues in the GTPase and FeS binding domains highlighted. One subunit is illustrated in blue, while the other subunit is shown in gray. In the GTPase domain the residues associated with GTP binding and hydrolysis are highlighted in cyan for distal GTP specificity (NKxD), blue for the G-5 loop domain, purple for the Walker A P-loop (GxxNxGKS) and magenta for the Walker B Mg^{2+} binding loop (LxDTxG). This magnified box view is rotated 90° counter clock-wise in the xy plane from the full dimer structure on the left. The FeS binding domain: the three cysteine residues highlighted are the only cysteine residues in the monomer. (Color scheme in expanded view: N blue; O red; S yellow; C, same color as highlighted stick) (Protein Data Bank ID code: 3QQ5) (Broderick J.B. et al., 2014).

When purified to homogeneity, this protein is a composite mixture of dimers and tetramers and structural characterization of the metal-free enzyme has suggested that FeS cluster(s) bind(s) at subunit interfaces (Cendron L. et al., 2011). Moreover, among the three maturases, only a purified HydF previously expressed in the presence of HydE and HydG is able to activate $HydA^{\Delta EFG}$. This activation is achieved in the absence of exogenously added proteins or small molecules, suggesting that HydF binds a precursor form of the H-cluster needed

to achieve maturation (McGlynn S.E. et al., 2008). The HydF protein plays a key role in the maturation pathway, since it acts as scaffold in which the precursor of the H-cluster active site is assembled, and as carrier for the transfer of this cluster to the hydrogenase (Shepard E.M. et al., 2010; Czech I. et al., 2010). In our laboratory experiments were designed to probe protein–protein interactions between the maturases and revealed that HydE and HydG do not bind to HydF concurrently, suggesting that the radical SAM enzymes associate with the same binding site on HydF (Vallese F. et al., 2012). Moreover, HydE and HydF bind to one another with an order of magnitude higher affinity than HydG binds to HydF, and addition of GTP during dissociative phases causes enhanced detachment rates for both HydE–HydF and HydG–HydF complexes (Vallese F. et al., 2012). Collectively, these results implicate that GTP binding and hydrolysis provides a mechanism for gating the interactions between HydE and HydG with the scaffold/carrier HydF, and this may be linked to structural changes in HydF dependent on the GTP (see below).

The three-dimensional structure of the HydF from *T. neapolitana* in the recombinant apo-form, *i.e.* completely devoid of both GTP or FeS centers, and therefore inactive, has been solved in our laboratory by X-ray crystallography (Cendron L. et al., 2011). The active form of the protein is likely a homodimer presenting an open structure, with the domains exposed and ready to interact with other maturases and then to transfer the cluster to the hydrogenase. Each monomer has three different domains, all characterized by a common folding, *i.e.* a parallel β-sheet flanked on both sides by α-helices (see figure 14):

- a GTP binding domain (I)
- a dimerization domain (II)
- an iron-sulfur cluster binding domain (III)

Based on this model, further biochemical studies have been performed in solution where the protein, unlike the crystal, keeps the ability to bind both a center FeS and the GTP. In particular, EPR (Electron Paramagnetic Resonance) and HYSCORE (hyperfine sublevel correlation spectroscopy) analysis have confirmed the fundamental role of the three conserved cysteines of the consensus

sequence CXHX (44-53) HCXXC, responsible for the binding of the *cluster* to the protein, and highlighted the variability of its fourth ligand, which may be different depending on the HydF belonging to different species (Berto P. et al., 2012; Albertini M. et al., 2014).

3.3.1 The HydF GTPase domain

NTPases are often involved in the assembly of metal cofactors of iron-sulfur proteins, wherein they participate in the transfer of the FeS center(s) to the apo-protein, or in the insertion of the metal(s) in the active site. In the case of [FeFe]-hydrogenases, site-directed mutagenesis experiments have demonstrated that the HydF GTPase domain is necessary for a correct maturation process of the enzyme active form (King P.W. et al., 2006). Similarly to other GTPases, the HydF GTPase domain has an extended structure formed by five parallel β-strands and one anti-parallel, flanked by three α-helices on one side and two on the other.

It presents conserved amino acids considered important for the binding and hydrolysis of GTP (Shepard E.M. et al., 2010; McGlynn S.E. et al., 2007). It has a long, extremely flexible loop that could rearrange becoming more ordered upon binding of the nucleotide (Cendron L. et al., 2011).

The exact role of GTP binding and/or hydrolysis in [FeFe]-hydrogenase maturation remains, however, still unresolved. It has been shown that the GTPase activity of HydF is not associated with the activation step of $HydA^{\Delta EFG}$ by HydFEG (Shepard E.M. et al., 2010). However, it was also observed that the rate of GTP hydrolysis was increased of about 50% when HydF was expressed in the presence of either HydE or HydG, leading to the hypothesis that GTP binding and hydrolysis may be linked to structural changes in HydF that result in altered interactions with HydE and HydG, and/or by perturbation of the electronic environment where the 2Fe subcluster is formed (Shepard E.M. et al., 2010).

It remains to clarify the details of the molecular interactions between the proteins involved in the formation of an active and properly assembled [FeFe]-hydrogenases. A greater knowledge of them could have interesting biotechnological applications since, as mentioned before, [FeFe]-hydrogenases show high specific activities in terms of hydrogen production. This led us to focus

our study on HydF and on its possible structural reorganization induced by the binding of GTP, that I will describe in the Results section.

The [NiFe]-hydrogenases

[NiFe]- and [FeFe]-hydrogenases are an excellent example of convergent evolution and it follows that their biosynthetic pathways exhibit both similarities and differences. Both the active site assembly pathways require multiple maturation proteins involved in intricate chemical transformations. Moreover, each system utilizes a key scaffold protein that belongs to the same subclass of GTPase enzymes, which are activated by alkali metals. Another intriguing aspect shared by these systems is the formation and transfer of Fe-diatomic species among proteins, even if the source of these diatomic ligands is disparate. Another common feature is the presence of endogenous CO and CN^- ligands bound to a Fe center in the active site. Finally, both types of enzymes contain hydrophobic gas channels. Differently from [FeFe]-hydrogenase, the Fe atom at the active site of the [NiFe]-hydrogenase is bridged to a Ni atom through bridging cysteine thiolates. The Ni atom is also terminally coordinated by two additional cysteine thiolates. In some hydrogenases one of the two terminal cysteines is replaced by a selenocysteine and these so-called [NiFeSe]-hydrogenases are considered variations of [NiFe]-hydrogenases. A feature that distinguishes the [NiFe]- from [FeFe]-hydrogenases is the absence of SAM proteins involved in the maturation process. Taxonomically, [NiFe]-hydrogenase are more widely distributed than [FeFe]-hydrognesae, indeed they are encoded by both aerobic and anaerobic bacteria and archaea but, differently from [FeFe]-hydrogenases, not by eukarya. To date, the question of whether the [FeFe]- or [NiFe]-hydrogenases appeared first in the course of biological evolution remains unanswered. The wider distribution in bacteria suggests that [NiFe]-hydrogenases appeared earlier than the [FeFe]-enzymes, an inference that is otherwise supported by indications of a close association of iron and nickel in prebiotic chemistry and primitive biochemistry (Fang H.H.P. et al., 2006). On the other hand, these hydrogenases might have been associated with their chaperone system since their origin, and this indicates that they appeared at a time when spontaneous assembly of the

active site was no longer feasible, thus placing them in a subsequent period than the [FeFe]-hydrogenases.

As represented in figure 15, the [NiFe]-hydrogenases are heterodimeric proteins consisting of two subunits, a large subunit (LSU) of about 60-kDa, hosting a unique, complex nickel iron center with coordination to 2 CN^- and one CO, forming a biologically unique metallocenter (Pierik A.J. et al.,1999), and a small subunit (SSU) of about 30-kDa, containing three highly conserved iron-sulfur clusters, *i.e.* two [4Fe–4S], proximal and distal, and one medial [3Fe–4S], that serve to shuttle electrons between the external electron carrier and the NiFe site.

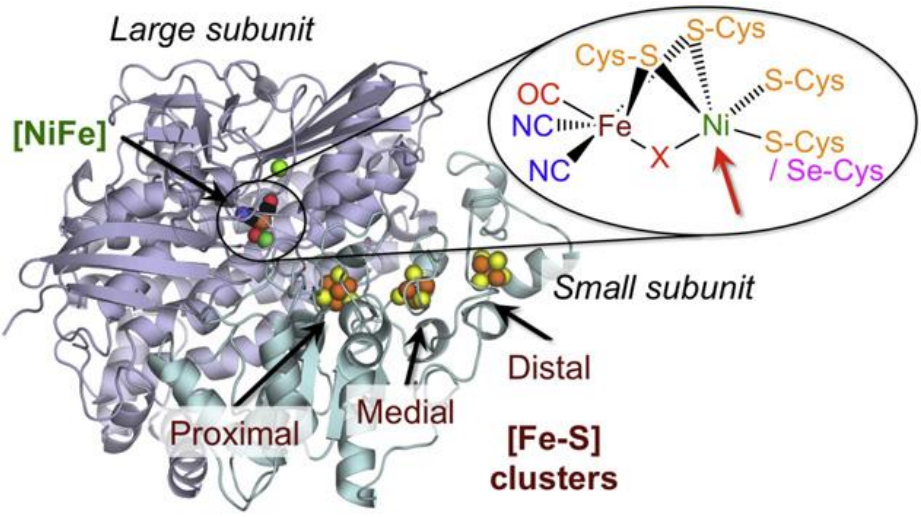

Figure 15. Protein structure of [NiFe]-hydrogenase. Active site, large and small subunits, [4Fe-4S] proximal and distal clusters, and [3Fe-4S] medial cluster are indicated. In the enlarged active site the red arrow indicates proposed H_2-binding site; the terminal cysteine that is replaced by selenocysteine is also shown. (Shafaat H.S. et al., 2013).

It was the crystal structures of *Desulfovibrio* hydrogenases that revealed that the two subunits interact extensively through a large contact surface and form a globular heterodimer (Volbeda A. et al., 1995, 1996; Higuchi Y. et al., 1997, 1999). The bimetallic NiFe center is deeply buried in the large subunit; it is coordinated to the protein by four cysteines. The [4Fe-4S] cluster proximal to the active site (within 14 Å) is essential to H_2 activation (Volbeda A. et al., 1995; Fontecilla-Camps J.C. et al., 1997). Hydrophobic channels linking the active site

to the surface of the molecule have been suggested to facilitate gas access to the active site (Fontecilla-Camps J.C. et al., 1997; Montet Y. et al., 1997).

1. [NiFe]-hydrogenase sensitivity to O_2

[NiFe]-hydrogenases are in general reversibly inhibited by oxygen and regain catalytic activity when placed back in an anaerobic reductive environment. The reason why [NiFe]- and [FeFe]-hydrogenases have different sensitivity to this gas is not clear, but is likely that the mechanism of this inhibition is very similar in both classes, given the strong similarity of their active sites, and that involves redox processes at this level. X-ray crystallography and molecular dynamics modeling in *Desulfovibrio gigas* and *D. fructosovorans* have identified a hydrophobic gas channel connecting the active site of [NiFe]-hydrogenase to its surface (Montet Y. et al., 1997). The fluctuations of the protein do not seem to interfere with the presence of this cavity, but are certainly crucial to allow the gas to pass through them. Several biochemical and molecular studies have focused on identifying amino acid residues more involved in the paths of gases diffusion, with particular attention to the [NiFe]-hydrogenases that show a partial oxygen tolerance. Experiments on the [NiFe]-hydrogenases of *Ralstonia eutropha* (Ludwig M. et al., 2008) led to the conclusion that oxygen tolerance is not due to a single factor, such as the diameter of the channel of the gas exchange, but rather is determined by the protein superficial charge and by the electronic structure of the active site, which, in this organism, appears slightly different as it coordinates two additional CN^- in the bimetallic center (Fontecilla-Camps J.C., 2007). It has been proposed that in [NiFe]-hydrogenases oxygen induces a conformational change in the active site due to the abundance of electrons at this level, resulting in the impairment of the catalytic activity; however, actually how oxygen inhibits, even in a reversible manner, the activity of these enzymes remains unclear.

2. [NiFe]-hydrogenase classification

[NiFe]-hydrogenases can be classified into four distinct functional groups that in general correspond to their putative physiological role (Vignais P.M. and Billoud B., 2001):

2.1 Group1. The uptake [NiFe]-hydrogenases

They are typically membrane-bound hydrogenases and are found in organisms that use hydrogen as an energy source. They are connected to the quinone pool of the respiratory chain in the membrane by a cytochrome *b* which, together with the hydrophobic C-terminus of the small subunit, anchors the hydrogenase dimer to the membrane. These enzymes serve to consume hydrogen coupling the oxidation of H_2 to the reduction of electron acceptors such as oxygen, nitrate, sulfate, or CO_2. Electrons from hydrogen are transferred to the quinone pool and the energy of hydrogen oxidation is recovered by proton transfer (Vignais P.M. et al., 2004). These uptake hydrogenases were found in *Proteobacteria* and in *Aquifex aeolicus* (Brugna-Guiral M. et al., 2003) and in the methanogenic archaeon *Methanosarcina mazei* Gö1 (Ide T. et al., 1999). Another type of uptake enzyme is the periplasmic hydrogenases of *Desulfovibrio* species and *Thiocapsa roseopersicina*. The uptake hydrogenases are characterized by the presence of a long signal peptide (30-50 amino acid residues) at the N-terminus of their small subunit. A conserved (S/T)RRxFxK motif in the peptide serves as signal recognition to target the fully folded heterodimer to the membrane and to the periplasm (Wu L.F. et al., 2000a, b; Berks B.C. et al., 2000).

2.2 Group 2. The cytoplasmic hydrogen sensors and the cyanobacterial uptake [NiFe]-hydrogenases

Group 2a. This subgroup includes hydrogenases of cyanobacteria as *Nostoc* (Oxelfelt F. et al., 1998) and *Anabaena variabilis* (Happe R.P. et al., 2000) that fix dinitrogen (N_2) using nitrogenase. These organisms contain a dimeric uptake hydrogenase (HupSL) to recapture energy lost as hydrogen during the reduction of N_2 (Berman-Frank I. et al., 2003). Electrons from hydrogen are then channeled into the quinone pool or function to reduce oxygen that deactivates the oxygen sensitive nitrogenase enzyme (Tamagnini P. et al., 2007; Zhang X. et al., 2014).

Group 2b. These hydrogenases, identified in *Rhodobacter capsulatus and Ralstonia eutropha,* are not exported but remain in the cytoplasm. Their role is to detect the presence of hydrogen in the environment and to trigger a cascade of cellular reactions controlling the synthesis of some uptake [NiFe]-hydrogenases (Vignais P.M. et al., 2007).

2.3 Group 3. The bidirectional heteromultimeric cytoplasmic [NiFe]-hydrogenases

This group has the dimeric hydrogenase module associated with other subunits that are able to bind soluble cofactors, such as cofactor 420 (F420, 8-hydroxy-5-deazaflavin), NAD(H) or NADP(H). They are termed bidirectional because, physiologically, they function reversibly and can thus reoxidize the cofactors under anaerobic conditions by using the protons of water as electron acceptors. Many members of this group are found in *Archaea*. They include the trimeric F420-reducing hydrogenases, the tetrameric bifunctional hydrogenases of hyperthermophiles, able to reduce S° to H_2S *in vitro* and to use NADPH as electron donor (Ma K. et al., 1994), and the F420-non-reducing hydrogenases. An additional subgroup consists of bidirectional heteromultimeric [NiFe]-hydrogenases (HoxHY) that are associated with an additional NADH oxidoreductase (diaphorase) module, which shows distinct homology to the some subunits of Complex I of the respiratory chain (Vignais P.M. et al., 2007). The bidirectional hydrogenases are found in aerobic H_2-utilizing organisms such as *Ralstonia eutropha*, in which they most likely catalyze hydrogen oxidation and supply reducing equivalents (NADH) to Complex I for energy generation or provide reductant for biosynthesis (Cramm R., 2009). Many cyanobacteria possess the bidirectional hydrogenase, which works to dispose of excess electrons derived from fermentation and photosynthesis (Tamagnini P. et al., 2007). It was shown that in the cyanobacterium *Synechocystis* sp. PCC 6803 it could also directly accept electrons from Fd or flavodoxin, which explains the production of H_2 by over reduction of the Fd pool in the light or fermentative metabolism under anoxic dark conditions (Gutekunst K. et al., 2014).

2.4 Group 4. The H_2-evolving, energy-conserving, membrane-associated hydrogenases

These multimeric (six subunits or more) enzymes reduce protons from water in order to dispose of excess reducing equivalents produced by the anaerobic oxidation of organic compounds of low potential, such as carbon monoxide or formate. The hydrogenase-3 from *E. coli*, which metabolizes formate to H_2 and CO_2, is the prototype of this group. The majority of hydrogenases belonging to

this group have been found in *Archaea* including *Methanosarcina barkeri* (Künkel A. et al., 1998), *Methanobacterium thermoautotrophicum* strain Marburg (now called *Methanothermobacter marburgensis)* (Tersteegen A. and Hedderich R., 1999) and *Pyrococcus furiosus*.

2.5 Group 5.

This group was recently proposed based on genome sequencing, phylogenetic reconstructions, and biochemical characterization of an enzyme from *Streptomyces* spp. that is capable of oxidizing hydrogen at very low levels (Constant P. et al., 2011; Schäfer C. et al., 2013; Constant P. et al., 2010). It appears that these hydrogenases are abundant among soil bacteria, where they presumably provide the capability to take advantage of low hydrogen concentrations (Meredith L.K. et al., 2014; Greening C. et al., 2014).

They are similar to the group 1 as they also consist of a small and large subunit and associate with the membrane, although, in this case, not through a cytochrome. No redox partners have been identified to date. Thus, while these hydrogenases appear to be biochemically similar to group 1, they are distinct from that because they are oxygen resistant. Moreover, their [NiFe] binding motifs are different (Constant P. et al., 2011).

3. [NiFe]-hydrogenase active site assembly

The synthesis of [NiFe]-hydrogenase is a highly complicated process which needs a number of accessory gene products that are required for metal (nickel and iron) capture, synthesis (CO and CN^-) as well as cluster insertion and protein maturation (figure 16).

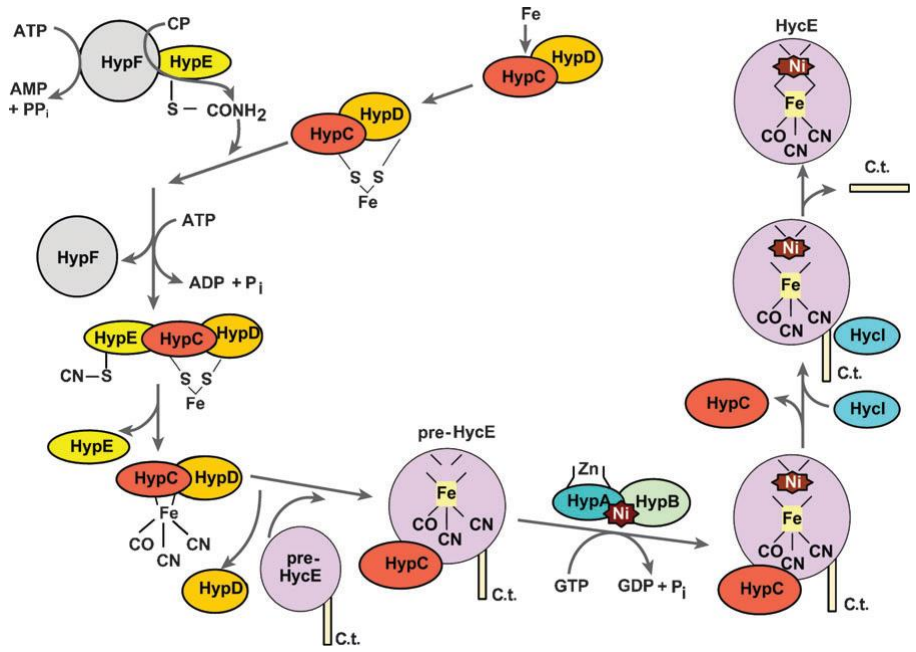

Figure 16. Network of hydrogenase maturation proteins. CP is carbomoyl phosphate, C.t. is the C terminus of the precursor to the large subunit HycE. (adapted from Blokesch M. and Böck A., 2002).

Six *hyp* genes denoted *hypA–hypF* (and their associated homologs) are required for biosynthesis and insertion of the NiFe(CN)$_2$CO catalytic cluster into the large subunit of [NiFe]-hydrogenases. HypC, D, E, and F proteins are involved in Fe(CN)$_2$CO biosynthesis and are absolutely needed for the maturation process (Maier T. et al., 1996; Jacobi A. et al., 1992; Lutz S. et al., 1991). The cyanide ligands of the active site cluster are derived from carbamoylphosphate in a series of reactions involving HypE and HypF (Reissmann S. et al., 2003). In the following, the mechanisms underlying the maturation of [NiFe]-hydrogenase are depicted and described in detail.

3.1 HypC and HypD: Fe(CN)$_2$CO cofactor biosynthesis

The insertion of Fe and Ni into the metal center is a sequential process in which Fe incorporation precedes that of Ni. The Fe donor is not identified, but it appears to be incorporated into a complex formed by HypC and HypD (Blokesch M. and Böck A., 2002). HypC is a protein of approximately 10 kDa that is associated with HypD and a precursor form of the catalitic subunit, moreover it forms a ternary complex with HypD and HypE (Böck A. et al., 2006).

HypD proteins are approximately 40 kDa in size and contain a unique C-terminal CX14CX6CX16C motif in domain III that coordinates a [4Fe–4S] cluster. This latter, together with a pair of cysteine residues that are in close proximity to it, is involved in a redox cascade that is extended to four other conserved motifs in HypD (CGXHXH, GPGCPVCX2P, GFETT, and PXHVSX3G). This has been proposed to play a role in the mechanism of iron cyanation (Watanabe S. et al., 2007; Soboh B. et al., 2012). Some results suggest that HypC delivers Fe–CO_2 to HypD, where the CO_2 is reduced to CO (Soboh B. et al., 2013); therefore, metabolic CO_2 would be the source of the CO ligand, although this has yet to be experimentally demonstrated. Co-expression studies revealed that substoichiometric amounts of HypE were associated with a HypC–HypD complex that accepted CN^- from HypE; HypC– HypD complex shared the coordination of the CN^- group since CN^- was not transferred to them when singly expressed (Blokesch M. et al., 2004). However, the exact details of diatomic ligand coordination to Fe at this stage of maturation are not fully resolved. A model wherein Cys2 and His51 of HypC and Cys41 and His44 of HypD (*E. coli* numbering) come together to coordinate a precursor Fe ion in a tetrahedral environment has been recently suggested; addition of the CO and the CN^- ligands results in HypC dissociation and addition of His201 to accomplish formation of the octahedrally coordinated $Fe(CN)_2CO$ unit on HypD (Stripp S.T. et al., 2013; Soboh B. et al., 2013). The assignment of His44 and His201 as the fourth and fifth ligands is not established with certainty.

3.2 HypF and HypE: synthesis of thiocyanate

This monomeric protein of ~82 kDa modifies carbamoylphosphate in two ATP-dependent steps: first, it converts it to carbamate, then to carbamoyladenylate before finally transferring the carbamoyl functional group to the C-terminal cysteine residue of HypE (Reissmann S. et al., 2003). Then, the dehydration coupled with ATP hydrolysis producing a thiocyanate adduct HypE takes place (Blokesch M. et al., 2004), followed by the cyano group transfer to the iron atom of the HypC-HypD complex. It was initially postulated that carbamoylphosphate also serves as the precursor of the CO ligand (Paschos A. et al., 2001), but recent labeling studies demonstrated that the CO is synthesized

from a different carbon source than the cyanides and involves a metabolic pathway that incorporates acetate (Roseboom W. et al., 2005). The intermediates produced by HypF are quite unstable, however, a mechanism for their formation is suggested by the HypE-HypF complex, a heterotetrameric structure comprised of a HypE dimer (monomeric size is ~35 kDa) flanked by two HypF molecules (Shomura Y. et al., 2012).

3.3 HypA and HypB: insertion of Ni^{2+}

HypA and HypB are involved in acquiring and inserting Ni^{2+} into the large subunit, which occurs only when the $Fe(CN)_2CO$ moiety is present (Böck A. et al., 2006). Evidence has been reported for cooperation between HypA and HypB during insertion of Ni into hydrogenase (Hube M. et al., 2002).

HypA is a 140 aminoacid protein that exists in both monomeric and dimeric states (Watanabe S. et al., 2009). HypA coordinates a single Ni^{2+} ion with micromolar affinity via an N-terminal MHE motif, and also binds Zn^{2+} through the cysteine thiolates of a zinc finger motif. Ni^{2+} and Zn^{2+} binding domains are independent of one another, but it seems that Ni^{2+} mediates protein-protein interactions influencing the orientation of these two domains .

HypB is a Ni^{2+}-metallo chaperone that has a conserved GTP-binding motif at the C-terminus, which is essential to achieve complete hydrogenase maturation (Maier T. et al., 1995). HypB dimerization is Ni^{2+}-dependent and its GTPase activity is modulated by metal binding (Sydor A.M. et al., 2014)

While the molecular mechanism for Ni^{2+} transfer to the large catalytic subunit is not yet fully resolved, delivery of nickel *in vivo* is likely modulated by protein-protein interactions and there are evidence that HypA, HypB, SlyD (a Ni^{2+}-metallo chaperone in *E. coli*), and HycE (the large subunit of hydrogenase 3 in *E. coli*) form complexes (Leach M.R. et al., 2007). The interaction of HypB with the large subunit requires the presence of HypA, providing support for HypA being the docking protein between HypB and HycE in the nickel delivery step (Chan Chung K.C. et al., 2011). Moreover, HypA selectively removes Ni^{2+} from the GTPase domain of HypB and this metal release appears to be stimulated by GTP hydrolysis (Douglas C.D. et al., 2013).

The final steps include the cleavage of a C-terminal fragment from the large subunit by an isoenzyme-specific endopeptidase to complete the active site (Theodoratou E. et al., 2005). The peptide length varies somewhat among different hydrogenases; a peptide of approximately 15 residues is most commonly cleaved, although maturation of *E. coli* hydrogenase 3 results in the removal of 32 residues (Soboh B. et al., 2013). Nickel promotes the recognition of the binding motif DPCXXCXXH/R consensus motif by the proteases and this explains why cleavage only occurs after Ni^{2+} has been inserted (Theodoratou E. et al., 2000b). The peptide extension of the large subunit is necessary for interaction with HypC, and its presence helps to keep the large subunit in an open conformation for both Ni^{2+} and $Fe(CN)_2CO$ insertion (Drapal N. et al., 1998; Blokesch M.A. et al., 2002). Upon cleavage of the C-terminal peptide, a conformational change in the active site environment is induced which effectively internalizes the $NiFe(CN)_2CO$ moiety and affords the active enzyme (Böck A. et al., 2006).

Hydrogenases have been the focus of extensive research in recent years. Some of these efforts are clearly driven by the potential of using these enzymes in future biotechnological applications to produce hydrogen as a renewable fuel. Although studies in the last decade have added new informations about hydrogenases, there are still several open questions that remains to be answered:

1) in first instance, in order to heterologously express recombinant active hydrogenases in host organisms it is still necessary to clarify the details that allow to assembly *in vivo* these enzymes. This issue concerns in particular the [FeFe]-hydrogenases and their still poorly elucidated maturation mechanism, since they are considered promising for hydrogen bioproduction due to a specific activity of two orders of magnitude higher than the [NiFe]-hydrogenases. In chapter two we tried to add a piece to complete this puzzle, going to investigate the HydF GTPase activity and its role in the dynamics of association/dissociation with the other two maturases, which are still unknown and under debate;

2) in second place, there is a more general but not trivial aspect to deepen that concerns the physiological role of hydrogenases, because it is certain that they are involved in hydrogen metabolism and that, in most cases, they are active only in anoxic/micro-oxic conditions. It is therefore particularly curious

that, in some organisms, these enzymes are expressed also in the presence of oxygen. This is the case of *Synechocystis* sp. PCC 6803, a cyanobacterial strain which possesses a bidirectional [NiFe]-hydrogenase that is expressed, with its throughout maturases network, even in the presence of oxygen. In chapter one we have investigated whether this enzyme could have some function, still unknown, even under these conditions.

It is easy to understand that we will not be able to fully exploit the potential of these enzymes for the biological production of hydrogen until these gaps will not be filled. Once clarified these aspects, the next step will involve the identification of organisms useful to express catalytically active recombinant hydrogenases. In this respect, during the last few years the interest of the scientific community towards cyanobacteria has significantly increased.

Cyanobacteria

Cyanobacteria are oxygenic photosynthetic gram negative bacteria. For a long time they have been called "blue green algae", since the term alga, in general, indicates any aquatic organism capable of photosynthesis. However, this definition was not correct since algae are eukaryotic organisms, on the contrary cyanobacteria are prokaryotes. Fossil traces of cyanobacteria have been found around 3.5 billions years ago, when they most probably played a key role in the formation of atmospheric oxygen. They are thought to have evolved into present-day from chloroplasts of algae and green plants (Tamagnini P. et al., 2007). Cyanobacterial cells are considered more complex than that of other bacteria, since they have an internal membrane system (as represented in figure 17).

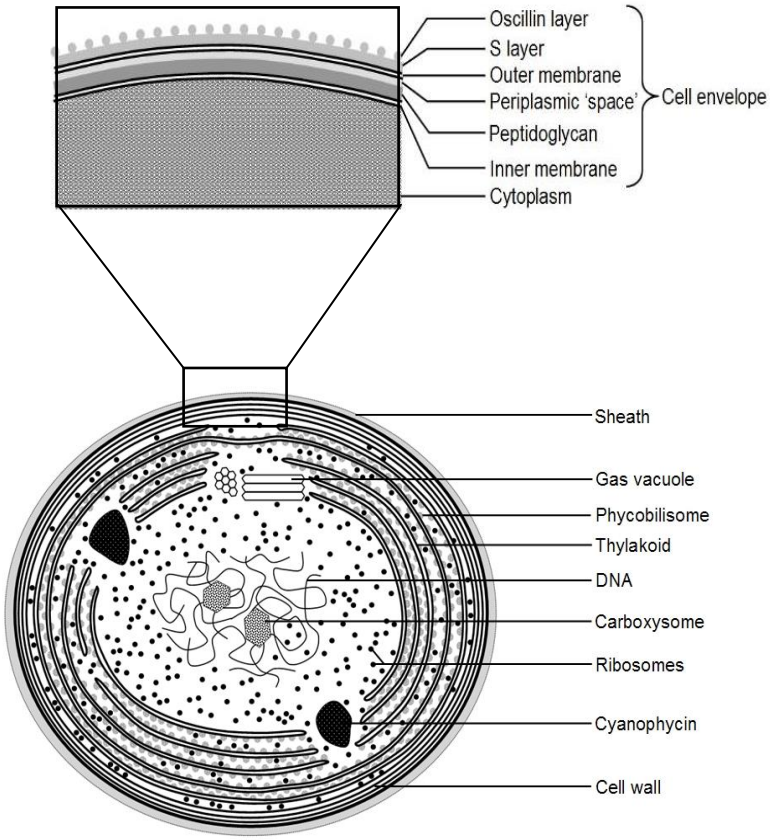

Figure 17. Structure of a cyanobacterial cell

Cells are surrounded by a cytoplasmic membrane and by a multilayered cell wall composed of an inner layer of peptidoglycan and an outer layer of lipo-polysaccharide (Hoiczyk E. and Hansel A., 2000). In addition to these layers, an external mucilaginous mass may also be present, which is a key feature for the colonization and survival of the organism. This layer is often variously pigmented and has different functions, including the protection by high radiation, especially ultraviolet light (UV) (Hoek C. van den et al., 1995). As prokaryotes, they do not have nuclear envelope and a nucleus, instead the DNA is circular and free in the cytosol though intricately folded and attached to special scaffolding proteins. Typical of bacteria, the DNA is often confined to a central region of the cell, the nucleoplasm, forming a nucleoid. The surrounding cytoplasm is rich in prokaryotic ribosomes. The peripheral cytoplasm contains the photosynthetic

apparatus. Flattened membrane vesicles called thylakoids harbour the pigments and proteins that make up the photosynthetic machinery. Each outer cytosolic surface of each thylakoid (the surface facing into the cytosol) is studded with particles called phycobilisomes, which consist of chlorophyll type a and accessory pigments, called phycobiliproteins, such as phycoerythrin (red) and phycocyanin (cyan). The accessory pigments both screen and protect the chlorophyll from damaging UV light and also trap photons and funnel them to the chlorophyll, acting as antennae and increasing the wavelengths of light that can be used for photosynthesis. Gas vacuoles, often present in aquatic forms, regulate buoyancy, helping the cells to float at the right depth where light levels are optimal for photosynthesis. Cyanophycin, typically located near the cell periphery, is a polypeptide (polymer or chain of amino acids) produced by a ribosome-independent mechanism and involved in nitrogen metabolism. Lipid droplets, storing lipids for later use, may also be found in the periphery of the cell. Large polyphosphate bodies are granules that store phosphate whereas tiny glycogen granules or rods are situated between the thylakoids and act as a store of glucose (for carbon and energy). Carboxysomes (polyhedral bodies) contain the main enzyme involved in photosynthesis, Rubisco (ribulose-1,5-bisphosphate carboxylase).

There are several fields in which these microorganisms are applied: they are known to produce compounds with therapeutical, industrial and agricultural significance (*i.e.* antiviral, antibacterial, antifungal, antimalarial, antitumoral and anti-inflammatory), moreover they are used in wastewater treatment and as food supplements. Cyanobacteria are also considered an ideal model system for studying fundamental processes such as photosynthesis.

Photosynthesis

This is the process by which algae, plants and in many species of bacteria convert the electromagnetic energy into chemical energy. Photosynthesis can be divided into two phases: a photochemical light period and a chemical dark phase.

In the first phase, the light energy is transformed into ATP and the $NADP^+$ is reducted to NADPH with the release of oxygen gas. In the dark period, also called phase of carbon fixation, ATP and NADPH provide energy and reducing power for CO_2 reduction. The overall reaction is:

$$CO_2 + H_2O \rightarrow O_2 + (CH_2O)$$

during which water is oxidized to oxygen and carbon dioxide is reduced to carbohydrates. Photosynthesis could be oxygenic or anoxygenic, the last requires reduced forms of sulfur (H_2S), molecular hydrogen or other organic compounds (Pupillo P. et al., 2003) and is typical of green sulfur bacteria, purple bacteria and heliobacteria. In cyanobacteria, thylakoid membranes, similar to the chloroplasts of higher plants, are the site of location of photosynthetic machinery and consist of a membrane system whose architecture allows to significantly increase the surface area exposed to light for the photosynthetic process. Four major protein complexes are integrated in thylakoid membranes: photosystem I and II (PSI and PSII, respectively) with their antenna proteins, the cytochrome b6f complex and the ATP synthase. Photosynthesis is carried out by multiprotein complexes PSII and PSI. Cyanobacterial PSII includes a reaction center, called "Type II" or "quinone", an internal and an external antenna. In the reaction center a pair of molecules of photochemically active chlorophyll a (P680) is present, whereas the antenna, located in the stromal side, is composed of phycobilisomes. These two photosynthetic pigments, together with carotenoids and xanthophylls, ensure the conversion of light energy into chemical energy, during the process. PSI is an integral membrane protein complex that normally functions to transfer electrons from the soluble electron carrier plastocyanin (Pc) to the soluble electron carrier ferredoxin (Fd). PSI lacks an external antenna. The PSI consists of a heterodimer (PsaA / PsaB) to which hundreds chlorophyll molecules are linked, basically acting as the antenna of the photosystem (Xu W. et al., 2001).

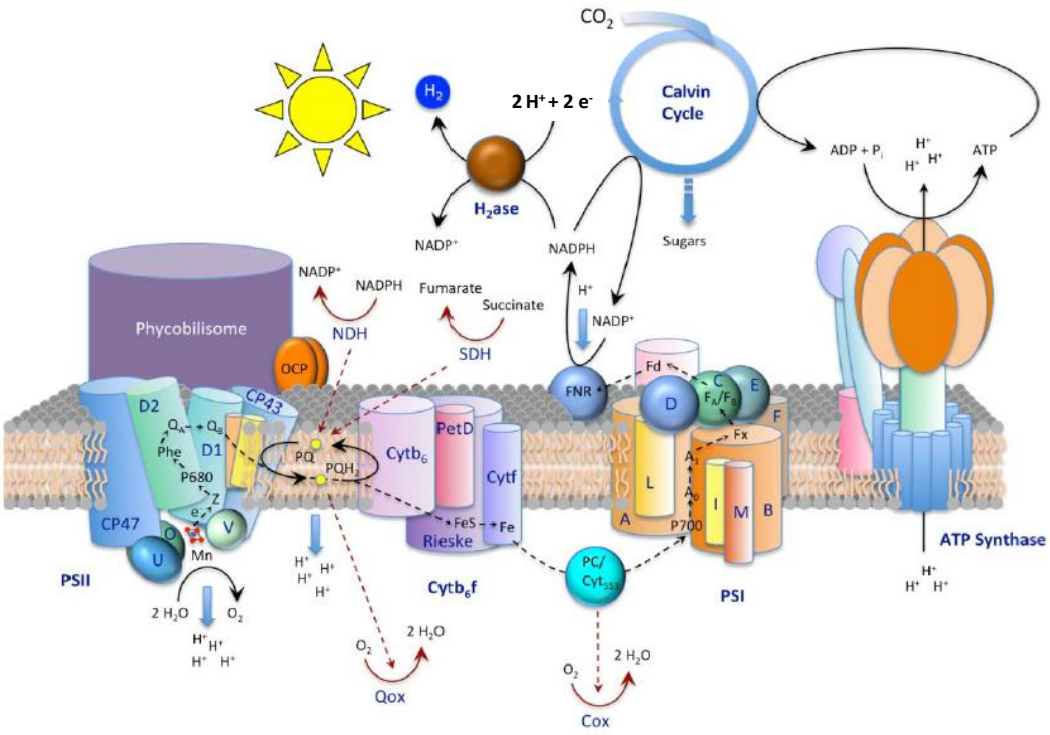

Figure 18. The photosynthetic machinery in cyanobacteria. (Modified from Jansson C. and Northen T., 2010).

The light energy captured by the photosynthetic system allows the oxidation of water at the photosystem II (PSII), with the release of protons and electrons that are then transferred through a complex transport chain to photosystem I (PSI) and here to ferredoxin. The latter, under physiological conditions, yields the electrons to $NADP^+$ reductase (FNR) which reduces it to NADPH, then used for the carbon dioxide fixation in the dark phase of photosynthesis. In anaerobic conditions, however, the ferredoxin gives the electrons to the hydrogenase resulting in the production of hydrogen. Electrons needed for the reduction of protons may also result from the oxidation of endogenous cellular substrates (*e.g.* via glycolysis or Krebs cycle), with their insertion at the level of the plastoquinone (PQ). The existence of this alternative pathway have been proven through the observation that the green alga *C. reinhardtii* can photoproduce hydrogen gas even when the activity of PSII is selectively inhibited with DCMU (3-(3,4-dichlorophenyl)-1,1-dimethylurea). The photosynthetic production of H_2, which uses water as a source of electrons, is only transient (lasting 60 to 90 seconds) because water photooxidation releases protons and electrons but also molecular oxygen, which,

as previously mentioned is a strong inhibitor of the hydrogenases (Ghirardi M.L. et al., 1997). Additionally, in *C. reinhardtii* oxygen also inactivates the transcription of the gene coding for the hydrogenase, exercising in this way a further negative control in hydrogen evolution.

In recent years, cyanobacteria have gained interest of researchers especially for producing third generation biofuels (*i.e.* biomass and hydrogen production), as they convert captured solar energy into biomass at high efficiencies (3%-9%). In cyanobacteria, hydrogen production *in vivo* depends on two enzymes: the nitrogenase and the reversible [NiFe]-hydrogenase, both sensitive to oxygen. The first one reduces protons to H_2 concomitantly with the reduction of N_2 to NH_4^+ and occurs only in N_2-fixing strains. In these organisms, however, H_2 production is limited due to an efficient recycling by an uptake hydrogenase. The second one raises up more interest for the development of solar hydrogen production technologies (see Chapter 1 for details).

Generally, cyanobacteria exhibit a range of advantageous features: first of all they are the most abundant photosynthetic organisms of our planet (Dismukes G.C. et al., 2008). They are found in cold and hot, alkaline and acidic, marine, freshwater, saline environments; indeed, they are able to establish competitive growth in any environment that has, at least temporarily, liquid water and sunlight. Furthermore, the simple nutritional requirements combined with their autotrophy and metabolic plasticity, as well as the availability of molecular tools for their genetic manipulation, make them promising 'low-cost' microbial cell factory (Abed R. et al., 2009; Thajuddin N. and Subramanian G., 2005). This is especially true in the case of the unicellular model strain *Synechocystis* sp. PCC 6803, which has a small genome (3,6 Mb and seven plasmids) that was completely sequenced in 1996 (Kaneko T. et al., 1996).

Synechocystis sp. PCC6803

This cyanobacterial strain was isolated for the first time from fresh water in California and now is considered a good model for scientific studies. It is spontaneously transformable, is able to integrate foreign DNA into its genome by homologous recombination (allowing targeted gene replacement) and can grow

photoautotrophycally and heterotrophically if a suitable fixed-carbon source such as glucose is provided.

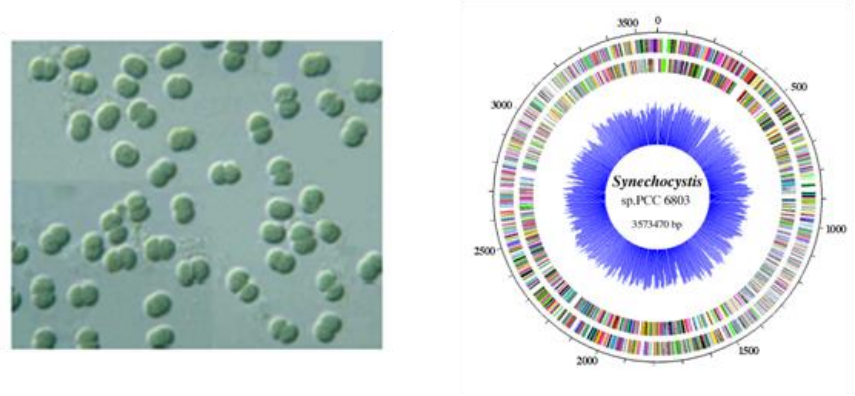

Figure 19. *Synechocystis* sp. PCC 6803: on the left microscopy image of *Synechocystis* sp.6803; on the right Genome Map of *Synechocystis* sp. PCC 6803 (Reference: http:// www.kazusa.or.jp/cyano/Synechocystis/map/click/cmap.html).

Synechocystis possesses only a multisubunits bidirectional [NiFe]-hydrogenase that comprises five protein-subunits, HoxEFUYH, and several [Fe-S] redox clusters (figure 20).

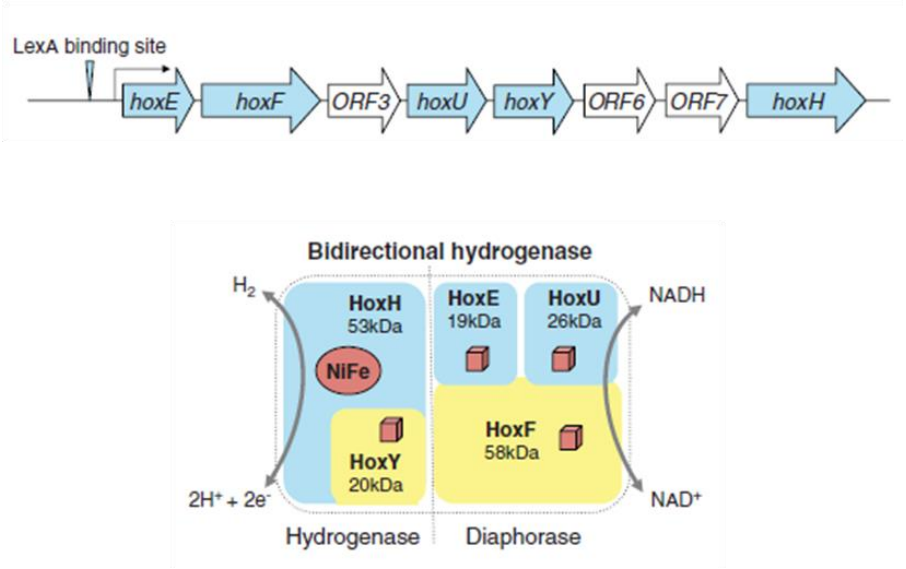

Figure 20. [NiFe]-hydrogenase and its gene structure in *Synechocystis* sp. PCC 6803. (Ghirardi M.L. et al., 2007).

The HoxYH is the hydrogenase sub-complex, in which HoxH, the large subunit, harbors conserved cysteines involved in binding nickel and iron to the active site. The HoxEFU subunits make up the diaphorase sub-complex that transfers the NAD(P)H-transported electrons produced by photosynthesis and/or sugar catabolism to the HoxHY sub-complex (Cournac L. et al., 2004). Recently, based on an *in vitro* analysis, it was also proposed that the Hox enzyme can be reduced by ferredoxin or flavodoxin (Gutekunst K. et al., 2014), similarly to the [FeFe]-hydrogenase of eukaryotic algae (Ghirardi M.L. et al., 2009). The physical organizations of the structural genes encoding the bidirectional hydrogenases are similar in different strains. The *hoxEFUYH* genes are clustered in an octacistronic operon, which comprises the *hoxE*, *hoxF*, *hoxU*, *hoxY*, and *hoxH* genes in that order, and also encodes three ORFs proteins (*sll1222*, *ssl2420*, *sll1225)* with unknown function (Tamagnini P. et al., 2007; Eckert C. et al 2012). The *hoxEFUYH* operon is regulated by various environmental conditions, such as hydrogen, light, nitrate, nickel, oxygen and sulfur availabilities (Oliveira P. et al 2009).

The transcript levels of all *hox* genes are increased (five to six fold) under microaerobic conditions (Kiss E. et al., 2009; Summerfield T.C. et al., 2008). Furthermore, the expression of the *hoxEFUYH* operon is controlled by three transcription factors: two positively acting regulators, LexA (*sll1626*) (Gutekunst K. et al., 2005; Oliveira P. et al., 2005) and AbrB1 (*sll*0359) (Oliveira P. et al., 2008), and one repressor AbrB2 (*sll0822*) (Dutheil J. et al., 2012).

The physiological role of the bidirectional [NiFe]-hydrogenase is unknown, but some hypotheses have been proposed: it has been reported that it could be involved in dark fermentation, act as an electron valve during photosynthesis, or even be part of the respiratory complex I (Antal T.K. and Lindblad P., 2005; Appel and Schulz, 1996; Appel J. et al., 2000; Gutthann F. et al., 2007; Troshina O. et al., 2002). Although the complex hydrogenase enzyme is neither ubiquitous in all cyanobacteria nor essential to the standard photoautotrophic growth of model strains (Carrieri D. et al., 2011), the analysis of gene deletion mutants showed that the presence of the Hox enzyme offers some growth advantages only in certain environmental conditions (Gutekunst K. et al.,

2014). Furthermore, it has been recently shown that the hydrogenase complex can be viewed as an important enzyme in cyanobacteria like *Synechocystis* operating as an electron valve to defende against redox stresses triggered by H_2O_2 or reduced carbon or nitrogen metabolites (Ortega-Ramos M. et al., 2014).

In conclusion, for all the features mentioned before, *Synechocystis* sp. PCC 6803 can be considered an excellent candidate as a device for producing hydrogen gas. An evidence of that occurred in my laboratory when a recombinant [FeFe]-hydrogenase from *C. reinhardtii* was heterologously expressed, in the absence of its specific chaperones set, in *Synechocystis* sp. PCC 6803 (which possesses only a bidirectional [NiFe]-hydrogenase), resulting catalytically active (Berto P. et al, 2011). This suggested that the [NiFe]-hydrogenase HypABCDE-F maturation proteins network is adaptable enough to drive the synthesis of a H-cluster and correctly fold a [FeFe]-hydrogenase. However, in this experiment the levels of hydrogen production were low, maybe due to the poor yields of heterologously produced enzyme, but also for the concomitant presence of the constitutively expressed bidirectional [NiFe]-hydrogenase, that consumes hydrogen (Berto P. et al, 2011). A better candidate to increase hydrogen production by this system might be a *Synechocystis* knock-out mutant strain lacking an active bidirectional hydrogenase (ΔHoxYH). This knock out strain has been characterized at different levels: physiological, proteomic and transcriptional (Pinto F. et al., 2012). The mutant exhibits similar growth behavior compared with the wild-type, reflecting *Synechocystis* plasticity and metabolic adaptability and underlying that it can be used as a photoautotrophic chassis for the integration of recombinant hydrogenases.

AIM OF THE THESIS

The work carried out during the PhD was part of a larger project aimed at developing systems able to produce hydrogen as a renewable source of clean energy from microorganisms through exploiting their hydrogenases, the key enzymes involved in hydrogen metabolism. To achieve this aim, it is necessary to overcome limitations and gaps related to these proteins, currently not yet solved.

At this purpose, in Chapter 1 I have investigated the physiological function of the bidirectional [NiFe]-hydrogenase from *Synechocystis* sp PCC 6803, the most studied cyanobacterial strain, which is currently considered as an unessential protein, at least under physiological conditions. Indeed, intriguingly, even if inactive in the presence of oxygen, this enzyme and the set of proteins involved in its maturation are nonetheless expressed in aerobiosis. I have generated several knock-out mutant strain of *Synechocystis* and compared their behavior to that of the wild type in a particular stress condition (*i.e.* growth under prolonged darkness in aerobiosis), in order to understand if *Synechocystis* could take an evolutionary advantage expressing this protein even in a condition in which its hydrogenase activity is inhibited.

The goal of the work reported in Chapter 2 was to provide new structural details on the maturation of [FeFe]-hydrogenases, as enzymes characterized by a high catalytic activity and therefore most promising for the production of biohydrogen. Our studies were focused on the domain I belonging to HydF protein from *T. neapolitana*, one of the three maturases that ensure the correct assembly of an active [FeFe]-hydrogenase. It is well known that HydF is able to bind and hydrolyze GTP, nevertheless the role of this nucleotide and its contribution in the maturation process have not been elucidated. To investigate these elusive issue, we produced site-specific mutations in the GTPase domain residues located in positions useful for our analysis. These sites were first marked individually and then in couples with a selective spin-probe. By means of advanced spectroscopic techniques, we have analyzed the possible conformational changes due to the binding/dissociation of GTP and the repercussions on the

whole HydF protein, opening new working perspectives on its role in the [FeFe]-hydrogenase maturation process.

CHAPTER 1

[NiFe]-hydrogenase is essential for cyanobacterium *Synechocystis* sp. PCC 6803 survival under long term darkness

The bidirectional [NiFe]-hydrogenase of Synechocystis sp. PCC 6803 is composed by five subunits combined in two functional units: the HoxYH hydrogenase and the HoxEFU diaphorase moieties. The precise physiological function of this enzyme is still under debate. Several experimental evidences suggest that it may play a role only under transient and/or specific growth conditions. Curiously, despite this enzyme is not-oxygen tolerant, the hox genes together with the hyp genes, coding for the maturation proteins involved in the active site assembly, are expressed also in the presence of oxygen, suggesting an additional role of the enzyme, at least in selected conditions. In this work we analyzed the phenotype of different Synechocystis hydrogenase mutant strains, lacking either hyp or hox genes, during prolonged, complete darkness in aerobiosis, a growth condition to which cyanobacteria are frequently exposed in nature. Our results indicate that the [NiFe]-hydrogenase could be involved in the adaptive response of Synechocystis to this environmental stress. Interestingly, a proteomic analysis of the wild type strain revealed a downregulation in the expression of several hydrophilic subunits of the NDH-1 respiratory complex under this stress condition, according to previously proposed hypothesis whereby these proteins may be somehow involved in respiration.

Chapter 1 is adapted from: De Rosa E., Checchetto V., Franchin C., Bergantino E., Berto P., Szabò I., Giacometti G. M., Arrigoni G, and Costantini P. [NiFe]-hydrogenase is essential for cyanobacterium *Synechocystis* sp. PCC 6803 survival under long term darkness. Manuscript submitted to: Scientific Reports.

Supplementary Tables 1-5 are available on the CD attached to the thesis

Introduction

The key enzymes involved in hydrogen metabolism, one of the most ancient and crucial processes of life (Tian F. et al., 2005), are the hydrogenases, which catalyze the reversible reduction of protons to hydrogen gas. According to the metal ion present in their active site, hydrogenases can be divided in two major classes: the [FeFe]-hydrogenases and the [NiFe]-hydrogenases, in general involved in proton reduction and in hydrogen oxidation respectively. Cyanobacteria possess two functionally distinct [NiFe]-hydrogenases: an uptake enzyme, which oxidizes H_2, and a bidirectional hydrogenase, which is able to both oxidize and produce molecular hydrogen from solar energy and water; these microorganisms are receiving considerable attention for photobiological hydrogen production. In particular, *Synechocystis* sp. PCC 6803, the most studied cyanobacterial strain, appears to have promising features in this field since it has a small and fully sequenced genome amenable to genetic manipulations (Kaneko T. et al., 1996; Kaneko T. et al., 2003); moreover, it is characterized by a natural aptitude to be transformed with exogenous DNA, its nutritional requirements are simple and it is able to grow both phototrophically, by oxygenic photosynthesis in sunlight, and heterotrophically, by glycolysis and oxidative phosphorylation in the dark. *Synechocystis* has been reported to possess only a bidirectional [NiFe]-hydrogenase, a heteropentameric enzyme that uses $NAD(P)^+$/NAD(P)H as a substrate and is encoded by the *hoxE-F-U-Y-H* genes belonging to a single operon together with additional ORFs interspersed between some of them (Appel J. et al., 1996; Schmitz O. et al., 2002). HoxH and HoxY form the catalytic subcomplex, in which the larger HoxH subunit harbours the NiFe active site and the HoxY small subunit which carries a [4Fe-4S] cluster mediating the electron transfer to and from HoxH. The HoxF, HoxU and HoxE subunits form the diaphorase moiety, a flavoprotein interacting with the $NAD(P)^+$/(NAD(P)H couple and likely working as a redox partner for the catalytic subcomplex. The assembly of catalytically active [NiFe]-hydrogenases depends on a highly coordinated network of accessory maturation proteins, encoded by the *hypABCDEF* operon (Lutz S. et al., 1991).

It is known that [NiFe]-hydrogenase is inactivated by molecular oxygen (Vignais P.M. et al., 2007) but its precise physiological function in *Synechocystis*, and more in general in cyanobacteria, expecially in oxygen-rich environments, is still under debate (Carrieri D. et al., 2011). It has been proposed that it could be involved in dark fermentation or work as an electron valve during photosynthesis under light (Appel J. et al., 1996; Antal T.K. and Lindblad P., 2005; Appel J. et al., 2000). Moreover, due to the homology of HoxE, F and U with the NuoE, F and G proteins, respectively, found in the respiratory complex I of other bacteria as well in mitochondria of eukaryotic cells, it is tempting to speculate that these Hox proteins could be somehow involved in respiration (Appel J. et al., 1996). However, cyanobacteria lacking the Hox hydrogenase do not display growth defects due to an impaired respiration, at least in physiological conditions (Howitt C.A. and Vermaas W.F.J., 1999). Several Hox mutants have been generated in order to gain new insights into the role of the cyanobacterial [NiFe]-hydrogenase (Appel J. et al., 2000; Boison G. et al., 1998; Antal T.K. et al., 2006; Gutthann F. et al., 2007; Aubert-Jousset E. et al., 2011; Pinto F. et al., 2012; Eckert C. et al., 2012; Gutekunst K. et al., 2013). Although the literature data are somewhat inconsistent, a general emerging consensus is that the Hox hydrogenase may play a role only under transient and/or specific growth conditions.

Interestingly, the *hox* and *hyp* genes are constitutively expressed in *Synechocystis* under both anaerobic and aerobic conditions (Appel J. et al., 2000; Gutekunst K. et al., 2005, McIntosh C.L. et al., 2011), even if the HoxEFUYH hydrogenase is clearly not-oxygen tolerant and is able to produce/consume H_2 only under strict anaerobiosis. This suggests that the Hox hydrogenase could have an additional function besides hydrogen production, at least in selected conditions. In this work we analyzed the phenotype of different *Synechocystis* hydrogenase mutant strains, lacking either *hyp* or *hox* genes, grown on a (stress) condition to which cyanobacteria are often subjected in nature, *i.e.* long term darkness. Our results indicate that the [NiFe]-hydrogenase could play a role in the survival of *Synechocystis* to this environmental stress, which has never been investigated before in hydrogenase mutant strains.

Materials and methods

Bacteria strains

Escherichia coli

XL1-Blue: genotype F', *end*A1, *gyr*A96, (nalR), *thi*-1, *rec*A1, *rel*A1, *lac*, *gln*V44, F'[::Tn10 *pro*AB^{+}, *lac*Iq Δ(*lac*Z)M15], *hsd*R17,(rK^{-} mK^{+})

BL21(DE3): genotype F^{-}, *omp*T, *hsd*S$_{B}$ (r_b^-, m_b^-), *gal*, *dcm*, (DE3)

Synechocystis sp. PCC 6803

WT (wild type)

ΔhoxE-H: strain deleted of the entire operon coding the [NiFe]-hydrogenase *i.e.* genes *hoxE, hoxF, hoxU, hoxY, hoxH* by the insertion of the gene cassette for kanamycin resistance (kindly provided by the group of Jens Appel, from the Botanical Institute of the Christian-Albrechts-University, Kiel, Germany).

ΔHypA: strain deleted of the gene *hypA1* (*srl1675*) coding for the HypA1 protein obtained by the insertion of the gene cassette for kanamycin resistance.

ΔHypB: strain deleted of the gene *hypB1* (*sll1432*) coding for the HypB1 protein obtained by the insertion of the gene cassette for kanamycin resistance.

ΔHoxYH: strain deleted of the genes *hoxYH* (*sll1224-sll1226*) coding for the HoxYH proteins obtained by the insertion of the gene cassette for kanamycin resistance.

ΔHoxEFU: strain deleted of the genes *hoxEFU* (*sll1220-sll1223*) coding for the HoxEFU proteins obtained by the insertion of the gene cassette for kanamycin resistance.

Bacteria colture media

Luria-Bertani (LB)

Liquid

Bacto Triptone (Difco)	1 %
Yeast extract (Difco)	0.5 %
NaCl	0.5 %

Solid: as the liquid with the addition of bacto-agar (Difco) 1,5%

When necessary, were added ampicillin antibiotic at a final concentration of 100 μg/ml or kanamycin antibiotic to a final concentration of 50 μg/ml

SOC

Bacto Tryptone	2 %
Yeast extract	0.5 %
NaCl	10 mM
KCl	2.5 mM
$MgCl_2$	10 mM
$MgSO_4$	10 mM
Glucose	20 mM

***Synechocystis* sp. PCC 6803 colture medium**

BG11

Liquid

$NaNO_3$	17.65 mM
$MgSO_4 7H_2O$	0.30 mM
$CaCl_2 2H_2O$	0.25 mM
Na_2CO_3	0.19 mM
Na-EDTA	0.003 mM
Acid citric	0.029 mM
Ammonium citrate ferric	0.030 mM
H_3BO_3	46 μM
$Co(NO_3)_2 6H_2O$	0.17 μM
$CuSO_4 5H_2O$	0.32 μM
$MnCl_2 4H_2O$	9.2 μM
$Na_2MoO_4 2H_2O$	1.6 μM
$ZnSO_4 7H_2O$	0.77 μM
$K_2HPO_4 3H_2O$	0.17 μM
HEPES-NaOH pH 8.2	10 mM

Solid: as the liquid with the addition of

bacto-agar (Difco)	1.5%
$Na_2S_2O_3 5H_2O$	0.3%

When necessary, was added kanamycin at different final concentrations: 5 μg/ml, 10 μg/ml, 20 μg/ml and 50 μg/ml.

Plasmids

pBluescript® II SK+/- (Phagemid Vectors, Agilent Technologies)

The pBluescript II phagemid (plasmid with a phage origin) is cloning vector designed to simplify commonly used cloning and sequencing procedures, including the construction of nested deletions for DNA sequencing, generation of RNA transcripts *in vitro* and site-specific mutagenesis and gene mapping. It present an extensive polylinker with 21 unique restriction enzyme recognition sites which interrupts the lacZ gene. This portion gene allows the synthesis of the fragment functional enzyme α-galactosidase and together with the possibility of α-complementation in the presence of the terminal fragment of the enzyme, allows to detect the transformants positive. The vector also contains the gene Amp^r for resistance to the ampicillin antibiotic, and the origin of replication for *E. coli*.

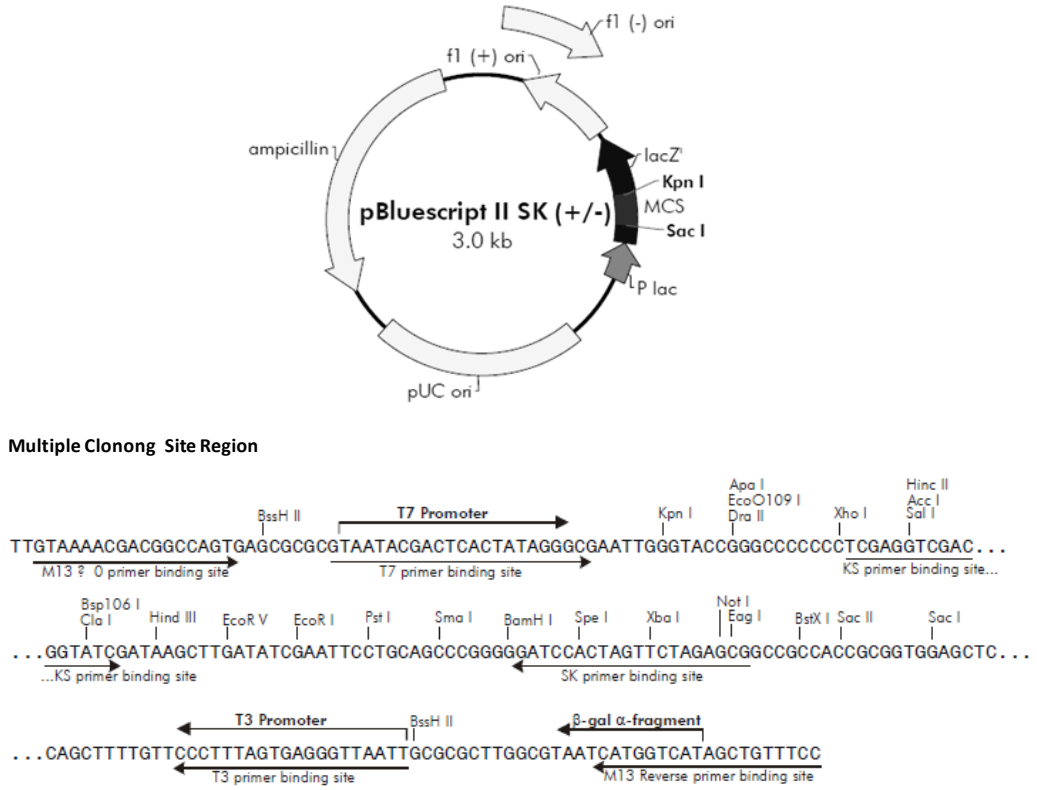

Figure 21. Circular Map of the plasmid pBluescript II phagemid (+/-).

Strains and standard growth conditions

The wild type *Synechocystis* sp. glucose-tolerant strain PCC 6803 as well as the *hox*/*hyp* deletion mutant strains (see below) were grown at 30 °C under continuous white light (50 μE m^{-2} s^{-1}), unless stated otherwise, in standard BG11 medium buffered at pH 8.0 with HEPES (*N*-2-hydroxyethylpiperazine-*N'*-2-ethanesulfonic acid) and supplemented with 5 mM glucose (sterilized by filtration using 0.2 μm filters from *Millex*®) for photoheterotrophic growth. When grown in the dark, cultures were kept in flasks wrapped with aluminium foil. Transformed *Synechocystis* strains (see below) were grown with 5 to 50 μg/ml kanamycin. For cultures grown on plates, BG11 medium was supplemented with 1.5% agar and 0.3% sodium thiosulfate. For liquid cultures, thiosulfate was omitted and the cultures were kept under continuous shaking. Cell growth was monitored as optical density at 730 nm (OD_{730}). When analyzed for the hydrogen evolution, liquid cultures were grown in sealed flasks in the presence of 5 μM (3-(3,4-dichlorophenyl)-1,1-dimethylurea) (DCMU), as previously described (Berto P. et al.,2011). *E. coli* XL1-Blue strain was used for DNA manipulation. The *E. coli* liquid medium was LB and solid medium was obtained by adding 1.5% agar.

Determination of chlorophyll content

One ml of liquid culture of *Synechocystis* was centrifuged for 10 minutes at 13000 x *g* and 100 μl of 100% methanol were added to the cell pellet obtained. Cells were broken mechanically with a pestle (Silicone Tubing, Pharmacia), then 900 μl of 100% methanol were further added and the suspension was centrifuged for 5 minutes at 13000 x *g*, in order to remove the insoluble fraction, thus obtaining chlorophyll a in the supernatant. Chlorophyll a concentration was obtained from the absorbance of the supernatant, using the coefficient of Mac Kinney (1941) as follows:

$$\text{Chl } (\mu g/ml) = (A_{666nm} - A_{730nm}) \times 12.6$$

Plasmids construction and generation of *Synechocystis* ΔHypA, ΔHypB, ΔHoxYH and ΔHoxEFU deletion mutants.

The *hypA1* (*srl1675*), *hypB1* (*sll1432*), *hoxYH* (*sll1224-sll1226*) and *hoxEFU* (*sll1220-sll1223*) knock-out strains were obtained, starting from *Synechocystis* PCC 6803 wild type strain, by homologous double recombination transferring into the respective genes a kanamycin-resistance cassette (*kan*^{r}), derived by BamHI digestion from plasmid pUC4K (Pharmacia). The plasmids used to generate these deletion mutants were based on the pBSKII vector (Agilent Technologies) and contained the *Synechocystis* chromosome regions flanking the genes to be deleted. The regions upstream and downstream these genes were amplified by a three-steps PCR strategy, using primers designed on the basis of the *Synechocystis* genome sequence accessible through CyanoBase and containing sequences with restriction sites for cloning purposes (listed in Table 1 and 2), and the high-fidelity Fusion DNA polymerase (Finnzymes). In the first step, a PCR-up and a PCR-down were separately performed using as template the *Synechocystis* genomic DNA, purified following standard protocols (Xu W. and McFadden B.A., 1997), and the following primers couples:

i) SacI*hypA1*_for/BamHI*hypA1*_rev
BamHI*hypA1*_for/EcoRV*hypA1*_rev (for *hypA1*$^-$)

ii) SacI*hypB1*_for/BamHI*hypB1*_rev
BamHI*hypB1*_for/EcoRV*hypB1*_rev (for *hypB1*$^-$)

iii) SpeI*hoxYH*_for/BamHI*hoxYH*_rev
BamHI*hoxYH*_for/HIndIII*hoxYH*_rev (for *hoxYH*$^-$)

iv) SacI*hoxEFU*_for/BamHI*hoxEFU*_rev
BamHI*hoxEFU*_for/HIndIII*hoxEFU*_rev (for *hoxEFU*$^-$)

In a second step, the products of these PCR-up and PCR-down were amplified using the primers couples:

i) SacI*hypA1*_for/EcoRV*hypA1*_rev (for *hypA1*$^-$)

ii) SacI*hypB1*_for/EcoRV*hypB1*_rev (for *hypB1*$^-$)

iii) SpeI*hoxYH*_for/HIndIII*hoxYH*_rev (for *hoxYH*$^-$)

iv) SacI*hoxEFU*_for/HIndIII*hoxEFU*_rev (for *hoxEFU*$^-$)

thus obtaining an overlapping band. In the last step, the overlapping bands were digested by the restriction enzymes and individually cloned in a pBSKII vector, which was finally digested with BamHI to introduce the *kan*^{r} cassette. The sequences of the primers listed above are reported in Table 1 and 2. The sequences of the resulting recombinant plasmids pBSKII_*hypA1*KO_ *kan*^{r} , pBSKII_*hypB1*KO_ *kan*^{r}, pBSKII_*hypYH*KO_ *kan*^{r}, pBSKII_*hypEFU*KO_ *kan*^{r} were confirmed by DNA sequencing (BMR Genomics, University of Padova). These plasmids were used to transform wild type *Synechocystis* sp. PCC 6803 (Kufryk G. et al., 2002). The complete segregation of recombinant chromosomes in mutant strains was confirmed by PCR using, as template, the genomic DNA of the respective knock out mutant strains and the following primers couples:

FL*hypA1*_for/FL*hypA1*_rev for the *hypA1*$^{-}$

FL*hypB1*_for/FL*hypB1*_rev for the *hypB1*$^{-}$

FL*hoxYH*_for/FLhox*YH*_rev for the hoxYH^{-}

FL*hoxEFU*_for/FL*hoxEFU*_rev for the hoxEFU^{-}

Primer name	Primer sequence
SacI*hypA1*_for	5’-TACGTTCAAGAGCTCAGCCCCGAAACC-3’
BamHI*hypA1*_rev	5’-CATATGCACGAAGGGATCCGGTGTGT-3’
BamHI*hypA1*_for	5’-GGATCCGGTGTGTTAGAACTGAGTTGA-3’
EcoRV*hypA1*_rev	5’-ACTGGGGTGGATATCGTCCAAAGAATTATC-3’
SacI*hypB1*_for	5’-ATGAGTCTGGGGAGCTCCGCTTCCG-3’
BamHI*hypB1*_rev	5’-TGTAGTGCGGTGGGAtCCGTTGCCC-3’
BamHI*hypB1*_for	5’-GGATCCGTTGCCCGCATTGGCCTAA-3’
EcoRV*hypB1*_rev	5’-CCGGGCCATAACGGTGGCGATATC-3’
FL*hypA1*_for	5’-GGGCTCAGCGCTCCCGTGCTGG-3’
FL*hypA1*_rev	5’- ATGCCCGCTGGCCCCGGTGGA-3’
FL*hypB1*_for	5’- CCAGCAACCGGGCGGAGCCGT-3’
FL*hypB1*_rev	5’- TGGATGGGGTCCAGGCTTTGGCCCA-3’

Table 1. List of primers used to generate ΔHypA and ΔHypB knock out mutant strains.

Primer name	Primer sequence
SpeI*hoxYH*_for	5’-CAGTTCAGCCAGCAACTAGTCCTTT-3’
BamHI*hoxYH*_rev	5’-TTAATCCCGCTGGAGGATCCGGTGTGT-3’
BamHI*hoxYH*_for	5’-GGATCCGGTGTGTTAGCCATGATTAAAAGTTTA-3’
HIndIII*hoxYH*_rev	5’-CACGAATAAGCTTATGCCCGCCTGC-3’
SacI*hoxEFU*_for	5’-GGTGTGTGAGCTCTCCTGAATAGCTATTTTGC-3’
BamHI*hoxEFU*_rev	5’-TCTTAAAAGTTCAACGGATCCGGTGTGT-3’
BamHI*hoxEFU*_for	5’-GGATCCGGTGTGTGGAAAAATCCTCAAA-3’
HIndIII*hoxEFU*_rev	5’-GTCATGCTCGAAGAAAGCTTGGTGTGT-3’
FL*hoxYH*_for	5’-TCCGCCCTTGGTGCAGGCCG-3’
FL*hoxYH*_rev	5’-CCATGCACAAACGACAGGCTGCCGC-3’
FL*hoxEFU*_for	5’-CGGCGATCGCCAAAGCATCCTGG-3’
FL*hoxEFU*_rev	5’-AGCCCAAGTCACCAGCCCAGCA-3’

Table 2 List of primers used to generate ΔHoxYH and ΔHoxEFU knock out mutant strains.

Transformation of *Synechocystis* sp. PCC 6803

Exogenous DNA is absorbed by the cells without any preparatory treatment since *Synechocystis* sp. PCC 6803 is a naturally competent strain. A saturated precolture of *Synechocystis* was inoculated in BG11 liquid with 5 mM glucose and grown until reaching the mid-exponential phase (OD_{730} = 0.5), and then centrifuged at room temperature at 3000 × *g* for 5 min. The cell pellet was suspended in fresh BG11 medium without glucose at a density of 1×10^{10} cells/ml and then mixed with exogenous DNA to a final concentration of 0.5 μg/ml. The mixture of cells and DNA was incubated for 5 hat 30 °C, and afterward spread onto a membrane filter resting on BG11 agar plates without antibiotic in order to allow the expression of the antibiotic resistance (kanamycin). After 24 h, the membrane filter was moved on BG11 agar plates containing 10 μg/ml kanamycin. Several single recombinant colonies, which tipically appear approximately after 10-15 days of growth, were subcloned on agar plates containing increasing antibiotic concentrations up to 50 μg/ml.

Purification of genomic DNA from cyanobacteria.

Cyanobacteria were inoculated in 500 ml of BG11 liquid medium with glucose 5 mM and incubated about 48h at 30 °C under agitation until reaching OD_{730} of 1-1.6. Then the culture was centrifuged at 6000 x *g* for 10 min at 25 °C and the resulting pellet was resuspended in 2.5 ml of saturated NaI and incubated at 37 °C for 30 min under mixing. The suspension was centrifuged again at 6000 x *g* for 10 min at 25 ° C, the resulting pellet was washed two times with deionized water and then frozen at -80 °C from 2h to overnight. Then, lysis buffer (2.5 ml; 50 mM glucose, 50 mM Tris-HCl pH 8, 10 mM EDTA) and lysozyme (15 mg/ml) were added, and the suspension incubated at 37 °C for 1h, under mixing. Then, 5 ml of a solution of 0.2% NaOH and 1% SDS were added and incubated 10 min on ice. Subsequently, 3.75 ml of NaAcetate 3M were added, incubated 30 min on ice and then centrifuged at 12000 x *g*, 10 min, at 4 °C. An equal volume of phenol: chloroform was added to the supernatant, then vortexed for 60 sec; the emulsion was centrifuged at 14,000 x *g* for 2 min, at 4 °C. Once recovered the upper phase, the extraction in phenol: chloroform was repeated once again. At this point, an equal volume of chloroform 100% was added to the upper phase and vortexed for

60 sec, the obtained emulsion was centrifuged at 14,000 x *g* for 2 min at 4 °C, and the upper phase recovered. Afterward, 1/10 volume of NaAcetate 3 M and 2.5 volumes of 100% cold ethanol were added. Once vortexed the mixture was incubated at at -20 °C, overnight, centrifuged at 16,000 x *g* for 30 min at 4 ° C, the supernatant removed and the pellet washed twice with 1 ml of ethanol 70%, each time centrifuging at maximum speed for 10 min, at 4 °C. The pellet was left to dry and then suspended in 70 µl of sterile water. RNase was added to the final concentration of 1.5 ng/µl and incubated for 30 min at 37 °C. The obtained DNA was stored at -20 °C.

Hydrogen evolution assay

Hydrogenase activity of whole cell extracts was measured *in vitro*, as previously described (Berto P. et al., 2011), as the evolution of hydrogen gas from reduced methyl viologen in nitrogen-flushed 13.5 ml sealed vials, using a Clarus 500 gas chromatographer equipped with an Elite-Molesieve column (0.53 mm i.d., length 30 m) (Perkin Elmer). All steps were performed under anaerobic conditions in a glove-box (MBRAUN MB 200B), using oxygen-free solutions.

Oxygen evolution measurements

Experiments were performed using a Clark electrode (CBID; Hansatech) as described (Cruz J.A. et al., 2005). The strains were cultured at 0 µE m^{-2} s^{-1} and at 50 µE m^{-2} s^{-1} for 5 days. The cells were collected (5000 rpm for 10 min, *Allegra*® 25R Centrifuge, Bekman Coulter) and transferred for 5 minutes to the measuring chamber in the dark; then a light with an intensity of 2000 µmol of photons m^{-2} s^{-1} was applied. All measurements were performed at 30 °C in the absence of 5 mM bicarbonate. The chlorophyll concentration in the experiments was 10 µg ml^{-1}.

The Fluorescence Induction Program (FIP) allowed the determination of the rate of oxygen evolution, expressed in V/s, by a linear fitting of the curves obtained under various conditions and the expression of it as µmol O_2/(mg Chl × h) by taking into account the chlorophyll concentration, the volume of the experimental mixture, the oxygen content of air-saturated water at 30 °C, and calibration of the oxygen electrode.

Growth experiments

Cultures of wild type and ΔHoxE-H *Synechocystis* mutant strains were grown up to the exponential phase (OD_{730} 2.5) and, before the beginning of the experiments, they were the transferred to fresh BG11 medium plus 5 mM glucose, and diluted to get a starting (*i.e.* day 0) optical density of about 0.2. Each experiment was performed in triplicate *i)* under continous white light (50 μE m^{-2} s^{-1}), *ii)* with 12 h light/12 h dark cycles or *iii)* complete darkness. To assess the capability to form colonies on plates, *Synechocystis* liquid cell cultures previously incubated five days in the dark were diluted to an OD_{730} = 0.3-0.4 (corresponding to $1x10^6$-$1.5x10^6$ cells/ml) and quantified using the cell counter Cellometer Auto X4 with a Cellometer SD100 counting chamber (from Nexcelom Bioscience LLC.). Fifty microliters of three serial dilutions (*i.e.* 1:2500, 1:5000, and 1:10000) were then plated on BG11 agar plates in the presence of 5 mM glucose and incubated at 30 °C in a 20 μE m^{-2} s^{-1} light regimen. Colonies, which usually appear after about ten days, were finally counted.

Electron microscopy

Pellets of cyanobacteria were fixed overnight at 4 °C in 3% glutaraldehyde in 0.1 M sodium cacodylate buffer (pH 6.9) and then processed for electron microscopy (Checchetto V. et al., 2012), at the electron microscopy facility of the Department of Biology, University of Padova. Ultrathin sections, cut with an ultramicrotome (LKB Ultratome V), were poststained with 1% osmium tetroxide/1% potassium ferrycyanide, embedded in a EPON 812 resin and examined under a transmission electron microscope (FEI Tecnai™ F12) operating at 100 kV.

Bacteria transformation (*E. coli*)

The bacterial transformation is a process that allows to introduce plasmid DNA in competent bacteria. Chemical transformation allows to introduce plasmid DNA in bacterial cells previously made chemocompetent by a pre-treatment with $CaCl_2$ at 4 °C, which modify the walls and the membranes-associated with a rapid

change in temperature (thermal shock). The plasmid (2-5 μl) is added to the solution containing an aliquot of competent bacteria and the suspension is placed for 30 minutes on ice, then for 30 seconds at 42 °C, and transferred again into ice, thus causing a thermal shock which makes the bacterial cells permeable to DNA. Then, 500 μl of SOC are quickly added to bacteria, and culture incubated for one hour at 37 °C under shaking. Finally, bacteria are plated on selective solid medium (LB + antibiotic) and grown overnight at 37 °C.

DNA electrophoretic running on agarose gel

The analysis of the double-stranded DNA was performed by electrophoresis on agarose gel 1% p/v (SIGMA). Agarose was dissolved in TBE buffer 0.5% (90 mM Tris, 90 mM boric acid, 2 mM EDTA, pH 8) supplemented with ethidium bromide to a final concentration of 0.5 mg/ml. This substance, which intercalates between planar rings of the double helix of DNA, if exposed to ultraviolet light has fluorescent properties and thus allows to reveal the DNA fragments migrated in the gel. Sample was prepared by adding 10 X Loading Buffer (0,25% blue bromophenol, 0,25% xylene cyanol, 30% glycerol) reaching the final concentration of 1 X; this promotes the DNA deposition in the wells and allows to display the migration front from the negative to the positive pole. The gel, in TBE buffer 0.5%, is subjected to an electric field of 50-100 V, depending on the size, until the front dye reaches approximately 3/4 of the gel length. The DNA can be observed with a UV transilluminator. The size of the DNA fragments is estimated by comparison with a marker of molecular weights, in this case 100bp ladder (Promega) or 1kb ladder (Promega). The concentrations of the samples are estimated by comparing the intensity of the bands obtained with that of a sample with a known concentration.

DNA extraction from agarose gel

The DNA fragments after electrophoresis on a 0.7% agarose gel, can be extracted by cutting the bands of interest from the gel and purified with the DNA through GelElute™ Gel Extraction Kit (SIGMA) following the protocol.

Purification of plasmid DNA from bacteria

Plasmid DNA is purified from a culture of transformed bacteria grown over-night using the GEN Elute® Plasmid Miniprep Kit (SIGMA), following the protocol of the supplier company.

***iTRAQ* (isobaric Tags for Relative and Absolute Quantitation)**

This technique enables the simultaneous identification and quantification of proteins in different samples. Thanks to its many advantages, it is widely used in proteomics research. After the proteolytic digestion, usually carried out with trypsin, which cuts residues of lysine and arginine of the proteome previously purified, isobaric reagents are used to mark the primary amino group of peptides of different samples which are then analyzed by tandem mass spectrometry or MS/MS (figure 22, panel B). Using four or eight isobaric tags, iTRAQ can analyze up to eight biological samples. The reagents used are called 114, 115, 116, 117 (if four samples are analyzed) to which reagents 113, 118, 119, 121 ca be then added (if eight samples are analyzed). Each reagent is composed of a peptide reactive group and an isobaric tag that consists of a reporter group and a balance group (see figure 22, panel A). The peptide reactive group reacts specifically with the primary amino group of the peptides, allowing their derivatization to the N-terminal. The reporter group is the charge portion of the molecule that gives a strong ion signal in the MS/MS and is used to determine the relative abundance of a peptide; it may have different mass values. The balance group, instead, equilibrates mass differences of the various regions reporter, ensuring that the combination between the masses of the reporter group and the balance group remains constant at 145 Da.

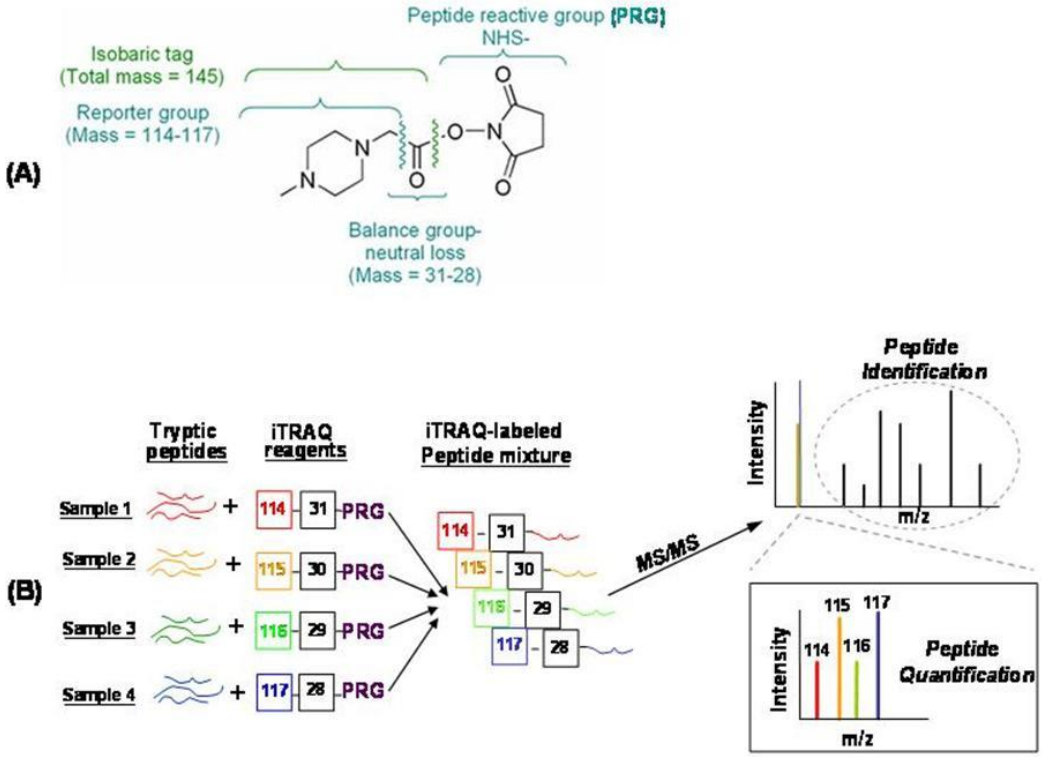

Figure 22. ***Panel A*** **structure of iTRAQ reagent,** ***panel B*** **schematic representation of the iTRAQ technique.**

In this way, peptides from the same protein, expressed differentially in various samples and linked to iTRAQ reagents with different reporter groups, have equal values in mass spectra MS, thanks to the balance due to the presence of the different balance groups. Following the fragmentation of the peptide of interest, bonds that hold together the three portions of the reagent are broken and the different reporter groups, released in ionic form, are recognized in the tandem mass spectrometry at m/z values between 114 and 117 (if four isobaric reagents were used). The steps performed in our analysis are described in the following.

Sample collection and protein extraction. Three biological replicates of *Synechocystis* sp. PCC 6803 (wild type and *hox* knock-out mutant strains) were grown for 5 days in continuous light and in the dark as described above. Cells were collected by 10 min centrifugation at 4 °C (Allegra® 25R Centrifuge, Beckman Coulter) at 5000 × *g*, frozen in liquid nitrogen, and stored at -20 °C until further use. Harvested cells were washed twice with 50 mM HEPES-KOH, pH 7.5, suspended in the same buffer with the addition of PMSF 1 mM, and split into

2 ml screw cap microtubes. After centrifugation the pellet was suspended in 150 µl of extraction buffer (50 mM HEPES-KOH, pH 7.5, 0.1% SDS, 0.1% Triton X-100, PMSF 1 mM) and an equal volume of glass beads (diameter 150-212 µm) was added. Cells were disrupted in a Mini Bead Beater (Biospec Products) by homogenizing three times at 3500 RPM for 15 sec, each time followed by incubation on ice for 1 min. Unbroken cells and glass beads were removed by centrifugation for 5 min at 1000 × *g* (Mikro 22R, Hettich) and the resulting supernatant was incubated for 30 min in 2% SDS (final concentration) to facilitate extraction of membrane proteins. Samples were centrifuged for 20 min at 12 000 × *g* at 4 °C, and the supernatant was transferred into a new tube and stored at -20 °C until further use. Protein concentration was determined by Bradford method (Bradford Reagent, Sigma-Aldrich). The proteins were precipitated in ice-cold acetone (1:4, v/v) at -20 °C overnight and stored at -80 °C until use.

Protein digestion and iTRAQ labeling. One hundred µg of protein pellets from each of the 6 preparations of *Synechocystis* sp. PCC 6803 (3 wild type and 3 *hox* knock-out mutant strains) were suspended in 40 µl Laemmli buffer and loaded into a NuPage 12% precast SDS-PAGE (Invitrogen). The electrophoretic process was carried out for few minutes, just enough to allow all proteins to enter the separating gel and focus in single narrow bands. Proteins were then stained using the SimplyBlue Safestain (Invitrogen), and each band was manually excised from the gel. After destaining, proteins were reduced for 1 h at 55 °C using 10 mM dithiotreitol (DTT) in 25 mM triethylammonium bicarbonate (TEAB). Cysteines were alkylated using 55 mM iodoacetamide in 25 mM TEAB for 45 min, in the dark and at room temperature. Gel slices were then thoroughly washed with 3 exchanges of 50 mM TEAB and acetonitrile (ACN) and dried under vacuum. Samples were incubated (37 °C, overnight) with 130 µl of sequencing grade modified trypsin (Promega, 12.5 ng/µl in 50 mM TEAB). Peptides were extracted from the gel slices by two consecutive treatments with 100 µl of 50% ACN (30 min, under constant agitation) and finally dried under vacuum. Each digested sample was dissolved in iTRAQ dissolution buffer and labeled with iTRAQ tags according to the manufacturer's instructions (AB Sciex). To reduce any potential variation introduced by the labeling reaction, samples from the 3

replicates were labeled with a tag-swapping strategy (mass tags 114, 115, and 117 for wild type samples; tags 116, 117, and 114 for mutant samples). To verify the labeling efficiency, 1 µg of each labeled sample was individually analyzed by liquid chromatography–tandem mass spectrometry (LC-MS/MS) as specified below. Acquired data were searched with Mascot search engine, setting iTRAQ labeling as variable modification. No unmodified peptides were identified from the search and all the peptides were correctly modified at the N-terminus and at each lysine residue. Finally, the iTRAQ labeled samples were combined in a 1:1 ratio (wild type: mutant) and the pools were vacuum dried in a SpeedVac system.

Strong Cation Exchange Fractionation. Strong cation exchange (SCX) was performed using a SCX cartridge (AB Sciex) following the manufacturer's protocol. Each iTRAQ labeled sample was suspended in 500 µl of equilibration buffer (5 mM KH_2PO_4, 25% ACN, pH 2.9) and loaded onto a SCX cartridge with a syringe-pump system at a flow rate of 50 µl/min. Peptides were eluted in a step-wise mode using 500 µl of the following concentrations of KCl in equilibration buffer: 30, 50, 80, 110, 140, 170, 200, 350 mM. Each SCX fraction was dried under vacuum, suspended in 500 µl of 0.1% formic acid (FA) and desalted using C18 cartridges (Sep-Pack, C18, Waters). Samples were finally dried under vacuum and stored at -20 °C until MS analyses were performed.

LC-MS/MS analyses. Samples were dissolved in 40 µl of 0.1% FA, and analyzed with a LTQ-Orbitrap XL mass spectrometer (ThermoFisher Scientific) coupled online with a nano-HPLC Ultimate 3000 (Dionex - Thermo Fisher Scientific). Analyses were carried out as previously described (Menegazzo L. et al., 2013). About 1 µg of peptides from each fraction was loaded onto a 10 cm chromatographic column packed in-house into a pico-frit (75 µm I.D., 15 µm tip, New Objective) with C18 material (Aeris Peptide 3.6 µm XB-C18, Phenomenex). Peptides were eluted using a 3%-50% linear gradient of ACN/0.1% FA in 90 min at a flow rate of 250 nL/min. The instrument performed a full scan at high resolution (60000) on the Orbitrap, followed by MS/MS scans on the three most intense ions both with CID and HCD fragmentation. After a first set of analysis, data were searched with Proteome Discoverer software (Thermo Fisher Scientific) as detailed below and all peptides identified with high (99%) or medium (95%)

confidence were used to create a static exclusion list that was then included in the instrument method. All samples were re-analyzed under identical instrumental and chromatographic conditions except for the application of the exclusion list. All data obtained were merged into a MudPIT protocol and analyzed as described below.

***Data analysis*.** Raw MS/MS files were analyzed using Proteome Discoverer 1.4 (Thermo Fisher Scientific) connected to a Mascot Search Engine server version 2.2.4 (Matrix Science), using a MudPIT protocol. Data were filtered to exclude MS/MS spectra containing less than 5 peaks and with a total ion count lower than 50. Spectra were searched against the Uniprot *Synechocystis* database (version March 2014, 3622 sequences), concatenated with a database of the most common contaminants found in proteomics experiments. Peptide and fragment tolerances were set to 10 ppm and 0.6 Da respectively. Enzyme specificity was set to Trypsin with up to 2 missed cleavages, carbamidomethylcysteine, 4-plex iTRAQ at N-terminus and Lys were set as fixed modifications, while oxidation of methionine was set as variable modification. Percolator and a search against the corresponding randomized database were used to calculate False Discovery Rates (FDR). Proteins were grouped into protein families according to the principle of maximum parsimony. Data were filtered considering as positive hits peptides identified with medium (95%) or high (99%) confidence, based on the q-value calculated by the Percolator algorithm. The final list of proteins was obtained by further filtering the data in order to consider as positive hits only proteins identified with at least two unique peptides and quantified with at least 2 independent peptides. A fold change of 1.5 combined with the results of a two-tailed Z Test were used to highlight proteins that showed in all replicates a significant change in their expression level between light and dark conditions.

Results

As mentioned in the Introduction, all *Synechocystis* deletion mutant strains characterized to date and lacking one or more *hox* genes of the *hoxE-H* operon display, under standard growth conditions, a behavior almost identical to that of the wild type strain. This makes the role of the cyanobacterial bidirectional [NiFe]-hydrogenase elusive. On the other hand, the puzzling constitutive expression of this enzyme, both in aerobic and anaerobic conditions, indicates an evolutionary advantage of retaining it, and suggests an additional role besides its primary function in hydrogen metabolism, at least under non-standard conditions. The majority of cyanobacteria are aerobic photoautotrophs, and sunlight driven oxygenic photosynthesis is their principal mode of energy metabolism. However, it is well known that in natural environment some cyanobacterial communities can experience and survive to regular prolonged periods of complete darkness, for example in lake sediments, in soil water as well as in dense aquatic accumulations produced in surface, conditions in which a metabolic shift to anaerobic fermentation is expected to take place (Stal L.J. and Moezelaar R., 1997). Interestingly, the *hox* genes are almost absent in cyanobacterial strains isolated from open oceans (Vignais P.M. and Billoud B., 2007; Barz M. et al., 2010), where both anaerobiosis and darkness are unlikely to be prevalent, suggesting that under these specific conditions the [NiFe]-hydrogenase function is especially important. To explore the potential contribution of the Hox bidirectional hydrogenase activity as a cellular strategy to overcome a darkness period, we analyzed the growth behavior under normal light and prolonged darkness of a *Synechocystis* mutant strain in which the whole *hox* operon has been deleted.

Physiological characterization of wild type and ΔHoxE-H Synechocystis strains under normal light and long term darkness.

To evaluate the possible effects of the whole *hox* operon deletion on the fitness of *Synechocystis* during prolonged dark periods (up to five days), the growth of both wild type and ΔHoxE-H deletion mutant strains were compared in the presence of glucose as carbon source and under two different light conditions, *i.e.* i) continuous white light (50 μE m^{-2} s^{-1}) and ii) complete darkness. Moreover,

since *Synechocystis* is known to possess a circadian clock system (Wiegard A. et al., 2013; Dörrich A.K. et al., 2014), as an additional control both strains were also grown in 12 h light/12 h dark cycles. Figure 23 shows that no significant differences in terms of growth for *Synechocystis* wild type and ΔHoxE-H mutant strains were found, both under continuous irradiance (panel A) and when cultured with a circadian rhythm of light/dark cycles (panel B). This result is in agreement with data previously obtained using different *hox* deletion mutants (Appel J. et al., 2000; Boison G. et al., 1998; Antal T.K. et al., 2006; Gutthann F. et al., 2007; Aubert-Jousset E. et al., 2011; Pinto F. et al., 2012; Eckert C. et al., 2012; Gutekunst K. et al., 2013). On the other hand, when cultures were maintained under complete darkness from the time of inoculation, the two strains displayed different behaviors. In the case of the wild type, as expected, glucose was still able to support the heterotrophic growth, even though at a rate which was reduced by 60-70% with respect to its growth under photoheterotrophic conditions (see figure legend for details). On the contrary, interestingly, the ΔHoxE-H mutant strain, displayed a severe defect in its growth when compared to the wild type strain cultured in the same conditions (figure 23, panel C) (see Materials and methods for experimental details).

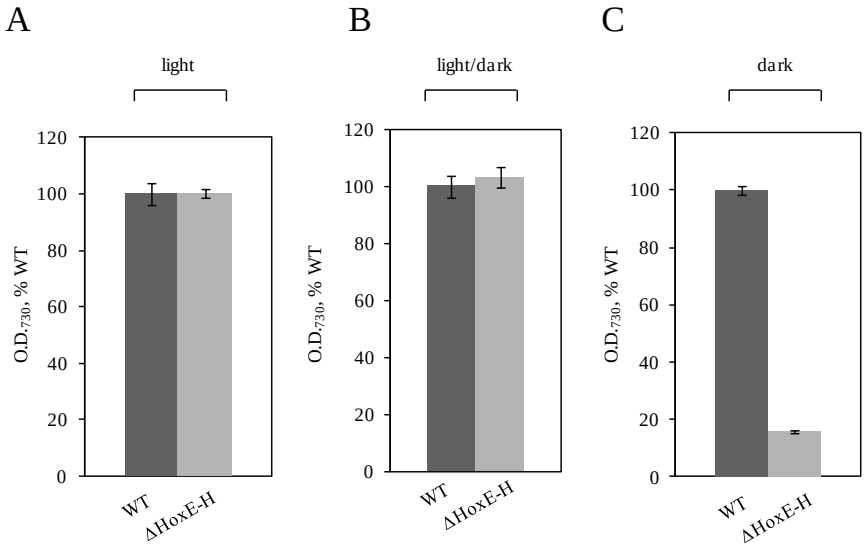

Figure 23. Wild type *Synechocystis* is more resistant to prolonged darkness than ΔHoxE-H mutant strain. *Panel A*, continuous white light (50 μE m^{-2} s^{-1}); *panel B*, 12 h light (50 μE m^{-2} s^{-1})/12 h dark; *panel C*, continuous darkness. Optical densities at 730 nm ($O.D._{730}$) of wild type (WT, dark grey) and ΔHoxE-H (light grey) liquid cultures were measured after five days of growth, and values normalized to the $O.D._{730}$ of the WT strain cultured in the same condition (*i.e.*, *panel A*, 5.2 ± 0.72; *panel B*, 4.03 ± 0.55; *panel C*, 1.8 ± 0.15). Reported data result from the mean of three independent experiments ± Standard Deviation.

These results were further confirmed by measurements of chlorophyll content (not shown), and suggest that the presence of an intact *hox* operon confers to *Synechocystis* an adaptive advantage enabling it to survive in the absence of photosyntethic activity. Interestingly, after shifting back these ΔHoxE-H cultures to normal light conditions, we observed that cells were suddenly able to resume their growth (figure 24, panel A), reaching in almost three days the same optical density of the wild type cells grown exactly in the same conditions (figure 24, panel B).

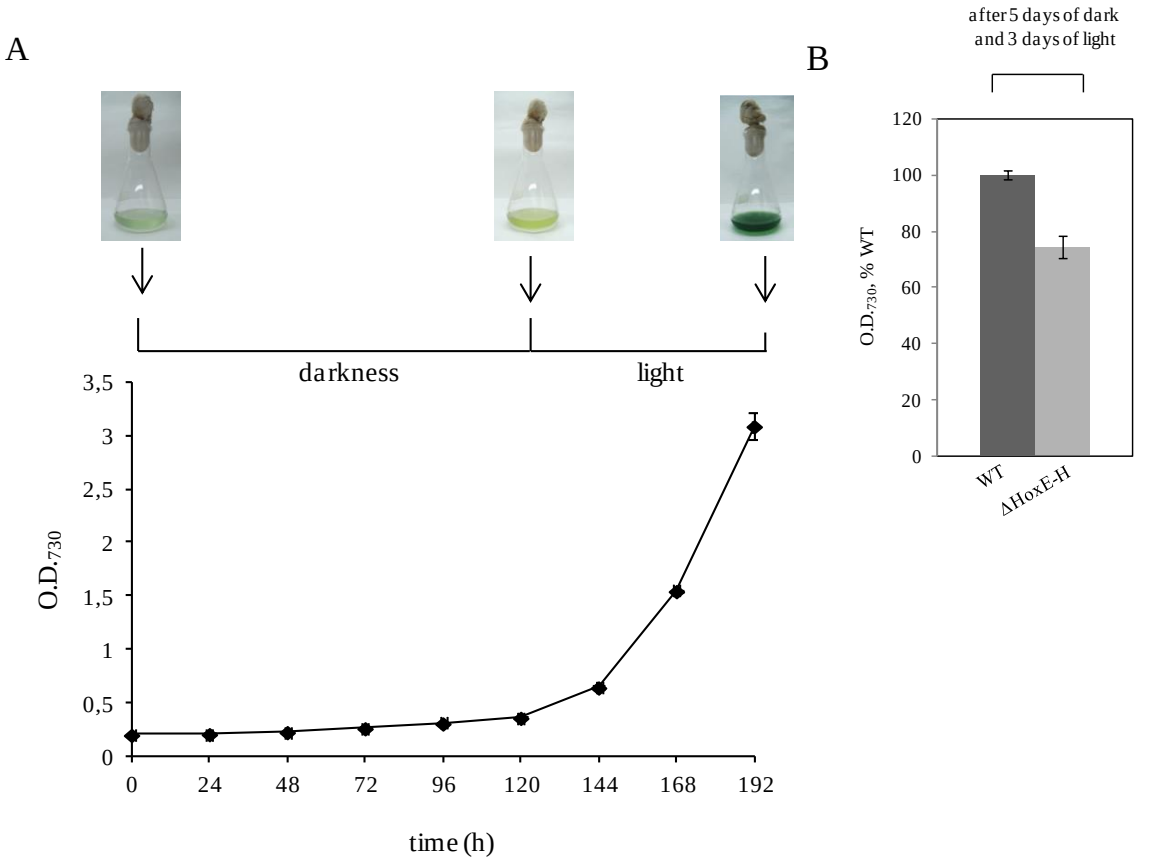

Figure 24. ΔHoxE-H *Synechocystis* mutant strain is able to resume its growth in the light after a five-day incubation under complete darkness. *Panel A*, growth curve of ΔHoxE-H *Synechocystis* mutant strain cultured up to five days in the dark and additional three days under normal light intensity. *Panel B*, optical densities at 730 nm ($O.D._{730}$) of wild type (WT, dark grey) and ΔHoxE-H (light grey) liquid cultures measured after five days of growth in the dark and additional three days under light. Values are normalized to the $O.D._{730}$ of the WT strain cultured in the same condition (*i.e.* 4.1± 0.07). In both panels, reported data result from the mean of three independent experiments ± Standard Deviation.

This outcome appeared very interesting because, by comparing the values achieved by the two strains after the dark conditions (*i.e.* OD=1.8 and OD=0.3 for the wild type and the mutant strains respectively) we would have expected the wild type strain to reach, after additional three days in the light, OD values higher to those obtained, hence an increased difference with the mutant. It is likely that the wild type strain, even in a stress condition, continues to perform its vital functions in the dark, consuming the nutrients in the medium; thus, when the colture is brought back to light, it would rapidly reach saturation and stop replicating. On the contrary, the knock out mutant strain seems to be in a quiescent state during the dark regimen. This result further indicates that the different behavior of the wild type and the mutant strains is probably due to the presence/absence of the [NiFe]-hydrogenase, and suggests that the alteration(s) induced in the ΔHoxE-H mutant strain by a prolonged darkness is (are) reversible. To explore the hypothesis that the entry into a quiescent but viable state is a survival mechanism that the *Synechocystis* mutant strain can adopt when exposed to a prolonged darkness in the absence of the [NiFe]-hydrogenase, we analyzed the ability of ΔHoxE-H cells previously incubated for five days in the dark in liquid medium of forming colonies on solid BG11 when moved back to normal light growth conditions. Plate counts (see Materials and methods for experimental details) clearly indicate that this is indeed the case (data not shown). These data were also confirmed by a transmission electron microscopy (TEM) morphological examination of ΔHoxE-H cells grown either in normal light or in the dark. TEM analysis showed that no gross ultra-structural difference could be detected in the cells grown under the two conditions (figure 25) (for a detailed description of the characteristics of cyanobacteria cells see the Introduction), further supporting the idea that the ΔHoxE-H *Synechocystis* deletion mutant strain remains viable, thus allowing the recovery of growth after prolonged exposure to darkness.

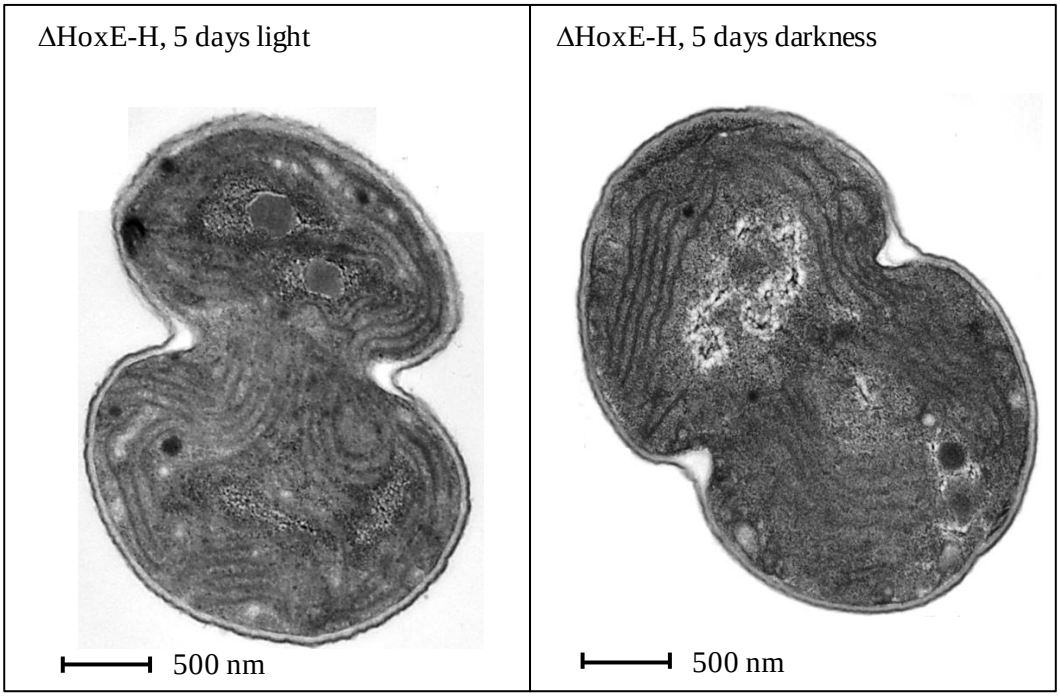

Figure 25. ΔHoxE-H *Synechocystis* mutant cells grown under light and in the dark display the same ultrastructural organization. Transmission Electron Microscopy of *Synechocystis* ΔHoxE-H mutant cells grown up to five days either in the light (*left panel*) or in complete darkness (*right panel*). Scale bar: 0.5 μm.

This analysis also allowed us to detect a peculiarity in the mutant cells compared to the wild type: in the first, the phycobilisomes resulted much more visible, in particular, in dark conditions, most of them appear enlarged (figure 26, right panel). These data have not been further explored, it will be readdressed and investigated in future.

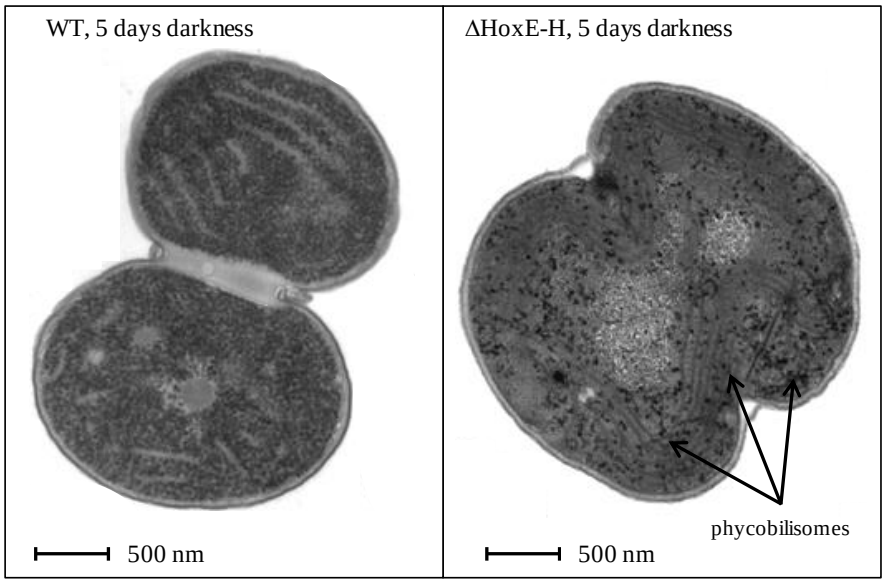

Figure 26. ΔHoxE-H *Synechocystis* mutant cells grown in the dark display noticeable phycobilisomes. Transmission Electron Microscopy of Synechocystis WT(*left panel*) and ΔHoxE-H (*right panel*) mutant cells grown up to five days in complete darkness. The black arrows emphasize phycobilisoes. Scale bar: 0.5 μm

It is worth noting that the results of the growth experiments described above were obtained in aerobic conditions, which are known to inhibit rapidly and completely the hydrogenase function of the Hox protein. The reactivity of several purified [NiFe]-hydrogenases toward O_2 has been extensively studied, and involves the conversion of the enzyme into a mixture of two inactive states, *e.g.* Ni-A and Ni-B, with an oxygenic ligand bridging the Ni and Fe atoms of the active site (De Lacey A.L. et al., 2007; Fernandez V.M. et al., 1986; Pandelia M.E. et al., 2010). This indicates that the wild type *Synechocystis* strain phenotype, under long term darkness, cannot rely on the ability of its [NiFe]-hydrogenase to evolve H_2. To further explore this issue, I generated two additional knock out deletion mutant strains, *i.e.* i) the ΔHypA and ii) the ΔHypB lacking, respectively, the hydrogenase accessory chaperones HypA and HypB involved in the last steps of the NiFe site assembly process. In such mutants the diaphorase activity of this bidirectional enzyme should be preserved while oxidation/reduction of molecular hydrogen should not take place.

Construction and physiological characterization of ΔHypA1 and ΔHypB1 Synechocystis strains under normal light and long term darkness.

As reported in the Introduction, the maturation of the [NiFe]-hydrogenases is driven by a complex, highly conserved pathway needed for the biosynthesis of their composite active site, and has been thoroughly characterized in several microorganisms, including cyanobacteria (Tamagnini P. et al., 2007; Casalot L. and Rousset M., 2001; Blokesh M. and Böck A., 2002; Ghirardi M.L. et al., 2007). Specifically, the auxiliary proteins HypA and HypB are responsible for the nickel insertion into the active site, prior to the very last step of the whole process, *i.e.* the hydrogenase C-terminus cleavage from the large subunit, culminating in enzyme activation (Blokesch M. et al., 2002). Two homologues of both *hypA* and *hypB* are present in *Synechocystis* (Kaneko T. et al., 1996) (figure 27); however, only the HypA1 and HypB1 couple is needed for the nickel insertion, while the HypA2 and HypB2 proteins probably have a chaperone role in the maturation of other metalloproteins in this microorganism (Hoffman D. et al., 2006).

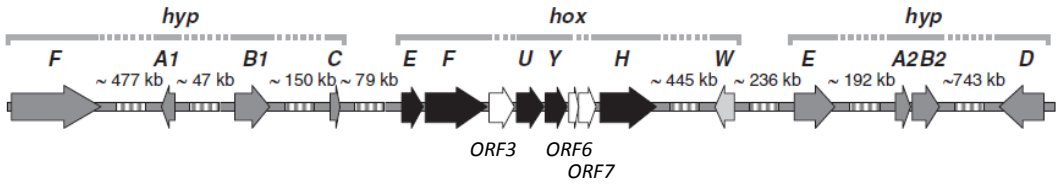

Figure 27. Organization of the loci containing the genes encoding the bidirectional hydrogenase of *Synechocystis*. The *hox* operon genes are depicted in black. The *hyp* genes encoding the accessory proteins involved in the hydrogenase maturation are depicted in gray. The three addictional ORFs are represented in white (modified from Tamagnini P. et al., 2007).

Based on this premise, we selectively replaced the *hypA1* (*slr1675*) and *hypB1* (*sll1432*) genes with a selection cassette conferring kanamycin resistance, as described in Materials and methods. Due to the existence of multiple genome copies in *Synechocystis*, the complete segregation of the recombinant chromosomes, usually reached by increasing the antibiotic concentration up to 50 μg/ml, was verified by PCR (see Materials and methods for details) (figure 28).

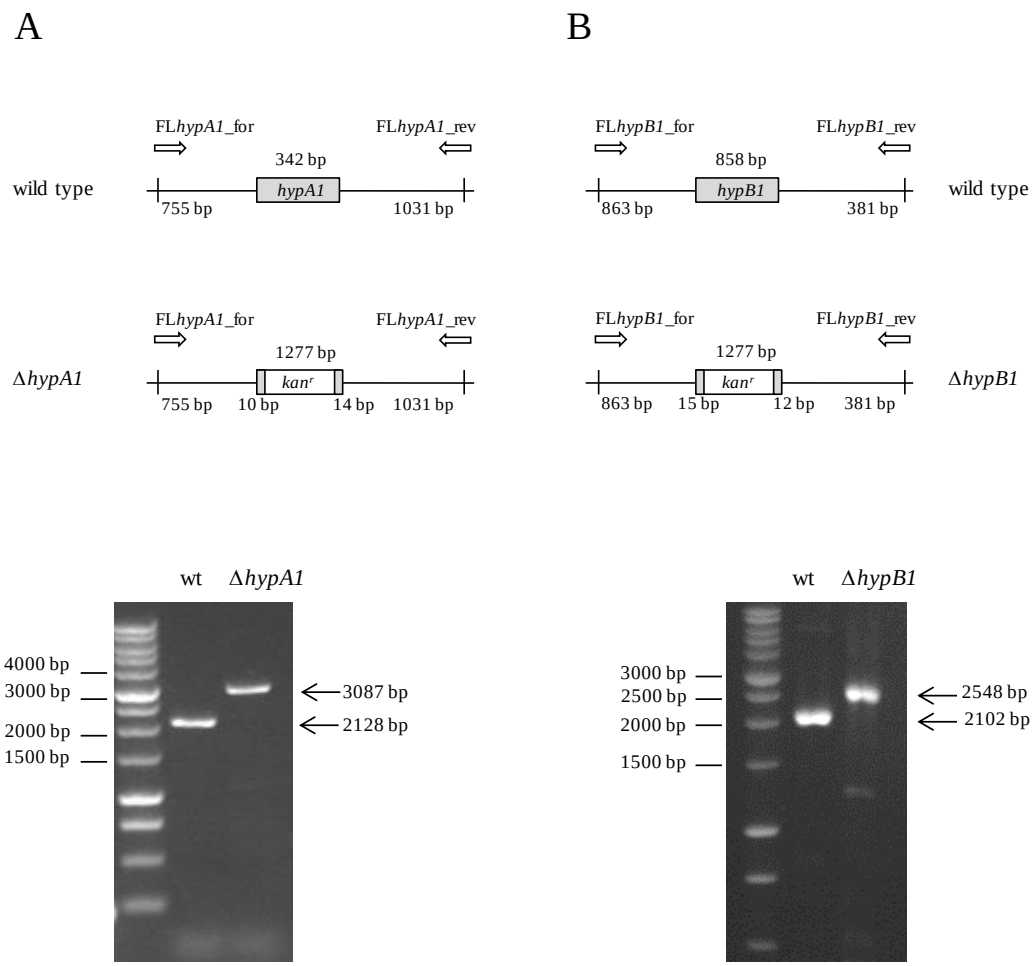

Figure 28. Construction of ΔHypA1 and ΔHypB1 *Synechocystis* mutant strains. *Upper panels*, schematic diagram of the construction of the ΔHypA1 (*panel A*) and ΔHypB1 (*panel B*) knock-out strain. The *hypA1* (*slr1675*) and *hypB1* (*sll1432*) genes were deleted and substituted by a kanamycin-resistance cassette (as detailed in Materials and methods). Positions of PCR primers used to verify correct insertion of the cassette are indicated (*FLhypA1_for/ FLhypA1_rev* and *FLhypB1_for/ FLhypB1_rev*). *Lower panels*, agarose gel electrophoresis of analytical PCR amplifications using as template genomic DNA from wild type and knock-out strains. *Lane 1*, molecular markers; *lane 2*, DNA from wild type; *lane 3*, DNA from knock-out.

Hydrogenase activity measured by gas chromatography (reported in table 3) confirmed the lack of an active enzyme in the two new knock out mutant strains (*i.e. ΔhypA1* and *ΔhypB1*).

Strain	nmol H_2 · mg · Chl^{-1} · min^{-1} ± SD[(a)]
wild type	30 ± 3.1
ΔhypA	NA[(b)]
ΔhypB1	NA[(b)]

Table 3. H_2 evolution activities of wild type, ΔHypA1 and ΔHypB1 mutant *Synechocystis* sp. PCC6803 strains. [(a)]Reported values represent the mean of three independent experiments ± Standard Deviation. [(b)]NA: not applicable.

These strains were then tested for their ability to grow both under normal light and prolonged darkness, as described above. We found that the lack of HypA1 and HypB1 proteins does not interfere with the aerobic growth of *Synechocystis* mutant strains when compared to the wild type strain, as assessed by $O.D._{730}$ monitoring (figure 29, panels A and B) and chlorophyll quantification (not shown), both under a normal light regimen and five day-long exposure to complete darkness. This result indicates that a correctly assembled, functional [NiFe]-hydrogenase active site is indeed not essential to confer to *Synechocystis* the ability to face this stress condition.

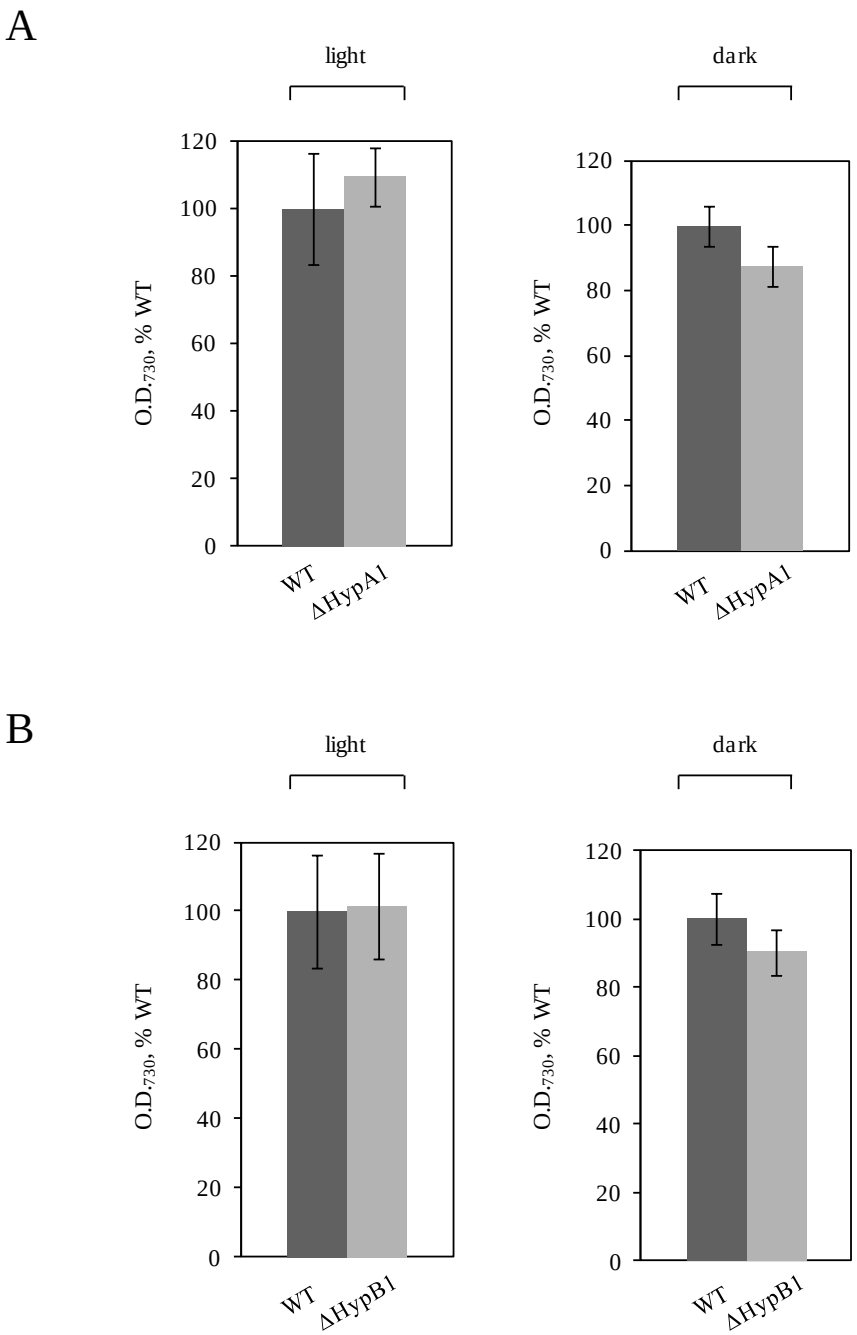

Figure 29. ΔHypA1 and ΔHypB1 *Synechocystis* mutant strains have the same growth phenotype of the wild type strain when cultured in the dark. *Panel A*, ΔHypA1; *panel B*, ΔHypB1. Strains were grown either under continuous white light (50 μE m^{-2} s^{-1}) or in the dark. Optical densities at 730 nm ($O.D._{730}$) of wild type (WT, dark grey) and mutants (light grey) liquid cultures were measured after five days, and values normalized to the $O.D._{730}$ of the WT strain cultured in the same condition (*i.e.* light, 5.8 ± 0.9; dark, 1.6 ± 0.5). In all panels, reported data result from the mean of three independent experiments ± Standard Deviation.

[NiFe]-hydrogenase is a heteropentameric enzyme that, as already described in the Introduction, possesses five related subunits combined in two functional units. One of these, the hydrogenase moiety (*i.e.* HoxYH), harbours the active site whose maturation tightly depends on HypA and HypB proteins, the other, the diaphorase moiety (*i.e.* HoxEFU), likely works as a redox partner for the catalytic subcomplex. To further validate the hypothesis that the phenotype observed under this stress condition is not due to the hydrogenase activity of the enzyme, I generated a new knock out mutant strain lacking the hydrogenase subcomplex, *i.e. ΔhoxYH.*

Construction and physiological characterization of ΔhoxYH Synechocystis strain under normal light and long term darkness.

The strategy used to obtain this knock out mutant strain was analogous to that of *ΔhypA1* and *ΔhypB1*, reported in Materials and Methods. I deleted the portion of the *Synechocystis* wild type genome between *sll1224 (hoxY)* and *sll1226 (hoxH)* genes inserting a kanamycin resistance cassette by double homologous recombination (figure 30, upper panel).

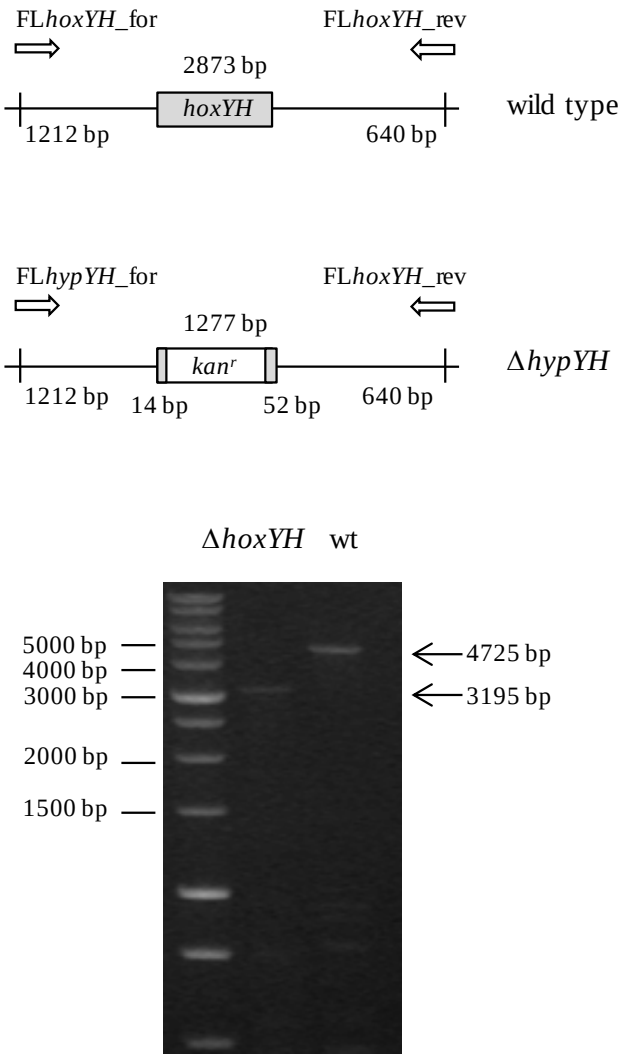

Figure 30. Construction of ΔHoxYH *Synechocystis* mutant strain. *Upper panel*, schematic diagram of the construction of the ΔHoxYH knock-out strain. The *hoxY-hoxH (sll1224-sll1226)* genes were deleted and substituted by a kanamycin-resistance cassette (as detailed in Materials and methods). Positions of PCR primers used to verify correct insertion of the cassette are indicated (*FLhoxYH_for/ FLhoxYH_rev*). *Lower panel*, agarose gel electrophoresis of analytical PCR amplifications using as template genomic DNA from wild type and knock-out strains. *Lane 1*, molecular markers; *lane 2*, DNA from knock-out; *lane 3*, DNA from wild type.

Trasformants were selected on plates containing 50 μg/ml of kanamycin. The correct segregation of the recombinant mutants was checked by PCR (see figure 30 lower panel and Materials and methods for the oligonucleotides used) and by

hydrogen evolution assay in which, as expected, the knock out strain was not able to evolve hydrogen gas (table 4).

Strain	nmol H_2 · mg · Chl^{-1} · min^{-1} ± SD[(a)]
wild type	27 ± 2.8
ΔYH	NA[(b)]

Table 4. H_2 evolution activities of wild type and ΔYH mutant *Synechocystis* sp. PCC6803 strains. [(a)]Reported values represent the mean of three independent experiments ± Standard Deviation. [(b)]NA: not applicable.

The growth of the *ΔhoxYH* mutant strain was then analyzed in normal lighting conditions (50 μE m^{-2} s^{-1}), and the observed behavior was similar to the wild type strain, in agreement with what is reported in literature (Pinto F. et al., 2012). Interestingly, similarly to the results obtained with *ΔhypA1* and *ΔhypB1* mutant strains under prolonged darkness, also *ΔhoxYH* grew in a comparable manner to the wild type strain (figure 31).

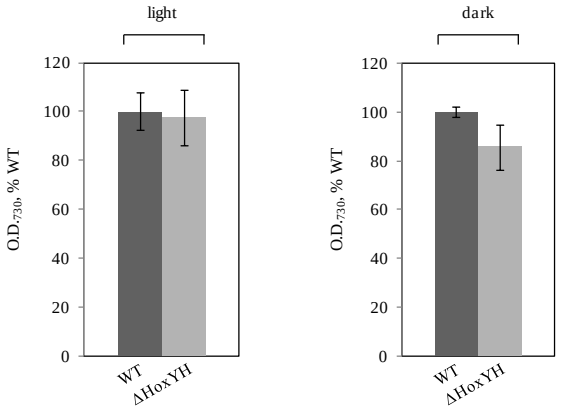

Figure 31. ΔHoxYH *Synechocystis* mutant strains have quite the same growth phenotype of the wild type strain when cultured in the dark. *Left panel*: the ΔHoxYH strain was grown under continuous white light (50 μE m^{-2} s^{-1}). *Right panel*: the ΔHoxYH strain was grown in the dark. Optical densities at 730 nm ($O.D._{730}$) of wild type (WT, dark grey) and mutant (light grey) liquid cultures were measured after five days, and values normalized to the $O.D._{730}$ of the WT strain cultured in the same condition (*i.e.* light, 5.4 ± 0.8; dark, 1.8± 0.1). In all panels, reported data result from the mean of three independent experiments ± Standard Deviation.

These new results have strengthened the original hypothesis that the adaptive advantage conferred to the wild type strain in our selected stressful conditions was not associated with the hydrogenase activity of the [NiFe]-hydrogenase. This led us to speculate that the diaphorase moiety, the other portion of the enzyme, could have a role in this phenotype, shedding light on the hydrogenase expression and function in aerobic conditions, which are not likely to prevent the NADP(H) oxidation/reduction activity. Therefore, I generated a new knock out mutant strain lacking the diaphorase moiety, *i.e. ΔhoxEFU*.

Construction and physiological characterization of ΔhoxEFU Synechocystis strain under normal light and long term darkness.

As in the previous knock out mutant strain, a kanamycin resistance cassette was inserted in the wild type to replace the genome sequence between *sll1220* (*hoxE)* and *sll1223 (hoxU)* genes. After subcloning at increasing concentration of antibiotic, the homoplasmy was reached with 50 μg/ml of kanamycin. As expected, the mutant strain was unable to produce H_2 (table 5).

Strain	nmol $H_2 \cdot mg \cdot Chl^{-1} \cdot min^{-1} \pm SD$[(a)]
wild type	31 ± 2.5
ΔEFU	NA[(b)]

Table 5. H_2 evolution activities of wild type and ΔEFU mutant *Synechocystis* sp. PCC6803 strains. [(a)]Reported values represent the mean of three independent experiments ± Standard Deviation. [(b)]NA: not applicable.

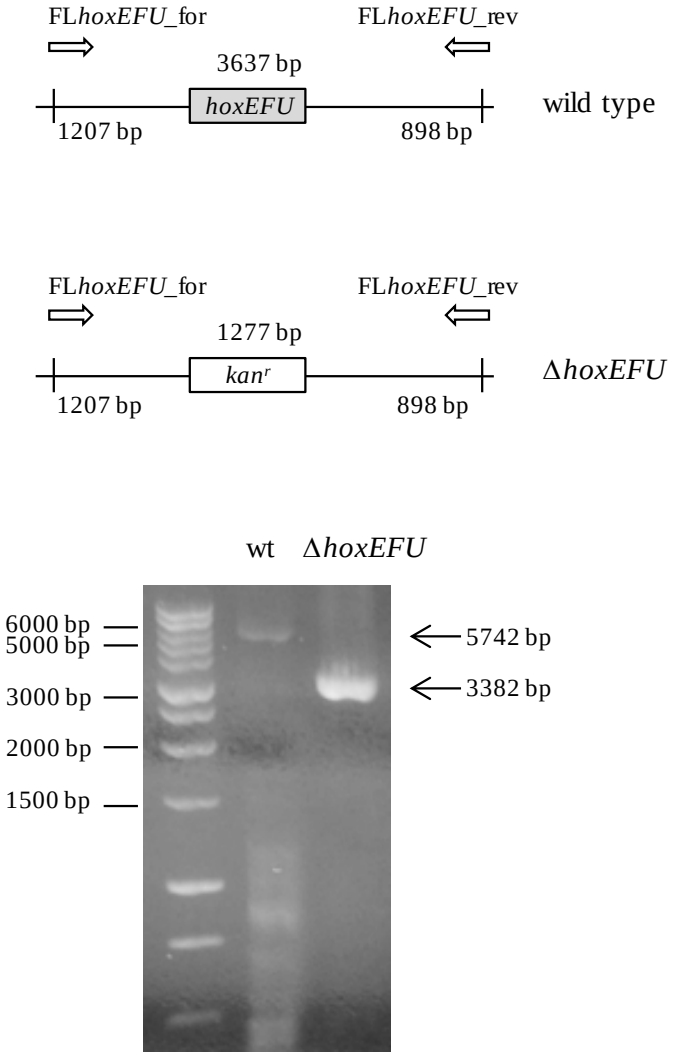

Figure 32. Construction of ΔHoxEFU *Synechocystis* mutant strain. *Upper panel*, schematic diagram of the construction of the ΔHoxEFU knock-out strain. The *hoxE*, *hoxF*, *hoxU (sll1220, sll1221, sll1223)* genes were deleted and substituted by a kanamycin-resistance cassette (as detailed in Materials and methods). Positions of PCR primers used to verify correct insertion of the cassette are indicated (*FLhoxEFU_for/ FLhoxEFU_rev*). *Lower panel*, agarose gel electrophoresis of analytical PCR amplifications using as template genomic DNA from wild type and knock-out strains. *Lane 1*, molecular markers; *lane 2*, DNA from wild type; *lane 3*, DNA from knock-out.

The mutant strain was first grown in continuous light condition and once again it was found to be capable of growing in a completely comparable way to the wild type (figure 33, panel A). Once it was subjected to the prolonged darkness, the results were nevertheless conflicting, not allowing us to confirm the hypothesis

previously made: in fact, among the biological replicates analyzed, in some cases there were a significant reduction in the mutant growth compared to the wild type (figure 33, panel B), whereas in other experiments the growth behavior was comparable to the WT strain (figure 33 panel C).

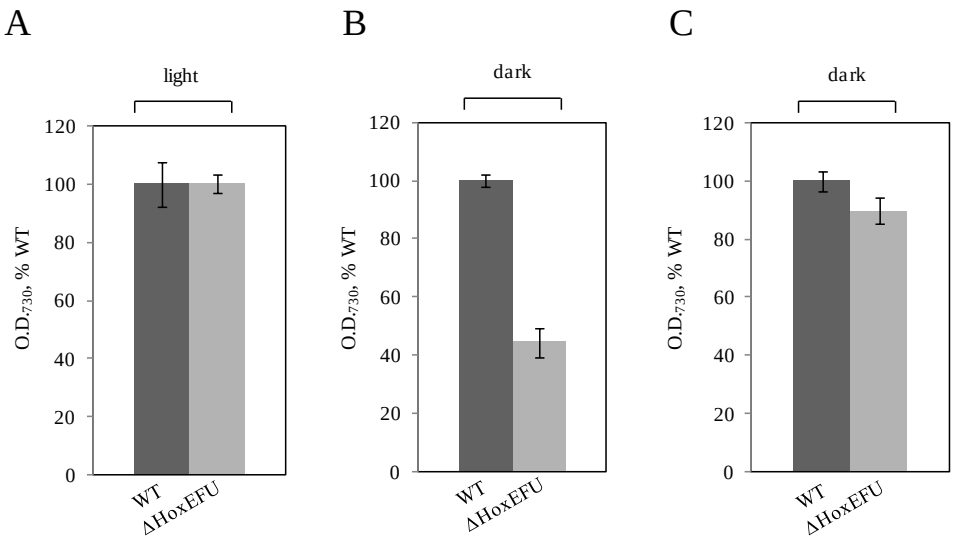

Figure 33. ΔHoxEFU *Synechocystis* mutant strains have the same growth phenotype of the wild type strain when cultured in the light, but not a clear behaviour in the dark. *Panel A*: the ΔHoxEFU strain was grown under continuous white light (50 μE m^{-2} s^{-1}). *Panel B and C*: the ΔHoxYH strain was grown in the dark. Optical densities at 730 nm ($O.D._{730}$) of wild type (WT, dark grey) and mutant (light grey) liquid cultures were measured after five days, and values normalized to the $O.D._{730}$ of the WT strain cultured in the same condition (*i.e.* light, 5.5 ± 0.9; dark (*panel B*) 2,1 ± 0.1). 5.4 ± 0.8; dark (*panel C*) 2± 0.3). In all panels, reported data result from the mean of three independent experiments ± Standard Deviation.

This may be due to an intrinsic biological variability of these organisms; furthermore, since the five *hox* genes coding for the whole [NiFe]-hydrogenase complex (*i.e. hoxE, hoxF, hoxU, hoxY* and *hoxH*) belong to a single operon, it is not easy to predict if and how their expression is affected when one or more of the other genes is/are deleted. In fact, studies on this topic have shown that the knock-out of one or more genes of the *hox* operon causes a downregulation in the expression of the other *hox* genes, at different extent depending on the deleted gene(s) (Eckert C. et al., 2012). Unfortunately, in the absence of specific antibodies against the five Hox subunits it is not possible to estimate the amount

of HoxYH and HoxEFU sub-complexes in our experiments, making difficult to intepretate the behavior observed for the ΔHoxYH and ΔHoxEFU *Synechocystis* mutant strains grown under prolonged darkness. Furthermore, a possible effect of a differential deletion of the three additional ORFs (*i.e. ORF3*, *ORF6* and *ORF7*) interspersed among the *hox* genes (see figure 25 to localize the position in the genome) in the sub-complexes assembly cannot be excluded, although their products are unlikely to be involved in the activities of the hydrogenase and diaphorase enzyme moietes (Schmitz O. et al., 2002). Thus, to date we cannot assign a specific role to the Hox diaphorase portion in the *Synechocystis* growth phenotype observed in the dark. The unresolved issues emerged in the characterization of the ΔYH and ΔEFU mutant strains will be further investigated in the future.

Taken together our results suggest that the [NiFe]-hydrogenase plays a key function in the response of *Synechocystis* to a longterm darkness exposure, and open a new perspective to gain clues on the role of this protein in selected stress conditions.

Several proteomic studies have been recently reported on different cyanobacteria, including *Synechocystis*, grown under various environmental stress conditions, such as for example UV light, high salt, cold temperature or CO_2 limitation, and revealed activation of distinct strategies by cyanobacteria against these perturbations (Gao Y. et al., 2009; Wegener K.M. et al., 2010; Battchikova N. et al., 2010; Rowland J.G. et al 2011; Li T. et al., 2012; Qiao J. et al., 2012). Thus, in order to get more insights into the involvement of the [NiFe]-hydrogenase in the metabolic response of *Synechocystis* to a prolonged darkness we analyzed and compared the proteomes of a wild type strain grown either in normal light regimen or in the dark. The same analysis was conducted on the ΔHoxE-H mutant strain in the aforementioned conditions, but the data are still under analysis (supplementary table 5) and they will be only briefly mentioned below.

Quantitative proteomics analysis and comparison of the proteome of wild type Synechocystis grown under normal light and in the dark. Unraveling a new clue on the potential [NiFe]-hydrogease functional role.

A proteomic approach based on isobaric tag for relative and absolute quantification (iTRAQ) technology and liquid chromatography-tandem mass spectrometry (LC-MS/MS) was applied to compare the expression level of proteins from wild type *Synechocystis*, cultured for five days either under light or in the dark (see Material and methods for more experimental details). The analysis was conducted on three independent biological replicates. Across all replicates a total of 780 distinct protein families were identified and quantified. All relevant information relative to proteins and pepetides identification and quantification are reported in supplementary tables 1-3 (available on the attached CD). Six hundred and two proteins, which constitutes 16.4% of the *Synechocystis* theoretical proteome (Kaneko T. et al., 1996), could be quantified in at least two out the three experiments, and were therefore used for the differential protein expression analysis. Unfortunately, hydrophobic proteins, including membrane-embedded subunits of thylakoid complexes (which are expected to be highly abundant in *Synechocystis*) are underestimated in our analysis, due to intrinsic limitations in the applied methodology, which relies on the use of trypsin as digestive enzyme. Nevertheless, we determined that 112 proteins were differentially regulated between light and darkness growth (p value <0.05), among which 58 showed an increased abundance (*i.e.* dark/light ratio ≥ 1.50) and 54 a decreased abundance (*i.e.* dark/light ratio ≤ 0.67). These proteins have been listed in supplementary table 4 (available at the end of this Chapter and also in the attached CD) and grouped in table 6 in different main categories according to their proven or predicted functions (when known).

Functional category	Up-regulated (dark/light ratio ≥ 1.5)	Down-regulated (dark/light ratio ≤ 0.67)
Nucleotides metabolism, Transcription, Translation	38	1
Metabolism	8	12
Aminoacids	6	5
Lipids	1	2
Carbohydrates	1	5
Photosynthesis	0	7
Respiration	0	4
Other functions	4	17
Unknown	8	13

Table 6. Distribution by functional groups of proteins differentially regulated between control and darkness *Synechocystis* growth.

A large number of proteins and enzymes involved in transcription and translation show an altered expression in the dark as compared to light conditions, indicating that the overall protein synthesis process is altered when *Synechocystis* is grown under prolonged darkness, as previously observed also for several other stress conditions affecting the *Synechocystis* physiology (Gao Y. et al., 2009; Pinto F. et al., 2012; Battchikova N. et al., 2010; Wegener K.M. et al., 2010; Rowland J.G. et al 2011; Li T. et al., 2012; Qiao J. et al., 2012). More specifically, as expected, several proteins/cofactors belonging to photosystems I and II and/or functionally correlated to photosynthesis, including the electron carrier flavodoxin, show a lower abundance when *Synechocystis* is grown in the absence of light, *i.e.* when glycolysis and oxidative pentose-phosphate metabolic pathways become prevalent. A thorough and complete analysis of the changes in the proteome of both wild type and ΔHoxE-H *Synechocystis* strains grown in the dark, and the close dissection of the metabolic pathways activated/affected in response to this stress condition, will be further conducted in the future. On the other hand, it is

worth mentioning that several subunits of the respiratory chain NADPH/plastoquinone oxidoreductase (NDH-1) complex were also found with a reduced expression. *Synechocystis* contains a respiratory electron transport chain on both the cytoplasmic and thylakoid membranes, working in an interwoven way with the photosynthetic electron transport chain (Mullineaux C.W., 2014). The two pathways share some components (*i.e.* plastoquinone, cytocrome b_6f and plastocyanin), whereas other complexes are specific for the respiratory electron flow, including NDH-1, succinate dehydrogenase (SDH), and the terminal oxidase. The cyanobacterial NDH-1 is a proton-pumping NADPH/plastoquinone oxidoreductase analogous to the mitochondrial Complex I and is composed, in *Synechocystis*, of 11 subunits encoded by the *ndh* genes (Kaneko T. et al., 1996; Berger S. et al., 1991; Yagi T., 1998; Battchikova N. and Aro E.M., 2007; Ogawa T. and Mi H., 2007). This multisubunit complex, organized into a membrane domain containing hydrophobic subunits and a perpendicular peripheral domain composed by hydrophilic proteins, moves the electrons from NADPH to the plastoquinone (PQ) pool. However, in cyanobacteria NADPH is preferentially used for the CO_2 fixation process and the role of NDH-1 as an electron transport route into the PQ pool is controversial. On the other hand, four distinct NDH-1 complexes with similar structure and different functions were predicted to exist in *Synechocystis* (Ogawa T. and Mi H., 2007), suggesting that NDH-1 may work with different specificities depending on the physiological state of the cell. Based on mutagenesis experiments (Cooley J.W. and Vermaas W.F., 2001), a general consensus has indeed emerged that in *Synechocystis* most respiratory electrons enter the PQ pool via SDH, a complex composed by three subunits (*i.e.* a flavoprotein subunit, an iron-sulfur protein subunit, and a membrane subunit) which oxidizes succinate to fumarate, moving the electrons to the PQ pool. Intriguingly, we found that when wild type *Synechocystis* is grown under prolonged darkness four out of the six NDH-1 complex hydrophilic subunits detected (*i.e.* subunits Ndh-J, -K, -M and -O, encoded by genes *ndhJ*/*slr1281*, *ndhK*/*slr1280*, *ndhM*/*slr1623*, *ndhO*/*sll1690* respectively) are downregulated in their expression. Furthermore, our data (supplementary tables 1-3) strongly suggest that also the subunits Ndh-I (gene *ndhI*/*sll0520*) and Ndh-H (gene *ndhH*/*slr0261*) are affected in the same way, but they have been excluded from

the final list of differentially expressed proteins either because the value is slightly higher than the established cutoff (as in the case of Ndh-I, average value 0.68) or due to the biological variability among the three replicates (as in the case of Ndh-H). Moreover, collected data indicate that also the expression of the SDH flavoprotein subunit (*sdhA*/*slr1233*) is reduced, although it was not included in the final list because it did not completely meet the chosen criteria (altered expression of at least 50% and $p<0.05$). The opposite seems to apply to other two proteins, *i.e.* iron superoxide dismutase (gene *sodB*/*slr1516*) and catalase-peroxidase (gene *katG*/*sll1987*), which act as antioxidant shields, show a trend of increased abundance (see supplementary tables 1-3) and are likely to be also overexpressed. This is consistent with a more reductive intracellular environment under this stress condition, causing an increased concentration of toxic oxygen species. Although a specific function has not been yet assigned to the Hox bidirectional [NiFe]-hydrogenase in *Synechocystis*, as reported in the Introduction, our proteomic data confirm that it may work as an electron valve to dissipate electron excess under specific conditions, as previously proposed (Appel J. and Schulz R., 1996; Antal T.K. and Lindblad P., 2005; Appel J. et al., 2000), and suggest that it could be essential when the photosynthetic or respiratory electron transport chains are transiently over-reduced, such as during growth under prolonged darkness (Vignais P.M. and Billoud B., 2007; Stal L.J. and Moezelaar R., 1997; Barz M. et al., 2010). This is also supported by additional experiments in which the wild type and ΔHox *Synechocystis* strains were grown under light in the presence of 5 μM DCMU, which inhibits the PSII-dependent oxygen evolution. Figure 34 shows that the growth of ΔHox mutant strain is indeed strongly affected if compared to the wild type when the photosynthetic electron transport is specifically inhibited by DCMU.

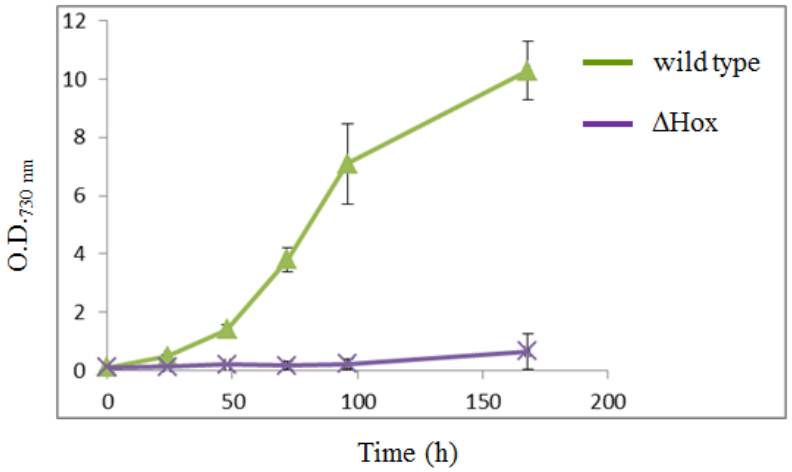

Figure 34. Growth curves of wild type (*green line*) and mutant ΔHox (*violet line*) *Synechocystis* strains cultured up to five days under normal light intensity in the presence of DCMU. Reported data result from the mean of three independent experiments ± Standard Deviation.

These results further confirm a key functional role of the [NiFe]-hydrogenase in *Synechocystis* when the overall electron flow is affected. To further explore this scenario, we analyzed the oxygen consumption rates of a wild type strain grown 48 hours either under light or in the dark.

It should be noted that the results of the proteomic analysis discussed before were obtained by analyzing the culture of the wild type strain after 5 days of growth. We could not analyze the same cultures for the oxygen consumption experiments since these measurements should be performed when bacteria are still in the exponential phase of their growth, that usually occurs after 48 h from the initial inoculum. Therefore, cultures of wild type strain were grown for two days in the presence of 5 mM glucose under i) continuous light and ii) prolonged darkness, and then analyzed by oxygraph as described in Materials and Methods. The preliminary obtained results (not shown) have been encouraging as they have shown a reduction by 20% in the amount of μmoles O_2/(mg Chl × h) consumed by the wild type strain grown in dark compared to that in light condition. Despite respiration in dark regimen resulted only slightly compromised, these data appear to be consistent with the proteomic data, and will be further addressed in the

future. Moreover, the same experiments will be also performed with the ΔHoxE-H mutant strain, since preliminary analysis of the proteomic data (supplementary table 5, available on the CD), acquired on this strain grown five days in the dark, revealed that several hydrophilic subunits of the NDH-1 complex seem to be also affected by this stress condition, exactly as in the wild type strain. This would confirm that [NiFe]-hydrogenase, when present, could confer to *Synechocystis* an adaptive advantage enabling it to cope with this stress condition.

Discussion

The bidirectional [NiFe]-hydrogenase expressed in *Synehcocystis* sp. PCC 6803 is an enzyme involved in the metabolism of hydrogen whose specific role in the physiology of this cyanobacterial strain is still not completely understood. Indeed, mutants lacking part or all of this enzyme appear to well survive, at least in standard growth conditions. In particular, the fact that the hydrogenase activity is inhibited by oxygen but the [NiFe]-hydrogenase and the protein set that promotes its maturation are expressed in these conditions arouses curiosity, since it suggests that the enzyme may have some additional activity besides hydrogen production, which has never been investigated before. To date, several studies have shown that this protein appears to be essential only in selected conditions. On this basis, we compared the behavior of the wild type strain and of a mutant lacking the entire *hox* operon coding for the enzyme (*i.e.* ΔHoxE-H) under continuous and prolonged darkness, an environmental stress condition to which cyanobacteria could be subjected, for example as in the case of strains populating lake sediments. The surprising result was that the knock out mutant strain had a marked reduction in its growth when compared to the wild type under prolonged oxygenic darkness. Interestingly, once it was brought back to light it was found to be able to grow again. Since this result was obtained in the conditions that, as known, inactivate the hydrogenase activity of the enzyme, *i.e.* in the presence of oxygen, we supposed that this phenotype was due to some other function of the [NiFe]-hydrogenase. I investigated this hypothesis with two strategies: in the first, I have generated the mutant strains lacking the HypA1 and HypB1 proteins, two

chaperones involved in the crucial phase of the Ni atom insertion in the active site of the enzyme; in the second, I have generated a knock out mutant strain lacking one of the two functional moieties of the [NiFe]-hydrogenase, the YH hydrogenase subcomplex, hosting the active site. In prolonged dark condition, *ΔhypA1* and *ΔhypB1* grown in a comparable way to the wild type, proving that *Synechocystis* is able to survive even if its active site is not properly formed. The results obtained with the second strategy have strengthened the hypothesis that the hydrogenase portion is unlikely to be involved in the observed phenotype; in fact, *ΔhoxYH* mutant strain grew likewise the wild type strain under dark regimen. This has opened new scenarios leading us to speculate that, therefore, there could be an involvement of the other functional moiety of the enzyme, the EFU diaphorasic portion. Thus, I have generated a mutant strain lacking this moiety, which normally acts conveying electrons to the YH portion. However, the conflicting data that I have obtained did not allow us to achieve a definitive conclusion. The question remains open and will be further investigated.

To identify possible effects on the metabolism of *Synechocystis* due to the [NiFe]-hydrogenase lack, we finally performed a proteomic analysis of the wild type strain grown for 5 days in normal light regimen or in the dark. As result, 780 distinct proteins were detected across all replicates and 112 of these were differentially regulate between control and darkness growth. In particular, we found very interesting that four out the six hydrophilic portions of NDH-1 complex showed a downregulated expression. This finding, along with other data on the SDH and on some proteins involved in oxidative stress response, have opened a new scenario suggesting that the overall respiration electron flow is affected in *Synechocystis* grown under prolonged darkness. Preliminary respiration experiments, performed on the wild type strain after 48 hours in the dark, gave a first encouraging result showing a reduction, even if by only 20%, in the oxygen consumption for the wild type strain grown in the dark. Interstingly, a *Synechocystis ndhB*-deficient mutant strain, which is completely devoid of NDH-1 complex (Ogawa T., 1991), has been previously shown to display a sustained H_2 photoevolution (Cournac L. et al., 2004), further supporting the idea that the bidirectional [NiFe]-hydrogenase can be functionally related to the photosynthetic

and respiratory electron transport pathways. This is also supported by preliminary proteomic data acquired on the *Synechocystis* ΔHoxE-H mutant strain grown five days in the dark, which reveal that several hydrophilic subunits of the NDH-1 complex seem to be affected by this stress condition in the same way as in the wild type strain. The analysis of these additional proteomic data will be completed in the future to get new insights into the enigmatic role of the [NiFe]-hydrogenase, and to characterize the ΔHox mutant strain as a model organism in which catalytically active hydrogenases can be expressed.

Conclusions

No matter what might be the evolutionary driving force which led to the current wide taxonomic distribution of different [NiFe]-hydrogenases, long time considered only as primordial proteins involved in early life hydrogen metabolism, increasing and independent experimental evidences converge on a common consensus that they could have a key role in controlling/buffering electron flow pathways, at least under specific growth conditions.

In my experiments I showed that the Hox bidirectional [NiFe]-hydrogenase is essential to the cyanobacterium *Synechocystis* sp. PCC 6803 to survive under long term darkness, either in anaerobic or aerobic conditions, when the growth is only supported by fermentative metabolism. Interestingly, I found that under this stress condition the expression of several hydrophilic subunits of the NDH-1 respiratory complex is downregulated. This would be consistent with the homology of the Hox [NiFe]-hydrogenase NAD(P)H oxidoreductase portion to the NADH input module of mitochondrial Complex I.

Taken together, these data add new clues pointing toward an active role of the bidirectional [NiFe]-hydrogenase in *Synechocystis*, and provide a molecular evidence supporting, more in general, the close evolutionary relationship between [NiFe]-hydrogenases and the Complex I of the aerobic respiratory chain.

Supplementary Table 4. List of proteins differentially regulated between control and darkness *Synechocystis* growth.

Accession	Description	ΣCoverage	Dark/Light Replicate 1	Dark/Light Replicate 2	Dark/Light Replicate 3	Average	p Value
Q55542	Slr0334 protein OS=Synechocystis sp. (st	13,64	4,43	7,59	18,92	10,31	3,88E-07
Q55168	Phytochrome-like protein cph1 OS=Synec	4,81	23,48	3,31	1,55	9,45	4,84E-02
P77970	Glutamate--ammonia ligase OS=Synecho	9,94	7,05	2,58	1,29	3,64	3,35E-02
P73309	50S ribosomal protein L24 OS=Synechocy	68,7	1,23	2,52	4,86	2,87	2,23E-02
P36239	50S ribosomal protein L19 OS=Synechocy	44,26	3,87	2,26	1,77	2,63	8,10E-05
P74446	Slr0147 protein OS=Synechocystis sp. (st	13,01	3,54	2,33	1,82	2,56	3,51E-06
Q55541	Slr0333 protein OS=Synechocystis sp. (st	37,74	1,92	2,29	3,25	2,48	1,05E-08
P42352	50S ribosomal protein L9 OS=Synechocys	61,18	1,97	2,73	2,39	2,36	5,21E-19
P74565	RNA polymerase sigma factor SigA OS=Sy	8	3,33	1,94	1,71	2,33	9,17E-05
P73296	50S ribosomal protein L17 OS=Synechocy	52,59	1,73	2,09	3,15	2,32	4,22E-06
P73318	50S ribosomal protein L23 OS=Synechocy	78,22	1,70	2,17	2,59	2,15	4,46E-10
P74390	Negative aliphatic amidase regulator OS=	41,48	1,27	2,61	2,51	2,13	2,45E-03
Q55484	Diaminopimelate decarboxylase OS=Syne	22,39	2,58	2,56	1,25	2,13	3,48E-03
P74450	Slr0151 protein OS=Synechocystis sp. (st	25,62	2,38	2,36	1,62	2,12	5,87E-09
P48957	50S ribosomal protein L20 OS=Synechocy	57,26	1,58	1,83	2,92	2,11	1,29E-04
P73320	50S ribosomal protein L3 OS=Synechocys	52,58	2,01	2,46	1,84	2,10	1,58E-17
P73848	3-hydroxyacyl-[acyl-carrier-protein] dehy	24,39	1,56	2,30	2,37	2,08	9,04E-08
P72866	30S ribosomal protein S15 OS=Synechocy	33,71	2,25	2,08	1,78	2,04	6,46E-25
P36237	50S ribosomal protein L11 OS=Synechocy	45,39	1,90	2,24	1,88	2,00	5,24E-35
P73306	50S ribosomal protein L6 OS=Synechocys	77,65	1,75	1,66	2,52	1,98	5,11E-07
P73293	30S ribosomal protein S9 OS=Synechocys	37,23	2,82	1,76	1,30	1,96	5,78E-03
P73303	50S ribosomal protein L15 OS=Synechocy	67,35	1,71	1,92	2,25	1,96	2,76E-17
P73315	50S ribosomal protein L22 OS=Synechocy	43,8	1,40	2,28	2,16	1,95	2,67E-05
Q55698	Slr0226 protein OS=Synechocystis sp. (st	2,9	2,94	1,38	1,52	1,94	1,09E-02
P73305	50S ribosomal protein L18 OS=Synechocy	20	1,72	1,89	2,19	1,93	8,96E-21
P74448	Slr0149 protein OS=Synechocystis sp. (st	20,51	2,29	1,71	1,71	1,90	1,02E-10
P73319	50S ribosomal protein L4 OS=Synechocys	55,71	1,89	2,10	1,69	1,89	5,09E-24
P73311	30S ribosomal protein S17 OS=Synechocy	66,67	2,63	1,59	1,41	1,88	1,91E-03
P73317	50S ribosomal protein L2 OS=Synechocys	61,59	1,87	1,58	2,15	1,87	5,29E-12
P73294	50S ribosomal protein L13 OS=Synechocy	78,81	1,37	1,56	2,65	1,86	3,87E-03
P73307	30S ribosomal protein S8 OS=Synechocys	51,88	2,78	1,50	1,29	1,86	1,68E-02
P80505	Glyceraldehyde-3-phosphate dehydroger	64,99	1,98	1,06	2,50	1,85	3,10E-02
P73308	50S ribosomal protein L5 OS=Synechocys	65,56	2,47	1,66	1,37	1,83	8,35E-04
Q55662	ATP-dependent Clp protease regulatory s	24,36	2,69	1,61	1,12	1,81	3,92E-02
P77962	Serine hydroxymethyltransferase OS=Syn	19,67	2,57	1,61	1,22	1,80	1,26E-02
P73316	30S ribosomal protein S19 OS=Synechocy	36,96	2,27	1,69	1,43	1,80	2,65E-05
P74071	30S ribosomal protein S2 OS=Synechocys	35,32	1,93	1,77	1,66	1,79	8,38E-40
P73290	Adenylosuccinate synthetase OS=Synech	12,16	2,67	1,42	1,24	1,78	2,87E-02
P74267	50S ribosomal protein L27 OS=Synechocy	59,77	1,73	1,51	2,06	1,77	3,62E-10
P73409	Slr1841 protein OS=Synechocystis sp. (st	17,78	1,58	1,92	1,72	1,74	7,79E-22
P73304	30S ribosomal protein S5 OS=Synechocys	61,27	2,29	1,64	1,28	1,74	2,05E-03
P73636	30S ribosomal protein S6 OS=Synechocys	44,25	1,51	1,80	1,87	1,73	9,28E-16
P74193	Threonine synthase OS=Synechocystis sp	26,7	1,86	1,59		1,73	2,16E-12
P73452	Nitrate transport protein NrtA OS=Synecl	38,12	1,12	1,76	2,16	1,68	1,25E-02
P48946	30S ribosomal protein S18 OS=Synechocy	64,79	1,99	1,65	1,38	1,68	1,53E-06
P73298	30S ribosomal protein S11 OS=Synechocy	32,31	2,25	1,53	1,07	1,62	4,17E-02
P23350	50S ribosomal protein L10 OS=Synechocy	22,54	1,50	1,50	1,81	1,61	1,68E-14
P74219	Slr1533 protein OS=Synechocystis sp. (st	29,57	1,55	1,56	1,66	1,59	8,34E-102
P72851	50S ribosomal protein L28 OS=Synechocy	61,54	2,08	1,31	1,34	1,58	3,79E-03
P74395	N utilization substance protein B homolo	24,89	1,68	1,69	1,31	1,56	1,53E-07
P74226	30S ribosomal protein S10 OS=Synechocy	45,71	1,82	1,49	1,33	1,54	3,12E-06
P48939	30S ribosomal protein S4 OS=Synechocys	28,22	2,01	1,54	1,03	1,53	4,58E-02
P36236	50S ribosomal protein L1 OS=Synechocys	43,28	1,46	1,44	1,66	1,52	1,59E-20
P73289	50S ribosomal protein L25 OS=Synechocy	65,31	1,04	1,93	1,56	1,51	3,52E-02
P73299	30S ribosomal protein S13 OS=Synechocy	54,33	1,15	1,54	1,83	1,51	3,91E-03

Accession	Description	ΣCoverage	Dark/Light Replicate 1	Dark/Light Replicate 2	Dark/Light Replicate 3	Average	p Value
P48959	50S ribosomal protein L35 OS=Synechocy	32,84	1,20	2,02	1,26	1,49	2,43E-02
P73098	Chaperone protein dnaK3 OS=Synechocy	3,24	1,49	1,46		1,48	6,87E-221
P74229	30S ribosomal protein S7 OS=Synechocys	53,85	1,58	1,52	1,31	1,47	1,76E-11
P19050	NAD(P)H-quinone oxidoreductase subun	23,79	0,83	0,59	0,59	0,67	2,84E-04
P73061	Urease subunit alpha OS=Synechocystis s	16,34	0,54	0,68	0,80	0,67	2,37E-04
P72977	16.6 kDa small heat shock protein, mole	33,56	0,57	0,78		0,67	9,33E-03
P19569	Photosystem I reaction center subunit II	52,48	0,63	0,68	0,67	0,66	0,00E+00
Q55360	Sll0888 protein OS=Synechocystis sp. (str	16,84	0,44	0,62	0,91	0,66	2,59E-02
P73103	Slr1908 protein OS=Synechocystis sp. (st	19,12	0,67	0,50	0,78	0,65	4,17E-04
P19125	NAD(P)H-quinone oxidoreductase subun	23,46	0,63	0,62	0,64	0,63	0,00E+00
P73004	Long-chain-fatty-acid CoA ligase OS=Syne	5,89		0,71	0,55	0,63	3,29E-04
P73807	Histidinol-phosphate aminotransferase C	27,79	0,39	0,55	0,94	0,63	3,53E-02
P73321	Uncharacterized protein slr1894 OS=Syn	49,36	0,37	0,61	0,90	0,63	3,84E-02
Q55410	Sll0540 protein OS=Synechocystis sp. (str	5,21	0,40	0,70	0,75	0,62	7,09E-03
Q55233	Protein DrgA OS=Synechocystis sp. (strai	39,05	0,87	0,46	0,52	0,61	7,02E-03
P72662	Cysteine synthase OS=Synechocystis sp.	24,62	0,84	0,59	0,38	0,61	1,54E-02
P74591	Shikimate dehydrogenase OS=Synechocy	16,21	0,69	0,52		0,61	2,81E-04
P09190	Cytochrome b559 subunit alpha OS=Syne	32,1	0,47		0,73	0,60	1,49E-02
P73720	Putative OxPP cycle protein OpcA OS=Syn	6,95	0,73	0,61	0,45	0,60	1,85E-04
Q55776	Sll0180 protein OS=Synechocystis sp. (str	11,98	0,71	0,56	0,47	0,58	2,18E-06
Q55199	Phosphate-binding protein OS=Synechoc	31,33	0,35	0,55	0,81	0,57	1,06E-02
Q55727	Slr0645 protein OS=Synechocystis sp. (st	57,77	0,27	0,61	0,83	0,57	4,73E-02
P32422	Photosystem I iron-sulfur center OS=Syn	65,43	0,44	0,59	0,67	0,57	4,10E-06
P74416	Glycine dehydrogenase (decarboxylating	6,51	0,42	0,66	0,60	0,56	1,70E-05
Q55835	Iron uptake protein A2 OS=Synechocystis	31,5	0,38	0,38	0,88	0,55	1,51E-02
Q55513	4-hydroxy-tetrahydrodipicolinate syntha	8,31	0,60	0,47		0,53	1,45E-07
P09192	Photosystem II D2 protein OS=Synechocy	10,8	0,75	0,37	0,47	0,53	1,05E-03
Q55865	Sll0585 protein OS=Synechocystis sp. (str	11,11	0,32	0,67	0,59	0,53	2,09E-03
P73511	Glycogen phosphorylase OS=Synechocys	32,51	0,38	0,43	0,76	0,52	1,08E-03
P16033	Photosystem Q(B) protein 2 OS=Synecho	16,67	0,82	0,37	0,38	0,52	5,40E-03
P73527	6,7-dimethyl-8-ribityllumazine synthase	29,27	0,37	0,68	0,44	0,50	6,33E-05
Q55517	Sll0529 protein OS=Synechocystis sp. (str	36,25	0,49	0,47	0,51	0,49	0,00E+00
P72939	Alkaline phosphatase OS=Synechocystis s	11,36	0,28	0,51	0,67	0,49	2,31E-03
P80046	Isocitrate dehydrogenase [NADP] OS=Syn	27,58	0,28	0,48	0,68	0,48	2,11E-03
Q55200	Protein SphX OS=Synechocystis sp. (strai	17,26	0,37	0,45	0,62	0,48	5,01E-07
P74338	NAD(P)H-quinone oxidoreductase subun	23,97	0,28	0,56	0,55	0,46	2,57E-04
P73914	Squalene-hopene-cyclase OS=Synechocys	10,36	0,30	0,43	0,61	0,45	2,70E-05
P74771	NAD(P)H-quinone oxidoreductase subun	40,28	0,45	0,45	0,44	0,44	0,00E+00
P73393	Sll1734 protein OS=Synechocystis sp. (str	16,71	0,57	0,41	0,36	0,44	2,01E-09
P73599	Uncharacterized protein sll1304 OS=Syne	11,15	0,48	0,37	0,47	0,44	0,00E+00
Q55196	Phosphate import ATP-binding protein P	25,65	0,55	0,36	0,40	0,43	3,30E-11
P72646	Sll1054 protein OS=Synechocystis sp. (str	9,09	0,26	0,61		0,43	2,94E-02
P72647	Sll1053 protein OS=Synechocystis sp. (str	7,31	0,19	0,39	0,65	0,41	4,75E-03
P73618	Deoxyribose-phosphate aldolase OS=Syn	10,22	0,37	0,44		0,40	0,00E+00
P72891	Slr1613 protein OS=Synechocystis sp. (st	12,76	0,27		0,51	0,39	1,84E-03
P74474	D-alanyl-D-alanine carboxypeptidase OS-	14,25	0,30	0,34	0,52	0,39	6,32E-09
Q55198	Phosphate transport system permease p	5,05		0,39	0,38	0,38	0,00E+00
P74250	Hydroperoxy fatty acid reductase gpx1 O	16,57	0,21	0,40	0,42	0,34	8,15E-07
P73954	Membrane-associated protein slr1513 O	48,18	0,16	0,35	0,48	0,33	2,10E-04
P72938	Extracellular nuclease OS=Synechocystis	6,55	0,16	0,33	0,51	0,33	4,25E-04
P73066	Ycf23 protein OS=Synechocystis sp. (stra	12,9	0,42	0,26	0,30	0,33	1,78E-14
P73862	Rubisco operon transcriptional regulator	14,24	0,48	0,15	0,27	0,30	9,28E-05
P72827	Iron uptake protein A1 OS=Synechocystis	39,44	0,18	0,24	0,38	0,27	3,47E-10
P73866	Potassium-transporting ATPase A chain C	4,84	0,54	0,09	0,13	0,25	2,01E-03
P27319	Flavodoxin OS=Synechocystis sp. (strain I	11,18	0,15	0,16	0,42	0,24	2,86E-06
P73867	Potassium-transporting ATPase B chain C	15,36	0,42	0,10	0,12	0,21	8,38E-05
P74625	Phycobilisome rod-core linker polypeptid	24,1	0,16	0,16	0,25	0,19	0,00E+00

CHAPTER 2

A conformational study of the GTPase domain of [FeFe]-hydrogenase maturation protein HydF, by PELDOR spectroscopy

[FeFe]-hydrogenases catalyze the reversible interconversion of protons to molecular hydrogen (H_2) at an active site called H-cluster. Their complex maturation pathway involves three proteins, HydE, HydF and HydG. It has been suggested that HydF interacts with HydE and HydG and, as a carrier, that it transfers the complete H-cluster to the hydrogenase; however, the exact molecular mechanism driving this translocation remains unclear. HydF is constituted by three different domains: a N-terminal GTP-binding domain, a dimerization domain and a C-terminal [4Fe4S]-cluster binding domain. To investigate possible conformational changes induced by the GTP binding in the N-terminal domain, we have expressed, in E. coli, a recombinant HydF protein from T. neapolitana including the GTP-binding domain only. Site-directed mutants were designed in which the native residues were substituted by cysteines and subsequently spin-labeled with the nitroxide MTSSL. CW-EPR was used to study the local mobility of the nitroxides at each site, and double spin labeled mutants have been investigated by PELDOR spectroscopy. We found that the binding of the nucleotide does not induce large conformational effects within the isolated GTP domain. However, the observed small changes in the distance between spin labels could affect the dimer form adopted by the whole HydF protein in solution and, as a consequence, the interactions with the other maturases.

Chapter 2 is adapted from: Maso L., Galazzo L., Vallese F., Di Valentin M., Albertini M., De Rosa E., Giacometti G. M., Costantni P., Carbonera D. (2015*). A conformational study of the GTPase domain of [FeFe]-hydrogenase maturation protein HydF, by PELDOR spectroscopy*. In press in Applied Magnetic Resonance, DOI: 10.1007/s00723-015-0641-z

Introduction

As assessed above, [FeFe]-hydrogenases are metalloenzymes, found both in bacteria and eukaryotes (Vignais P.M. and Billoud B., 2007) that catalyze the reversible interconversion of protons to molecular hydrogen (H_2) at a very complex active site, referred to as the H-cluster. The structure of this 6Fe-cluster has been determined by X-ray crystallographic analysis (Peters J.W. et al., 1998; Nicolet Y. et al., 1999). Extensive research is beginning to define the catalytic mechanism of the [FeFe]-hydrogenases (Lubitz W. et al., 2014), however, it still remains unclear how the H-cluster is formed within the cell. To date only a partial knowledge of the machinery driving its assembly *in vivo* is available (Lubitz W. et al., 2014; Shepard E.M. et al., 2014; Peters J.W. and Broderick J.B., 2012). This pathway involves three proteins: HydE and HydG, that are both radical S-adenosylmethionine (SAM) enzymes (Posewitz M.C. et al., 2004; Ruback J.K. et al., 2005), and HydF, a GTPase containing a FeS cluster binding motif (Posewitz M.C. et al., 2004; Brazzolotto X. et al., 2006). Different models have been proposed to describe the maturation pathway involving these proteins. Several *in vitro* and/or cell-free experiments using purified recombinant proteins led to a two-step model (Shepard E.M. et al., 2014; Peters J.W. and Broderick J.B., 2012), in which first HydE and HydG drive the chemical modifications of a H-cluster precursor working on HydF as a scaffold protein, and then HydF transfers this cluster to the hydrogenase (HydA) completing the maturation process (McGlynn S.E. et al., 2008; Mulder D.W. et al., 2010; Czech I. et al., 2011). However, the exact molecular mechanism that allows this traslocation from HydF is still under investigation and represents a key point to be elucidated in order to complete the knowledge of the [FeFe]-hydrogenases activation. The X-ray structure of the apo-HydF from *T. neapolitana* has been solved in our laboratory (PDB ID: 3QQ5) (Cendron L. et al., 2011), showing the presence of three different domains: a N-terminal GTP-binding domain (I), a dimerization domain (II) and a C-terminal metal-cluster binding domain (III). Moreover, the HydF GTPase activity, which has been shown to be essential for the H-cluster biosynthesis (Posewitz M.C. et al., 2004), has been fully characterized *in vitro* with recombinant proteins from different microorganisms (Brazzolotto X. et al., 2006; Shepard E.M. et al., 2010;

Vallese F. et al., 2012), but its exact contribution to the [FeFe]-hydrogenase maturation and activation is still elusive, and the role of GTP binding/hydrolysis remains uncertain. Since both HydE and HydG have been shown to increase by 50% the rate of GTP hydrolysis of a recombinant HydF protein from *C. acetobutylicum* (Shepard E.M. et al., 2010), it has been proposed that GTP binding and/or hydrolysis are associated with interactions of HydF with the other accessory proteins, rather than with the hydrogenase. Interestingly, we recently found that the binding of GTP (either as such or as non-hydrolyzable analogue) induces the dissociation of HydE and HydG from HydF (Vallese F. et al., 2012). Furthermore, the 3D structure of the apo-HydF protein showed that the GTPase domain includes a flexible loop region, which could in principle become ordered upon GTP binding (Cendron L. et al., 2011). This could in turn facilitate structural rearrangements driving the interactions of HydF scaffold with the two other maturation proteins. It has also been reported that the presence of GTP significantly affects the EPR spectral properties of the HydF FeS cluster (Shepard E.M. et al., 2010), suggesting a communication between the GTP and the iron-sulfur cluster binding domains, where the H-cluster precursor is probably finally assembled.

Prompted by these experimental evidences, we wanted to investigate possible intrinsic conformational changes induced by the nucleotide binding at the interface of the GTPase domain with either the [4Fe4S] cluster binding or the dimerization domains. For this purpose, in the present study, we have expressed in *E. coli* a recombinant HydF protein from *T. neapolitana* including only the GTP-binding domain. Five single site-directed mutants were designed in which the native amino acids were substituted by cysteine residues and subsequently spin-labeled with the thiol-selective reagent nitroxide MTSSL. CW-EPR was used to study the local mobility of the nitroxides in each site, and to choose the suitable positions for spin-labeled double mutants to be investigated by pulse electron-electron double resonance (PELDOR) spectroscopy, a technique that is known to be very useful for monitoring distances between couples of spin labels, in the nanometric scale.

Materials and Methods

Bacteria strains

E. coli

XL1-Blue: genotype *rec*A1, *end*A1, *gyr*A96, *thi*-1, *hsd*R17, *sup*E44, *rel*A1, lac [F´ proAB *lac*I^q ZΔM15 Tn10 (Tetr)]

Rosetta(DE3)pLysS: F^- genotype, *omp*T, *hsd*S_B(R_B^- m_B^-), *gal*, *dcm* λ; (DE3 [lacI lacUV5-T7 *gene* 1 *ind*1 *sam*7 *nin*5]); (pLysSRARE [Cam^R and genes for the tRNA: *arg*U, *arg*W, *ile*X, *gly*T, *leu*W, *pro*L, *met*T, *thr*T, *tyr*U e *thr*U, that supply the rare codons AGG, AGA, AUA, CUA, CCC and GGA])

Bacteria colture media

Luria-Bertani (LB): see Chapter 1.

When necessary, the antibiotic kanamycin (50 μg/ml) was added to select bacteria transformed with the pET-28a(+) plasmid that carries the kanamycin resistance, and chloramphenicol (34 μg/ml) to allow exclusively the growth to Rosetta(DE3)pLysS cells carrying the resistance for this antibiotic.

SOC: see Chapter 1.

Plasmids

pET-28b(+) (Novagen)

The pET-28a(+) is a plasmid vector for the expression of proteins in bacteria. It brings a kanamycin resistance (Kan^r) and the T7 phage promoter. It also has a His-Tag/thrombin/T7-tag at the N-terminus and a His-Tag at the C-terminus to facilitate purification, by affinity chromatography, of the protein of interest encoded by the gene cloned into the plasmid. The map of the plasmid is shown in figure 35.

.

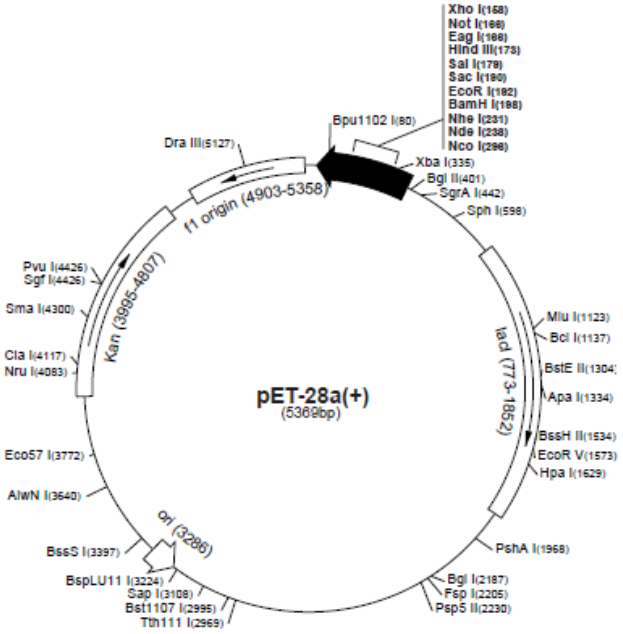

Figure 35. Circular Map of the plasmid pET-28b(+).

Bacteria transformation (*E. coli*): see Chapter 1.

DNA electrophoretic running on agarose gel: see Chapter 1.

DNA extraction from agarose gel: see Chapter 1.

Purification of plasmid DNA from bacteria: see Chapter 1.

Nucleotide and amino acid sequences of the $HydF_{T.n.}$ GTPase domain

Wild type gene sequence encoding the GTPase domain of the maturase HydF from *T. neapolitana* ($HydF_{T.n.}$), in frame with the sequence coding for a hexahistidine epitope at the 5'-end. The start and stop codons are indicated in red whereas bases modified in the different mutants have been underlined in green (the remaining bases of codons involved in mutagenesis are underlined in black).

5′CATCATCATCATCATCACAGCAGCGGCCTGGTGCCGCGCGGCAGCCATATGAG
ACTGCCGGACGCCGGTTTCAGAAGATACATCGTTGTTGCGGGAAGAAGGAACGTT
GGAAAATCCTCTTTCATGAACGCCTTAGTTGGTCAGAACGTGTCCATCGTGAGCG
ATTATGCGGGAACAACGACCGATCCCGTCTACAAATCCATGGAACTTCATCCTAT
CGGTCCCGTCACCCTCGTGGACACCCCTGGACTCGACGACGTGGGAGAACTTGGA
AGACTGAGGGTAGAGAAGGCAAGGAGGGTGTTCTACAGGGCAGATTGTGGAATTC
TCGTGACAGACAGCGCACCAACTCCCTACGAAGACGACGTTGTCAATCTTTTCAA
AGAGATGGAAATTCCCTTCGTAGTTGTCGTAAACAAAATCGACGTTCTTGGAGAA
AAGGCCGAAGAGCTGAAGGGACTCTACGAAAGCCGTTACGAAGCGAAAGTACTCC
TTGTCTCGGCTTTGCAGAAAAAGGGATTCGACGATATCGGGAAGACCATCTCCGA
AATTCTTCCGGGTGATGAAGAGATTTAACTCGAG 3′

Amino acidic sequence of the wild type GTPase domain of $HydF_{T.n.}$ with the six histidines tag fused at the N-terminal. The amino acids modified in different mutants are underlined in green, in blue the amino acids involved in the GTP binding.

HHHHHHSSGLVPRGSHMRLPDAGFRRYIVVAGRRNVGKSSFMNALVGQNVSIVSD
YAGTTTDPVYKSMELHPIGPVTLVDTPGLDDVGELGRLRVEKARRVFYRADCGIL
VTDSAPTPYEDDVVNLFKEMEIPFVVVVNKIDVLGEKAEELKGLYESRYEAKVLL
VSALQKKGFDDIGKTISEILPGDEEI

Cloning of $HydF_{T.n.}$ GTPase domain

The sequence coding for the GTPase N-terminal domain (domain I, residues 1 to 185) of the HydF protein from *T. neapolitana* ($HydF_{T.n.}$I) was PCR amplified using as template a vector containing the *$hydF_{T.n.}$* gene, previously obtained in our laboratory (Cendron L. et al., 2011), and the following primers:

$HydF_{T.n.}$I for, 5’-CATATGAGACTGCCGGACGCCGGT-3’ and
$HydF_{T.n.}$I rev, 5’-CTCGAGTTAAATCTCTTCATC-3’.

These primers were designed to contain unique restriction sites allowing the directional subcloning of the amplified sequence in frame with a 6His-tag

sequence at the 5'-terminus in a pET-28b vector (from Novagen®) suitable for T7 driven expression in *E. coli*. The sequence and reading frame were confirmed by DNA sequencing (BMR Genomics, University of Padova). The *pET-28b/hydF$_{T.n.}$I* plasmid was used as template to introduce different mutations in the wild type *hydF* coding sequence (see below).

Heterologous expression of HydF$_{T.n}$ GTPase domain.

E. coli Rosetta (DE3) cells were transformed with the *pET-28b/hydF$_{T.n.}$I* plasmid, and positive clones were selected by antibiotic resistance. Transformed cells were grown overnight in selective LB medium and then subcultured the following day in fresh medium. The expression of the 6His-tagged HydF$_{T.n.}$I proteins, either wild type or mutant, was induced by adding 1 mM isopropyl-β-thiogalactopyranoside (IPTG) in LB medium and incubating the cells at 30 °C overnight.

French Pressure Cell Press

At the end of induction cells were harvested at 5000 x *g* , for 10 minutes, at 4 °C. The pellet was resuspended in lysis buffer (25mM Tris-HCl pH 8, 200 mM KCl), adding the protease inhibitors: pepstatin A (1μg/ml), leupeptin (1μg/ml), and PMSF (phenyl-methyl-sulfonyl-fluoride) (3.3μg/ml), and lysed by French press performing a single cicle and applying a 1.35 kbar pressure.

Purification of HydF$_{T.n}$ GTPase domain

Following the French press, the obtained lysate was centrifuged to separate the supernatant, corresponding to the soluble protein fraction, from the pellet, which contains membranes residues, precipitated proteins and cellular debris. The presence of the protein of interest in the soluble fraction of the total lysate was checked by SDS-PAGE, as described in the following paragraphs, then it is was purified to homogeneity by combining a nickel affinity chromatography and a gel filtration chromatography.

Affinity chromatography

The ion metal affinity chromatography (IMAC) is based on the ability of the six histidines, fused to the polypeptide chain of the protein of interest (in our case at the N-terminal), to act as electron donors and reversibly bind the metal ion nickel (Ni^{2+}), which is immobilized by a chelating group NTA (nitrilotriacetic acid) on a matrix of agarose. The soluble fraction of cell lysate was added to the HIS-Select^{TM} Nickel Affinity Gel (SIGMA) resin, previously equilibrated with the lysis buffer (25 mM Tris-HCl pH 8, 200 mM KCl) and left to slowly stirring for one hour, at 4 °C. After the incubation, the suspension was transferred in the column and the resin allowed to pack by gravity. The resin was washed three times with 10 volumes of washing buffer (25 mM Tris-HCl pH 8, 200 mM KCl) and the protein was finally eluted with 8 volumes of elution buffer (25 mM Tris-HCl pH 8, 200 mM KCl and 300 mM imidazole).

Gel filtration FPLC (Fast Protein Liquid Chromatography)

Size exclusion was performed using Superose 12 10/300 GL (GE Healthcare Life Sciences) column. The fraction eluted from the affinity chromatography was concentrated to a volume slightly less than 500 µl using Vivaspin® Centrifugal Concentrators, 10,000 MWCO (Sartorius Stedim Biotech). The sample were then loaded into the loop and automatically injected into the column previously equilibrated in lysis buffer (25 mM Tris-HCl pH 8, 200 mM KCl). Each run was performed by injecting the appropriate sample volume at a flow rate of 0.75 ml/min and monitoring the UV absorbance at 280 nm, by a fixed wavelength detector. To estimate the molecular weight of the analyzed samples, the column was equilibrated in the lysis buffer and calibrated with the standards thyroglobulin (669,000 Da), ferritin (440,000 Da), catalase (232,000 Da), aldolase (158,000 Da), bovine serum albumin (67,000 Da), ovalbumin (43,000 Da), ribonuclease (13,700 Da). Proteins coming out were collected automatically from fractionator in aliquots of 500 µl. Samples of purified protein obtained after gel filtration were concentrated again with the concentrators described above to a volume suitable for EPR characterization (see below), giving rise to a final concentration ranging from 800 µM to 3 mM, as determined with a Micro BCA

Protein Assay Kit (from Thermo Scientific Pierce Protein Research). Purified proteins were analyzed by 12% SDS-PAGE.

Sample preparation for protein analysis

One ml of cells is taken from the liquid culture, and the optical density (OD_{600}) measured; the pellet obtained after centrifugation is resuspended in 1X SB buffer (62.5 mM Tris-HCl pH 6.8, 2% SDS, 10%glycerol, 5% β-mercaptoethanol, 0.1% blue bromophenol) in an amount equal to 100 µl for each unit of OD_{600}. Each sample is treated by adding SB buffer 2X and boiled for 10 minutes before gel electrophoresis.

Electrophoresis of proteins in polyacrylamide denaturing gel (SDS-PAGE)

Proteins are separated by polyacrylamide gel electrophoresis 12% in the presence of SDS. The separating gel (running gel) is composed of 12% acrylamide/0.4% bisacrilamide, 0.37 M Tris-HCl, pH 8.8, 0.1% SDS, and TEMED and APS as catalysts. The stacking gel is composed of 4% acrylamide, 0.125 M Tris-HCl pH 6.8, 0.1%, SDS to which TEMED and APS are added. The running buffer consists of 25 mM Tris-HCl pH 8.3, 192 mM glycine, 0.1% SDS. Electrophoresis was performed by applying a constant current of 20 mA before passing the stacking gel and of 30-35 mA in running gel. The separated proteins are then displayed on gel by Coomassie Brilliant Blue staining. The size of the protein bands are estimated by comparison with a marker of molecular weight.

Site-directed mutagenesis of $hydF_{T.n.}I$ sequence.

Site-directed mutagenesis of the *$hydF_{T.n.}$* gene was performed with the QuickChange® II Site-Directed Mutagenesis Kit (from Stratagene Agilent Technologies), using as template *pET-28b/$hydF_{T.n.}I$* recombinant plasmid. Oligonucleotides, listed in table 7, were designed according to the manufacturer's guidelines and the mutant constructs analyzed by DNA sequencing.

Primer name	Primer sequence
C91S_for	5′-TCTACAGGGCAGATTCTGGAATTCTCGTGAC-3′
C91S_rev	5′-GTCACGAGAATTCCAGAATCTGCCCTGTAGA-3′
M26C_for	5′-GTTGGAAAATCCTCTTTCTGCAACGCCTTAGTTGGTCAG-3′
M26C_rev	5′-CTGACCAACTAAGGCGTTGCAGAAAGAGGATTTTCCAAC-3′
R84C_for	5′-TGAGGGTAGAGAAGGCAAGGTGCGTGTTCTACAGGGCAGATTG-3′
R84C_rev	5′-CAATCTGCCCTGTAGAACACGCACCTTGCCTTCTCTACCCTCA-3′
A15C_for	5′-GAAGATACATCGTTGTTTGCGGAAGAAGGAACGTTGG-3′
A15C_rev	5′-CCAACGTTCCTTCTTCCGCAAACAACGATGTATCTTC-3′
T164C_for	5′-GATTCGACGATATCGGGAAGTGCATCTCCGAAATTCTTCCGGG-3′
T164C_rev	5′-CCCGGAAGAATTTCGGAGATGCACTTCCCGATATCGTCGAATC-3′
R88C′_for	5′-GGCAAGGTGCGTGTTCTACTGCGCAGATTGTGGAATTCTCG-3′
R88C′_rev	5′-CGAGAATTCCACAATCTGCGCAGTAGAACACGCACCTTGCC-3′

Table 7. List of primers used in this study. The modified bases are underlined

GTP hydrolysis assay.

The purified recombinant wild type $HydF_{T.n.}I$ protein was assayed for the ability to hydrolyze GTP using the protocol optimized by Shepard and co-workers (2010), with slight modifications. Briefly, the affinity purified protein was incubated at a concentration of 10 μM for 10 minutes at 30 °C in 20 mM Tris-HCl buffer, pH 8.0, containing 200 mM KCl and 2 mM $MgCl_2$ with different concentrations of GTP (ranging from 125 μM to 2 mM). Aliquots with different concentrations of substrate were collected and assayed for production of GDP. Assay aliquots were incubated at 95 °C for 3 minutes, centrifuged at 14,000 rpm at 4 °C in a benchtop microcentrifuge, and the supernatants analyzed by reverse phase HPLC on a Synergi MAX-RP 80A (150 × 4.6 mm, 4 μm, Phenomenex). The samples were eluted with an isocratic mobile phase of 50 mM sodium phosphate buffer, pH 7.0, 10 mM tetrabutylammonium bromide, 10% CH_3CN. The guanosine nucleotides were detected by their absorbance at 254 nm. Under

these conditions, GDP and GTP were eluted after 8.1 and 18.6 min, respectively. Integration of peak areas (using software Agilent Chemstation) of the samples taken at identical time points allowed the quantification of the μmoles of GDP produced L^{-1} min^{-1}, from which the ratio between the k_{cat} were finally determined.

EPR (Electron Paramagnetic Resonance)

The magnetic resonance spectroscopy of electron spin EPR (Electron Paramagnetic Resonance) is a technique that allows to detect and characterize species containing unpaired electrons, such as free radicals, photoexcited states, metal complexes. This technique is also applicable to the study of substances not intrinsically paramagnetic, through the use of spin labels (the most used is the MTSSL described below) appropriately inserted in macromolecules of interest. A very advantageous aspect of this technique is that it can be used for structure and conformation analysis in non denaturing conditions, in solution, without the need of complex processes such as the crystallization. Several EPR techniques exist, in this work the CW-EPR and DEER have been used. Samples were analyzed in the absence and in the presence of the non-hydrolysable GTP analog, GTPγS (Jena Bioscience), to a concentration of 50 mM (with $MgCl_2$ 10 mM), incubating for 10 minutes at 30 °C under stirring, before the EPR analysis, or freezing in the case of DEER analysis.

The instrument used for the EPR is illustrated in figure 36 and is composed by: a magnet that generates the field necessary to separate the electronic spin levels, a resonant cavity, where the microwaves are sent and the sample is placed, a microwave bridge, which contains the source of radiation, the detector and a console for the electronic management of the experiment and data processing. In the case of pulsed spectroscopy, as for the DEER technique used in our experiments, it is necessary to have a unit for the impulses formation. The instrument is also equipped with liquid helium cryostat to maintain the sample at low temperatures, where necessary, in order to slow down as much as possible protons relaxations that make criticism signal detection.

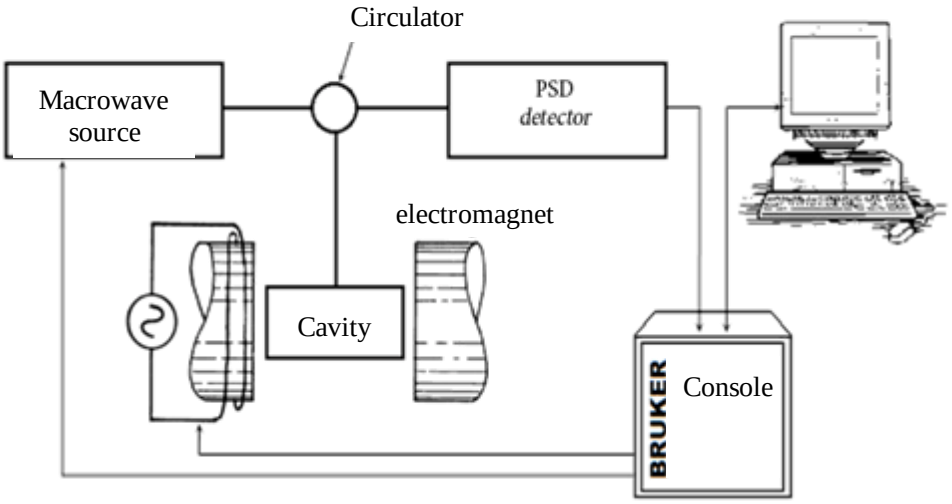

Figure 36. Schematic block diagram of a EPR CW instrument.

Proteins labeling with spin label MTSSL

Proteins intrinsically non paramagnetic are detectable by EPR spectroscopy, thanks to spin probes, *i.e.* species containing unpaired electrons. This process, called spin labeling, allows to exploit the thiol group of cysteine residues naturally present in the proteins or inserted by site-specific mutagenesis, to bind subsequently, by disulfide bound, different types of nitroxides, species containing an unpaired electron localized in the •NO group; the residues are thus marked with a spin probe. This process requires cysteines only in the desired sites and any other cysteine present is usually replaced with serine or alanine. The most used spin label is the nitroxide MTSSL ((1-Oxyl-2,2,5,5-tetramethylpyrroline-3-methyl) methanethiosulfonate) (Enzo Life Sciences), thanks to its specificity for the thiol group, its compact volume, similar to that of a side chain of a tryptophan residue, and its flexibility that allows labeled proteins to maintain the native conformation. The reactions of the site-specific spin labeling are shown in figure 37.

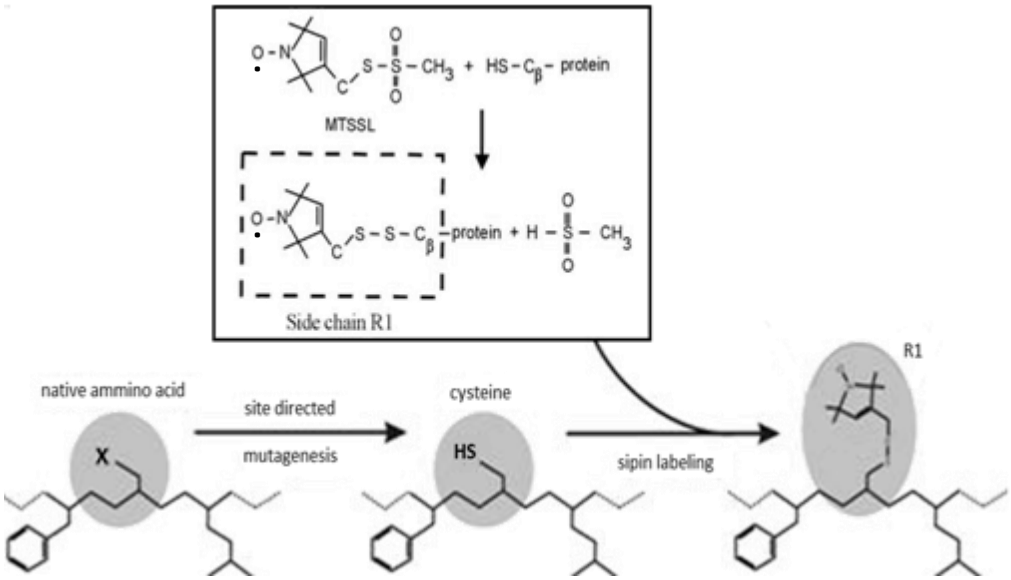

Figure 37. Diagram representing the spin labeling specific site process. In the high box the spin probe MTSSL and its binding reaction to cysteine residue.

The spin label is dissolved in DMSO (dimethyl sulfoxide) and not in aqueous solvent to avoid its dimerization in the mother solution

- CW-EPR (Continuous Wave Electron Paramagnetic Resonance)

In this technique, the sample is irradiated with electromagnetic radiation with fixed frequency microwave of about 9 GHz, while the intensity of a static magnetic field is varied continuously. The resonance conditions are reached when the energy difference between levels of electron spin determined by the static magnetic field and the characteristics of the sample equals the energy associated with microwave radiation. Thanks to this technique, it is possible to obtain informations on the dynamics of the spin probes in the interested species. The shape of the spectrum obtained, in fact, is strongly influenced by the orientational motion of the spin probe, and as a result of its mobility and its around. The spectra associated with spin probes-containing nitroxides are more enlarged and with pronunced variations in the intensity of the peaks as the nitroxides lose mobility,

instead they present three narrow peaks when the spin probe is free, as shown in figure 38.

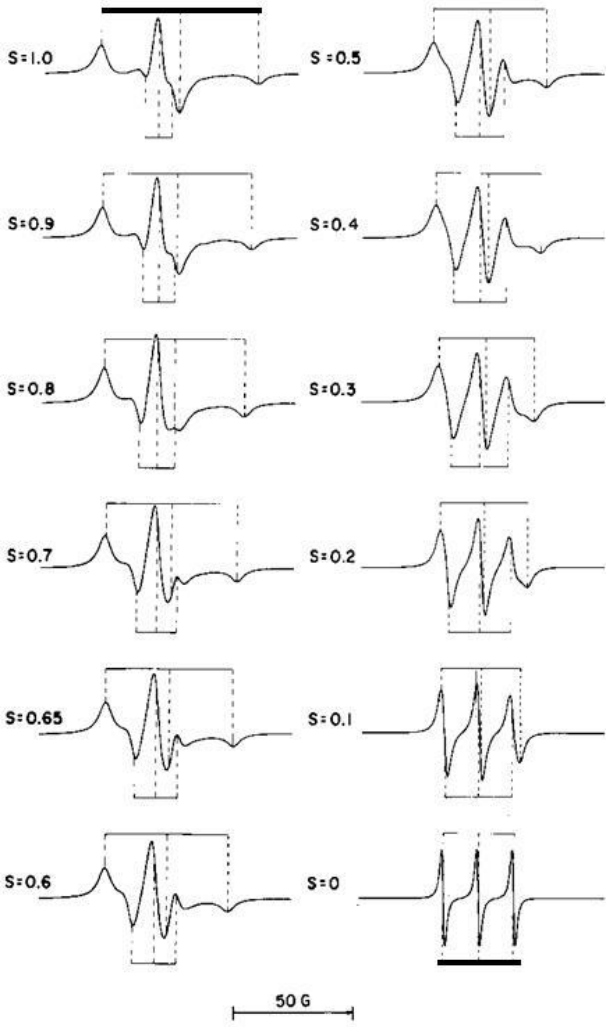

Figure 38. **Changes in the EPR spectrum in continuous wave of a nitroxide**. Spectra with decreasing S parameter, index of mobility of the probe at the site where it is located. S value = 1 when the probe is immobile (*above*); S = 0 when the probe is completely free to move (*below*).

Samples for EPR (about 100 μM protein labeled with MTSSL spin label in lysis buffer) were obtained by adding to the purified protein a fivefold molar excess of MTSSL (dissolved in DMSO) and incubating the protein at 4 °C overnight in the dark. Excess of non-ligated spin label was removed from the protein by several cycles of dilution with the lysis buffer and concentration by centrifugal filters. Twenty microliters of each sample with a protein concentration of about 150 μM, were loaded into quartz capillaries with 0.6 mm ID and 0.8 mm OD. Non-hydrolyzable GTP analogous (GTPγS, 50 mM) and 10 mM MgCl were added to

the samples and incubated 30 min at 37 °C before starting the EPR measurements. EPR spectra were collected at room temperature (298 K) on an Elexsys E580 Xband spectrometer (Bruker) using a Super High Sensitivity cavity. The field modulation frequency was set at 100 kHz, with a field modulation amplitude of 0.03 mT and a microwave power of 6.4 mW. Simulations of the CW-EPR spectra were performed using the EasySpin function"chili" to obtain the correlation times for the nitroxide in the different mutants (Stoll S. and Schweiger A., 2006). Rotamers of the spin label in the different mutated sites were evaluated, starting from the X ray structure, using the molecular modeling software MMM2013 (Polyhach Y. et al., 2010). The EPR measurements were performed at the Department of Chemical Sciences of Padua, in collaboration with Prof. Donatella Carbonera.

- D.E.E.R. (Double Electron-Electron Resonance)

The DEER or PELDOR (pulse electron–electron double resonance) technique is more complex and is able to provide information on the distances between spin probes (between 17 Å and 80 Å), thanks to weak dipolar interactions between the spin. The technique is often used for proteins bis-labelled with nitroxides, in order to measure significant distances between them. For the realization of an experiment of pulsed EPR the same CW-EPR apparatus is used, equipped with a unit for the formation of pulses and an additional source of microwave, thanks to which two different populations of spin are excited. Measures of distances are derived from the intensity of the dipolar interactions. This is possible because there is a correlation between the intensity of these interactions and the distance where the two spin interacting are, *i.e.*:

$$D = f\,(1 / r3)$$

where D is the dipolar interaction, r is the distance between the spin and f is a function of dipole moments and the permeability of space. The DEER signal (figure 39, left panel) is given by two components: the stress relaxing due to to the intermolecular interactions between unpaired spin (background signal), and

periodic oscillations generated by intramolecular interactions of spin. From frequency oscillations, which reflect the strength of the dipolar interaction between the two populations of spin, by suitable elaboration, the distance between the spin probes inserted in the examined species is obtained.

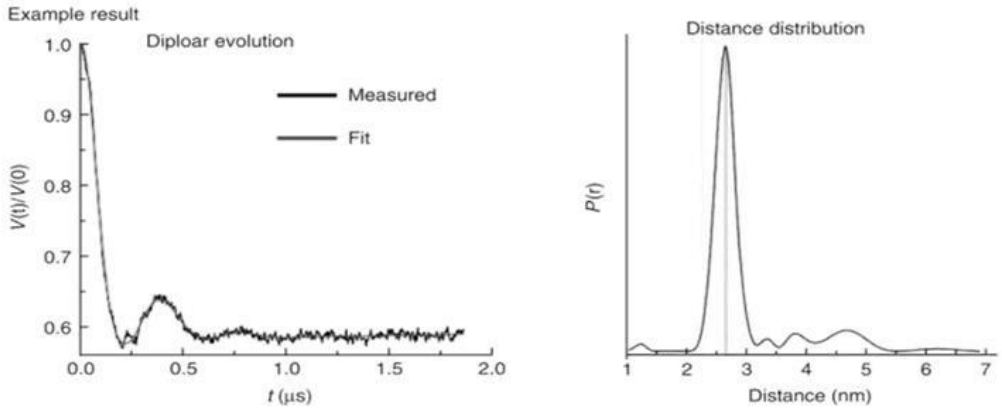

Figure 39. DEER experiment carried out on a protein bis-labelled. On the *left panel* the signal DEER normalized at t = 0, with phase and base line correction and with the best fitting. Processing the time-dependent trace is obtained the distribution of the distances between the spin probes (*right panel*).

Samples for PELDOR analysis were concentrated and exchanged with deuterated buffer. Deuterated glicerol (40% w/v) was also added to the samples before freezing. The final protein concentration was about 300 μM for all the samples. In the nucleotide binding experiments, 50 mM GTPγS and 10 mM $MgCl_2$ were added to the samples and incubated 30 minutes at 37 °C before freezing. Pulsed EPR was performed with the same EPR spectrometer equipped with a Bruker split-ring resonator ER4118X-MS3 (microwave frequency = 9.55 GHz) and an Oxford CF935 cryostat. The measurements were done at a temperature of 50 K. For PELDOR experiments, a standard four pulse sequence was applied; the microwave power was adjusted to obtain an observer sequence of 16/32/32 ns and a pump pulse of 16 ns. Samples were loaded into quartz capillaries with 2.0 mm ID and 3.0 mm OD. The difference between the pump (nitroxide) and observer (nitroxide) frequency was set to 70 MHz. A two-step phase cycle was applied for base-line correction while deuterium nuclear modulations were suppressed using an 8 step τ cycle from a 180 ns starting value with 56 ns increment steps. Data on each sample were collected for about 15 hours. Distance distributions were

extracted from PELDOR experiments by using DeerAnalysis2013 (Tsvetkov Y.D. et al., 2008). The measurements were performed at the Department of Chemical Sciences of Padua, in collaboration with Prof. Donatella Carbonera.

Results

As assessed in the Introduction, an active HydF GTPase domain is essential to produce a functional [FeFe]-hydrogenase, both *in vivo* and *in vitro* (Posewitz M.C. et al., 2004; King P.W. et al., 2006). However, the role of GTP binding and/or hydrolysis in the H-cluster assembly is still elusive. To explore the dynamic behavior required for the HydF scaffold/carrier role in the [FeFe]-hydrogenase maturation, we obtained a recombinant $HydF_{T.n.}$ protein including only its GTPase domain (domain I, residues 1-185), *i.e.* $HydF_{T.n.}I$, and analyzed by EPR spectroscopy several spin-labeled mutants where cysteine residues were introduced at proper sites by site-directed mutagenesis. The selected sequence includes the five consensus motifs shared by all NTPases and essential to bind and hydrolyze GTP (*i.e.* P-loop: GRRNVGKS, and G2 to G4 loops: TTT, DTPG and NKID, respectively, were the conserved amino acids underlined (figure 40), and a short extra stretch of residues belonging to the loop between domains I and II has also been conserved in the construct.

MLEDPRRYTMRLPDAGFRRYIVVAGRRNVGKSSFMNALVGQNVSIVSDYAGTTTD
PVYKSMELHPIGPVTLVDTPGLDDVGELGRLRVEKARRVFYRADCGILVTSAPTP
YEDDVVNLFKEMEIPFVVVVNKIDVLGEKAEELKGLYESRYEAKVLLVSALQKKG
FDDIGKTISEILPGDEEI

Figure 40. Consensus sequences of the $HydF_{T.n.}$ GTPase domain involved in the binding of GTP. GRRNVGKS: sequence responsible for the binding of α and β phosphates of GTP (P-loop); TTT: one of these three residues correspond to the conserved threonine in the G2-loop involved in the binding of Mg^{2+}; DTPG: it forms the G3-loop involved in the interaction with the GTP γ phosphate and Mg^{2+}; NKID: G4-loop,which is supposed to interact with the GTP; moreover TSA: G5-loop, it recognizes the base (guanine) of GTP.

Heterologous expression, purification and preliminary biochemical characterization of wild type $HydF_{T.n.}I$.

The recombinant protein $HydF_{T.n.}I$ was expressed in *E. coli* Rosetta (DE3) cells in frame with a 6His-tag at the N-terminus, as described in the Materials and

Methods, and purified by combining a NiNTA affinity and a gel filtration chromatography. A shown in figure 41, the isolated domain I can be indeed purified to homogeneity (lane 7) and as a single monomeric species, as assessed by the gel-filtration chromatogram (figure 42, red curve).

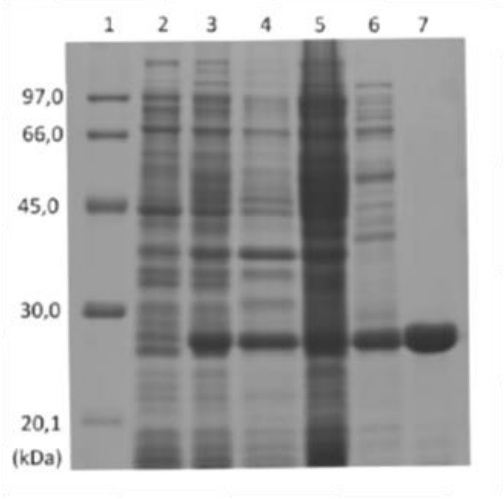

Figure 41. Expression and purification by affinity chromatography and gel filtration of the $HydF_{T.n.}$ GTPase domain. *Lane 1*, molecular weight markers; *lane 2*, not induced strain; *lane 3*, induced strain; *lane 4*, insoluble protein fraction (5 µl); *lane 5*, soluble protein fraction (10 µl); *lane 6*, protein fraction purified by affinity chromatography (20 µl); *lane 7*, protein fraction purified by affinity chromatography and gel filtration and reconcentrated (20 µl). SDS-PAGE, 12% poliacrylamide gel, stained with Coomassie Brilliant Blue.

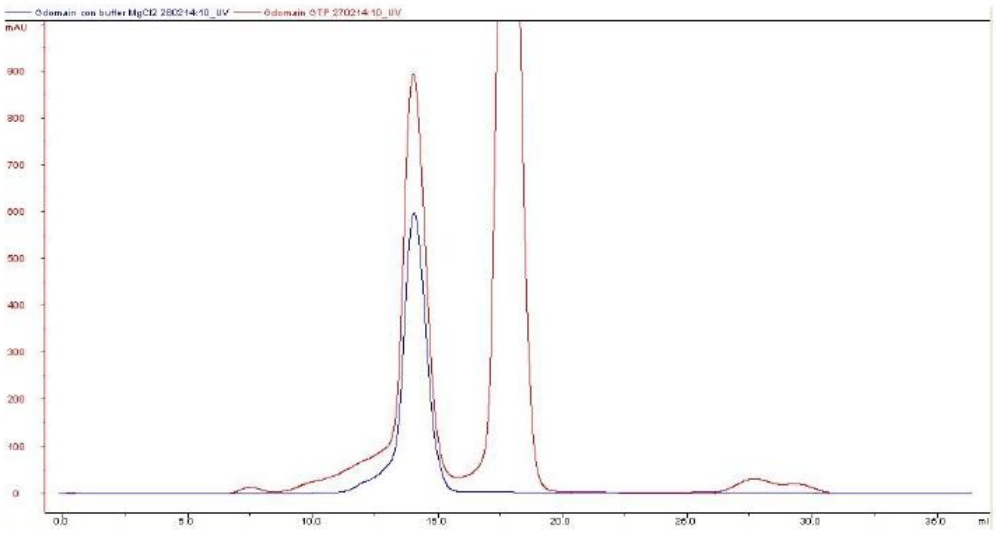

Figure 42. Gel filtration chromatographic profiles of $HydF_{T.n.}$ GTPase domain incubated in the presence (red curve) and in the absence (blue curve) of GTPγS. The overlapping of the two chromatograms shows that in both cases only one species is present. The peak relative to the elution volume of about 18 ml corresponds to GTPγS.

The same elution profile has been obtained in the presence of GTPγS (figure 42, blue curve) at the same concentration used for the following spectroscopic analysis (*i.e.* 50 mM).

The capability of this protein to bind and hydrolyze GTP has been then evaluated, as described in Materials and Methods, and compared with activity of the full-length protein, previously characterized in our laboratory. As reported in table 8, the isolated domain, obtained in a soluble form, keeps indeed its capability of GTP hydrolysis. According to the measurements, in the isolated domain the catalytic rate constant (k_{cat}) increases about ten times when compared to that the whole protein, which is comparable to that reported before for the HydF proteins from *T. maritima* and *C. acetobutilycum* (Brazzolotto X. et al., 2006; Shepard E.M. et al., 2010). The higher enzymatic activity of the isolated domain is likely due to a higher accessibility of the active site.

Protein	**[GTP]**	**k_{cat} (min^{-1})**
$HydF_{T.n.}$ (full-length protein)	62 μM–2 mM	1.13 ± 0.08
$HydF_{T.n.}$ I (GTPase domain)	125 μM–1.5 mM	11.2 ± 0.6

Table 8. Rate constant of GTP hydrolysis by HydF proteins from *T. neapolitana.*

Site-directed spin-label of $HydF_{T.n.}I$

A close look to the HydF GTPase domain suggested several useful positions for cysteine residues to be introduced and derivatized using thiol-specific spin labels. The wild type domain contains a single cysteine (*i.e.* C91), depicted in red in the X-ray structure of the whole $HydF_{T.n.}$ protein shown in figure 43.

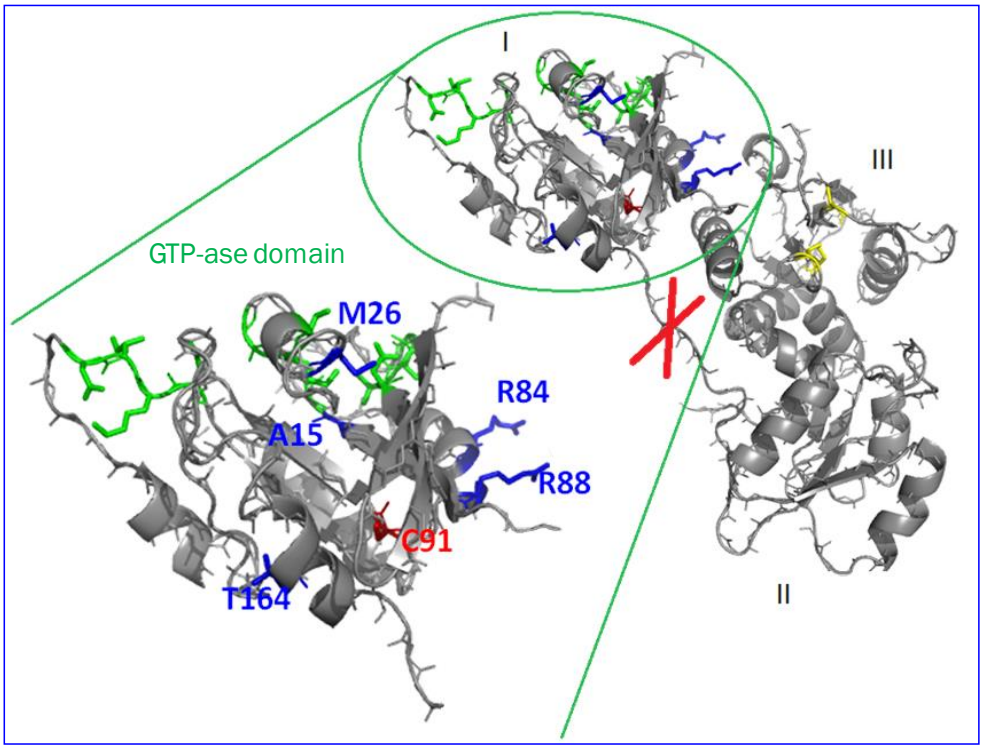

Figure 43. Structure of HydF protein (PDB code 3QQ5) showing the mutated residues in the single cysteine mutants of the GTP domain (I) circled. *Green sticks* correspond to residues involved in GTP binding. Circled and enlarged in *green* is the GTPase domain.

Five additional sites were chosen to introduce the cysteine residues to evaluate the potential effect of GTP binding on the protein conformation, *i.e.*: residues A15 and M26, close to the GTP-binding site; residues R84 and R88, located at the interface of domain I and III; and residue T164, which belongs to the terminal part of an α-helix connecting domain I and II via a long loop. The positions of the five residues selected to introduce new cysteines are highlighted in blue in figure 43, which also reports the cutting site in the long loop connecting domain I with domain II (red cross). To obtain single labeled species and evaluate the spin labeling efficiency at each site, the native cysteine C91 was first substituted by serine (C91S) in all the mutants.

All new recombinant mutant proteins were assayed for the expression in *E. coli* and solubility, and purified by the double chromatography approach described above (figure 44).

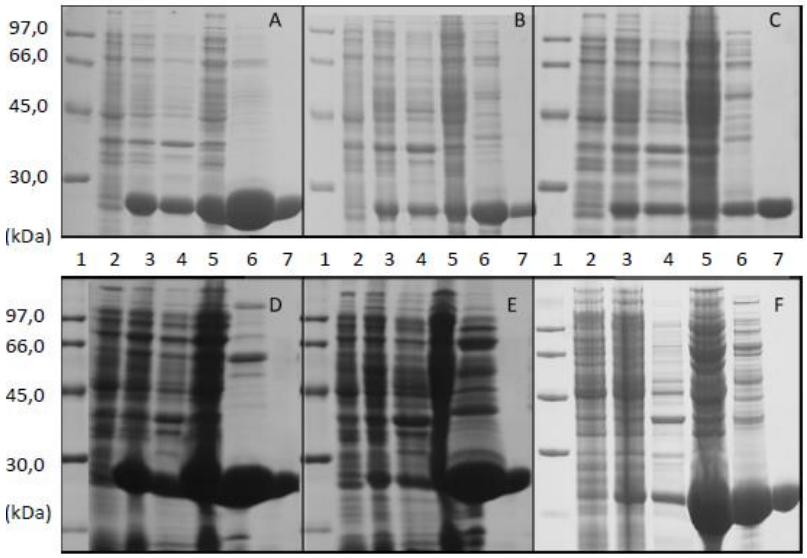

Figure 44. Expression and purification to homeogeneity in *E. coli* of the wild type and mutant GTPase domain of $HydF_{T.n.}$. A, C91wild type protein; B, C15 mutant protein; C, C26mutant protein**;** D, C84 mutant protein; E, C88 mutant protein; F, C164 mutant protein. In all panels: *lane 1*, molecular weight markers; *lane 2*, not induced strain; *lane 3*, induced strain; *lane 4*, insoluble fraction of the total lysate (5 µl); *lane 5*, the soluble fraction of the lysate total (10 µl); *lane 6*, protein purified by affinity (20 µl); *lane 7*, purified protein by affinity and subsequent gel filtration (20 µl). SDS-PAGE, 12% acrylamide gels, stained with Coomassie Brilliant Blue.

Spin labeling of $HydF_{T.n.}$I wild type and mutant proteins and EPR analysis.

The wild type (containing C91) and the five mutant (A15C-C91S, M26C-C91S, R84C-C91S, R88C-C91S, T164C-C91S) proteins were labeled using the spin label MTSSL, as described in details in Materials and Methods. The labeling yield is reported in table 9 and was calculated by spin quantification of double integral of the EPR spectra of the samples in comparison with those of standard solutions of the free spin label MTSSL.

Mutant	Labeling yield (%)
WT (C91)	23
C15	40
C26	50
C84	40
C88	65
C164	46

Table 9. Spin-labeling yield, as percentage of labeled protein, of the wild type and mutant $HydF_{T.n.}I$ proteins.

In figure 45 the CW-EPR spectra of the single mutants, with the simulations (*chili* program (Polyhach Y. et al., 2010)) and the corresponding correlation times in each site are reported.

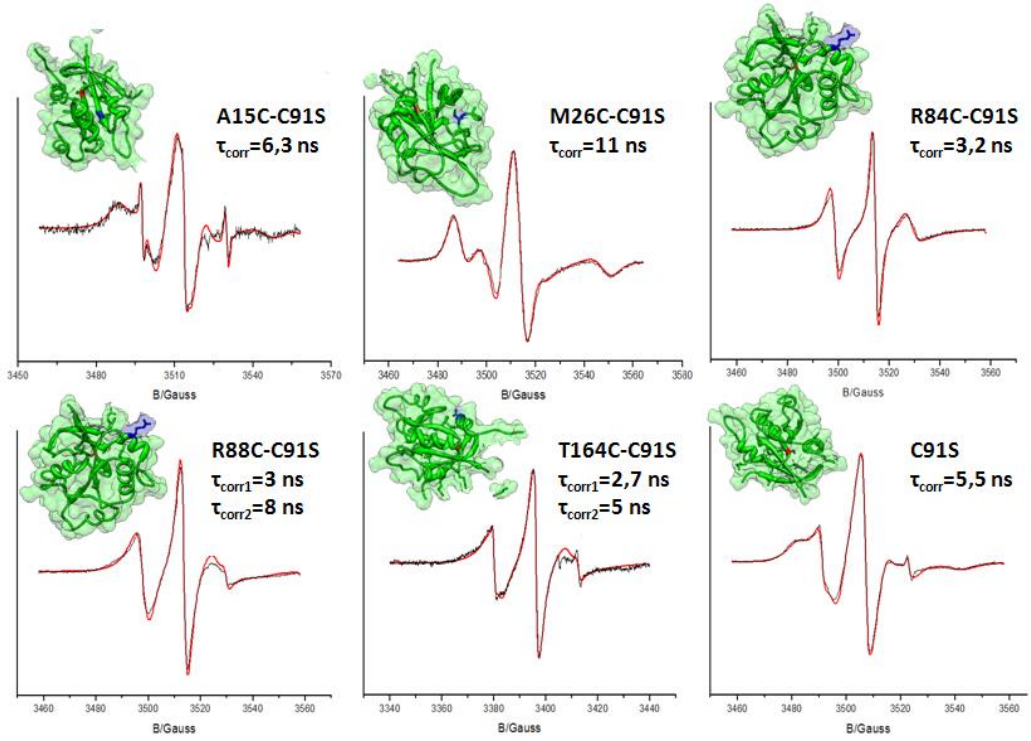

Figure 45: Room temperature experimental X band CW-EPR spectra (*black*) and simulations (*red*) of single-labeled samples. Positions of the labels in the protein sequence are indicated together with the correlation times derived from simulations. In the simulation of R88C-C91S and T164C-C91S, two components are present in relative amounts of 0.75:1 and 0.37:1, respectively. Small amount of free spin label is present in the C15 and C91 spectra (*narrow peaks*). Rotamers, calculated using the software MMM (Polyhach Y. et al., 2010), are shown as *red*/*blue balls* and *sticks*

The mobility of the nitroxides derived from simulations is in good qualitative agreement with the distributions of rotamers calculated with the software MMM (Polyhach Y. et al., 2010), starting from the crystallographic data, and is displayed in figure 45. In fact, as expected, nitroxides at positions R88, T164 and R84 possess high mobility, although an extra contribution of a slower component is required to simulate the spectra of T164 and R84, while those in the sites C91 and A15 are more buried and characterized by slow motion. Unexpectedly, the most

immobilized nitroxide, among the six selected positions, is found at position 26, the correlation time derived from the simulation of the EPR spectrum being very close to the estimated tumbling time of the protein in solution (11 ns). On the basis of the rotamers calculated with the software MMM at position 26, starting from the X-ray structure of the apo-protein, the nitroxide was expected to show high mobility at this site. However, residue 26 is located close to a protein portion (residues 32-44) which was not resolved in the X-ray structure and therefore was not included in the MMM calculations. This missing region in the diffraction map was suggested to correspond to a flexible loop (Cendron. L. et al., 2011). Therefore, it is likely that in solution this loop is largely responsible for the immobilization of the spin label at position 26.

Taken together the EPR data indicate that the isolation of the GTPase domain, from the rest of the HydF protein, does not alter the structure significantly. In all the mutant and wild-type samples, the addition of 50 mM GTPγS did not change the line shapes of the CW-EPR spectra (data not shown), indicating that the nitroxide mobility of the spin labels does not undergo dramatic changes upon GTP binding.

On the basis of the labeling yield of single mutants, the more suitable positions for a double labeling, necessary for PELDOR experiments, were chosen. The proteins containing the cysteines at positions either C91 or C84 were discharged because of the low labeling yield (C91) and tendency to dimerization (C84), respectively (not shown). Triple mutants (R88C-C91S-M26C and R88C-C91S-T164C) were produced, using, as template for the mutagenesis, the plasmid *pET-28b/hydF$_{T.n.}$I_C91S-R88C*, purified as described above, and after reaction with the spin label MTSSL double spin labeled samples were finally obtained. The PELDOR traces of M26C-R88C-C91S and R88C-C91S-T164C mutants, are shown in figure 46 a/b.

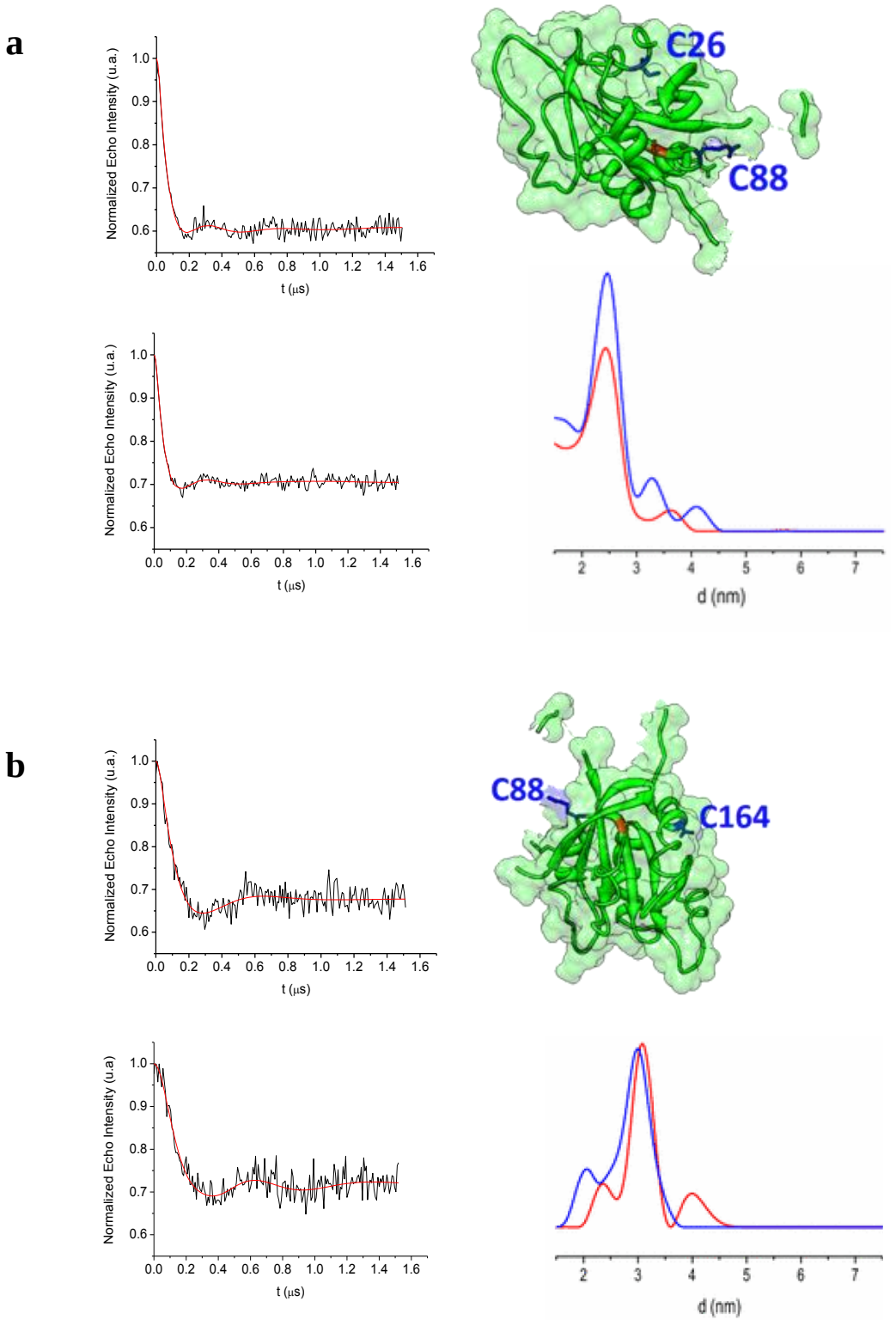

Figure 46. ***Left*****: background corrected PELDOR data for the M26C-R88C-C91S(a) andR88C-T164C-C91S(b) spin-labeled samples in the absence (*black, upper trace*) and after the addition of 50 mM GTPγS (*black, bottom trace*). *Right*: Tikhonov derived distance distributions for samples in the absence (*blue*) and in the presence (*red*) of the nucleotide analogous.** Double labeling positions are indicated in the protein structure.

Tikhonov-derived distance distributions provide main values which correspond, roughly, to those expected on the basis of the X-ray structure of the apo-HydF protein (*i.e.*, 1.9 and 2.1nm) measured at the α-carbon atoms for M26-R88 and R88-T164 couples, respectively) (Cendron L. et al., 2011). When the GTP analogous was added to the M26C-R88C-C91S sample (figure 46a), only very little differences at distances larger than 3.3 nm were detected. On the other hand, the distance distribution detected for R88C-T164C-C91S undergoes a higher effect upon GTPγS binding. In fact, a contribution centered at 4 nm appears, which was not present in the absence of the nucleotide and, at the same time, the two main distance distributions (at about 2.0 and 3.0 nm) shift toward longer distances (2.5 and 3.2 nm).

Discussion

The N-terminal GTPase domain of HydF is essential to its role in [FeFe]-hydrogenase maturation, since mutations in the Walker P-loop prevent the formation of an active HydA *in vitro* (King P.W. et al., 2006). It has been demonstrated that HydE and HydG increase the rate of GTP hydrolysis by 50% (Shepard E.M. et al., 2010), suggesting a direct interaction of HydF with the other accessory proteins, and that the binding of GTP during the dissociation of the HydE and HydG from HydF may have an effect on the interactions between the maturases (Vallese F. et al., 2012). Thus, the GTP binding and/or hydrolysis might be responsible for structural changes in HydF itself leading to a change in the interactions with HydG and/or HydE. With this working hypothesis, we have started a structural study in solution to monitor the intrinsic conformational changes of the isolated GTP binding domain of HydF, by EPR techniques. Indeed, as assessed above, the X-ray crystal structure of the apo-$HydF_{T.n.}$ suffers the lack of nucleotide, thus hindering a clarification of its binding effect on the protein structure.

The measurements of the GTPase activity and the analysis of the CW-EPR spectra of five single-labeled mutants as well as of the wild type domain carrying the native cysteine C91 show that the isolated domain maintains the functional

characteristics and the general structure of the whole protein. Some diagnostic positions for couples of spin labels have been designed to monitor, by PELDOR spectroscopy, the conformational changes at the interface regions of domains I with the other two domains of the whole HydF protein. The PELDOR results show that the distance between the residues 26 and 88, belonging to the protein region close to the GTP binding site and to the interface with the domain III, respectively, remains substantially unaffected upon binding of the nucleotide. Instead, an effect is found for the couple of spin labels at the 88 and 164 sites. In this case, the binding of the nucleotide induces an average increase of the distance, although the main component centered at 3.0 nm is only slightly affected. Since the labeled position 88 is common to both double mutants under investigation, it is likely that the protein rearrangement takes place mainly in the region close to T164, rather than to R88. Interestingly, T164 belongs to an α-helix element connecting a loop close to the GTP binding site with a long protein loop (highlighted in green in figure 47) which connects domain I with the dimerization domain (II).

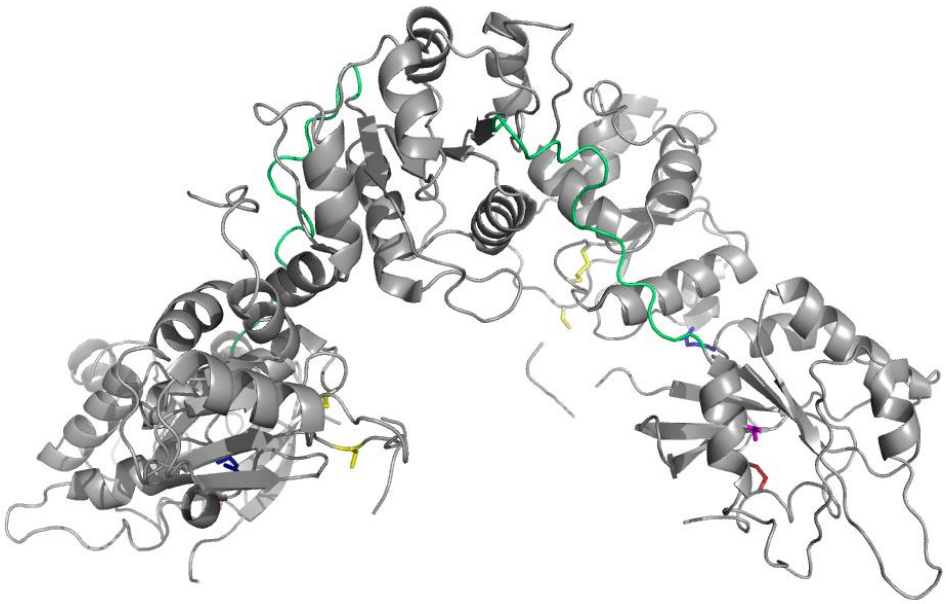

Figure 47. Cartoon representation of the HydF dimer. The two monomers are related by a twofold axis, approximately parallel to the plane of the paper in the *vertical* direction. Cysteine side chain residues, which are the putative ligand of the [4Fe4S] cluster of domain III, are in *yellow*; T164 side chain in *magenta*, R88 side chain in *blue* and M26 side chain in *red*. The long loop (residues 169–186) connecting domain I and II is colored in *green*.

As suggested by the crystal structure, the dimeric form of HydF (figure 47), which is the prevalent state in solution, represents an open form of the protein with both the [4Fe4S] cluster and the GTP-binding sites fully accessible. It is plausible that the open dimer interacts with the maturase partners in the extended conformation revealed by the X-ray structure. As the PELDOR experiments suggest, the binding of the nucleotide does not induce dramatic effects in the conformation within the GTP domain, at the level of the diagnostic positions investigated in this work, however, subtle changes are observed which may reflect large scale effects in the dimer conformation, as suggested by the involvement of residue T164 which is close to the long loop connecting the GTPase with the dimerization domain.

Conclusions

The specific role of GTPase domain of HydF in the maturation process of HydA is likely related to conformational changes of the protein upon ligation/hydrolysis of the nucleotide. Using a non-hydrolyzable analogous of GTP we have investigated the effect due to the binding of the nucleotide in the truncated protein domain. We found that the binding of the nucleotide does not induce large effects within the GTP domain, at least at the level of the elements investigated in this work. However, subtle changes are observed which may produce diffuse effects in the supramolecular dimeric assembly of the whole HydF protein. It is worth noting that not only the binding but also the hydrolysis of GTP could facilitate structural rearrangements, promoting interactions also with HydA facilitating the transfer of the 2Fe subcluster.

In order to obtain more significant data, further investigation will be carried out by designing new site-directed mutants of residues belonging to the above mentioned long loop and to the unstructured region reported in the X-ray structure (residues 32-44). Spin labeling of the GTPase domain in the whole protein will be also performed.

CONCLUSIONS

Hydrogen is a viable replacement to the current economy principally based on non-renewable energy sources and is one of the chances to overcome the current energy crisis. Hydrogen economy, however, is still unfavorable compared to other energy technologies that already exist. An alternative and clean method of hydrogen production is the one that exploits biological processes based on the use of some microorganisms whose hydrogen metabolism is regulated by hydrogenases. Although in recent years many advances have been made to get a greater understanding of how these enzymes work, there are different aspects that still remain to clarify. Through this work we have tried to shed light on two of the major classes of hydrogenases, going to investigate the functional role of the [NiFe]-hydrogenase from *Synechocistis* sp. PCC 6803 and completing the biochemical characterization of HydF from *T. neapolitana*, one of the maturation protein of [FeFe]-hydrogenases. The physiological function of the bidirectional [NiFe]-hydrogenase, object of our studies, is a topic still under debate: there are several hypotheses, but independent experimental evidences have suggested that it may play a role only under transient and/or specific growth conditions. The fact that this enzyme is expressed in the presence of oxygen, while being inhibited in this condition, makes even more elusive its role.

In the first part of the thesis, I have investigated the physiological role of the bidirectional [NiFe]-hydrogenase, comparing different *Synechocistis* knock out mutant strains to the wild type, in complete and prolonged darkness in aerobiosis. We discovered that the enzyme is in fact essential for the survival of this cyanobacterial strain, at least in the selected stressful conditions. Furthermore, the proteomic analysis performed on the wild type strain, as well as on a knock out mutant strain lacking of the entire *hox* operon coding for the enzyme, grown under this stress condition has highlighted a downregulation of several hydrophilic subunits of the NDH-1 complex belonging to the respiratory chain. This seems to be in agreement with the theories suggesting a close evolutionary relationship between [NiFe]-hydrogenase and this complex. As future prospect, we will complete this analysis to get new insights into the [NiFe]-hydrogenase

role and to characterize the knock out mutant strain as an ideal organism for the heterologous expression of recombinant [FeFe]-hydrogenases which possess, in terms of molecular hydrogen production, specific activity higher than the [NiFe]-hydrogenases.

In the second part we have got new clues on HydF, one of the proteins involved in the maturation of [FeFe]-hydrogenases. This protein has a GTPase activity that is required for the proper assembly of the enzyme but the role of the binding and/or hydrolysis of the nucleotide is still unclear. The crystal structure of HydF from *T. neapolitana*, previously obtained in our laboratory as apo-protein (*i.e.* without FeS clusters and GTP), showed the presence of three domains: a GTP-binding domain, a dimerization domain and a C-terminal [4Fe4S]-cluster binding domain. We isolated and expressed in *E. coli* the HydF GTP-binding domain, with the aim of studying the possible conformational changes induced by the nucleotide binding. We identified five residues useful to our purpose. In order to perform spectroscopic analysis, these sites were mutated in cysteines, spin labeled with the thiol-selective reagent MTSSL, and finally analyzed individually and in couples. Although there were no evidence of great movements of the mutated residues analyzed after the addition of GTP, we found small variations between the distances of the couple C88-C164. This was especially interesting for the 164 residue as it is close to the long loop that connects the domain I with that of dimerization, and suggested a possible involvement of the GTP binding in the conformational changes of the whole structure of HydF, as well as in its interactions with the two other maturases. In the future, we will further investigate this hypothesis generating new site-directed mutants near the position 164, in order to study this loop region, and extending the investigation to the whole HydF protein, in order to clarify the role of the GTP in the maturation process of the [FeFe]-hydrogenases.

REFERENCES

Abed R. M., Dobretsov S., Sudesh K. (2009). *Applications of cyanobacteria in biotechnology*. J Appl Microbiol 106, 1-12.

Adams M.W.W. (1990). *The structure and mechanism of iron-hydrogenases*. Biochim. Biophys. Acta 1020, 115-45.

Albertini M., Vallese F., Di Valentin M., Berto P., Giacometti G. M., Costantini P., Carbonera D. (2014). *The proton iron-sulfur cluster environment of the [FeFe]-hydrogenase maturation protein HydF from Thermotoga neapolitana*. International Journal of Hydrogen Energy 39, 18574–18582.

Antal T.K., Oliveira P., Lindblad, P. (2006). *The bidirectional hydrogenase in the cyanobacterium Synechocystis sp. strain PCC 6803*. Int. J. Hydrogen Energy 31, 1439-1444.

Antal T.K and Lindblad P. (2005). *Production of H_2 by sulphur-deprived cells of the unicellular cyanobacteria Gloeocapsa alpicola and Synechocystis sp. PCC 6803 during dark incubation with methane or at various extracellular pH*. J. Appl. Microbiol. 98, 114-120.

Appel J., Phunpruch S., Steinmuller K., Schulz, R. (2000). *The bidirectional hydrogenase of Synechocystis sp. PCC 6803 works as an electron valve during photosynthesis*. Arch. Microbiol. 173, 333-338.

Appel J. and Schulz R. (1996). *Sequence analysis of an operon of a NAD(P)-reducing nickel hydrogenase from the cyanobacterium Synechocystis sp. PCC 6803 gives additional evidence for direct coupling of the enzyme to NAD(P)H-dehydrogenase (complex I)*. Biochim. Biophys. Acta 1298, 141-147.

Aubert-Jousset E., Cano M., Guedeney, G., Richaud, P., Cournac, L. (2011). *Role of HoxE subunit in Synechocystis PCC6803 hydrogenase*. FEBS J. 278, 4035-4043.

Barz M., Beimgraben C., Staller T., Germer F., Opitz F., Marquardt C., Schwarz C., Gutekunst K., Vanselow K.H., Schmitz R., LaRoche J., Schulz R., Appel J. (2010). *Distribution analysis of hydrogenases in surface waters of marine and freshwater environments*. PLoS ONE 5 e13846.

Battchikova N, Vainonen J.P., Vorontsova N., Keranen M., Carmel D., Aro E.M. (2010). *Dynamic changes in the proteome of Synechocystis 6803 in response to CO(2) limitation revealed by quantitative proteomics*. J Proteome Res. 9, 5896-912.

Battchikova N., and Aro E.M. (2007). *Cyanobacterial NDH-1 complexes: multiplicity in function and subunit composition*. Physiol. Plant. 131, 22-32.

Bennett B., Lemon B.J., Peters J.W. (2000). *Reversible carbon monoxide binding and inhibition at the active site of the Fe-only hydrogenase*. Biochemistry 39, 7455-7460.

Berger S., Ellersiek U., Steinmüller K. (1991). *Cyanobacteria contain a mitochondrial complex I-homologous NADH-dehydrogenase*. FEBS Lett. 286, 129-132.

Berggren G, Adamska A, Lambertz C, Simmons T.R., Esselborn J., Atta M., Gambarelli S., Mouesca J.M., Reijerse E., Lubitz W., Happe T., Artero V., Fontecave M. (2013). *Biomimetic assembly and activation of [FeFe]-hydrogenases*. Nature 499, 66-69.

Berkessel A. (2001). *Activation of dihydrigen without transition metals*. Curr Opin Chem Biol 5, 486-490.

Berks B.C., Sargent F., Palmer T. (2000). *The Tat protein export pathway*. Mol. Microbiol. 35, 260-274.

Berman-Frank I., Lundgren P., Falkowski P. (2003). *Nitrogen fixation and photosynthetic oxygen evolution in cyanobacteria*. Res. Microbiol. 154 157-164.

Bethel R.D., Singleton M.L., Darensbourg M.Y. (2010). *The modular assembly of clusters is the natural synthetic strategy for the active site of [FeFe] hydrogenase*. Angew. Chem. Int. Ed. Engl. 49, 8567-8569.

Berto P., Di Valentin M., Cendron L., Vallese F., Albertini M., Salvadori E., Giacometti G. M., Carbonera D., Costantini P. (2012). *The [4Fe-4S]-cluster coordination of [FeFe]-hydrogenase maturation protein HydF as revealed by EPR and HYSCORE spectroscopies*. Biochim Biophys Acta 1817, 2149-57

Berto P., D'Adamo S., Bergantino E., Vallese F., Giacometti G.M., Costantini, P. (2011). *The cyanobacterium Synechocystis sp. PCC 6803 is able to express an active [FeFe]-hydrogenase without additional maturation proteins*. Biochem. Biophys. Res. Commun. 405, 678-683.

Blokesch M., Albracht S.P., Matzanke B.F., Drapal N.M., A. Jacobi A., Bock A. (2004). *The com-plex between hydrogenase-maturation proteins HypC and HypD is an intermedi-ate in the supply of cyanide to the active site iron of [NiFe]-hydrogenases*. J. Mol.Biol. 344 155-167.

Blokesh M. and Böck A. (2002). *Maturation of [NiFe]-hydrogenases in Escherichia coli: the HypC cycle*. J. Mol. Biol. 324, 287-296.

Blokesch M., Paschos A., Theodoratou E., Bauer A., Hube M., Huth, S., Böck, A. (2002). *Metal insertion into [NiFe]-hydrogenases*. Biochem. Soc. Trans. 30, 674-680.

Böck A., King P.W., Blokesch M., Posewitz M.C. (2006). *Maturation of hydrogenases*. Adv Microb Physiol , 51(Suppl.), 1-71.

Boison G., Schmitz O., Schmitz B., Bothe H. (1998). *Unusual gene arrangement of the bidirectional hydrogenase and functional analysis of its diaphorase subunit HoxU in respiration of the unicellular cyanobacterium Anacystis nidulans*. Curr. Microbiol. 36, 253-258.

Brazzolotto X., Rubach J. K., Gaillard J., Gambarelli S., Atta M., Fontecave M. (2006). *The [FeFe]-hydrogenase maturation protein HydF from Thermotoga maritima is a GTPase with an iron-sulfur cluster*. J. Biol. Chem. 281, 769-774.

Broderick J.B., Duffus B.R., Duschene K.S., Shepard E.M. (2014). *Radical S-adenosylmethionine enzymes*. Chem. Rev. 114: 4229-317.

Brugna-Guiral M., Tron P., Nitschke W., Stetter K.O., Burlat B., Guigliarelli B., Bruschi M., and Giudici- Orticoni M.T. (2003). *[NiFe] hydrogenases from the hyperthermophilic bacterium Aquifex aeolicus: properties, function, and phylogenetics*. Extremophiles. 7, 145-157.

Bui E.T. and Johnson P.J. (1996). *Identification and characterization of [Fe]-hydrogenases in the hydrogenosome of Trichomonas vaginalis*. Mol. Biochem. Parasitol. 76, 305-310.

Carrieri D., Wawrousek K., Eckert C., Yu J., Maness P.C. (2011). *The role of the bidirectional hydrogenase in cyanobacteria*. Bioresour. Technol. 102, 8368-8377.

Casalot L. and Rousset M. (2001). *Maturation of the [NiFe] hydrogenases*. Trends in Microbiology 9, 228-237.

Cendron L., Berto P., D'Adamo S., Vallese F., Govoni C., Posewitz M. C., Giacometti G. M., Costantini P., Zanotti G. (2011). *Crystal structure of HydF scaffold protein provides insights into [FeFe]-hydrogenase maturation*. J. Biol. Chem. 286, 43944-43950.

Chan Chung K.C. and Zamble D.B. (2011). *Protein interactions and localization of the Escherichia coli accessory protein HypA during nickel insertion to [NiFe]- hydrogenase*. J. Biol. Chem. 286, 43081-43090.

Checchetto V., Segalla A., Allorent G., La Rocca N., Leanza L., Giacometti G.M., Uozumi N., Finazzi G., Bergantino E., Szabò I. (2012). *Thylakoid potassium channel is required for efficient photosynthesis in cyanobacteria*. Proc. Natl. Acad. Sci. USA 109, 11043-11048.

Cohen J., Kim K., Posewitz M., Ghirardi M. L., Schulten K., Seibert M., King P. (2005). *Molecular dynamics and experimental investigation of H_2 and O_2 diffusion in [Fe]-hydrogenase*. Biochem Soc Trans. 33, 80-82.

Constant P., Chowdhury S.P., Hesse L., Pratscher J. (2011). *Conrad R., Genome data mining and soil survey for the novel group 5 [NiFe]-hydrogenase to explore the diversity and ecological importance of presumptive high-affinity H2-oxidizing bacter*. Appl. Environ. Microbiol. 77, 6027-6035. 1505.

Constant P., Chowdhury S.P., Pratscher J., Conrad R. (2010). *Streptomycetes contributing to atmospheric molecular hydrogen soil uptake are widespread and encode a puta- tive high-affinity [NiFe]-hydrogenase*. Environ. Microbiol. 12, 821–829. 1510.

Cooley J.W. and Vermaas W.F. (2001). *Succinate dehydrogenase and other respiratory pathways in thylacoid membrane of Synechocystis sp. PCC 6803: capacity comparisons and physiological function*. J. Bacteriol. 183, 4251-4258

Cournac L., Guedeney G., Peltier G., Vignais P.M. (2004). *Sustained photoevolution of molecular hydrogen in a mutant of Synechocystis sp. strain PCC 6803 deficient in the type I NADPH-dehydrogenase complex*. J. Bacteriol. 186, 1737-1746.

Cramm R. (2009). *Genomic view of energy metabolism in Ralstonia eutropha H16*. J. Mol. Microbiol. Biotechnol. 16, 38-52.

Cruz J.A., Kanazawa A., Treff N., Kramer D.M. (2005). *Storage of light-driven transthylakoid proton motive force as an electric field (Deltapsi) under steady-state conditions in intact cells of Chlamydomonas reinhardtii*. Photosynth Res 85, 221-233.

Czech I., Stripp S., Sanganas O., Leidel N., Happe T., Haumann M. (2011). *The [FeFe]-hydrogenase maturation protein HydF contains a H-cluster like [4Fe4S]-2Fe site*. FEBS Lett. 585, 225-230.

Czech I., Silakov, A., Lubitz, W., Happe, T. (2010). *The [FeFe]-hydrogenase maturase HydF from Clostridium acetobutylicum contains a CO and CN_ ligated iron cofactor*. FEBS Lett. 584, 638-642.

De Lacey A.L., Fernandez V.M., Rousset M., Cammack R. (2007). *Activation and inactivation of hydrogenase function and the catalytic cycle: spectroelectrochemical studies*. Chem. Rev. 107, 4304-4330.

Dismukes G.C., Carrier D., Bennette N., Ananyev G.M., Posewitz M. (2008). *Aquatic phototrophs: efficient alternative to land-based crops for biofuels*. Current Opinion in Biotechnology 19, 235-240.

Dörrich A.K., Mitschke J., Siadat O., Wilde A. (2014). *Deletion of the Synechocystis sp. PCC 6803 kaiAB1C1 gene cluster causes impaired cell growth under light-dark conditions*. Microbiology, doi: 10.1099/mic.0.081695-0.

Douglas C.D., Ngu T.T., H. Kaluarachchi H., Zamble D.B. (2013). *Metal transfer within the Escherichia coli HypB-HypA complex of hydrogenase accessory proteins*. Biochemistry 52, 6030-6039.

Drapal N. and Bock A. (1998). *Interaction of the hydrogenase accessory protein HypC with HycE, the large subunit of Escherichia coli hydrogenase 3 during enzyme maturation*. Biochemistry 37, 2941-2948.

Driesener R.C., Challand M.R., McGlynn S.E., Shepard E.M., Boyd E.S., Broderick J.B., Peters J.W., Roach P.L. (2010). *[FeFe]-hydrogenase cyanide ligands derived from S-adenosylmethionine-dependent cleavage of tyrosine*. Angew. Chem. Int. Ed. Engl. 49, 1687-1690.

Dutheil J., Saenkham P., Sakr S., Leplat C., Ortega-Ramos M., Bottin H., Cournac L., Cassier-Chauvat C., Chauvat F. (2012). *The AbrB2 autorepressor, expressed from an atypical promoter, represses the hydrogenase operon to regulate hydrogen production in Synechocystis strain PCC6803*. J. Bacteriol. 194, 5423-5433.

Eckert C., Boehm M., Carrieri D., Dubini A., Nixon P.J., Maness P.C. (2012). *Genetic analysis of the Hox hydrogenase in the cyanobacterium Synechocystis sp. PCC 6803 reveals subunit roles in association, assembly, maturation, and function*. J. Biol. Chem. 287, 43502-43515.

Esselborn J., Lambertz C., Adamska-Venkatesh A., Simmons T., Berggren G., Noth J., Siebel J., Hemschemeier A., Artero V., Reijerse E., Fontecave M., Lubitz W., Happe T. (2013). *Spontaneous activation of [FeFe]-hydrogenases by an inorganic [2Fe] active site mimic*. Nat Chem Biol 9, 607-609.

Fang H.H.P., Zhu H., Zhang T. (2006). *Phototrophic hydrogen production from glucose by pure and co-culture of Clostridium butyricum and Rhodobacter sphaeroides*. Int J Hydrogen Energy 31, 2223-30.

Fedorov A.S., Tsygankov A.A., Rao K.K., Hall D.O. (1998). *Hydrogen photoproduction by Rhodobacter sphaeroides immobilized on polyurethane foam*. Biotechnology Letters 20, 1007-9.

Fernandez V.M., Hatchikian E.C., Patil D.S., Cammack R. (1986). *ESR-detectable nickel and iron-sulphur centres in relation to the reversible activation of Desulfovibrio gigas hydrogenase*. Biochim. Biophys. Acta 883, 145-154.

Florin L., Tsokoglou A., Happe T. (2001). *A novel type of iron hydrogenase in the green alga Scenedesmus obliquus is linked to the photosynthetic electron transport chain*. J Biol Chem. 276, 6125-32.

Fontecilla-Camps J.C., Volbeda A., Cavazza C., Nicolet Y. (2007). *Structure/function relationships of [NiFe]- and [FeFe]-hydrogenases*. Chem Rev. 107, 4273-4303.

Fontecilla-Camps J.C. and Fernandez V.M. (1997). *Infrared-spectrochemical characterization of the [NiFe] hydrogenase of Desulfovibrio gigas*. J. Am. Chem. Soc. 119, 7181-7189.

Frey M. (2002). *Hydrogenases: hydrogen-activating enzymes*. Chembiochem 3, 152-160.

Friedrich B., Fritsch J., and Lenz O. (2011). *Oxygen-tolerant hydrogenases in hydrogen-based technologies*. Curr. Opin. Biotechnol. 22, 358-364.

Gaffron H. and Rubin J. (1942). *Fermentative and photochemical production of hydrogen in algae*. J Gen Physiol 26, 219-40.

Gao Y., Xiong W., Li X., Gao C.F., Zhang Y.L., Li H. and Wu Q.Y. (2009). *Identification of the proteomic changes in Synechocystis sp. PCC 6803 following prolonged UV-B irradiation*. J. Exp. Bot. 60, 1141-1154.

Garcin E., Vernede X., Hatchikian E. C., Volbeda A., Frey M., Fontecilla-Camps J. C. (1999). *The crystal structure of a reduced [NiFeSe] hydrogenase provides an image of the activated catalytic ceter*. Structure, 7, 557-66.

Ghirardi M.L., Dubini A., Yu J., Maness P.C. (2009). *Photobiological hydrogen-producing systems*. Chem. Soc. Rev. 38, 52-61.

Ghirardi M.L., Posewitz M.C., Maness P.C., Dubini A., Jianping Y., Seibert M. (2007). *Hydrogenases and hydrogen photoproduction in oxygenic photosynthetic organisms*. Annu. Rev. Plant. Biol. 58, 71-91.

Ghirardi M.L., Togasaki R.K., Seibert M. (1997). *Oxygen sensitivity of algal H2-production*. Appl Biochem Biotechnol 63-65, 141-51.

Greening C., Berney M., Hards K., Cook G.M., Conrad R. (2014). *A soil actinobacteriumscav-enges atmospheric H2 using two membrane-associated, oxygen-dependent [NiFe] hydrogenase*. Proc. Natl. Acad. Sci. 111, 4257-4261. 1516.

Gutekunst K., Chen X., Schreiber K., Kaspar U., Makam S., Appel J. (2014). *The bidirectional NiFe-hydrogenase in Synechocystis sp. PCC 6803 is reduced by flavodoxin and fer-redoxin and is essential under mixotrophic, nitrate-limiting conditions*. J. Biol. Chem. 289, 1930-1937.

Gutekunst K., Phunpruch S., Schwarz C., Schuchardt S., Schulz-Friedrich R., Appel J. (2005). *LexA regulates the bidirectional hydrogenase in the cyanobacterium Synechocystis sp. PCC 6803 as a transcription activator*. Mol. Microbiol. 58, 810-823.

Gutthann, F., Egert M., Marques A., Appel, J. (2007). *Inhibition of respiration and nitrate assimilation enhances photohydrogen evolution under low oxygen concentrations in Synechocystis sp. PCC 6803*. Biochim. Biophys. Acta 1767, 161-169.

Hallenbeck P.C. (2012). Microbial technologies in advanced biofuels production. Springer 2:15-28.

Hallenbeck P.C. and Ghosh, D. (2009). *Advances in fermentative biohydrogen production: the way forward?* Trends Biotechnol. 27, 287-297.

Hallenbeck P.C. and Benemann J.R.. (2002). *Biological hydrogen production; fundamentals and limiting processes*. Int J Hydrogen Energy 27,1185-1193.

Happe, R.P., Roseboom, W., Egert, G., Friedrich, C. G., Massanz, C., Friedrich B., Albracht S.P. (2000). *Unusual FTIR and EPR properties of the H_2-activating site of the cytoplasmic NAD-reducing hydrogenase from Ralstonia eutropha*. J. FEBS Lett. 466, 259-63.

Happe R.P., Roseboom W., Pierik A.J., Albracht S. P. J., Bagley K.A. (1997). *Biological activation of hydrogen*. Nature, 385, 126.

Harwood C.S. (2008). *Nitrogenase-catalyzed hydrogen production by purple nonsulfur photosynthetic bacteria*. In: Wall, J.D., Harwood, C.S., Demain, A. (Eds.), Bioenergy. ASM Press, Washington, D.C., pp. 259-271.

Higuchi Y., Ogata H., Miki K., Yasuoka N., Yagi T. (1999). *Removal of the bridging ligand atom at the Ni-Fe active site of [NiFe] hydrogenase upon reduction with H2, as revealed by X-ray structure analysis at 1.4 A resolution*. Structure 7, 549-556.

Higuchi Y., Yagi T., Yasuoka N. (1997). *Unusual ligand structure in Ni-Fe active center and an additional Mg site in hydrogenase revealed by high resolution X-ray structure analysis*. Structure 5, 1671-1680.

Hiromoto T., Warkentin E., Moll J., Ermler U., Shima S. (2009). *The crystal structure of an [Fe]-hydrogenase-substrate complex reveals the framework for H2 activation*. Angew. Chem. Int. Ed. Engl. 48, 6457-6460.

Hoek C. van den, Mann D.G., Jahns H.M. [Eds] (1995). *Algae:(An Introduction to Phycology)*. Cambridge University Press, Cambridge, 623 pp.

Hoffman D., Gutekunst K., Klissenbauer M., Schulz-Friedrich R., Appel J. (2006). *Mutagenesis of hydrogenase accessory genes of Synechocystis sp. PCC 6803. Additional homologues of hypA and hypB are not active in hydrogenase maturation*. FEBS J. 273, 4516-4527.

Hoiczyk E. and Hansel A. (2000). *Cyanobacterial cell walls: News from an unusual prokaryotic envelope*. Journal of Bacteriology, 182(5), 1191-1199.

Horner D.S., Heil B., Happe T., Embley T.M. (2002). *Iron hydrogenases-ancient enzymes in modern eukaryotes*. Trends Biochem. Sci. 27, 148-153.

Howitt C.A. and Vermaas W.F.J. (1999). *Subunits of the NAD(P)-reducing nickel-containing hydrogenase do not act as part of the type-1 NAD(P)H-dehydrogenase in the cyanobacterium Synechocystis sp. PCC 6803*. In: Peschek G.A., Löffelhardt W., Schmetterer G., (Eds.) The Phototrophic Prokaryotes. Kluwer Academic/Plenum Publisher, New York, NY USA, pp. 595-601.

Hu B., Chen D., Hu X. (2014). *Synthesis and Reactivity of Mononuclear Iron Models of [Fe]-Hydrogenase that Contain an Acylmethylpyridinol Ligand*. Chemistry, A European Journal, 20, 1677-1682.

Hube M., Blokesch M., Böck A. (2002). *Network of hydrogenase maturation in Escherichia coli: role of accessory proteins HypA and HybF*. J. Bacteriol. 184, 3879-3885.

Ide T., Bäumer S., Deppenmeier U. (1999). *Energy conservation by the H2:heterodisulfi de oxidoreductase from Methanosarcina mazei Gö1: identifi cation of two proton-translocating segments*. J. Bacteriol. 181, 4076-4080.

Jackson D.D. and Ellms J.W. (1896). *On odors and tastes of surface waters with special reference to Anabaena, a microscopial organism found in certain water supplies of Massachusetts*. Rep Mass State Board Health 410-20.

Jacobi A., Rossmann R., Bock A. (1992). *The hyp operon gene products are required for the maturation of catalytically active hydrogenase isoenzymes in Escherichia coli, Arch. Microbiol*. 158, 444-451.

Jansson C. and Northen T. (2010). *Calcifying cyanobacteria—The potential of biomineralization for carbon capture and storage*. Curr. Opin. Biotechnol., 21, 365-371.

Kamp C., Silakov A., Winkler M., Reijerse E.J., Lubitz W., Happe, T. (2008). *Isolation and first EPR characterization of the [FeFe]-hydrogenases from green algae*. Biochim. Biophys. Acta 1777, 410-416.

Kaneko T., Nakamura Y., Sasamoto S., Watanabe A., Kohara M., Matsumoto M., Shimpo S., Yamada M., Tabata, S. (2003). *Structural analysis of four large plasmids harboring in a unicellular cyanobacterium, Synechocystis sp. PCC 6803*. DNA Res. 10, 221-228.

Kaneko T., Sato S., Kotani H., Tanaka A., Asamizu E., Nakamura Y., Miyajima N., Hirosawa M., Sugiura M. et al. (1996). *Sequence analysis of the genome of the unicellular cyanobacterium Synechocystis sp. strain PCC6803*. II. Sequence determination of the entire genome and assignment of potential protein-coding regions. DNA Res. 3, 109-136.

King P. W., Posewitz M. C., Ghirardi M. L., Seibert M. (2006). *Functional studies of [FeFe]-hydrogenase maturation in an Escherichia coli biosynthetic system*. J. Bacteriol. 188, 2163-2172.

Kiss E., Kos P.B., Vass I. (2009). *Transcriptional regulation of the bidirectional hydrogenase in the cyanobacterium Synechocystis 6803*. J. Biotechnol. 142, 31-37.

Koku H., Eroglu I., Gunduz U., Yucel M., Turker L. (2003). *Kinetics of biological hydrogen production by the photosynthetic bacterium Rhodobacter sphaeroides O.U. 001*. Int J Hydrogen Energy 28, 381-388.

Kuchenreuther J. M., Myers W. K., Suess D. L., Stich T. A., Pelmenschikov V., Shiigi S. A., Cramer S. P., Swartz J. R., Britt R. D., George S.J. (2014). *The HydG enzyme generates an Fe(CO)2(CN) synthon in assembly of the FeFe hydrogenase Hcluster*. Science. 6169, 424-7.

Kuchenreuther J.M., George S.J., Grady-Smith C.S., Cramer S.P., Swartz J.R. (2011). *Cell-free H-cluster synthesis and [FeFe] hydrogenase activation: all five CO and CN ligands derive from tyrosine*. PLoS One 6 e20346.

Kufryk G., Sachet M., Schmettere G., Vermaas W.F.J. (2002). *Transformation of the cyanobacterium Synechocystis sp. PCC 6803 as a tool for genetic mapping: optimization of efficiency*. FEMS Microbiology Letters 206, 215-219.

Künkel A., Vorholt J.A., Thauer R.K., Hedderich R. (1998). *An Escherichia coli hydrogenase-3-type hydrogenase in methanogenic archaea*. Eur. J. Biochem. 252, 467-476.

Leach M.R. and Zamble D.B. (2007). *Metallocenter assembly of the hydrogenase enzyme*. Curr. Opin. Chem. Biol. 11, 159-165.

Lemon B.J. and Peters, J.W. (1999). *Binding of exogenously added carbon monoxide at the active site of the iron-only hydrogenase (CpI) from Clostridium pasterianum*. Biochemistry 38, 12969-12973.

Li T., Yang H.M., Cui S.X., Suzuki I., Zhang L.F., Li L., Bo T.T., Wang J., Murata N., Huang F. (2012). *Proteomic study of the impact of Hik33 mutation in Synechocystis sp. PCC 6803 under normal and salt stress conditions*. J. Proteome Res. 11, 502-514.

Lubitz W., Ogata H., Rüdiger O., Reijerse E. (2014). *Hydrogenases*. Chem. Rev. 114, 4081-4148.

Lubitz W., Reijerse E., van Gastel M. (2007). *[NiFe] and [FeFe] hydrogenases studied by advanced magnetic resonance techniques*. Chem Rev. 107, 4331-65.

Ludwig M., Cracknell JA., Vincent KA., Armstrong FA., Lenz O. (2008). *Oxygen-tolerant H2 oxidation by membrane-bound [NiFe]-hydrogenases of Ralstonia species: coping with low-level H2 in air*. JBC 284, 465-77.

Lutz S., Jacobi A., Schlensog V., Böhm R., Sawers G., Böck A. (1991). *Molecular characterization of an operon (hyp) necessary for the activity of the three hydrogenases isoenzymes in Escherichia coli*. Mol. Microbiol. 5, 123-135.

Lyon E.J., Shima S., Boecher R., Thauer R.K., Grevels F.W., Bill E., Roseboom W., Albracht S.P.J. (2004). *Carbon monoxide as an intrinsic ligand to iron in the active site of the iron–sulfur-cluster-free hydrogenase H2-forming methylenetetrahydromethanopterin dehydrogenase as revealed by infrared spectroscopy*. J. Am. Chem. Soc. 126, 14239-14248.

Lyon E. J., Shima S., Buurman G., Chowdhuri S., Batschauer A., Steinbach K., Thauer R. K. (2004). *UV-A/blue-light inactivation of the "metal-free" hydrogenase (Hmd) from methanogenic archea*. Eur J Biochem, 271, 195-204.

Ma K., Zhou Z.H., Adams M.W.W. (1994). *Hydrogen production from pyruvate by enzymes purifi ed from the hyperthermophilic archaeon, Pyrococcus furiosus: A key role for NADPH*. FEMS Microbiol. Lett. 122, 245-250.

Maier T., Binder U., Bock A. (1996). *Analysis of the hydA locus of Escherichia coli: two genes (hydN and hypF) involved in formate and hydrogen metabolism*. Arch. Microbiol. 165, 333-341. 1736.

Maier T., Lottspeich F., Bock A. (1995). *GTP hydrolysis by HypB is essential for nickel inser-tion into hydrogenases of Escherichia coli*. Eur. J. Biochem. 230, 133-138.

Malki S., Saimmaime I., De Luca G., Rousset M., Dermoun Z., Belaich J.-P. (1995). *Characterization of an operon encoding an NADP-reducing hydrogenase in Desulfovibrio fructosovorans*. J. Bacteriol. 177, 2628-2636.

McGlynn S. E., Shepard E. M., Winslow M. A., Naumov A. V., Duschene K. S., Posewitz M. C., Broderick W. E., Broderick J. B., Peters J. W. (2008). *HydF as a scaffold protein in [FeFe] hydrogenase H-cluster biosynthesis*. FEBS Lett. 582, 2183-2187.

McGlynn S.E., Ruebush S.S., Naumov A., Nagy L.E., Dubini A., King P.W., Broderick J.B., Posewitz M.C., Peters J.W. (2007). *In vivo activation of [FeFe] hydrogenase: new insights into hydrogenase maturation*. J Biol Inorg Chem 12, 443-447.

McIntosh C.L., Germer F., Schulz R., Appel J., Jones A.K. (2011). *The [NiFe]-hydrogenase of the cyanobacterium Synechocystis sp. PCC 6803 works bidirectionally with a bias to H_2 production*. J. Am. Chem. Soc. 133, 11308-11319.

Melis A., Zhang L., Forestier M., Ghirardi M.L., Seibert M. (2000). *Sustained photobiological hydrogen gas production upon reversible inactivtion of oxygen evolution in the green alga Chlamydomonas reinhardtii*. Plant Physiol. 122, 127-135.

Menegazzo L., Albiero M., Millioni R., Tolin S., Arrigoni G., Poncina N., Tessari P., Avogaro A., Fadini G.P. (2013). *Circulating myeloid calcifying cells have antiangiogenic activity via thrombospondin-1 overexpression*. FASEB J. 27, 4355-4365.

Meredith L.K., Rao D., Bosak T., Klepac-Ceraj V., Tada K.R., Hansel C.M., Ono S., Prinn R.G. (2014). *Consumption of atmospheric hydrogen during the life cycle of soil-dwelling actinobacteria*. Environ. Microbiol. Rep. 6, 226-238. 1513.

Meyer J. (2007). *[FeFe] hydrogenases and their evolution: a genomic perspective*. Cell Mol Life Sci. 64, 1063-1084.

Montet Y., Amara P., Volbeda A., Vernede X., Hatchikian E.C., Field M.J., Frey M., Fontecilla-Camps J.C. (1997). *Gas access to the active site of Ni-Fe hydrogenases probed by X-ray crystallography and molecular dynamics*. Nat. Struct. Biol. 4, 523-526.

Mulder D.W., Boyd E.S., Sarma R., Lange R. K., Endrizzi J.A., Broderick J. B., Peters J.W. (2010). *Stepwise [FeFe]-hydrogenase H-cluster assembly revealed in the structure of HydA(ΔEFG)*. Nature 465, 248-251.

Mullineaux C.W. (2014). *Co-existence of photosynthetic and respiratory activities in cyanobacterial thylacoid membranes*. Biochim. Biophys. Acta 1837, 503-511.

Nath K. and Das D. (2004). *Improvement of fermentative hydrogen production: various approaches*. Appl Microbiol Biotechnol. 65, 520-9

Nicolet Y. and Fontecilla-Camps J.C. (2012). *Structure-function relationships in [FeFe]-hydrogenase active site maturation*. J Biol Chem. 287, 13532-40.

Nicolet Y., Martin L., Tron C., Fontecilla-Camps J.C. (2010). *A glycyl free radical as the precursor in the synthesis of carbon monoxide and cyanide by the [FeFe]-hydrogenase maturase HydG*. FEBS Lett. 584, 4197-4202.

Nicolet Y., Amara P., Mouesca J.M., Fontecilla-Camps J.C. (2009). *Unexpected electron transfer mechanism upon AdoMet cleavage in radical SAM proteins*. Proc. Natl. 1 Acad. Sci. U. S. A. 106, 14867-14871.

Nicolet Y., Rubach J.K., Posewitz M.C., Amara P., Mathevon C., Atta M., Fontecave M., Fontecilla-Camps J.C. (2008). *X-ray structure of the [FeFe]-hydrogenase maturase HydE from Thermotoga maritima*. J. Biol. Chem. 283, 18861-18872.

Nicolet Y., Lemon B.J., Fontecilla-Camps J.C., Peters J.W. (2000). *A novel FeS cluster in Fe-only hydrogenases*. Trends Biochem. Sci. 25, 138-143.

Nicolet Y., Piras C., Legrand P., Hatchikian C.E., Fontecilla-Camps J.C. (1999). *Desulfovibrio desulfuricans iron hydrogenase: the structure shows unusual coordination to an active site Fe binuclear center*. Structure 7, 13-23.

Ogawa T. and Mi H. (2007). *Cyanobacterial NADPH dehydrogenase complexes*. Photosynth. Res. 93, 69-77.

Ogawa T. (1991). *A gene homologous to the subunit-2 gene of NADH dehydrogenase is essential to inorganic carbon transport of Synechocystis sp. PCC 6803*. Proc. Natl. Acad. Sci. USA 88, 4275-4279.

Oliveira P. and Lindblad P. (2009). *Transcriptional regulation of the cyanobacterial bidirectional Hox-hydrogenase*. Dalton Trans 45, 9990-9996.

Oliveira P. and Lindblad, P. (2008). *An AbrB-Like protein regulates the expression of the bidirectional hydrogenase in Synechocystis sp. strain PCC 6803*. J. Bacteriol. 190, 1011-1019.

Oliveira P. and Lindblad P. (2005). *LexA, a transcription regulator binding in the promoter region of the bidirectional hydrogenase in the cyanobacterium Synechocystis sp. PCC 6803*. FEMS Microbiol Lett 251, 59-66.

Ortega-Ramos M., Jittawuttipoka T., Saenkham P., Czarnecka-Kwasiborski A., Bottin H., Cassier-Chauvat C., Chauvat F. (2014). *Engineering Synechocystis PCC6803 for hydrogen production: influence on the tolerance to oxidative and sugar stresses*. PLoS One, 9, e89372.

Oxelfelt F., Tamagnini P., Lindblad P. (1998). *Hydrogen uptake in Nostoc sp. strain PCC 73102. Cloning and characterization of a hupSL homolog*. Arch. Microbiol. 169, 267-274.

Pandelia M.E., Ogata H., Lubitz W. (2010). *Intermediates in the catalytic cycle of hydrogenase: functional spectroscopy of the active site*. ChemPhysChem 11, 1127-1140.

Paschos A, Glass RS, Böck A.(2001). *Carbamoylphosphate requirement for synthesis of the active center of [NiFe]-hydrogenases*. FEBS Lett, 488:9-12.

Peters J.W., and Broderick J.B. (2012). *Emerging paradigms for complex ironsulfur cofactor assembly and insertion*. Annu. Rev. Biochem. 81, 429-450.

Peters J.W., Szilagyi R.K., Naumov A., Douglas T. (2006). *A radical solution for the biosynthesis of the H-cluster of hydrogenase*. FEBS Lett. 580, 363-367.

Peters J.W., Lanzilotta W.N., Lemon B.J., Seefeldt, L.C. (1998). *X-ray crystal structure of the Fe-only hydrogenase (CpI) from Clostridium pasteurianum to 1.8 angstrom resolution*. Science 282, 1853-1858.

Pierik A.J., Roseboom W., Happe R.P., Bagley K.A., Albracht S.P.J. (1999). *Carbon monoxide and cyanide as intrinsic ligands to iron in the active site of [NiFe]-hydrogenases*. NiFe(CN)2CO, Biology's way to activate H2. J Biol Chem 274, 3331-7.

Pierik A. J., Hulstein M., Hagen W. R., Albracht S. P. J. (1998). *A low-spin iron with CN and CO as intrinsic ligands forms the core of the active site in [Fe]-hydrogenases*. Eur. J. Biochem, 258, 572-8.

Pinto F., van Elburg K.A., Pacheco C.C., Lopo M., Noirel J., Montagud A., Urchueguía J.F., Wright P.C., Tamagnini P. (2012). *Construction of a chassis for hydrogen production. Physiological and molecular characterization of a Synechocystis sp. PCC 6803 mutant lacking a functional bidirectional hydrogenase*. Microbiology 158, 448-464.

Polyhach Y,. Bordignon E., Jeschke G. (2011). *Rotamer libraries of spin labelled cysteines for protein studies*. Phys Chem Chem Phys. 13, 2356-66.

Posewitz M.C., Mulder D.W., Peters J.W. (2008). *New frontiers in hydrogenase structure and biosynthesis*. Curr. Chem. Biol. 2, 178-199.

Posewitz M.C., King P.W., Smolinski S.L., Zhang L., Seibert M., Ghirardi M.L. (2004). *Discovery of two novel radical S-adenosylmethionine proteins required for the assembly of an active [Fe] hydrogenase*. J. Biol. Chem. 279, 25711-20.

Pupillo P., Cervone F., Cresti M., Rascio N. (eds) (2003). Biologia vegetale XII+483 pp., Zanichelli.

Qiao J., Wang J., Chen L., Tian X., Huang S., Ren X. (2012). *Quantitative iTRAQ LC-MS/MS proteomics reveals metabolic responses to biofuel ethanol in cyanobacterial Synechocystis sp. PCC 6803*. J. Proteome Res. 11, 5286-5300.

Reissmann S., Hochleitner E., Wang H., Paschos A., Lottspeich F., Glass R.S., Böck, A. (2003). *Taming of a poison: biosynthesis of the NiFe-hydrogenase cyanide ligands*. Science. 299, 1067-1070.

Roseboom W., Blokesch M., Bock A., Albracht S.P. (2005). *The biosynthetic routes for car-bon monoxide and cyanide in the Ni-Fe active site of hydrogenases are different*. FEBS Lett. 579, 469-472.

Rowland J.G., Simon W.J., Prakash J.S., Slabas A.R. (2011). *Proteomics reveals a role for the RNA helicase crhR in the modulation of multiple metabolic pathways during cold acclimation of Synechocystis sp. PCC6803*. J. Proteome Res. 10, 3674-3689.

Rubach J.K., Brazzolotto X., Gaillard J., Fontecave M. (2005). *Biochemical characterization of the HydE and HydG iron-only hydrogenase maturation enzymes from Thermatoga maritima*. FEBS Lett 579, 5055-60.

Rupprecht J., Hankamer B., Mussgnug J.H., Ananyev G., Dismukes C., Kruse O. (2006). *Perspectives and advances of biological H_2 production in microorganisms*. Appl. Microbiol. Biotechnol. 72, 442-449.

Schmitz O., Boison G., Salzmann H., Bothe H., Schuz K., Wang S.H., Happe, T. (2002). *Hox-E--a subunit specific for the pentameric bidirectional hydrogenase complex (HoxEFUYH) of cyanobacteria*. Biochim. Biophys. Acta 1554, 66-74.

Shafaat H.S., Rüdiger O., Ogata H., Lubitz W. (2013). *[NiFe] hydrogenases: A common active site for hydrogen metabolism under diverse conditions*. Biochim. Biophys. Acta Bioenerg. 1827, 986-1002. 1556.

Shepard E.M., Mus F., Betz J.N., Byer A.S., Duffus B.R., Peters J.W., Broderick J.B. (2014). *[FeFe]-hydrogenase maturation.* Biochemistry. 53, 4090-4104.

Shepard E.M., Boyd E.S., Broderick J.B., Peters J.W. (2011). *Biosynthesis of complex iron- sulfur enzymes*. Curr. Opin. Chem. Biol. 15, 319-327.

Shepard E.M., McGlynn S.E., Bueling A.L., Grady-Smit, C.S., George S.J., Winslow M.A., Cramer S.P., Peters J.W., Broderick J.B. (2010). *Synthesis of the 2Fe sublcuster of the [FeFe]-hydrogenase H cluster on the HydF scaffold*. Proc. Natl. Acad. Sci. 107, 10448-10453.

Shima S., Pilak O., Vogt S., Schick M., Stagni M.S., Meyer-Klaucke W., Warkentin E., Thauer R.K., Ermler U. (2008). *The crystal structure of [Fe]-hydrogenase reveals the geometry of the active site*. Science 321, 572-5.

Shima S. and Thauer R.K. (2007). *A third type of hydrogenase catalyzing H2 activation*. Chem. Rec. 7, 37-46.

Shomura Y. and Higuchi Y. (2012). *Structural basis for the reaction mechanism of Scarbamoylation of HypE by HypF in the maturation of [NiFe]-hydrogenases*. J. Biol. Chem. 287, 28409-28419.

Soboh B., Stripp S.T., Bielak C., Lindenstrauss U., Braussemann M., Javaid M., Hallensleben M., Granich C., Herzberg M., Heberle J., Sawers R.G. (2013). *The [NiFe]-hydrog-enase accessory chaperones HypC and HybG of Escherichia coli are iron- and car- bon dioxide-binding proteins*. FEBS Lett. 587, 2512-2516.

Soboh B., Stripp S.T., Muhr E., Granich C., Braussemann M., Herzberg M., Heberle J., Gary R. (2012). *Sawers, [NiFe]-hydrogenase maturation: isolation of a HypC-HypD complex carrying diatomic CO and CN^- ligands*. FEBS Lett. 586, 3882-3887.

Soboh B., Linder D., Hedderich R. (2004). *Amultisubunitmembrane-bound [NiFe] hydrog- enase and an NADH-dependent Fe-only hydrogenase in the fermenting bacterium Thermoanaerobacter tengcongensis*. Microbiology 150, 2451-2463.

Stal L.J. and Moezelaar R. (1997). *Fermentation in cyanobacteria*. Fems Microbiol. Rev. 21, 179-211.

Stoll S. and Schweiger A. (2006). *EasySpin, a comprehensive software package for spectral simulation and analysis in EPR*. J Magn Reson. 178, 42-55.

Strickland L.H. (1929). *The bacterial decomposition of formate*. Biochem J 23, 1187.

Stripp S.T., Soboh B., Lindenstrauss U., Braussemann M., Herzberg M., Nies D.H., Sawers R.G., Heberle J. (2013). *HypD is the scaffold protein for Fe-(CN)2CO cofactor assembly in [NiFe]-hydrogenase maturation*. Biochemistry 52, 3289-3296.

Stripp S.T., Goldet G., Brandmayr C., Sanganas O., Vincent K.A., Haumann M., Armstrong F.A., Happe T. (2009a). *How oxygen attacks [FeFe] hydrogenases from photosynthetic organisms*. Proc. Natl. Acad. Sci. USA 106, 17331-17336.
Summerfield T.C., Toepel J., Sherman L.A. (2008). *Low-oxygen induction of normally cryptic psbA genes in cyanobacteria*. Biochemistry, 47, 12939-12941.

Suzuoki Z. and Suzuoki T. (1951). *Carbohydrate metabolism of Trichomonas foetus*. J. Biochem. 38, 237-254.

Sydor A.M., Lebrette H., Ariyakumaran R., Cavazza C., Zamble D.B. (2014). *Relationship be-tween Ni(II) and Zn(II) coordination and nucleotide binding by the Helicobacter pylori [NiFe]-hydrogenase and urease maturation factor HypB*. J. Biol. Chem. 289, 3828-3841.

Tamagnini P., Leitao E., Oliveira P., Ferreira D., Pinto F., Harris D.J., Heidorn T., Lindblad P. (2007). *Cyanobacterial hydrogenases: diversity, regulation and applications*. Fems. Microbiol. Rev. 31, 692-720.

Tersteegen A. and Hedderich R. (1999). *Methanobacterium thermoautotrophicum encodes two multisubunit membrane-bound [NiFe] hydrogenases. Transcription of the operons and sequence analysis of the deduced proteins*. Eur. J. Biochem. 264, 930-943.

Thajuddin N. and Subramanian G. (2005). *Cyanobacterial biodiversity and potential applications in biotechnology*. Curr Sci 89, 47–57.

Thauer R.K., Klein A.R., Hartmann G.C. (1996). *Reactions with Molecular Hydrogen in Microorganism: Evidence for a Purely Organic Hydrogenation Catalyst*. Chem Rev 96, 3031-3042.

Theodoratou E., Huber R., Bock A. (2005). *[NiFe]-Hydrogenase maturation endopeptidase: structure and function*. Biochem. Soc. Trans. 33, 108-111.

Theodoratou E., Paschos A., Magalon A., Fritsche E., Huber R., and Böck A. (2000b). *Nickel serves as a substrate recognition motif for the endopeptidase involved in hydrogenase maturation*. Eur. J. Biochem. 267, 1995-1999.

Tian F., Toon O.B., Pavlov A.A., De Sterck, H. (2005). *A hydrogen-rich early earth atmosphere*. Science 308, 1014-1017.

Tosatto S.C., Toppo S., Carbonera D., Giacometti G. M., Costantini P. (2007). *Comparative analysis of [FeFe]-hydrogenase from Thermotogales indicates the molecular basis of resistance to oxygen inactivation*. Int. J. hydrogen Energy. 33, 570-578.

Tron C., Cherrier M.V., Amara P., Lydie M., Fauth F., Fraga E., Correard M., Fontecave M, Nicolet Y, Fontecilla-Camps J.C. (2011). *Further characterization of the [FeFe]-hydrogenase maturase HydG*. Eur J Inorg Chem 1121-1127.

Troshina O., Serebryakova L., Sheremetieva M, Lindblad P. (2002). *Production of H2 by the unicellular cyanobacterium Gloeocapsa alpicola CALU 743 during fermentation*. Int J Hydrogen Energy 27, 1283-1289.

Tsvetkov Y.D., Milov A.D., Maryasov A.G.(2008). *Pulsed Electron-Electron Double Resonance (PELDOR) as EPR Spectroscopy in Nanometer Range*. Russ Chem Rev. 77, 487-520.

Vallese F., Berto P., Ruzzene M., Cendron L., Sarno S., De Rosa E., Giacometti G.M., Costantini P. (2012). *Biochemical analysis of the interactions between the proteins involved in the [FeFe]-hydrogenase maturation process*. J Biol Chem. 287, 36544-55.

Van Ooteghem S. A., Jones A., Van Der Lelie D., Dong B., Mahajan D. (2004). *H(2) production and carbon utilization by Thermotoga neapolitana under anaerobic and microaerobic growth conditions*. Biotechnol Lett. 15, 1223-32.

Verhagen M.F., O'Rourke T., Adams . W. (1999). *The hyperthermophilic bacterium, Thermotoga maritima, contains an unusually complex iron-hydrogenase: amino acid sequence analyses versus biochemical characterization*. Biochim. Biophys. Acta 1412, 212-229.

Vignais P.M. and Billoud B. (2007). *Occurrence, classification, and biological function of hydrogenases: an overview*. Chem. Rev. 107, 4206-4272.

Vignais P.M. and Colbeau A. (2004). *Molecular biology of microbial hydrogenases*. Curr Issues Mol Biol. 6, 159-88.

Vignais P.M., Billoud B., Meyer J. (2001). *Classification and phylogeny of hydrogenases*. FEMS Microbiol. Rev. 25, 455-501.

Volbeda A., Garcin E., Piras C., de Lacey A.L., Fernandez V.M., Hatchikian E.C., Frey M., Fontecilla-Camps J.C. (1996). *Structure of the [NiFe] hydrogenase active site: evidence for biologically uncommon Fe ligands*. J. Am. Chem. Soc. 118, 12989-12996.

Volbeda A., Charon M.H., Piras C., Hatchikian E.C., Frey M., Fontecilla-Camps J.C. (1995). *Crystal structure of the nickel-iron hydrogenase from Desulfovibrio gigas*. Nature 373, 580-587.

Watanabe S., Arai T., Matsumi R., Atomi H., Imanaka T., Miki K. (2009). *Crystal structure of HypA, a nickel-binding metallochaperone for [NiFe] hydrogenase maturation*. J. Mol. Biol. 394, 448–459.

Watanabe S., Matsumi R., Arai T., Atomi H., Imanaka T., Miki K. (2007). *Crystal structures of [NiFe] hydrogenase maturation proteins HypC, HypD, and HypE: insights into cyanation reaction by thiol redox signaling*. Mol. Cell 27, 29-40.

Weare N.M. and Benemann J.R. (1974). *Nitrogenase activity and photosynthesis by Plectonema boryanum 594*. J Bacteriol 119, 258-265.

Wegener K.M., Singh A.K., Jacobs J.M., Elvitigala T., Welsh E.A., Keren N., Gritsenko M.A., Ghosh B.K., Camp D.G. 2nd, Smith R.D., Pakrasi, H.B. (2010). *Global proteomics reveal an atypical strategy for carbon/nitrogen assimilation by a cyanobacterium under diverse environmental perturbations*. Mol. Cell. Proteomics 9, 2678-2689.

Wiegard A., Dörrich A.K., Deinzer H.T., Beck C., Wilde A., Holtzendorff J., Axmann I.M. (2013). *Biochemical analysis of three putative KaiC clock proteins from Synechocystis sp. PCC 6803 suggests their functional divergence*. Microbiology 159, 948-958.

Wu L.F., Ize B., Chanal A., Quentin Y., Fichant G. (2000a). *Bacterial twin-arginine signal peptide-dependent protein translocation pathway: evolution and mechanism*. J. Mol. Microbiol. Biotechnol. 2, 179-189.

Wu L.F., Chanal A., Rodrigue A. (2000b). *Membrane targeting and translocation of bacterial hydrogenases*. Arch. Microbiol. 173, 319-324.

Wu L. F. and Mandrand M. A.(1993). *Microbial hydrogenases: primay structure, classification, signatures and phylogeny*. FEMS Microbiol. Rev. 10, 243-69.

Xu W., Tang H., Wang Y., Chitnis P.R. (2001). *Proteins of the cyanobacterial photosystem I. Biochimica Et Biophysica Acta (BBA)-Bioenergetics*. 1507, 32-40.

Xu W. and McFadden B.A. (1997). *Sequence analysis of plasmid pCC5.2 from cyanobacterium Synechocystis PCC 6803 that replicates by a rolling circle mechanism*. Plasmid 37, 95-104.

Yagi T. (1998). *Prokaryotic complex I (NDH-1), an overview*. Biochim. Biophys. Acta 1364, 125-133.

Zhang X., Sherman D.M., Sherman L.A (2014). *The uptake hydrogenase in the unicellular diazotrophic cyanobacterium Cyanothece sp. strain PCC 7822 protects nitrogenase from oxygen toxicity*. J. Bacteriol. 196, 840–849.

PAPERS

MANUSCRIPT SUBMITTED TO: SCIENTIFIC REPORTS

[NiFe]-hydrogenase is essential for cyanobacterium *Synechocystis* sp. PCC 6803 survival under long term darkness

Edith De Rosa[1], Vanessa Checchetto[1,2], Cinzia Franchin[2,3], Elisabetta Bergantino[1], Paola Berto[2], Ildikò Szabò[1], Giorgio M. Giacometti[1], Giorgio Arrigoni[2,3,*], and Paola Costantini[1,*]

[1]Department of Biology and [2]Department of Biomedical Sciences, University of Padova, Viale G. Colombo 3, 35131 Padova, Italy; [3]Proteomics Center of Padova University, Via G. Orus 2/B, 35129 Padova, Italy

*Co-corresponding authors

Mailing address: Paola Costantini, Department of Biology, University of Padova, Viale G. Colombo 3, 35131 Padova, Italy, Phone: +39-049-8276323, fax: +39-049-8276300, e-mail: paola.costantini@unipd.it; Giorgio Arrigoni, Proteomics Center of Padova University, Via G. Orus 2/B, 35129 Padova, Italy, Phone: +39-049-8217449, fax: +39-049-8217468, e-mail: giorgio.arrigoni@unipd.it

Abstract

Synechocystis sp. PCC 6803 is a cyanobacterial strain which holds a bidirectional [NiFe]-hydrogenase allowing it to exploit solar energy to produce molecular hydrogen. *Synechocystis* received great attention in the field of hydrogen production biotechnologies, also due to its simple nutritional requirements and to the availability of several tools for its genetic manipulation. Many biochemical and functional data have been provided which describe the *Synechocystis* [NiFe]-hydrogenase and the maturation proteins involved in the assembly of its active site. However, its physiological function is still under debate, and during the years a general consensus has been shared that [NiFe]-hydrogenase is not essential to *Synechocystis* fitness, at least under standard growth conditions. In this work we analyze the phenotype during prolonged darkness of different *Synechocystis* hydrogenase mutant strains, lacking either the [NiFe]-hydrogenase or its maturases. Our results indicate that this protein is in fact strictly required to survive to this stress condition. The proteomic analysis of wild type *Synechocystis* grown in the dark revealed that the expression of several NDH-1 respiratory complex hydrophilic subunits is downregulated, indicating a key functional role of the [NiFe]-hydrogenase when photosynthetic or respiratory electron transport chains are transiently over-reduced, and growth is only supported by fermentative metabolism.

Introduction

Hydrogen metabolism is one of the most ancient and crucial processes of life [1]. Today, most of the microorganisms able to use molecular hydrogen (H_2) as an energy source are prokaryotes belonging to the bacteria and archaea domains, although lower eukaryotes, such as unicellular green algae, anaerobic fungi and parasitic protozoas also have the ability to evolve H_2. The key enzymes of hydrogen metabolism are the hydrogenases, a general class of metalloproteins which catalyze the reversible reduction of protons to molecular hydrogen. With respect to the metal composition of their active site, hydrogenases can be divided in two major classes, *i.e.* i) the [FeFe]-hydrogenases, found in some unicellular green algae, as well as in strict anaerobes, fungi and protists, ii) the [NiFe]-hydrogenases, widespread among all bacteria families, including archaea, eubacteria and cyanobacteria [2] (see [3] for a recent comprehensive review on this topic). Hydrogenases' activity is generally biased toward proton reduction to hydrogen gas (H_2) for [FeFe]-hydrogenases, and toward hydrogen oxidation for the [NiFe]-hydrogenases. Several microorganisms harbor multiple hydrogenases, and in some cases a combination of both [FeFe] and [NiFe] enzymes. Cyanobacteria possess two functionally distinct [NiFe]-hydrogenases: an uptake enzyme, which oxidizes H_2, and a bidirectional hydrogenase, which is able to both oxidize and produce molecular hydrogen from solar energy and water. Among the diverse hydrogenases, the latter are of great interest for the development and improvement of solar hydrogen production technologies. Indeed, although green algae are currently recognized as the best photobiological hydrogen producers, thanks to the high specific activity of their hydrogenases, cyanobacteria are also receiving considerable attention in the field. In particular, *Synechocystis* sp. PCC 6803 (referred as *Synechocystis* in the following) appears to be the favourite microorganism, due to its simple nutritional requirements and to its ability of both phototrophic growth by oxygenic photosynthesis in sunlight and heterotrophic growth by glycolysis and oxidative phosphorylation in the dark. Moreover, the complete genomic sequence is available for this microorganism [4, 5]

together with the availability of molecular tools for its genetic manipulation exploiting its natural aptitude to be transformed with exogenous DNA. These properties have made *Synechocystis* a model organism both for functional studies and biotechnological applications.

Synechocystis has been reported to possess only a bidirectional [NiFe]-hydrogenase, a heteropentameric enzyme that uses $NAD(P)^+$/NAD(P)H as a substrate and is encoded by a single operon named *hox*, in which the *hox-E-F-U-Y-H* genes are clustered together with additional ORFs interspersed between some of them [6, 7]. HoxH and HoxY form the catalytic subcomplex, in which the larger HoxH subunit harbors the NiFe active site catalyzing the oxidation/reduction of H_2, and the HoxY small subunit carries a [4Fe-4S] cluster mediating the electron transfer to and from the enzyme active site. The FeS clusters-containing subunits HoxF, HoxU and HoxE form the diaphorase moiety, a flavoprotein interacting with the $NAD(P)^+$/(NAD(P)H couple and likely working as a redox partner for the catalytic subcomplex. As all other [NiFe]-hydrogenases, the Hox hydrogenase needs a highly coordinated network of accessory maturation proteins, encoded by the *hypABCDEF* operon [8], to be assembled and activated to the functional enzyme. This biosynthetic pathway has been described in details in *Escherichia coli*, and is specifically involved in the assembly of the hydrogenase FeS cluster active site contained in the catalytic HoxYH subcomplex (see [9-12] for comprehensive reviews in this topic).

The role of the Hox bidirectional hydrogenase can be different in distinct microorganisms, but in any case the enzyme works only in anoxic/micro-oxic conditions, due to its prompt and complete inactivation by molecular oxygen [2]. The precise physiological function of this enzyme in *Synechocystis*, and more in general in cyanobacteria, is still under debate, especially in oxygen-rich environments, [13]. It has been proposed that Hox could be involved in dark fermentation or work as an electron valve during photosynthesis under light [6, 14, 15]. Moreover, due to the homology of HoxE, F and U respectively with the NuoE, F and G proteins found in the respiratory complex I of other bacteria as well in mitochondria of eukaryotic cells it is tempting to speculate

that these Hox proteins could be somehow involved in respiration [6]. However, cyanobacteria lacking the Hox hydrogenase do not display growth defects due to an impaired respiration, at least in physiological conditions (see below in Results and Discussion) [16]. Several Hox mutants have been generated in order to gain new insights into the role of the cyanobacterial [NiFe]-hydrogenase [15, 17-23]. Although the literature data are somewhat inconsistent, a general emerging consensus is that the Hox hydrogenase may play a role only under transient and/or specific growth conditions.

Interestingly, the *hox* and *hyp* genes are constitutively expressed in *Synechocystis* under both anaerobic and aerobic conditions [15, 24, 25], even if the HoxEFUYH hydrogenase is clearly not-oxygen tolerant and is able to produce/consume H_2 only under strict anaerobiosis. This suggests that the Hox hydrogenase could have an additional function, at least in selected conditions. In this work we analyzed the phenotype of different *Synechocystis* hydrogenase mutant strains, lacking either *hyp* or *hox* genes, during prolonged, complete darkness in aerobiosis, a growth condition to which cyanobacteria are frequently exposed in nature. Our results indicate that the [NiFe]-hydrogenase could be involved in the adaptive response of *Synechocystis* to this environmental stress, which has never been investigated before in hydrogenase mutant strains.

Methods

All chemicals were of the highest purity commercially available.

Strains and standard growth conditions. The wild type *Synechocystis* sp. glucose-tolerant strain PCC 6803 as well as the *hox*/*hyp* deletion mutant strains (see below) were grown at 30 °C under continuous white light (50 μE m^{-2} s^{-1}), unless stated otherwise, in standard BG11 medium [26] buffered at pH 8.0 with HEPES (*N*-2-hydroxyethylpiperazine-*N'*-2-ethanesulfonic acid) and supplemented with 5 mM glucose (sterilized by filtration using 0.2 μm filters from *Millex*®) for photoheterotrophic growth. When grown in the dark, cultures were kept in flasks wrapped with aluminium foil. Transformed *Synechocystis* strains (see below) were grown with 5 to 50 μg/ml

kanamycin. For cultures grown on plates, BG11 medium was supplemented with 1.5% agar and 0.3% sodium thiosulfate. For liquid cultures, thiosulfate was omitted and the cultures were kept under continuous shaking. Cell growth was monitored as optical density at 730 nm (OD_{730}). When analyzed for the hydrogen evolution, liquid cultures were grown in sealed flasks in the presence of 5 μM (3-(3,4-dichlorophenyl)-1,1-dimethylurea) (DCMU), as previously described [27]. Chlorophyll concentration was determined spectrophotometrically in 100% methanol cell extracts as described in [28]. *Escherichia coli* XL1-Blue strain was used for DNA manipulation. The *E. coli* liquid medium was LB (1% Bactotryptone, 0.5% yeast extract, 0.5% NaCl and, when requested, 50 μg/ml kanamycin). Solid medium was obtained by adding 1.5% agar. The *hox*$^-$ strain (ΔHoxE-H, kanamycin resistant) was kindly provided by Jens Appel (from the Botanical Institute of the Christian-Albrechts-University, Kiel, Germany).

Plasmids construction and generation of Synechocystis ΔHypA and ΔHypB deletion mutants. The *hypA1* (*srl1675*) and *hypB1* (*sll1432*) knock-out strains were obtained, starting from *Synechocystis* PCC 6803 wild type strain, by homologous double recombination transferring into the respective genes a kanamycin-resistance cassette (*kan*^{r}), derived by BamHI digestion from plasmid pUC4K (Pharmacia). The plasmids used to generate these deletion mutants were based on the pBSKII vector (Agilent Technologies) and contained the *Synechocystis* chromosome regions flanking the *srl1675* and *sll1432* genes, respectively. The regions upstream and downstream *srl1675* and *sll1432* were amplified by a three-steps PCR strategy, using primers designed on the basis of the *Synechocystis* genome sequence accessible through CyanoBase and containing sequences with restriction sites for cloning purposes (listed in Table 1), and the high-fidelity Fusion DNA polymerase (Finnzymes). In the first step, a PCR-up and a PCR-down were separately performed using as template the *Synechocystis* genomic DNA, purified following standard protocols [29], and the primers couples *i)* SacI*hypA1*_for/BamHI*hypA1*_rev and BamHI*hypA1*_for/EcoRV*hypA1*_rev (for *hypA1*$^-$) or *ii)* SacI*hypB1*_for/BamHI*hypB1*_rev and

BamHI*hypB1*_for/EcoRV*hypB1*_rev (for *hypB1*$^-$). In a second step, the products of these PCR-up and PCR-down were amplified using the primers couples *i)* SacI*hypA1*_for/EcoRV*hypA1*_rev (for *hypA1*$^-$) or *ii)* SacI*hypB1*_for/EcoRV*hypB1*_rev (for *hypB1*$^-$), thus obtaining an overlapping band. In the last step, the overlapping bands were digested by the restriction enzymes SacI and EcoRV and individually cloned in a pBSKII vector, which was finally digested with BamHI to introduce the *kan*^{r} cassette. The sequences of the primers listed above are reported in Table 1. The sequences of the resulting recombinant plasmids pBSKII_*hypA1*KO_ *kan*^{r} and pBSKII_*hypB1*KO_ *kan*^{r} were confirmed by DNA sequencing (BMR Genomics, University of Padova). These plasmids were used to transform wild-type *Synechocystis* sp. PCC 6803 [30]. To this end, a *Synechocystis* culture was grown until reaching the mid-exponential phase (OD_{730} = 0.5) and centrifuged at room temperature at 3000 × *g* for 5 min. The cell pellet was suspended in fresh BG11 medium without glucose at a density of 1×10^{10} cells/ml and then mixed with exogenous DNA to a final concentration of 0.5 μg/ml. The mixture of cells and DNA was incubated for 5 h, and afterward spread onto a membrane filter resting on BG11 agar plates without antibiotic. After 24 h, the membrane filter was moved on BG11 agar plates containing 10 μg/ml kanamycin. Several single recombinant colonies appeared approximately after 10-15 days of growth, were subcloned on agar plates containing increasing antibiotic concentrations up to 50 μg/ml. The complete segregation of recombinant chromosomes in mutant strains was confirmed by PCR using primers couples FL*hypA1*_for/FL*hypA1*_rev and FL*hypB1*_for/FL*hypB1*_rev for the *hypA1* and *hypB1* knock-out mutant strains respectively.

Hydrogen evolution assay. Hydrogenase activity of whole cell extracts was measured *in vitro*, as previously described [27], as the evolution of hydrogen gas from reduced methyl viologen in nitrogen-flushed 13.5 ml sealed vials, using a Clarus 500 gas chromatographer equipped with an Elite-Molesieve column (0.53 mm i.d., length 30 m) (Perkin Elmer). All steps were performed under anaerobic conditions in a glove-box (MBRAUN MB 200B), using oxygen-free solutions.

Growth experiments. Cultures of wild type and ΔHoxE-H *Synechocystis* mutant strains were grown up to the exponential phase (OD_{730} 2.5) and, before the beginning of the experiments, they were the transferred to fresh BG11 medium plus 5 mM glucose, and diluted to get a starting (*i.e.* day 0) optical density of about 0.2. Each experiment was performed in triplicate i) under continous white light (50 μE m^{-2} s^{-1}), ii) with 12 h light/12 h dark cycles or iii) complete darkness. To assess the capability to form colonies on plates, *Synechocystis* liquid cell cultures previously incubated five days in the dark were diluted to an OD_{730} = 0.3-0.4 and quantified using the cell counter Cellometer Auto X4 with a Cellometer SD100 counting chamber (from Nexcelom Bioscience LLC.). Fifty microliters of three serial dilutions (*i.e.* 1:2500, 1:5000 and 1:10000) of the starting culture ($1x10^6$-$1.5x10^6$ cells/ml) were then plated on BG11 agar plates in the presence of 5 mM glucose and incubated at 30 °C in a 20 μE m^{-2} s^{-1} light regimen. Colonies, usually appeared after about ten days, were finally counted. Experiments were made in triplicate.

Electron microscopy. Pellets of cyanobacteria were fixed overnight at 4 °C in 3% glutaraldehyde in 0.1 M sodium cacodylate buffer (pH 6.9) and then processed for electron microscopy according to [31], at the electron microscopy facility of the Department of Biology, University of Padova. Ultrathin sections, cut with an ultramicrotome (LKB Ultratome V), were poststained with 1% osmium tetroxide/1% potassium ferrycyanide, embedded in a EPON 812 resin and examined under a transmission electron microscope (FEI Tecnai™ F12) operating at 100 kV.

Sample collection and protein extraction. Three biological replicates of *Synechocystis* sp. PCC 6803 wild type and *hox* knock-out mutant strains were grown for 5 days in continuous light and in the dark as described above. Cells were collected by 10 min centrifugation at 4 °C (Allegra® 25R Centrifuge, Beckman Coulter) at 5000 × *g*, frozen in liquid nitrogen, and stored at -20 °C until further use. Harvested cells were washed twice with 50 mM HEPES-KOH, pH 7.5, suspended in the same buffer with the addition of PMSF 1 mM, and split into 2 ml screw cap microtubes. After centrifugation the pellet was suspended in 200 μl of extraction buffer (50 mM HEPES-KOH, pH

7.5, 0.1% SDS, 0.1% Triton X-100, PMSF 1 mM) and an equal volume of glass beads (diameter 150-212 μm) was added. Cells were disrupted in a Mini Bead Beater (Biospec Products) by homogenizing three times at 3500 RPM for 15 sec, each time followed by incubation on ice for 1 min. Unbroken cells and glass beads were removed by centrifugation for 5 min at 1000 × *g* (Mikro 22R, Hettich) and the resulting supernatant was incubated for 30 min in 2% SDS (final concentration) to facilitate extraction of membrane proteins. Samples were centrifuged for 20 min at 12 000 × *g* at 4 °C, and the supernatant was transferred into a new tube and stored at -20 °C until further use. Protein concentration was determined by Bradford method (Bradford Reagent, Sigma-Aldrich). The proteins were precipitated in ice-cold acetone (1:4, v/v) at -20 °C overnight and stored at -80 °C until use.

Protein digestion and iTRAQ labeling. One hundred μg of protein pellets from each of the 6 preparations of *Synechocystis* sp. PCC 6803 (3 wild type and 3 *hox* knock-out mutant strains) were suspended in 40 μl Laemmli buffer and loaded into a NuPage 12% precast SDS-PAGE (Invitrogen). The electrophoretic process was carried out for few minutes, just enough to allow all proteins to enter the separating gel and focus in single narrow bands. Proteins were then stained using the SimplyBlue Safestain (Invitrogen), and each band was manually excised from the gel. After destaining, proteins were reduced for 1 h at 55°C using 10 mM dithiotreitol (DTT) in 25 mM triethylammonium bicarbonate (TEAB). Cysteines were alkylated using 55 mM iodoacetamide in 25 mM TEAB for 45 min, in the dark and at room temperature. Gel slices were then thoroughly washed with 3 exchanges of 50 mM TEAB and acetonitrile (ACN) and dried under vacuum. Samples were incubated (37°C, overnight) with 130 μl of sequencing grade modified trypsin (Promega, 12.5 ng/μl in 50 mM TEAB). Peptides were extracted from the gel slices by two consecutive treatments with 100 μl of 50% ACN (30 min, under constant agitation) and finally dried under vacuum. Each digested sample was dissolved in iTRAQ dissolution buffer and labeled with iTRAQ tags according to the manufacturer's instructions (AB Sciex). To reduce any potential

variation introduced by the labeling reaction, samples from the 3 replicates were labeled with a tag-swapping strategy (mass tags 114, 115, and 117 for wild type samples; tags 116, 117, and 114 for mutant samples). To verify the labeling efficiency, 1 μg of each labeled sample was individually analyzed by liquid chromatography – tandem mass spectrometry (LC-MS/MS) as specified below. Acquired data were searched with Mascot search engine, setting iTRAQ labeling as variable modification. No unmodified peptides were identified from the search and all the peptides were correctly modified at the N-terminus and at each lysine residue. Finally, the iTRAQ labeled samples were combined in a 1:1 ratio (wild type: mutant) and the pools were vacuum dried in a SpeedVac system.

Strong Cation Exchange Fractionation. Strong cation exchange (SCX) was performed using a SCX cartridge (AB Sciex) following the manufacturer's protocol. Each iTRAQ labeled sample was suspended in 500 μl of equilibration buffer (5 mM KH_2PO_4, 25% ACN, pH 2.9) and loaded onto a SCX cartridge with a syringe-pump system at a flow rate of 50 μl/min. Peptides were eluted in a step-wise mode using 500 μl of the following concentrations of KCl in equilibration buffer: 30, 50, 80, 110, 140, 170, 200, 350 mM. Each SCX fraction was dried under vacuum, suspended in 500 μl of 0.1% formic acid (FA) and desalted using C18 cartridges (Sep-Pack, C18, Waters). Samples were finally dried under vacuum and stored at -20 °C until MS analyses were performed.

LC-MS/MS analyses. Samples were dissolved in 40 μl of 0.1% FA, and analyzed with a LTQ-Orbitrap XL mass spectrometer (ThermoFisher Scientific) coupled online with a nano-HPLC Ultimate 3000 (Dionex - Thermo Fisher Scientific). Analyses were carried out as previously described [32]. About 1 μg of peptides from each fraction was loaded onto a 10 cm chromatographic column packed in-house into a pico-frit (75 μm I.D., 15 μm tip, New Objective) with C18 material (Aeris Peptide 3.6 μm XB-C18, Phenomenex). Peptides were eluted using a 3%-50% linear gradient of ACN/0.1% FA in 90 min at a flow rate of 250 nl/min. The instrument performed a full scan at high resolution (60000) on the Orbitrap, followed by MS/MS scans on the

three most intense ions both with CID and HCD fragmentation. After a first set of analysis, data were searched with Proteome Discoverer software (Thermo Fisher Scientific) as detailed below and all peptides identified with high (99%) or medium (95%) confidence were used to create a static exclusion list that was then included in the instrument method. All samples were re-analyzed under identical instrumental and chromatographic conditions except for the application of the exclusion list. All data obtained were merged into a MudPIT protocol and analyzed as described below.

Data analysis. Raw MS/MS files were analyzed using Proteome Discoverer 1.4 (Thermo Fisher Scientific) connected to a Mascot Search Engine server version 2.2.4 (Matrix Science), using a MudPIT protocol. Data were filtered to exclude MS/MS spectra containing less than 5 peaks and with a total ion count lower than 50. Spectra were searched against the Uniprot *Synechocystis* database (version March 2014, 3622 sequences), concatenated with a database of the most common contaminants found in proteomics experiments. Peptide and fragment tolerances were set to 10 ppm and 0.6 Da respectively. Enzyme specificity was set to Trypsin with up to 2 missed cleavages, carbamidomethylcysteine, 4-plex iTRAQ at N-terminus and Lys were set as fixed modifications, while oxidation of methionine was set as variable modification. Percolator and a search against the corresponding randomized database were used to calculate False Discovery Rates (FDR). Proteins were grouped into protein families according to the principle of maximum parsimony. Data were filtered considering as positive hits peptides identified with medium (95%) or high (99%) confidence, based on the q-value calculated by the Percolator algorithm. The final list of proteins was obtained by further filtering the data in order to consider as positive hits only proteins identified with at least two unique peptides and quantified with at least 2 independent peptides. A fold change of 1.5 combined with the results of a two-tailed Z Test were used to highlight proteins that showed in all replicates a significant change in their expression level between light and dark conditions.

Results and discussion

As mentioned in the Introduction, all *Synechocystis* deletion mutant strains characterized to date and lacking one or more *hox* genes of the *hoxE-H* operon display, under standard growth conditions, a behavior almost identical to that of the wild type strain. This makes the role of the cyanobacterial bidirectional [NiFe]-hydrogenase elusive. On the other hand, the puzzling constitutive expression of this enzyme, both in aerobic and anaerobic conditions, indicates an evolutionary advantage of retaining it, and suggests an additional role besides its primary function in hydrogen metabolism, at least under non-standard conditions. The majority of cyanobacteria are aerobic photoautotrophs, and sunlight-driven oxygenic photosynthesis is their principal mode of energy metabolism. However, it is well known that in natural environment some cyanobacterial communities can experience and survive to regular prolonged periods of complete darkness, for example in lake sediments, soil water or in dense aquatic accumulations produced at the surface. In these conditions a metabolic shift to anaerobic fermentation is expected to take place [33]. Interestingly, the *hox* genes are almost absent in cyanobacterial strains isolated from open oceans [2, 34], where both anaerobiosis and darkness are unlikely to be prevalent, suggesting that it is in the latter specific conditions that [NiFe]-hydrogenase function is especially important. To explore the potential contribution of the Hox bidirectional hydrogenase activity as a cellular strategy to overcome darkness, we analyzed the growth behavior under normal light and prolonged darkness of a *Synechocystis* mutant strain in which the whole *hox* operon has been deleted.

Physiological characterization of wild type and ΔhoxE-H *Synechocystis* strains under normal light and long term darkness. To evaluate the possible effects of the whole *hox* operon deletion on the fitness of *Synechocystis* during prolonged dark periods (up to five days), the growth of both wild type and ΔHoxE-H deletion mutant strains were compared in the presence of glucose as carbon source and under two different light conditions, *i.e. i)* continuous white light (50 μE m^{-2} s^{-1}) and *ii)* complete darkness. Moreover, since *Synechocystis* is known to possess a circadian clock system

[*e.g.* 35, 36], as an additional control, wild type and the mutant strains were also grown in 12 h light/12 h dark cycles. Figure 1 shows that no significant differences in terms of growth for *Synechocystis* wild type and ΔHoxE-H mutant strains were found, both under continuous irradiance (panel A) and when cultured with a circadian rhythm of light/dark cycles (panel B). This result is in agreement with data previously obtained using different *hox* deletion mutants [15, 17-23]. Instead, wild type and *hox* mutants displayed different behaviour when cultures were maintained under complete darkness from the time of inoculation. In the case of the wild type strain, as expected, glucose was able to support heterotrophic growth, even though at a rate which was reduced by 60-70% with respects to that observed under photoheterotrophic conditions (see figure legend for details). In the case of the ΔHoxE-H mutant strain, growth displayed a severe defect as compared to wild type strain cultured in the same conditions (figure 1, panel C) (see Materials and methods for experimental details). These observations, further confirmed by measurements of chlorophyll content (not shown), suggest that the presence of an intact *hox* operon confers to *Synechocystis* an adaptive advantage enabling it to survive in the absence of photosynthetic activity. Interestingly, after shifting back these ΔHoxE-H cultures to normal light conditions we observed that cells were suddenly able to resume their growth (figure 2). This suggests that the functional alteration(s) induced in the ΔHoxE-H mutant strain by a prolonged darkness is (are) reversible pointing to the hypothesis that the entry into a quiescent but viable state is a survival mechanism that the mutant strain can adopt when exposed to a prolonged darkness in the absence of the [NiFe]-hydrogenase. We then analyzed the ability of ΔHoxE-H cells, previously incubated for five days in the dark in liquid medium, of forming colonies on solid BG11 when moved back to normal light growth conditions. Plate counts clearly indicate that this is indeed the case (see Materials and methods for experimental details). These data were also confirmed by a transmission electron microscopy (TEM) morphological examination of ΔHoxE-H cells grown either in normal light or in the dark. TEM analysis show that no gross ultra-structural difference could be detected in the cells grown

under the two conditions (representative images are shown in figure 3), further supporting the idea that the ΔHoxE-H *Synechocystis* deletion mutant strain remains viable, thus allowing recovery of growth after prolonged exposure to darkness.

It is worth noting that the results of the growth experiments described above were obtained both in anaerobic (not shown) and in aerobic conditions, which are known to inhibit rapidly and completely the hydrogenase function of the Hox protein. The reactivity of several purified [NiFe]-hydrogenases toward O_2 has been extensively studied, and involves the conversion of the enzyme into a mixture of two inactive states, ***e.g.*** Ni-A and Ni-B, with an oxygenic ligand bridging the Ni and Fe atoms of the active site [37-39]. This indicates that the observed phenotype of the wild type *Synechocystis* strain under long term darkness cannot depend on the ability of its [NiFe]-hydrogenase to evolve H_2. To further investigate this point, we generated two additional knock out deletion mutant strains, ***i.e.*** i) the ΔHypA and ii) the ΔHypB lacking, respectively, the hydrogenase accessory chaperones HypA and HypB involved in the last steps of the NiFe site assembly process. In such mutants the diaphorase activity should be preserved while oxidation/reduction of molecular hydrogen should not take place.

Construction and physiological characterization of ΔHypA1 and ΔHypB1 *Synechocystis* strains under normal light and long term darkness. As reported in the Introduction, the maturation of the [NiFe]-hydrogenases is driven by a complex, highly conserved pathway needed for the biosynthesis of their composite active site, and has been thoroughly characterized in several microorganisms, including cyanobacteria [9-12]. Specifically, the auxiliary proteins HypA and HypB are responsible for the nickel insertion into the active site, prior to the very last step of the whole process, ***i.e.*** the hydrogenase C-terminus cleavage from the large subunit, culminating in enzyme activation [40]. Two homologues of both *hypA* and *hypB* are present in *Synechocystis* [4]; however, only the HypA1 and HypB1 couple is needed for the nickel insertion, while the HypA2 and HypB2 proteins probably have a chaperone role in the maturation of other metalloproteins in

this microorganism [41]. Based on this premise, we selectively replaced the *hypA1* (*slr1675*) and *hypB1* (*sll1432*) genes with a selection cassette conferring kanamycin resistance, as described in Materials and methods. Given the existence of multiple genome copies in *Synechocystis*, the complete segregation of the recombinant chromosomes, usually obtained by increasing the antibiotic concentration up to 50 μg/ml, was verified by PCR (see Materials and methods for details) (figure 4). Hydrogenase activity measured by gas chromatography (not shown) confirmed the lack of an active enzyme in the two new knock out mutant strains (*i.e. ΔhypA1* and *ΔhypB1*), which were then tested for their ability to grow both under normal light and prolonged darkness, as described above. We found that the lack of HypA1 and HypB1 proteins does not interfere with the aerobic growth of *Synechocystis* mutant strains when compared to the wild type strain, as assessed by $O.D._{730}$ monitoring (figure 5, panels A and B) and chlorophyll quantification (not shown), both under a normal light regimen and five day- long exposure to complete darkness. This result indicates that a correctly assembled, functional [NiFe]-hydrogenase active site is indeed not essential to confer to *Synechocystis* the ability to face this stress condition.

As assessed above, the *Synechocystis* ΔHoxE-H mutant strain has been obtained by removing the entire *hox* operon, which is composed by five structural *hox* genes (*i.e. hoxE*, *hoxF*, *hoxU*, *hoxY* and *hoxH*) clustered together, with three additional ORFs (*i.e. ORF3*, *ORF6* and *ORF7*) interspersed among them. The number and identity of these ORFs are different in distinct cyanobacterial strains, and their products are not involved in the activities of the hydrogenase and diaphorase enzyme moieties [42], indicating that their role in the observed growth phenotype is unlikely.

Taken together, these results suggest that the [NiFe]-hydrogenase plays a key function in the response of *Synechocystis* to a long term darkness exposure, and open a new perspective to gain clues on the role of this protein in selected stress conditions.

Several proteomic studies have recently been reported on different cyanobacteria, including *Synechocystis*, grown under various environmental stress conditions, such as for example UV light, high salt, cold temperature or CO_2 limitation, and revealed activation of distinct strategies by cyanobacteria against these perturbations [43-48]. Thus, in order to get more insights into the involvement of the [NiFe]-hydrogenase in the metabolic response of *Synechocystis* to a prolonged darkness we analyzed and compared the proteomes of a wild type strain grown either in normal light regimen or in the dark.

Quantitative proteomics analysis and comparison of the proteome of wild type *Synechocystis* grown under normal light and in the dark. Unraveling a new clue on the potential [NiFe]-hydrogenase functional role. A proteomic approach based on isobaric tag for relative and absolute quantification (iTRAQ) technology and liquid chromatography-tandem mass spectrometry (LC-MS/MS) was applied to compare the expression level of proteins from wild type *Synechocystis*, cultured for five days either under light or in the dark (see Material and methods for more experimental details). The analysis was conducted on three independent biological replicates. Across all replicates a total of 780 distinct protein families were identified and quantified. All relevant information relative to proteins and peptides identification and quantification are reported in supplementary tables 1-3. Six hundred and two proteins (which constitutes 16.4% of the *Synechocystis* theoretical proteome [4]) could be quantified in at least two out the three experiments, and were therefore used for the differential protein expression analysis. Unfortunately, hydrophobic proteins, including membrane-embedded subunits of thylakoid complexes (which are expected to be highly abundant in *Synechocystis*) are underestimated in our analysis, due to intrinsic limitations in the applied methodology, which relies on the use of trypsin as digestive enzyme. Nevertheless, we determined that 112 proteins were differentially regulated between light and darkness grown organism (p value <0.05), among which 58 showed an increased abundance (*i.e.* dark/light ratio ≥ 1.50) and 54 a decreased abundance (*i.e.* dark/light ratio ≤ 0.67). These proteins

have been listed in supplementary table 4 and grouped in Table 2 into different main categories according to their proven or predicted functions (when known). A large number of proteins and enzymes involved in transcription and translation show an altered expression in the dark as compared to light conditions, indicating that the overall protein synthesis process is altered when *Synechocystis* is grown under prolonged darkness, as previously observed also for several other stress conditions affecting the *Synechocystis* physiology [21, 43-48]. More specifically, as expected, several proteins/cofactors belonging to photosystems I and II and/or functionally correlated to photosynthesis, including the electron carrier flavodoxin, show a lower abundance when *Synechocystis* is grown in the absence of light, *i.e.* when glycolysis and oxidative pentose-phosphate metabolic pathways become prevalent. A thorough and complete analysis of the changes in the proteome of both wild type and ΔHoxE-H *Synechocystis* strains grown in the dark, and close dissection of the metabolic pathways activated/affected in response to this stress condition, are beyond the aim of this work and are currently underway in our laboratory. On the other hand, it is worth mentioning that several subunits of the respiratory chain NADPH/plastoquinone oxidoreductase (NDH-1) complex were also found underexpressed. *Synechocystis* contains a respiratory electron transport chain on both the cytoplasmic and thylakoid membranes, working in an interwoven way with the photosynthetic electron transport chain (see [49] for a recent review on this topic). The two pathways share some components (*i.e.* plastoquinone, cytocrome b_6f and plastocyanin), whereas other complexes are specific for the respiratory electron flow, including NDH-1, succinate dehydrogenase (SDH), and the terminal oxidase. The cyanobacterial NDH-1 is a proton-pumping NADPH/plastoquinone oxidoreductase analogous to the mitochondrial Complex I and is composed, in *Synechocystis*, of 11 subunits encoded by the *ndh* genes [4, 50-53]. This multisubunit complex, organized into a membrane domain containing hydrophobic subunits and a perpendicular peripheral domain composed by hydrophilic proteins, moves the electrons from NADPH to the plastoquinone (PQ) pool. However, in cyanobacteria NADPH is preferentially used for the CO_2 fixation process and the role of NDH-1 as an electron transport route into the PQ pool is

controversial. On the other hand, four distinct NDH-1 complexes with similar structure and different functions were predicted to exist in *Synechocystis* [53], suggesting that NDH-1 may work with different specificities depending on the physiological state of the cell. Based on mutagenesis experiments [54], a general consensus has indeed emerged that in *Synechocystis* most respiratory electrons enter the PQ pool via SDH, a complex composed by three subunits (*i.e.* a flavoprotein subunit, an iron-sulfur protein subunit, and a membrane subunit) which oxidizes succinate to fumarate, moving the electrons to the PQ pool. Intriguingly, we found that when wild type *Synechocystis* is grown under prolonged darkness four out of the six NDH-1 complex hydrophilic subunits detected (*i.e.* subunits Ndh-J, -K, -M and -O, encoded by genes *ndhJ*/*slr1281*, *ndhK*/*slr1280*, *ndhM*/*slr1623*, *ndhO*/*sll1690* respectively) are downregulated in their expression. Furthermore, our data (supplementary tables 1-3) strongly suggest that also the subunits Ndh-I (gene *ndhI*/*sll0520*) and Ndh-H (gene *ndhH*/*slr0261*) are affected in the same way, but they have been excluded from the final list of differentially expressed proteins either because the value is slightly higher than the established cutoff (as in the case of Ndh-I, average value 0.68) or due to the biological variability among the three replicates (as in the case of Ndh-H). Moreover, collected data indicate that also the expression of the SDH flavoprotein subunit (*sdhA*/*slr1233*) is reduced, although it was not included in the final list because it did not completely meet the chosen criteria (altered expression of at least 50% and $p<0.05$). The opposite seems to apply to two other proteins, *i.e.* iron superoxide dismutase (gene *sodB*/*slr1516*) and catalase-peroxidase (gene *katG*/*sll1987*), which act as antioxidant shields and show a trend of increased abundance (see supplementary tables 1-3) indicating that they are also likely to be overexpressed. This is consistent with a more reductive intracellular environment under this stress condition, causing an increased concentration of toxic oxygen species.

The altered expression of all these proteins, and in particular of the NDH-1 hydrophilic subunits, is suggestive of a scenario where the overall respiration electron flow is affected when

Synechocystis is grown in the dark. Interestingly, a *Synechocystis ndhB*-deficient mutant strain, which is completely devoid of NDH-1 complex [55], has been previously shown to display a sustained H_2 photoevolution [56], further supporting the idea that the bidirectional [NiFe]-hydrogenase can be functionally related to the photosynthetic and respiratory electron transport pathways. Although a specific function has not been yet assigned to the Hox bidirectional [NiFe]-hydrogenase in *Synechocystis*, as reported in the Introduction, our proteomic data confirm that it may work as an electron valve to dissipate electron excess under specific conditions, as previously proposed [6, 14, 15], and suggest that it could become strategic when the photosynthetic or respiratory electron transport chains are transiently over-reduced during growth under prolonged darkness [2, 33, 34]. Preliminary proteomic data acquired on the *Synechocystis* ΔHoxE-H mutant strain grown five days in the dark reveal that several hydrophilic subunits of the NDH-1 complex seem to be affected by this stress condition (not shown). Thus, [NiFe]-hydrogenase, when present, could confer to *Synechocystis* an adaptive advantage enabling it to cope with this stress condition.

Conclusions

No matter what might be the evolutionary driving force which led to the current wide taxonomic distribution of different [NiFe]-hydrogenases, for long time considered only as primordial proteins involved in early life hydrogen metabolism, increasing and independent experimental evidences converge on a common consensus that they could have a key role in controlling/buffering electron flow pathways, at least under specific growth conditions.

In this work we show that in the cyanobacterium *Synechocystis* sp. PCC 6803 the Hox bidirectional [NiFe]-hydrogenase is essential to survive under long term darkness, either in anaerobic or aerobic conditions, when the growth is only supported by fermentative metabolism. Interestingly, we found that under this stress condition the expression of several hydrophilic subunits of the NDH-1 respiratory complex is downregulated. This would be consistent with the

homology of the Hox [NiFe]-hydrogenase NAD(P)H oxidoreductase portion to the NADH input module of mitochondrial Complex I.

Taken together, our data add new clues pointing toward an active role of the bidirectional [NiFe]-hydrogenase in *Synechocystis*, and provide a molecular evidence supporting, more in general, the close evolutionary relationship between [NiFe]-hydrogenases and the Complex I of the aerobic respiratory chain.

Acknowledgements

This work was supported by a grant MIPAF (Ministero delle Politiche Agricole e Forestali, 2007) to Giorgio M. Giacometti.

References

1. Tian, F., Toon, O.B., Pavlov, A.A. & De Sterck, H. A hydrogen-rich early earth atmosphere. *Science* **308**, 1014-1017 (2005).

2. Vignais, P.M. & Billoud, B. Occurrence, classification, and biological function of hydrogenases: an overview. *Chem. Rev.* **107**, 4206-4272 (2007).

3. Peters, J.W., Schut, G.J., Boyd, E.S., Mulder, D.W., Shepard, E.M., Broderick, J.B., King, P.W. & Adams, M.W.W. [FeFe]- and [NiFe]-hydrogenase diversity, mechanism, and maturation. *Biochim. Biophys. Acta*, doi:10.1016/j.bbamcr.2014.11.021 (2014).

4. Kaneko, T., Sato, S., Kotani, H., Tanaka, A., Asamizu, E., Nakamura, Y., Miyajima, N., Hirosawa, M., Sugiura, M. *et al.* Sequence analysis of the genome of the unicellular cyanobacterium *Synechocystis* sp. strain PCC6803. II. Sequence determination of the entire genome and assignment of potential protein-coding regions. *DNA Res.* **3**, 109-136 (1996).

5. Kaneko, T., Nakamura, Y., Sasamoto, S., Watanabe, A., Kohara, M., Matsumoto, M., Shimpo, S., Yamada, M. & Tabata, S. Structural analysis of four large plasmids harboring in a unicellular cyanobacterium, *Synechocystis* sp. PCC 6803. *DNA Res.* **10**, 221-228 (2003).

6. Appel J. & Schulz, R. Sequence analysis of an operon of a NAD(P)-reducing nickel hydrogenase from the cyanobacterium *Synechocystis* sp. PCC 6803 gives additional evidence for direct coupling of the enzyme to NAD(P)H-dehydrogenase (complex I). *Biochim. Biophys. Acta* **1298**, 141-147 (1996).

7. Schmitz, O., Boison, G., Salzmann, H., Bothe, H., Schuz, K., Wang, S.H. & Happe, T. Hox-E – a subunit specific for the pentameric bidirectional hydrogenase complex (HoxEFUYH) of cyanobacteria. *Biochim. Biophys. Acta* **1554**, 66-74 (2002).

8. Lutz, S., Jacobi, A., Schlensog, V., Böhm, R., Sawers, G. & Böck, A. Molecular characterization of an operon (*hyp*) necessary for the activity of the three hydrogenases isoenzymes in *Escherichia coli*. *Mol. Microbiol.* **5**, 123-135 (1991).

9. Tamagnini, P., Leitao, E., Oliveira P., Ferreira, D., Pinto, F., Harris, D.J., Heidorn, T. & Lindblad, P. Cyanobacterial hydrogenases: diversity, regulation and applications. *Fems. Microbiol. Rev.* **31**, 692-720 (2007).

10. Casalot, L. & Rousset, M. Maturation of the [NiFe] hydrogenases. *Trends in Microbiology* **9**, 228-237 (2001).

11. Blokesh, M. & Böck, A. Maturation of [NiFe]-hydrogenases in *Escherichia coli*: the HypC cycle. *J. Mol. Biol.* **324**, 287-296 (2002).

12. Ghirardi, M.L., Posewitz, M.C., Maness, P.C., Dubini, A., Jianping Y. & Seibert, M. Hydrogenases and hydrogen photoproduction in oxygenic photosynthetic organisms. *Annu. Rev. Plant. Biol.* **58**, 71-91 (2007).

13. Carrieri, D., Wawrousek, K., Eckert ,C., Yu, J. & Maness, P.C. The role of the bidirectional hydrogenase in cyanobacteria. *Bioresour. Technol.* **102**, 8368-8377 (2011).

14. Antal, T.K & Lindblad, P. Production of H_2 by sulphur-deprived cells of the unicellular cyanobacteria *Gloeocapsa alpicola* and *Synechocystis* sp. PCC 6803 during dark incubation with methane or at various extracellular pH. *J. Appl. Microbiol.* **98**, 114-120 (2005).

15. Appel, J., Phunpruch, S., Steinmuller, K. & Schulz, R. The bidirectional hydrogenase of *Synechocystis* sp. PCC 6803 works as an electron valve during photosynthesis. *Arch. Microbiol.* **173**, 333-338 (2000).

16. Howitt, C.A. & Vermaas, W.F.J. Subunits of the NAD(P)-reducing nickel-containing hydrogenase do not act as part of the type-1 NAD(P)H dehydrogenase in the cyanobacterium *Synechocystis* sp. PCC 6803. In Peschek, G.A., Löffelhardt, W., Schmetterer, G. (Eds.) *The Phototrophic Prokaryotes. Kluwer Academic/Plenum Publisher, New York, NY USA*, pp. 595-601 (1999).

17. Boison, G., Schmitz, O., Schmitz, B. & Bothe, H. Unusual gene arrangement of the bidirectional hydrogenase and functional analysis of its diaphorase subunit HoxU in respiration of the unicellular cyanobacterium *Anacystis nidulans*. *Curr. Microbiol.* **36**, 253-258 (1998).

18. Antal, T.K., Oliveira, P. & Lindblad, P. The bidirectional hydrogenase in the cyanobacterium *Synechocystis* sp. strain PCC 6803. *Int. J. Hydrogen Energy* **31**, 1439-1444 (2006).

19. Gutthann, F., Egert, M., Marques, A. & Appel, J. Inhibition of respiration and nitrate assimilation enhances photohydrogen evolution under low oxygen concentrations in *Synechocystis* sp. PCC 6803. *Biochim. Biophys. Acta* **1767**, 161-169 (2007).

20. Aubert-Jousset, E., Cano, M., Guedeney, G., Richaud, P. & Cournac, L. Role of HoxE subunit in *Synechocystis* PCC6803 hydrogenase. *FEBS J.* **278**, 4035-4043 (2011).

21. Pinto, F., van Elburg, K.A., Pacheco, C.C., Lopo, M., Noirel, J., Montagud, A., Urchueguía, J.F., Wright, P.C. & Tamagnini, P. Construction of a chassis for hydrogen production. Physiological and molecular characterization of a *Synechocystis* sp. PCC 6803 mutant lacking a functional bidirectional hydrogenase. *Microbiology* **158**, 448-464 (2012).

22. Eckert, C., Boehm, M., Carrieri, D., Dubini, A., Nixon, P.J. & Maness, P.C. Genetic analysis of the Hox hydrogenase in the cyanobacterium *Synechocystis* sp. PCC 6803 reveals subunit roles in association, assembly, maturation, and function. *J. Biol. Chem.* **287**, 43502-43515 (2012).

23. Gutekunst, K., Chen, X., Schreiber, K., Kaspar, U., Makam S. & Appel, J. The bidirectional NiFe-hydrogenase in *Synechocystis* sp. PCC 6803 is reduced by flavodoxin and ferredoxin and is essential under mixotrophic, nitrate-limiting conditions. *J. Biol. Chem.* **289**, 1930-1937 (2013).

24. Gutekunst, K., Phunpruch, S., Schwarz, C., Schuchardt, S., Schulz-Friedrich, R. & Appel, J. LexA regulates the bidirectional hydrogenase in the cyanobacterium *Synechocystis* sp. PCC 6803 as a transcription activator. *Mol. Microbiol.* **58**, 810-823 (2005).

25. McIntosh, C.L., Germer, F., Schulz, R., Appel, J. & Jones, A.K. The [NiFe]-hydrogenase of the cyanobacterium *Synechocystis* sp. PCC 6803 works bidirectionally with a bias to H_2 production. *J. Am. Chem. Soc.* **133**, 11308-11319 (2011).

26. Stanier, R.Y., Kunisawa, R., Mandel, M. & Cohen-Bazire, G. Purification and properties of unicellular blue-green algae (order *Chroococcales*). *Bacteriol. Rev.* **35**, 171-205 (1971).

27. Berto, P., D'Adamo, S., Bergantino, E., Vallese, F., Giacometti, G.M. & Costantini, P. The cyanobacterium *Synechocystis* sp. PCC 6803 is able to express an active [FeFe]-hydrogenase without additional maturation proteins. *Biochem. Biophys. Res. Commun.* **405**, 678-683 (2011).

28. McKinney, G. Absorption of light by chlorophyll solutions. *J. Biol. Chem.* **140**, 315-322 (1941).

29. Xu, W. & McFadden, B.A. Sequence analysis of plasmid pCC5.2 from cyanobacterium *Synechocystis* PCC 6803 that replicates by a rolling circle mechanism. *Plasmid* **37**, 95-104 (1997).

30. Kufryk, G., Sachet, M., Schmettere, G. & Vermaas, W.F.J. Transformation of the cyanobacterium *Synechocystis* sp. PCC 6803 as a tool for genetic mapping: optimization of efficiency. *FEMS Microbiology Letters* **206** , 215-219 (2002).

31. Checchetto, V., Segalla, A., Allorent, G., La Rocca, N., Leanza, L., Giacometti, G.M., Uozumi, N., Finazzi, G., Bergantino, E. & Szabò, I. Thylakoid potassium channel is required for efficient photosynthesis in cyanobacteria. *Proc. Natl. Acad. Sci. USA* **109**, 11043-11048 (2012).

32. Menegazzo, L., Albiero, M., Millioni, R., Tolin, S., Arrigoni, G., Poncina, N., Tessari, P., Avogaro, A. & Fadini, G.P. Circulating myeloid calcifying cells have antiangiogenic activity via thrombospondin-1 overexpression. *FASEB J*. **27**, 4355-4365 (2013).

33. Stal, L.J. & Moezelaar, R. Fermentation in cyanobacteria. *Fems Microbiol. Rev.* **21**, 179-211 (1997).

34. Barz, M., Beimgraben, C., Staller, T., Germer, F., Opitz, F., Marquardt, C., Schwarz, C., Gutekunst, K., Vanselow, K.H., Schmitz, R., LaRoche, J., Schulz, R. & Appel, J. Distribution analysis of hydrogenases in surface waters of marine and freshwater environments. *PLoS ONE* **5**, e13846 (2010).

35. Wiegard, A., Dörrich, A.K., Deinzer, H.-T., Beck, C., Wilde, A., Holtzendorff, J. & Axmann I.M. Biochemical analysis of three putative KaiC clock proteins from *Synechocystis* sp. PCC 6803 suggests their functional divergence. Microbiology **159**, 948-958 (2013).

36. Dörrich, A.K., Mitschke, J., Siadat, O. & Wilde, A. Deletion of the *Synechocystis* sp. PCC 6803 kaiAB1C1 gene cluster causes impaired cell growth under light-dark conditions. Microbiology, doi: 10.1099/mic.0.081695-0 (2014).

37. De Lacey, A.L., Fernandez, V.M., Rousset, M. & Cammack, R. Activation and inactivation of hydrogenase function and the catalytic cycle: spectroelectrochemical studies. *Chem. Rev.* **107**, 4304-4330 (2007).

38. Fernandez, V.M., Hatchikian, E.C., Patil, D.S. & Cammack, R. ESR-detectable nickel and iron-sulphur centres in relation to the reversible activation of *Desulfovibrio gigas* hydrogenase. *Biochim. Biophys. Acta* **883**, 145-154 (1986).

39. Pandelia, M.E., Ogata, H. & Lubitz, W. Intermediates in the catalytic cycle of hydrogenase: functional spectroscopy of the active site. *ChemPhysChem* **11**, 1127-1140 (2010).

40. Blokesch, M., Paschos, A., Theodoratou, E., Bauer, A., Hube, M., Huth, S. & Böck, A. Metal insertion into NiFe-hydrogenases. *Biochem. Soc. Trans.* **30**, 674-680 (2002).

41. Hoffman, D., Gutekunst, K., Klissenbauer, M., Schulz-Friedrich, R. & Appel, J. Mutagenesis of hydrogenase accessory genes of *Synechocystis* sp. PCC 6803. Additional homologues of *hypA* and *hypB* are not active in hydrogenase maturation. *FEBS J.* **273**, 4516-4527 (2006).

42. Schmitz, O., Boison, G., Bothe, H., Schütz, K., Wang, S.H. & Happe, T. HoxE: a subunit specific for the pentameric bidirectional hydrogenase complex (HoxEFUYH) of cyanobacteria. *Biochim.Biophys. Acta* **1554**, 66-74 (2002).

43. Gao, Y., Xiong, W., Li, X., Gao, C.F., Zhang, Y.L., Li, H. & Wu, Q.Y. Identification of the proteomic changes in *Synechocystis* sp. PCC 6803 following prolonged UV-B irradiation. *J. Exp. Bot.* **60**, 1141-1154 (2009).

44. Wegener, K.M., Singh, A.K., Jacobs, J.M., Elvitigala, T., Welsh, E.A., Keren, N., Gritsenko, M.A., Ghosh, B.K. & Camp, D.G. 2nd, Smith, R.D. & Pakrasi, H.B. Global proteomics reveal an atypical strategy for carbon/nitrogen assimilation by a cyanobacterium under diverse environmental perturbations. *Mol. Cell. Proteomics* **9**, 2678-2689 (2010)

45. Battchikova, N., Vainonen, J.P., Vorontsova, N., Keränen, M., Carmel, D. & Aro, E.M. Dynamic changes in the proteome of *Synechocystis* 6803 in response to CO_2 limitation revealed by quantitative proteomics. *J. Proteome Res.* **9**, 5896-5912 (2010).

46. Rowland, J.G., Simon, W.J., Prakash, J.S. & Slabas, A.R. Proteomics reveals a role for the RNA helicase crhR in the modulation of multiple metabolic pathways during cold acclimation of *Synechocystis* sp. PCC6803. *J. Proteome Res.* **10**, 3674-3689 (2011).

47. Li, T., Yang, H.M., Cui, S.X., Suzuki, I., Zhang, L.F., Li, L., Bo, T.T., Wang, J., Murata, N. & Huang, F. Proteomic study of the impact of Hik33 mutation in *Synechocystis* sp. PCC 6803 under normal and salt stress conditions. *J. Proteome Res.* **11**, 502-514 (2012).

48. Qiao, J., Wang J., Chen, L., Tian, X., Huang, S. & Ren, X. Quantitative iTRAQ LC-MS/MS proteomics reveals metabolic responses to biofuel ethanol in cyanobacterial *Synechocystis* sp. PCC 6803. *J. Proteome Res.* **11**, 5286-5300 (2012).

49. Mullineaux, C.W. Co-existence of photosynthetic and respiratory activities in cyanobacterial thylacoid membranes. *Biochim. Biophys. Acta* **1837**, 503-511 (2014).

50. Berger, S., Ellersiek, U. & Steinmüller, K. Cyanobacteria contain a mitochondrial complex I-homologous NADH-dehydrogenase. *FEBS Lett.* **286**, 129-132 (1991).

51. Yagi, T. Prokaryotic complex I (NDH-1), an overview. *Biochim. Biophys. Acta* **1364**, 125-133 (1998).

52. Battchikova, N. & Aro, E.M. Cyanobacterial NDH-1 complexes: multiplicity in function and subunit composition. *Physiol. Plant.* **131**, 22-32 (2007).

53. Ogawa, T. & Mi, H. Cyanobacterial NADPH dehydrogenase complexes. *Photosynth. Res.* **93**, 69-77 (2007).

54. Cooley, J.W. & Vermaas, W.F. Succinate dehydrogenase and other respiratory pathways in thylacoid membrane of *Synechocystis* sp. PCC 6803: capacity comparisons and physiological function. *J. Bacteriol.* **183**, 4251-4258 (2001).

55. Ogawa, T. A gene homologous to the subunit-2 gene of NADH dehydrogenase is essential to inorganic carbon transport of *Synechocystis* sp. PCC 6803. *Proc. Natl. Acad. Sci. USA* **88**, 4275-4279 (1991).

56. Cournac L., Guedeney, G., Peltier, G. & Vignais, P.M. Sustained photoevolution of molecular hydrogen in a mutant of *Synechocystis* sp. strain PCC 6803 deficient in the Type I NADPH-dehydrogenase complex. *J. Bacteriol.* **186**, 1737-1746 (2004).

Figure legends

Figure 1. Wild type *Synechocystis* is more resistant to prolonged darkness than ΔHoxE-H mutant strain. *Panel A*, continuous white light (50 µE m^{-2} s^{-1}); *panel B*, 12 h light (50 µE m^{-2} s^{-1})/12 h dark; *panel C*, continuous darkness. Optical densities at 730 nm ($O.D._{730}$) of wild type (WT, dark grey) and ΔHoxE-H (light grey) liquid cultures were measured after five days of growth, and values normalized to the $O.D._{730}$ of the WT strain cultured in the same condition (*i.e.*, *panel A*, 5.2 ± 0.72; *panel B*, 4.03 ± 0.15; *panel C*, 1.8 ± 0.55). Reported data result from the mean of three independent experiments ± Standard Deviation.

Figure 2. ΔHoxE-H *Synechocystis* mutant strain is able to resume its growth in the light after a five-day incubation under complete darkness. Growth curve of ΔHoxE-H *Synechocystis* mutant strain cultured up to five days in the dark and additional three days under normal light intensity. Reported data result from the mean of three independent experiments ± Standard Deviation.

Figure 3. ΔHoxE-H *Synechocystis* mutant cells grown under light and in the dark display the same ultrastructural organization. Transmission Electron Microscopy of *Synechocystis* ΔHoxE-H mutant cells grown up to five days either in the light (*left panel*) or in complete darkness (*right panel*). Scale bar: 0.5 μm.

Figure 4. Construction of ΔHypA1 and ΔHypB1 *Synechocystis* mutant strains. *Upper panels*, schematic diagram of the construction of the ΔHypA1 (panel A) and ΔHypB1 (panel B) knock-out strain. The *hypA1* (*slr1675*) and *hypB1* (*sll1432*) genes were deleted and substituted by a kanamycin-resistance cassette (as detailed in Materials and methods). Positions of PCR primers used to verify correct insertion of the cassette are indicated (*FLhypA1_for/ FLhypA1_rev* and *FLhypB1_for/ FLhypB1_rev*). *Lower panels*, agarose gel electrophoresis of analytical PCR amplifications using as template genomic DNA from wild type and knock-out strains. *Lane 1*, molecular markers; *lane 2*, DNA from wild type; *lane 3*, DNA from knock-out.

Figure 5. ΔHypA1 and ΔHypB1 *Synechocystis* mutant strains have the same growth phenotype of the wild type strain when cultured in the dark. *Panel A*, ΔHypA1; *panel B*, ΔHypB1. Strains were grown either under continuous white light (50 μE m^{-2} s^{-1}) or in the dark. Optical densities at 730 nm ($O.D._{730}$) of wild type (WT, dark grey) and mutants (light grey) liquid cultures were measured after five days, and values normalized to the $O.D._{730}$ of the WT strain cultured in the same condition (*i.e.* light, 5.8 ± 0.9; dark, 1.6 ± 0.1). In all panels, reported data result from the mean of three independent experiments ± Standard Deviation.

Table 1. List of primers used in this study

Primer name	Primer sequence
SacI*hypA1*_for	5'-TACGTTCAAGAGCTCAGCCCCGAAACC-3'
BamHI*hypA1*_rev	5'-CATATGCACGAAGGGATCCGGTGTGT-3'
BamHI*hypA1*_for	5'-GGATCCGGTGTGTTAGAACTGAGTTGA-3'
EcoRV*hypA1*_rev	5'-ACTGGGGTGGATATCGTCCAAAGAATTATC-3'
SacI*hypB1*_for	5'-ATGAGTCTGGGGAGCTCCGCTTCCG-3'
BamHI*hypB1*_rev	5'-TGTAGTGCGGTGGGAtCCGTTGCCC-3'
BamHI*hypB1*_for	5'-GGATCCGTTGCCCGCATTGGCCTAA-3'
EcoRV*hypB1*_rev	5'-CCGGGCCATAACGGTGGCGATATC-3'
FL*hypA1*_for	5'-GGGCTCAGCGCTCCCGTGCTGG-3'
FL*hypA1*_rev	5'- ATGCCCGCTGGCCCCGGTGGA-3'
FL*hypB1*_for	5'- CCAGCAACCGGGCGGAGCCGT-3'
FL*hypB1*_rev	5'- TGGATGGGGTCCAGGCTTTGGCCCA-3'

Table 2. Distribution by functional groups of proteins differentially regulated between control and darkness *Synechocystis* growth

Functional category	**Up-regulated** (dark/light ratio ≥ 1.5)	**Down-regulated** (dark/light ratio ≤ 0.67)
Nucleotides metabolism, Transcription, Translation	38	1
Metabolism	8	12
- Aminoacids	- 6	- 5
- Lipids	- 1	- 2
- Carbohydrates	- 1	- 5
Photosynthesis	0	7
Respiration	0	4
Other functions	4	17
Unknown	8	13

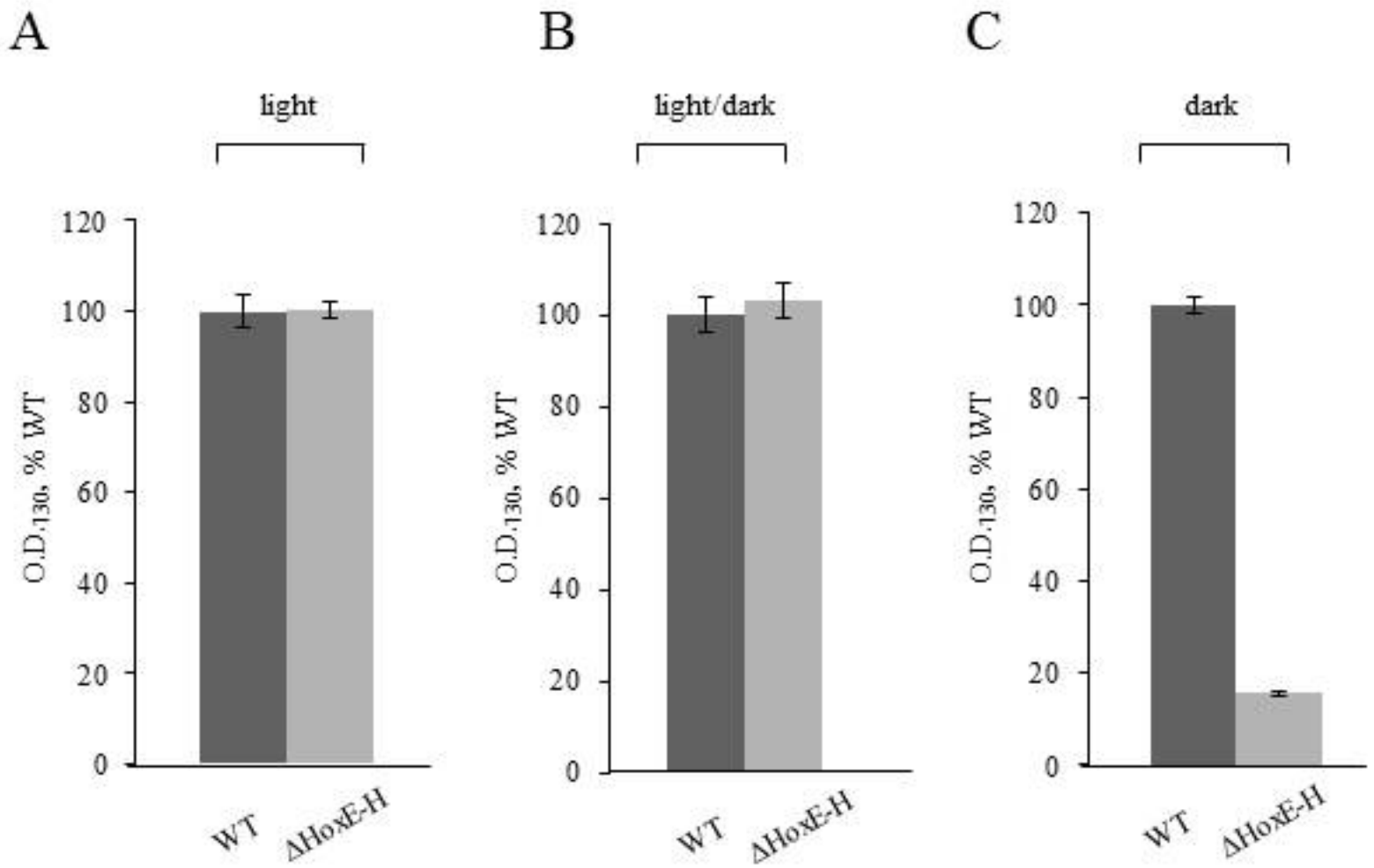
A
B
C
light
light/dark
dark
120
100
80
60
40
20
0
O.D.130, % WT
WT
ΔHoxE-H

Figure 1

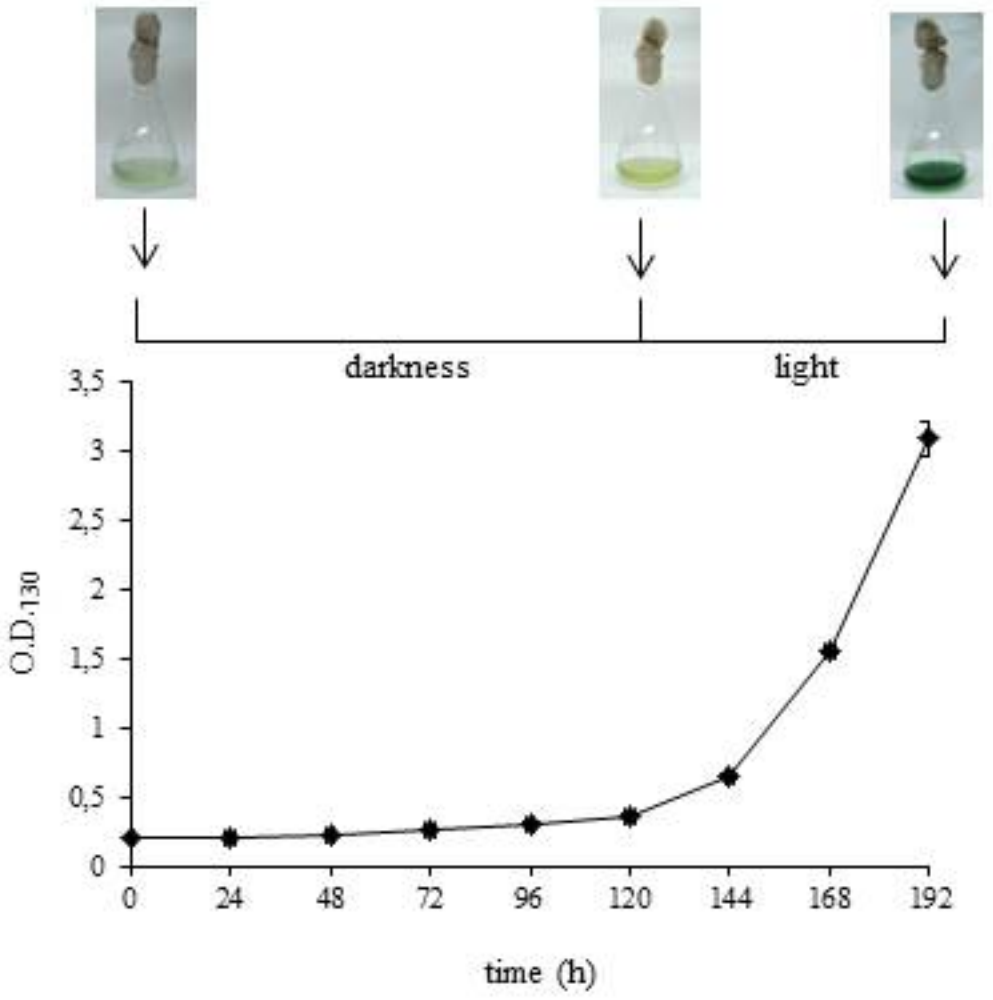
darkness
light
3,5
3
2,5
2
1,5
1
0,5
0
O.D.130
0
24
48
72
96
120
144
168
192
time (h)

Figure 2

ΔHoxE-H, 5 days light

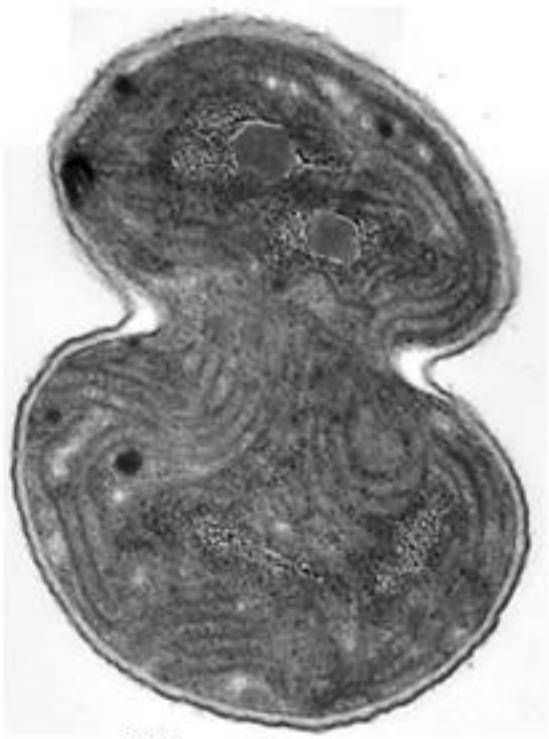

500 nm

ΔHoxE-H, 5 days darkness

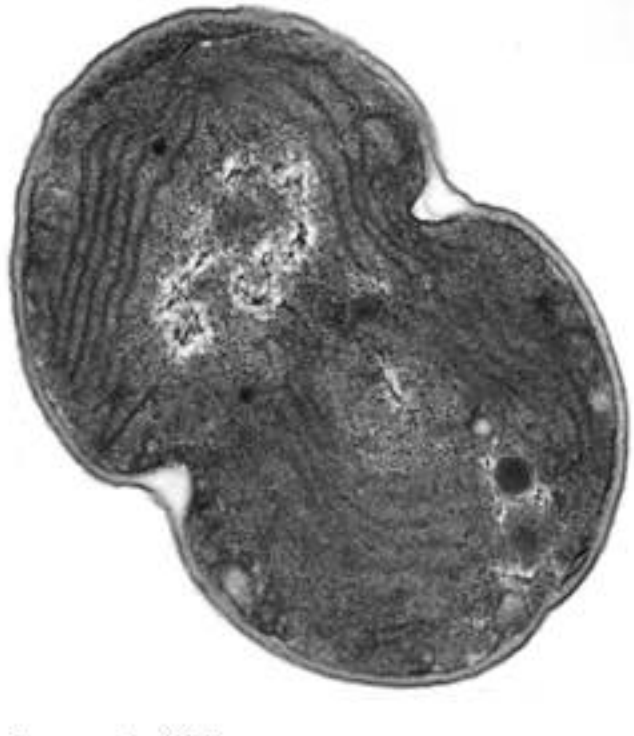

500 nm

Figure 3

A

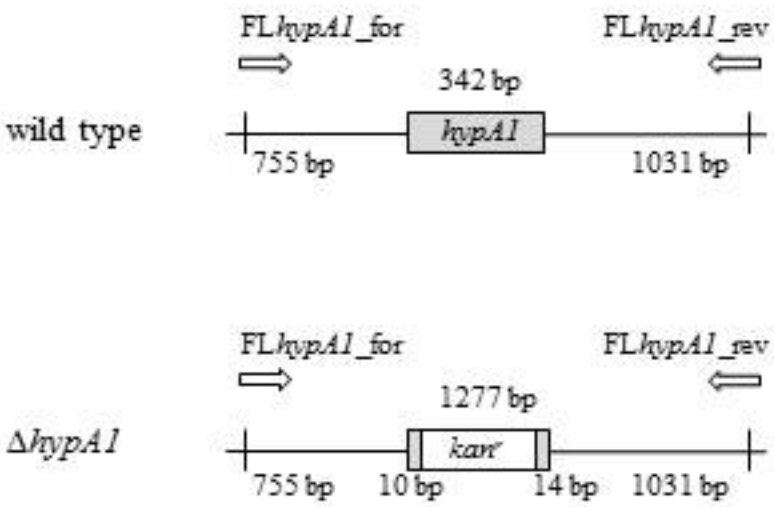
FL*hypA1*_for
FL*hypA1*_rev
342 bp
wild type
hypA1
755 bp
1031 bp
FL*hypA1*_for
FL*hypA1*_rev
1277 bp
Δ*hypA1*
*kan*r
755 bp
10 bp
14 bp
1031 bp

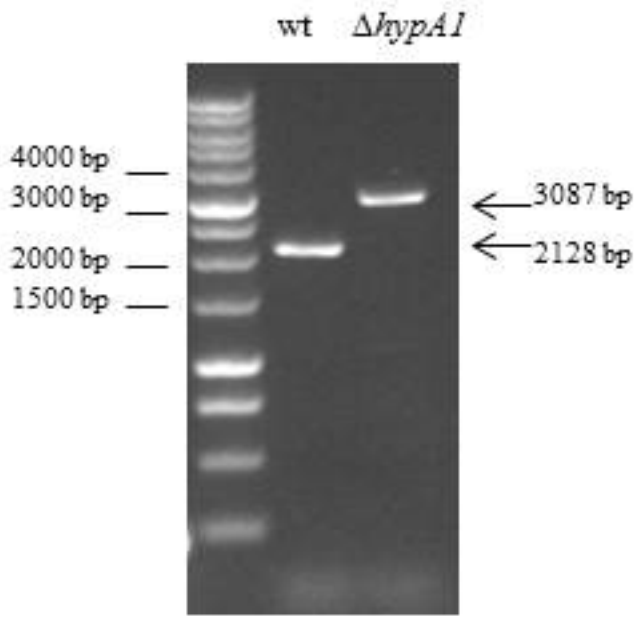
wt
Δ*hypA1*
4000 bp
3000 bp
2000 bp
1500 bp
3087 bp
2128 bp

B

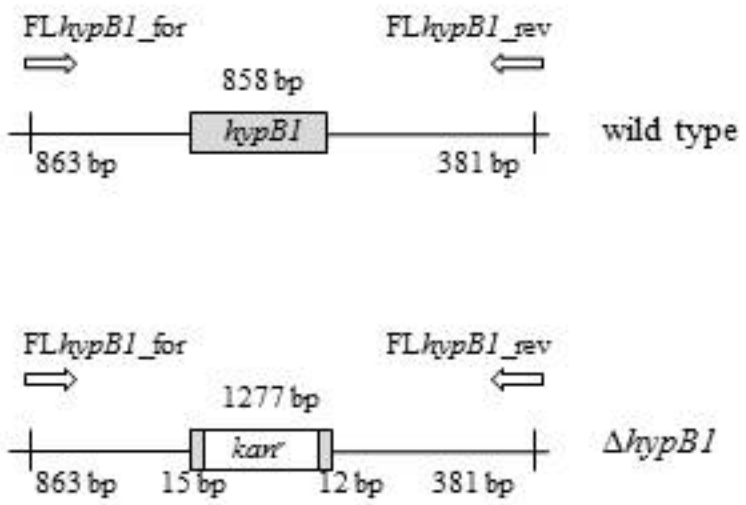
FL*hypB1*_for
FL*hypB1*_rev
858 bp
hypB1
wild type
863 bp
381 bp
FL*hypB1*_for
FL*hypB1*_rev
1277 bp
*kan*r
Δ*hypB1*
863 bp
15 bp
12 bp
381 bp

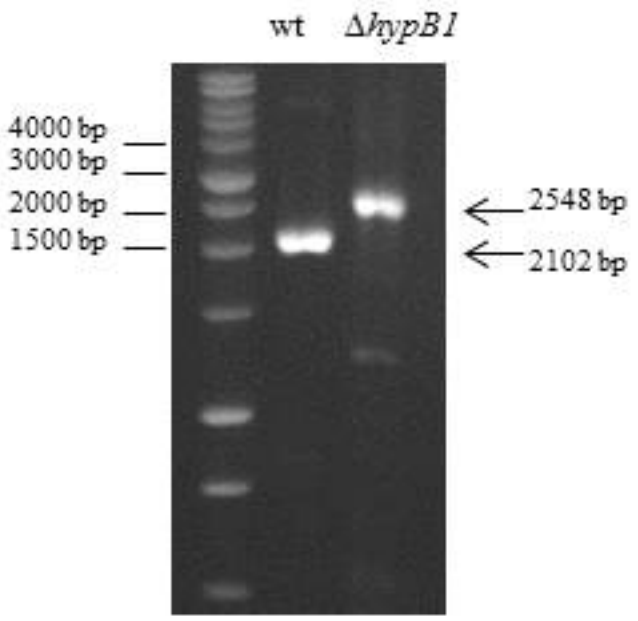
wt
Δ*hypB1*
4000 bp
3000 bp
2000 bp
1500 bp
2548 bp
2102 bp

Figure 4

A

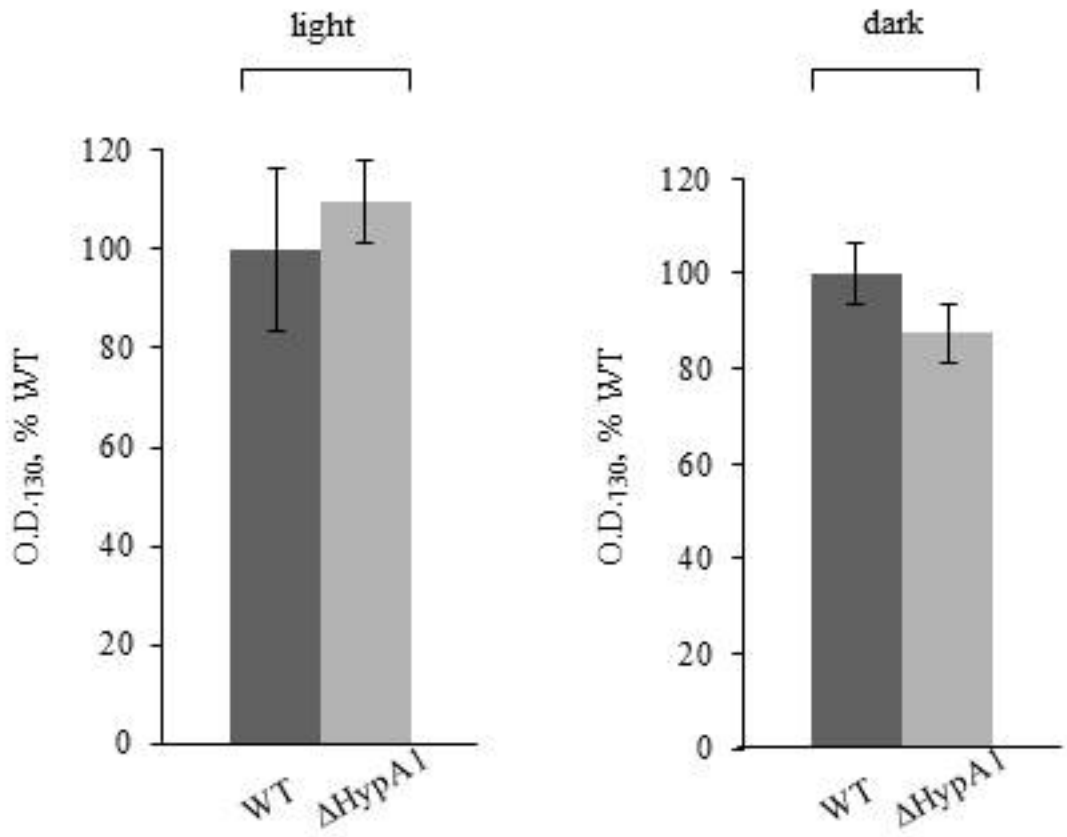
light
dark
120
100
80
60
40
20
0
O.D.130, % WT
WT
ΔHypA1

B

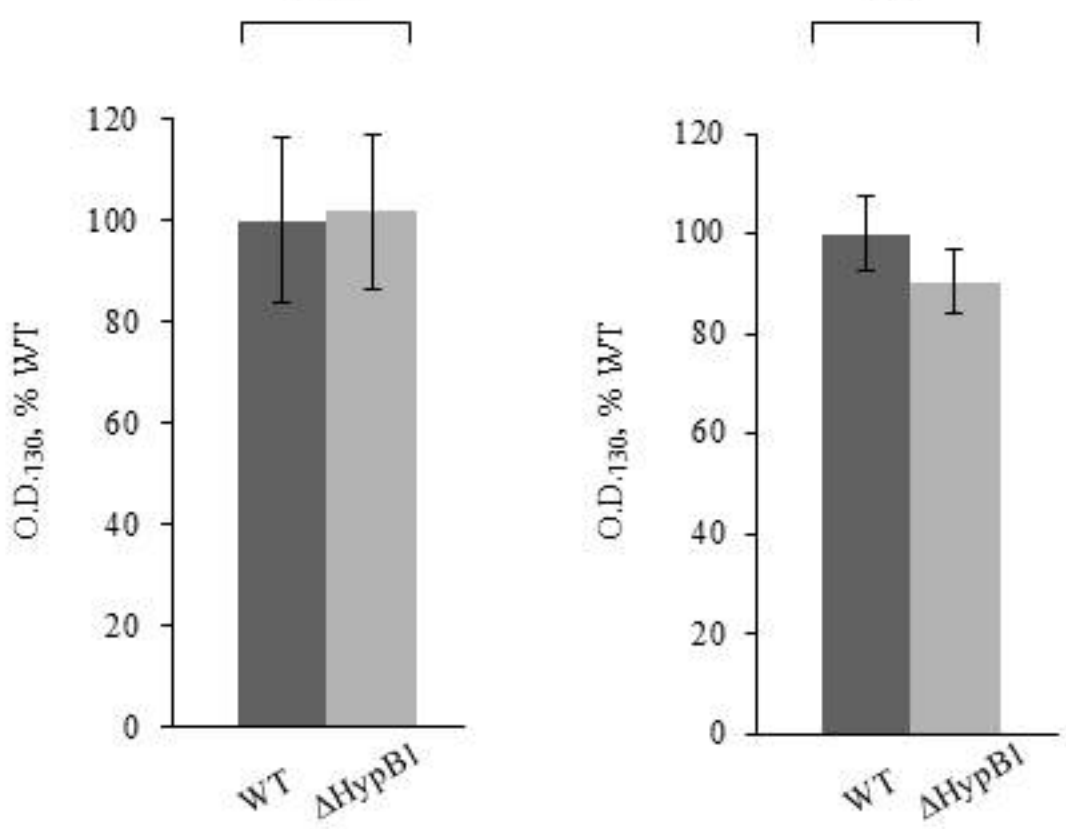
light
dark
120
100
80
60
40
20
0
O.D.130, % WT
WT
ΔHypB1

Figure 5

A conformational study of the GTPase domain of [FeFe]-hydrogenase maturation protein HydF, by PELDOR spectroscopy

Lorenzo Maso[a], Laura Galazzo[b], Francesca Vallese[a], Marilena Di Valentin[b], Marco Albertini[b], Edith De Rosa[a], Giorgio M. Giacometti[a], Paola Costantini[a*] and Donatella Carbonera[b*]

[a] *Department of Biology, University of Padova, Viale G. Colombo 3, 35131 Padova, Italy*

[b] *Department of Chemical Sciences, University of Padova, Via F. Marzolo 1, 35131 Padova, Italy*

e-mail: donatella.carbonera@unipd.it; paola.costantini@unipd.it

Abstract

[FeFe]-hydrogenases catalyze the reversible interconversion of protons to molecular hydrogen (H_2) at an active site called H-cluster. The maturation pathway of these enzymes is a complex process involving three proteins, HydE, HydF and HydG. The maturase protein HydF has been suggested to interact with HydE and HydG and to be the transferase that shuttles the complete H-cluster to the hydrogenase; however the exact molecular mechanism driving this translocation remains unclear. HydF is constituted by three different domains: a N-terminal GTP-binding domain, a dimerization domain and a C-terminal [4Fe4S]-cluster binding domain. To investigate possible conformational changes induced by the GTP binding in the N-terminal domain, we have expressed, in *Escherichia coli*, a recombinant HydF protein from *Thermotoga neapolitana* including the GTP-binding domain only. Site-directed mutants were designed in which the native residues were substituted by cysteines and subsequently spin-labeled with the nitroxide MTSSL. CW-EPR was used to study the local mobility of the nitroxides at each site, and double spin-labeled mutants have been investigated by PELDOR spectroscopy. We found that the binding of the nucleotide does not induce large conformational effects within the isolated GTP domain, at least at the level of the elements investigated in this work. However, small changes in the distance between spin labels were observed which might reflect diffuse structural rearrangements. We suggest that the variations following the GTP binding could affect the dimer form adopted by the whole HydF protein in solution and, as consequence, the interactions with the other maturases.

1 Introduction

[FeFe]-hydrogenases are metalloenzymes, found both in bacteria and eukaryotes [1], that catalyze the reversible interconversion of protons to molecular hydrogen (H_2) at a very complex active site, referred to as the H-cluster. The structure of this 6Fe-cluster has been determined by X-ray crystallographic analysis [2, 3] and comprises a [4Fe4S] subcluster, produced by canonical Fe-S cluster biosynthesis proteins, linked via a cysteine bridge to a 2Fe unit with two terminal CN^- ligands, two terminal CO ligands, and azadithiolate and CO bridges. Extensive research is devoted to define the catalytic mechanism of the [FeFe]-hydrogenases (see [4] for a recent review); however, it still remains unclear how the H-cluster is formed within the cell and only a partial knowledge of the machinery driving its assembly *in vivo* is available (see [4-6] for comprehensive reviews on this topic). This pathway involves three proteins, *i.e.* HydE, HydF and HydG, which have been originally discovered in the unicellular green alga *Chlamydomonas reinhardtii* [7] and then found in all microorganisms containing a [FeFe]-hydrogenase. HydE and HydG are both radical S-adenosylmethionine (SAM) enzymes [7, 8], and HydF is a GTPase containing an FeS cluster-binding motif [7, 9]. Different models have been proposed to describe the maturation pathway involving these proteins. Several *in vitro* and/or cell-free experiments using purified recombinant proteins led to a two step model (reviewed in [5, 6]), in which (a) HydE and HydG drive the chemical modifications of a H-cluster precursor working on HydF as a scaffold protein, (b) HydF transfer this cluster to the hydrogenase (HydA), completing the maturation process [10-12]. This model has been further supported by independent *in vitro* experiments showing that a H-cluster synthetic mimic can be loaded on a recombinant HydF protein and then transferred to an apo-hydrogenase, confirming the key role of this scaffold protein [13, 14]. On the other hand, Kuchenreuther and co-workers [15] have recently proposed that the iron, carbon monoxide, and cyanide components of the 2Fe unit in the active H-cluster of HydA, originate all from the chemistry which takes place in one of the two [4Fe4S] centers of the HydG protein, with a diiron subsite forming from two HydG synthons. The transfer of these components to the apo-hydrogenase HydA (which contains the [4Fe4S] cluster of the H-cluster but not the [2Fe] subsite) would lead to the functional protein, as proved by ^{57}Fe-labeling experiments showing that Fe in the [2Fe] subcluster is in fact provided by HydG [15]. However, how the two complex units would assemble together with a dithiolate bridge to form the [2Fe] subcluster remains to be clarified. Moreover, a recent study in cell-free conditions has shown that a synthetic diiron subsite [16] can be captured from solution by apo-HydA to give an active [FeFe]-hydrogenase without participation of HydE or

HydF. Nevertheless, these two proteins have a role in the maturation process both *in vitro* [17] and *in vivo*, since *C. reinhardtii* recombinant mutant strains lacking single or combinations of maturases are completely unable to express an active [FeFe]-hydrogenase [7].

A key point, which must be addressed to complete the knowledge of the [FeFe]-hydrogenases activation, is related to the molecular mechanism allowing an accurate delivery of the H-cluster precursor to the apoprotein. As assessed above, HydF has been suggested to be the transferase that shuttles the complete [2Fe] subcluster to the hydrogenase, but the exact molecular mechanism driving this translocation is still under investigation. The X-ray structure of the apo-HydF from *T. neapolitana* has been solved (PDB ID: 3QQ5) [18], showing the presence of three different domains: a N-terminal GTP-binding domain (I), a dimerization domain (II) and a C-terminal metal cluster-binding domain (III). In a previous work, we explored the [4Fe4S] cluster coordination sphere of HydF from *Clostridium acetobutylicum* and *T. neapolitana* by means of continuous-wave Electron Paramagnetic Resonance (CW-EPR) and Hyperfine Sublevel Correlation (HYSCORE) spectroscopies [19]. Our results showed that, despite the presence of the highly conserved FeS cluster $CxHx_{46-53}HCxxC$ putative coordination motif, alternative metal ligation of the FeS cluster exists in the HydF proteins from the two microorganisms, and that the non-cysteinyl ligand is easily exchangeable. This lead us to suggest a possible role for the unusually coordinated Fe in the catalytic process of HydF. On the other side, the HydF GTPase activity, which has been shown to be essential for the H-cluster biosynthesis [7], has been fully characterized *in vitro* with recombinant proteins from different microorganisms [9, 20, 21], but its exact contribution to the [FeFe]-hydrogenase maturation and activation is still elusive, and the role of GTP binding/hydrolysis remains uncertain. Since both HydE and HydG have been shown to increase by 50% the rate of GTP hydrolysis of a recombinant HydF protein from *C. acetobutylicum* [20], it has been proposed that GTP binding and hydrolysis are associated with interactions of HydF with the other accessory proteins, rather than with hydrogenase. Interestingly, we found that the binding of GTP (either as such or as non-hydrolyzable analog) induces the dissociation of HydE and HydG from HydF [21]. Furthermore, the 3D structure of the apo-HydF protein showed that the GTPase domain includes a flexible loop region, which could in principle become ordered upon GTP binding [18]. This could in turn facilitate structural rearrangements driving the interactions of HydF scaffold with the two other maturation proteins. It has also been reported that the presence of GTP significantly affects the EPR spectral properties of the HydF [4Fe4S] cluster [20], suggesting a communication between the GTP- and the iron-sulfur cluster binding domains, where the H-cluster precursor is probably finally assembled. This latter possibility would be analogous to the case of the GTPase MnmE [22] or to the case of the nitrogenase Fe protein [23-25].

Prompted by these experimental evidences, to investigate possible intrinsic conformational changes induced by the nucleotide binding at the interface of the GTPase domain with either the [4Fe4S] cluster-binding or the dimerization domains, we have expressed in *E. coli* a recombinant HydF protein from *T. neapolitana* including only the GTP-binding domain. Five single site-directed mutants have been designed in which the native amino acids were substituted by cysteine residues and subsequently spin labeled with the nitroxide MTSSL. CW-EPR was used to study the local mobility of the nitroxides at each site, and to determine the spin-labeling efficency and choose the suitable positions for labeling of double mutants to be investigated by pulse electron-electron double resonance (PELDOR) spectroscopy. This spectroscopic method is known to be very useful for monitoring distances and distance distributions between couples of spin labels, in the nanometric scale [26-30].

2. Experimental

All chemicals were of the highest purity commercially available.

Cloning of $HydF_{T.n.}$ GTPase domain. The sequence coding for the GTPase N-terminal domain (domain I, residues 1-185) of the HydF protein from *T. neapolitana* ($HydF_{T.n.}I$) was PCR amplified using as template a vector containing the *$hydF_{T.n.}$* gene, previously obtained in our laboratory [18], and the following primers:

$HydF_{T.n.}I$ for, 5'-CATATGAGACTGCCGGACGCCGGT-3' and

$HydF_{T.n.}I$ rev, 5'-CTCGAGTTAAATCTCTTCATC-3'.

These primers were designed to contain unique restriction sites allowing the directional subcloning of the amplified sequence in frame with a 6His-tag sequence at the 5' terminus in a pET-28b vector (from Novagen®) suitable for T7-driven expression in *E. coli*. The sequence and reading frame were confirmed by DNA sequencing (BMR Genomics, University of Padova). The *pET-28b/$hydF_{T.n.}I$* plasmid was used as template to introduce different mutations in the wild-type *hydF* coding sequence (see below).

Heterologous expression and purification of $HydF_{T.n}$ GTPase domain. E. coli Rosetta (DE3) cells were transformed with the *pET-28b/$hydF_{T.n.}I$* plasmid, and positive clones were selected by antibiotic resistance. Transformed cells were grown overnight in selective LB medium and then subclutured the following day in fresh medium. The expression of the 6His-tagged $HydF_{T.n.}I$ proteins, either wild-type or mutant, was induced by adding 1 mM isopropyl-β-thiogalactopyranoside (IPTG) in LB medium and incubating the cells at 30 °C overnight. The proteins were purified starting from 1 L cultures. In brief, cells were harvested by centrifugation,

resuspended in lysis buffer (25 mM Tris-HCl pH 8, 200 mM KCl, and protease inhibitors 1μg/ml pepstatin A, 1 μg/ml leupeptin, 1 μg/ml antipain, 1 mM PMSF) and lysed by French press. The supernatant fractions were isolated from cell debris by centrifugation and the proteins purified to homogeneity by combining a nickel affinity chromatography (HIS-Select® Nickel Affinity Gel, from Sigma-Aldrich) and a gel filtration chromatography using a Superose 12 10/300 GL column (from GE Healthcare, Italy), equilibrated in lysis buffer. Each run was performed by injecting the appropriate sample volume at a flow rate of 0.75 ml/min and monitoring the UV absorbance at 280 nm, by a fixed wavelength detector. To estimate the molecular weight of the analyzed samples, the column was equilibrated in the lysis buffer and calibrated with the standards such as thyroglobulin (669,000 Da), ferritin (440,000 Da), catalase (232,000 Da), aldolase (158,000 Da), bovine serum albumin (67,000 Da), ovalbumin (43,000 Da), ribonuclease (13,700 Da). For each purification, the eluted fractions were pooled together and concentrated by centrifugal filters (Vivaspin® Centrifugal Concentrators, 10,000 MWCO, from Sartorius Stedim Biotech) to a volume suitable for EPR characterization (see below), giving rise to a final concentration ranging from 800 μM to 3 mM, as determined with a Micro BCA Protein Assay Kit (from Thermo Scientific Pierce Protein Research). Purified proteins were analyzed by 12% SDS-PAGE.

Site-directed mutagenesis of $HydF_{T.n.}I$. Site-directed mutagenesis of the *$hydF_{T.n.}$* gene was performed with the QuickChange® II Site-Directed Mutagenesis Kit (from Stratagene), using as template *pET-28b/$hydF_{T.n.}I$* recombinant plasmid. Oligonucleotides, listed in Table 1, were designed according to the manufacturer's guidelines and the mutant constructs analyzed by DNA sequencing.

GTP hydrolysis assay. The purified recombinant wild-type $HydF_{T.n.}I$ protein was assayed for the ability to hydrolyze GTP using the protocol optimized by Shepard and co-workers [20], with slight modifications. In brief, the affinity purified protein was incubated at a concentration of 10 μM for 10 minutes at 30 °C in 20 mM Tris-HCl buffer, pH 8.0, containing 200 mM KCl and 2 mM $MgCl_2$ with different concentrations of GTP (ranging from 125 μM to 2 mM). Aliquots with different concentrations of substrate were collected and assayed for production of GDP. Assay aliquots were incubated at 95°C for 3 minutes, centrifuged at 14,000 rpm at 4 °C in a bench top microcentrifuge, and the supernatants analyzed by reverse phase HPLC on a Synergi MAX-RP 80A (150 × 4.6 mm, 4 μm, Phenomenex). The samples were eluted with an isocratic mobile phase of 50 mM sodium phosphate buffer, pH 7.0, 10 mM tetrabutylammonium bromide, 10% CH_3CN. The guanosine nucleotides were detected by their absorbance at 254 nm. Under these conditions, GDP and GTP were eluted after 8.1 and 18.6 min, respectively. Integration of peak areas (using software Agilent

Chemstation) of the samples taken at identical time points allowed the quantification of the μmoles of GDP produced L^{-1} min^{-1}, from which the ratio between the k_{cat} were finally determined.

CW-EPR experiments. Samples for EPR (about 100 μM protein labeled with MTSSL spin label in lysis buffer) were obtained by adding to the purified protein a fivefold molar excess of MTSSL (dissolved in DMSO) and incubating the protein at 4 °C overnight in the dark. Excess of non-ligated spin label was removed from the protein by several cycles of dilution with the lysis buffer and concentration by centrifugal filters. Twenty microliters of each sample with a protein concentration of about 150 μM, were loaded into quartz capillaries with 0.6 mm ID and 0.8 mm OD. Non-hydrolysable GTP analogous (GTPγS) 50 mM and $MgCl_2$ were added to the samples and incubated 30 minutes at 37 °C before starting the EPR measurements. EPR spectra were collected at room temperature (298 K) on an Elexsys E580-X-band spectrometer (Bruker) using a Super High Sensitivity cavity. The field modulation frequency was set at 100 kHz, with a field-modulation amplitude of 0.3 mT and a microwave power of 6.4 mW. Simulations of the CW-EPR spectra were performed using the EasySpin function "chili" to obtain the correlation times for the nitroxide in the different mutants [30]. Rotamers of the spin label in the different mutated sites were evaluated, starting from the X-ray structure, using the molecular modeling software MMM2013 [31].

PELDOR experiments. Samples for PELDOR were concentrated and exchanged with deuterated buffer. Deuterated glicerol (40% w/v) was also added to the samples before freezing. The final protein concentration was about 300 μM for all the samples. In the nucleotide-binding experiments 50 mM GTPγS and 10 mM $MgCl_2$ were added to the samples and incubated 30 minutes at 37 °C before freezing. Samples were loaded into quartz capillaries with 2.0 mm ID and 3.0 mm OD. Pulsed EPR was performed with the same EPR spectrometer equipped with a Bruker ER4118X-MS3 split-ring resonator (microwave frequency = 9.55 GHz) and an Oxford CF935 cryostat. The measurements were done at a temperature of 50 K. For PELDOR experiments a standard four-pulse sequence was applied; the microwave power was adjusted to obtain an observer sequence of 16/32/32 ns and a pump pulse of 16 ns. The difference between the pump (nitroxide) and observer (nitroxide) frequency was set to 70 MHz. A two-step phase cycle was applied for baseline correction while deuterium nuclear modulations were suppressed using an eight-step τ cycle from a 180 ns starting value with 56 ns increment steps. Data on each sample were collected for about 15 h. Distance distributions were extracted from PELDOR traces using DeerAnalysis2013 [32].

3 Results

As assessed in the Introduction, an active HydF GTPase domain is essential to produce a functional [FeFe]-hydrogenase, both *in vivo* and *in vitro* [7, 17]. However, the role of GTP binding and/or hydrolysis in the H-cluster assembly is still unknown. To explore the dynamic behavior required for the HydF scaffold/carrier role in the [FeFe]-hydrogenase maturation, we obtained a recombinant $HydF_{T.n.}$ protein including only its GTPase domain (domain I, residues 1 to 185), *i.e.* $HydF_{T.n.}I$, and analyzed by EPR spectroscopy several spin-labeled mutants, where cysteine residues were introduced at proper sites by site-directed mutagenesis. The selected sequence includes the five consensus motifs shared by all NTPases and essential to bind and hydrolyze GTP (*i.e.* P-loop: GRRNVGKS, and G2 to G4 loops: TTT, DTPG and NKID respectively, with the conserved aminoacids underlined), and a short extra stretch of residues belonging to the loop between domains I and II has been also included in the construct.

3.1. Heterologous expression, purification and preliminary biochemical characterization of wild-type $HydF_{T.n.}I$. The recombinant protein $HydF_{T.n.}I$ was expressed in *E. coli* Rosetta (DE3) cells in frame with a 6His-tag at the N terminus, as described in Sect. 2, and purified by combining a NiNTA affinity and a gel filtration chromatography. A shown in Fig. 1, the isolated domain I can be indeed purified to homogeneity (lane 2) and as a single monomeric species, as assessed by the gel filtration chromatogram (not shown). The same elution profile has been obtained in the presence of GTPγS (not shown) at the same concentration used for the following spectroscopic analysis (*i.e.* 50 mM).

The capability of this protein to bind and hydrolyze GTP has been then evaluated, as described in Sect. 2, and compared with activity of the full-length protein, previously characterized in our laboratory. As reported in Table 2, the isolated domain, obtained in a soluble form, keeps the capability of GTP hydrolysis. According to the measurements, in the isolated domain the catalytic rate constant (k_{cat}) increases about ten times when compared to that the whole protein, which is comparable to that reported before for the HydF proteins from *T. maritima* and *C. acetobutilycum* [9, 20]. The higher enzymatic activity of the isolated domain is likely due to a higher accessibility of the active site.

3.2. Site-directed spin-label of $HydF_{T.n.}I$. A close look to the HydF GTPase domain suggested several useful positions for cysteine residues to be introduced and derivatized using thiol-specific spin labels. The wild-type domain contains a single cysteine (*i.e.* C91), depicted in red in the X-ray structure of the whole $HydF_{T.n.}$ protein shown in Fig. 2. Five additional sites were chosen to

introduce the cysteine residues to evaluate the potential effect of GTP binding on the protein conformation, *i.e.*, residues A15 and M26, close to the GTP-binding site; residues R84 and R88, located at the interface of domain I and III; and residue T164, which belongs to the terminal part of an α-helix connecting domain I and II via a long loop. The positions of the five residues selected to introduce new cysteines are highlighted in blue in Fig. 2, which also reports the cutting site in the long loop connecting domain I with domain II. To obtain single labeled species and evaluate the spin-labeling efficiency at each site, the native cysteine C91 was first substituted by serine (C91S) in all the mutants.

The new recombinant mutant proteins were assayed for the expression and solubility, and were purified by the double chromatography approach described above (data not shown).

3.3. Spin labeling of $HydF_{T.n.}I$ wild-type and mutant proteins and EPR analysis. The wild-type (containing C91) and the five mutant (A15C-C91S, M26C-C91S, R84C-C91S, C88R-C91S, T164C-C91S) proteins were labeled using the spin label MTSSL, as described in details in Sect. 2 . The labeling yield, calculated by spin quantification of the EPR spectrum double integral of the samples and comparison with those of standard solutions of the free spin label MTSSL, is reported in Table 3.

In Fig. 3 the CW-EPR spectra of the single mutants, with the simulations and the characteristic correlation times at each site, are reported. The mobility of the nitroxides derived from simulations is in good qualitative agreement with the distributions of rotamers calculated with the software MMM [31], starting from the crystallographic data, and displayed in Fig. 3. In fact, as expected, nitroxides at positions R88, T164 and R84 possess high mobility, although an extra contribution of a slower component is required to simulate the spectra of T164 and R84, while those in the sites C91 and A15, are more buried and characterized by slow motion. Unexpectedly, the most immobilized nitroxide, among the six selected positions, is found at position 26, the correlation time derived from the simulation of the EPR spectrum being very close to the estimated tumbling time of the protein in solution (11 ns). On the basis of the rotamers calculated with the software MMM at position 26, starting from the X-ray structure of the apo-protein, the nitroxide was expected to show high mobility at this site. However, the 26 residue is located close to a protein portion (residues 32–44) which was not resolved in the X-ray structure and therefore was not included in the MMM calculations. This missing region in the diffraction map was suggested to correspond to a flexible loop [18]. Therefore, it is likely that in solution this loop is largely responsible for the immobilization of the spin label at position 26.

Taken together the EPR data indicate that the isolation of the GTPase domain, from the rest of the HydF protein, does not alter the structure significantly.

In all the mutant and wild-type samples, the addition of 50 mM GTPγS did not alter the line shapes of the CW-EPR spectra (data not shown), indicating that the nitroxide mobility of the spin label does not undergo dramatic changes upon GTP binding.

On the basis of the labeling yield of single mutants, the more suitable positions for a double labeling, necessary for PELDOR experiments, were chosen. The proteins containing the cysteines at positions either C91 or C84 were discharged because of the low labeling yield (C91) and tendency to dimerization (C84) respectively (not shown). Triple mutants (R88C-C91S-M26C and R88C-C91S-T164C) were produced, using as template for the mutagenesis the plasmid *pET-28b/hydF$_{T.n.}$I_C91S-R88C*, purified as described above, and after reaction with the spin label MTSSL double spin labeled samples were finally obtained.

The PELDOR traces of M26C-R88C-C91S and R88C-C91S-T164C mutants are shown in Fig. 4. Tikhonov-derived distance distributions provide main values which correspond, roughly, to those expected on the basis of the X-ray structure of the apo-HydF protein (*i.e.*, 1.9 and 2.1 nm, measured at the α-carbon atoms for M26-R88 and R88-T164 couples, respectively)[18]. When the GTP analogous was added to the M26C-R88C-C91S sample (Fig. 4a), only very little differences at distances larger than 3.3 nm were detected. On the other hand, the distance distribution detected for R88C-C91S T164C undergoes a higher effect upon GTPγS binding. In fact a contribution centered at 4 nm appears, which was not present in the absence of the nucleotide and, at the same time, the two main distance distributions (at about 2.0 and 3.0 nm) shift toward longer distances (2.5 and 3.2 nm).

4 Discussion

The N-terminal GTPase domain of HydF is essential to its role in [FeFe]-hydrogenase maturation, since mutations in the Walker P-loop prevent the formation of an active HydA *in vitro* [17].It has been demonstrated that HydE and HydG increase the rate of GTP hydrolysis by 50% [20], suggesting a direct interaction of HydF with the other accessory proteins, and a possible effect of the binding of GTP in the dissociation of the HydE and HydG from HydF [21]. Thus, the GTP binding and/or hydrolysis might be responsible for structural changes in HydF itself leading to a change in the interactions with HydG and/or HydE. With this working hypothesis, we have started a structural study in solution to monitor the intrinsic conformational changes of the isolated GTP-binding domain of HydF, by EPR techniques. Indeed, as assessed above, the X-ray crystal structure

of the apo-HydF$_{T.n.}$ suffers the lack of the GTP nucleotide, thus hindering a clarification of its binding effect on the protein structure.

The measurements on the GTPase activity and the analysis of the CW-EPR spectra of five single-labeled mutants as well as of the wild-type domain carrying the native cysteine C91 show that the isolated domain maintains the functional characteristics and the general structure of the whole protein. Some diagnostic positions of couple of spin labels have been designed to monitor, by PELDOR spectroscopy, the conformational changes at the interface regions of domain I with the other two domains of the whole HydF protein. The PELDOR results show that the distance between the residues 26 and 88, belonging to the protein region close to the GTP-binding site and to the interface with the domain III respectively, remains substantially unaffected upon binding of the nucleotide. Instead an effect is found for the couple of spin labels at the 88 and 164 sites. In this case, the binding of the nucleotide induces an average increase of the distance, although the main component centered at 3.0 nm is only slightly affected. Since the labeled position 88 is common to both the studied double mutants under investigation, it is likely that the protein rearrangement takes place mainly in the region close to T164, rather than to R88. Interestingly, T164 belongs to an α-helix element connecting a loop close to the GTP-binding site with a long protein loop (highlighted in green in Fig. 5) which connects domain I with the dimerization domain (II).

As suggested by the crystal structure, the dimeric form of HydF (Fig. 5), which is the prevalent state in solution, represents an open form of the protein with both the [4Fe4S] cluster and the GTP-binding site are fully accessible. It is plausible that the open dimer interacts with the maturase partners in the extended conformation revealed by the X-ray structure. As the PELDOR experiments suggest, the binding of the nucleotide does not induce dramatic effects in the conformation within the GTP domain, at the level of the diagnostic positions investigated in this work. However, subtle changes are observed which may reflect large scale effects in the dimer conformation, as suggested by the involvement of residue T164 which is close to the long loop connecting the GTPase with the dimerization domain.

5. Conclusions

The specific role of GTPase domain of HydF in the maturation process of HydA is likely related to conformational changes of the protein upon ligation/hydrolysis of the nucleotide. Using a non-hydrolizable analogous of GTP, we have investigated the effect due to the binding of the nucleotide in the truncated protein domain. We found that the binding of the nucleotide does not induce large effects within the GTP domain, at least at the level of the elements investigated in this

work. However, subtle changes are observed which may reflect diffuse effects in the supramolecular dimeric assembly of the whole hydF protein. It is worth noting that, not only the binding but also the hydrolysis of GTP could facilitate structural rearrangements and promote interactions also with HydA facilitating the transfer of the 2Fe subcluster.

To obtain more significant data, further investigation will be carried out by designing new site-directed mutants of residues belonging to the above mentioned long loop and to the unstructured region reported in the X-ray structure (residues 32-44). Spin labeling of the GTPase domain in the whole protein will be also performed.

6. Acknowledgements

This work has been supported by the CARIPARO Foundation (M3PC project) by the MIUR (PRIN2010-2011 prot. 2010FM38P_004).

7. References

1. P.M. Vignais, B. Billoud, Chem. Rev. **107**, 4206-4272 (2007)

2. J.W.Peters, W.N. Lanzilotta, B.J. Lemon, L.C. Seefeldt, Science **282**, 1853-1858 (1998)

3. Y. Nicolet, C. Piras, P. Legrand, C.E. Hatchikian, J.C. Fontecilla-Camps, Structure **7**, 13-23(1999)

4. W. Lubitz, H. Ogata, O. Rüdiger, E. Reijerse, Chem. Rev. **114**, 4081-4148 (2014)

5. E.M. Shepard, F. Mus, J.N. Betz, A.S. Byer, B.R. Duffus, J.W. Peters, J.B. Broderick, Biochemistry **53**, 4090-4104 (2014)

6. J.W. Peters, J.B. Broderick, Annu. Rev. Biochem. **81**, 429-450 (2012)

7. M.C. Posewitz, P.W. King, S.L. Smolinski, L. Zhang, M. Seibert, M.L. Ghirardi, J. Biol. Chem. **279**, 25711-25720 (2004)

8. J.K. Ruback, X. Brazzolotto, J. Gaillard, M. Fontecave, FEBS Lett. **579**, 5055-5060 (2005)

9. X. Brazzolotto, J. K. Rubach, J. Gaillard, S. Gambarelli, M. Atta, M. Fontecave, J. Biol. Chem. **281**, 769-774(2006)

10. S.E. McGlynn, E.M. Shepard, M.A. Winslow, A.V. Naumov, K.S. Duschene, M.C. Posewitz, W.E. Broderick, J.B. Broderick, J.W. Peters, FEBS Lett. **582**, 2183-2187 (2008)

11. D.W. Mulder, E.S. Boyd, R. Sarma, R.K. Lange, J.A. Endrizzi, J.B. Broderick, J.W. Peters, Nature **465**, 248-251 (2010)

12. I. Czech, S. Stripp, O. Sanganas, N. Leidel, T. Happe, M. Haumann, FEBS Lett. **585**, 225-230 (2011)

13. G. Berggren, A., Adamska, C. Lambertz, T.R. Simmons, J. Esselborn, M. Atta, S. Gambarelli, J.M. Mouesca, E. Reijerse, W. Lubitz, T. Happe, V. Artero, M. Fontecave, Nature **499**, 66-69 (2013)

14. J. Esselborn, C. Lambertz, A. Adamska-Venkatesh, T. Simmons, G. Berggren, J. Noth, J. Siebel, A. Hemschemeier, V. Artero, E. Reijerse, M. Fontecave, W. Lubitz, T. Happe, Nat. Chem. Biol. **9**, 607-609 (2013)

15. J.M. Kuchenreuther, W.K. Myers, D.L.M. Suess, T.A. Stich, V. Pelmenschikov, S.A. Shiigi, S.P. Cramer, J.R. Swartz, R.D. Britt, S.J. George, Science **343**, 424-427 (2014)

16. J.D. Lawrence, H.X. Li, T.B. Rauchfuss, M. Benard, M.M. Rohmer, Angew. Chem. Int. Ed. **40**, 1768-1771 (2001)

17. P.W. King, M.C. Posewitz, M.L. Ghirardi, M.Seibert, J. Bacteriol. **188**, 2163-2172 (2006)

18. L. Cendron, P. Berto, S. D'Adamo, F. Vallese, C. Govoni, M.C. Posewitz, G.M. Giacometti, P. Costantini, G. Zanotti, J. Biol. Chem. **286**, 43944-43950 (2011)

19. P. Berto, M. Di Valentin, L. Cendron, F. Vallese, M. Albertini, E. Salvadori, G.M. Giacometti D. Carbonera, P. Costantini, BBA-Bioenergetics **1817**, 2149-2157 (2012)

20. E.M. Shepard, S.E. McGlynn, A.L. Bueling, C.S. Grady-Smith, S.J. George, M.A. Winslow, S.P. Cramer, J.W. Peters, J.B. Broderick, Proc. Natl. Acad. Sci. U. S. A. **107**, 10448-10453 (2010)

21. F. Vallese, P. Berto, M. Ruzzene, L. Cendron, S. Sarno, E. De Rosa, G.M. Giacometti, P. Costantini, J. Biol. Chem. **287**, 36544-36555 (2012)

22. A. Scrima, A. Wittinghofer, EMBO J. **25**, 2940-2951 (2006)

23. M.J. Ryle, W.N. Lanzilotta, L.C. Seefeldt, Biochemistry **35**, 9424-9434 (1996)

24. S.B. Jang, M.S. Jeong, L.C. Seefeldt, J.W. Peters, J. Biol. Inorg. Chem. **9**, 1028-1033 (2004)

25. H.J. Chiu, J.W. Peters, W.N. Lanzilotta, M.J. Ryle, L.C. Seefeldt, J.B. Howard, D.C. Rees, Biochemistry **40**, 641-650 (2001)

26. G. Jeschke, M. Pannier, H.W. Spiess, in Distance Measurements in Biological Systems, vol. 19, ed. by L.J. Berliner, S.S. Eaton, G.R. Eaton (Kluwer Academic, New York, 2000), pp. 493–512

27. O. Schiemann, T.F. Prisner, Quart. Rev. Biophys. 40, 1 (2007)

28. Y.D. Tsvetkov, A.D. Milov, A.G. Maryasov, Russ. Chem. Rev. 77, 487 (2008)

29. G. Jeschke, Annu. Rev. Phys. Chem. 63, 419 (2012)

30. S. Stoll, A. Schweiger, J. Magn. Res. 178, 42–55 (2006)

31. Y. Polyhach, E. Bordignon, G. Jeschke, Phys. Chem. Chem. Phys. 13, 2356–2366 (2010)

32. G. Jeschke, V. Chechik, P. Ionita, A. Godt, H. Zimmermann, J. Banham, C.R. Timmel, D. Hilger, H. Jung, Appl. Magn. Res. 30, 473–498 (2006)

Table 1

Primer name	Primer sequence
C91S_for	5’-TCTACAGGGCAGATTCTGGAATTCTCGTGAC-3’
C91S_rev	5’-GTCACGAGAATTCCAGAATCTGCCCTGTAGA-3’
M26C_for	5’-GTTGGAAAATCCTCTTTCTGCAACGCCTTAGTTGGTCAG-3’
M26C_rev	5’-CTGACCAACTAAGGCGTTGCAGAAAGAGGATTTTCCAAC-3’
R84C_for	5’-TGAGGGTAGAGAAGGCAAGGTGCGTGTTCTACAGGGCAGATTG-3’
R84C_rev	5’-CAATCTGCCCTGTAGAACACGCACCTTGCCTTCTCTACCCTCA-3’
R88C_for	5’-GGCAAGGAGGGTGTTCTACTGCGCAGATTGTGGAATTCTCG-3’
R88C_rev	5’-CGAGAATTCCACAATCTGCGCAGTAGAACACCCTCCTTGCC-3’
A15C_for	5’-GAAGATACATCGTTGTTTGCGGAAGAAGGAACGTTGG-3’
A15C_rev	5’-CCAACGTTCCTTCTTCCGCAAACAACGATGTATCTTC-3’
T164C_for	5’-GATTCGACGATATCGGGAAGTGCATCTCCGAAATTCTTCCGGG-3’
T164C_rev	5’-CCCGGAAGAATTTCGGAGATGCACTTCCCGATATCGTCGAATC-3’
R88C’_for	5’-GGCAAGGTGCGTGTTCTACTGCGCAGATTGTGGAATTCTCG-3’
R88C’_rev	5’-CGAGAATTCCACAATCTGCGCAGTAGAACACGCACCTTGCC 3’

Table 2

Protein	[GTP]	k_{cat} (min^{-1})
$HydF_{T.n.}$ (full lenght protein)	62 µM ÷ 2 mM	1.13±0.08
$HydF_{T.n.}I$ (GTPase domain)	125 µM ÷ 1.5 mM	11.2±0.6

Table 3

Mutant	*Labeling yield*
WT (C91)	23%
C15	40%
C26	50%
C84	40%
C88	65%
C164	46%

Tables Captions

Table 1 List of primers used in this study (with the modified bases underlined)

Table 2 Rate constant of GTP hydrolysis by HydF proteins from *T. neapolitana* ([KCl = 200mM; $[MgCl_2]$=10 mM; T=298 K)

Table 3 Spin-labeling yield, as percentage of labeled protein, of the wild-type and mutant $HydF_{T.n.}I$ proteins

Figure Captions

Fig. 1 $HydF_{T.n.}I$ expression and purification. Lane 1, affinity-purified protein (20 µl); lane 2, protein purified by a combination of affinity and size-exclusion chromatography (20 µl). 12% SDS-PAGE, Coomassie Brilliant Blue staining.

Fig. 2 Structure of HydF protein (PDB code 3QQ5) showing the mutated residues in the single cysteine mutants of the GTP-domain (I). Green sticks correspond to residues involved in GTP binding.

Fig. 3 Room temperature (T = 293 K) X-band CW-EPR spectra (black) in the 1st derivative representation of single labeled samples. Positions of the labels in the protein sequence and structure are indicated. Simulations are shown as red lines. Small amount of free spin label is present in the C15 and C91 spectra (narrow peaks). Rotamers calculated using the software MMM [27] are shown as ref/blue balls and sticks.

Fig. 4 Left: background-corrected PELDOR data for the M26C-R88C-C91S (a) and R88C-T164C-C91S (b) spin-labeled samples alone (black, upper trace) and following the addition of 50 mM GTPγS (black, bottom trace). Right, Tikhonov-derived distance distributions for the sample in the absence (blue) and in the presence (red) of the nucleotide analogous. Distance distributions obtained from Deer analysis [28].

Fig. 5 Cartoon representation of the HydF dimer. The two monomers are related by a 2-fold axis, approximately parallel to the plane of the paper in the vertical direction. Cysteine side chain residues, which are the putative ligand of the [4Fe4S] cluster of domain III, are in yellow; T164 side chain in magenta, R88 side chain in blue and M26 side chain in red. The long loop (residues 169-186) connecting domain I and II is coloured in green.

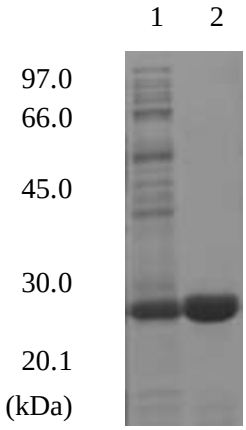

Figure 1

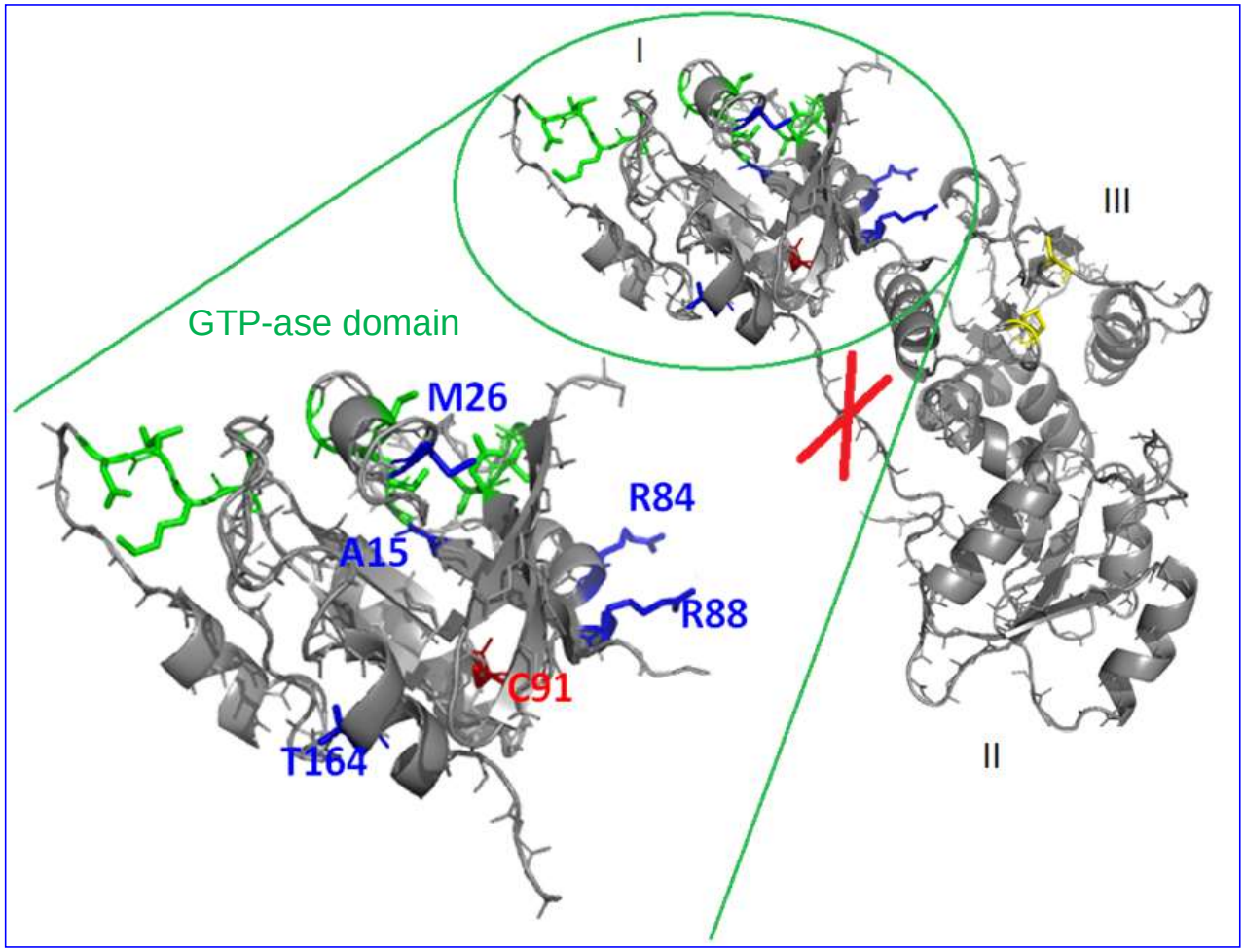

Figure 2

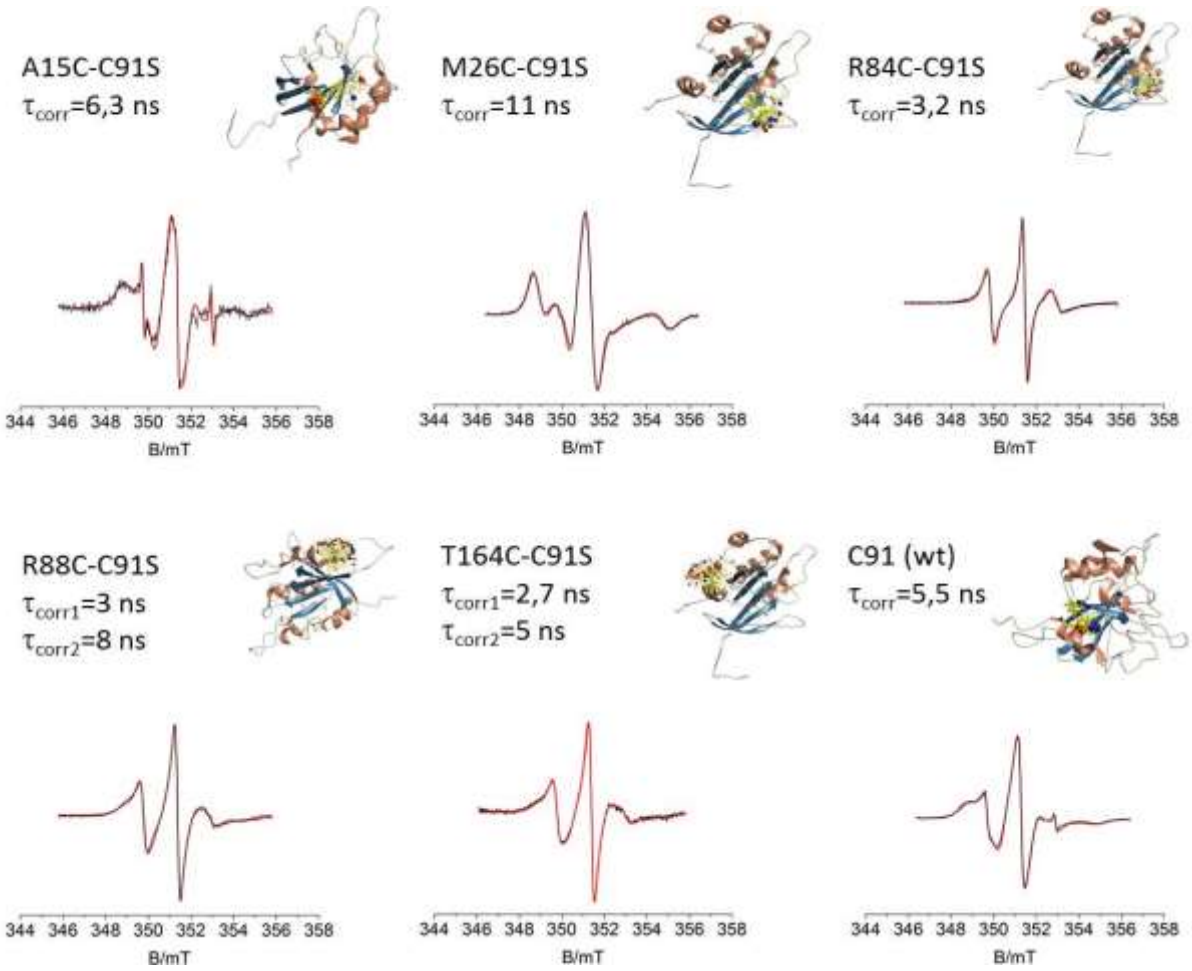
A15C-C91S
τ_{corr}=6,3 ns
M26C-C91S
τ_{corr}=11 ns
R84C-C91S
τ_{corr}=3,2 ns
R88C-C91S
τ_{corr1}=3 ns
τ_{corr2}=8 ns
T164C-C91S
τ_{corr1}=2,7 ns
τ_{corr2}=5 ns
C91 (wt)
τ_{corr}=5,5 ns
344 346 348 350 352 354 356 358
B/mT

Figure 3

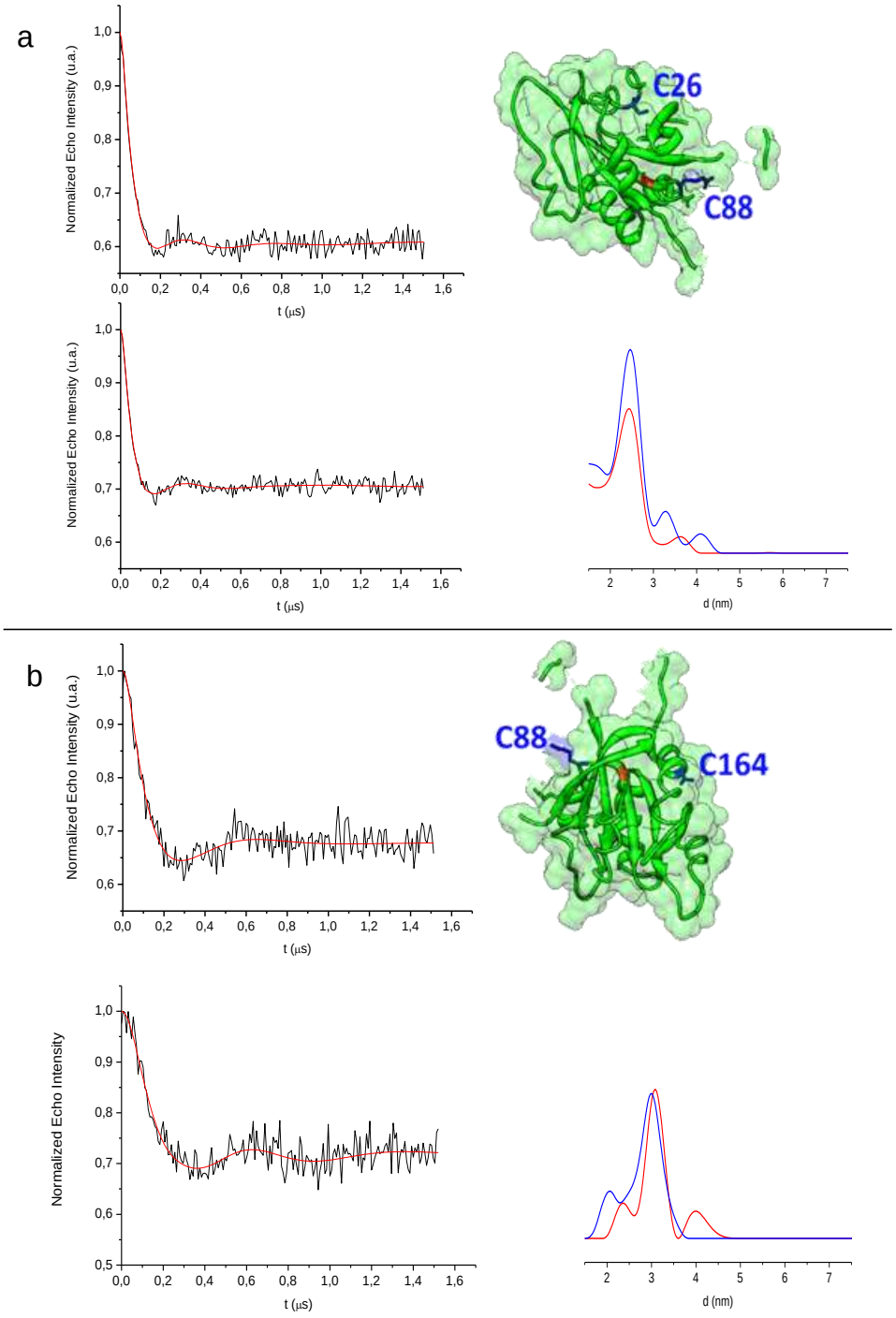
a
Normalized Echo Intensity (u.a.)
t (µs)
C26
C88
d (nm)
b
C88
C164
Normalized Echo Intensity

Figure 4

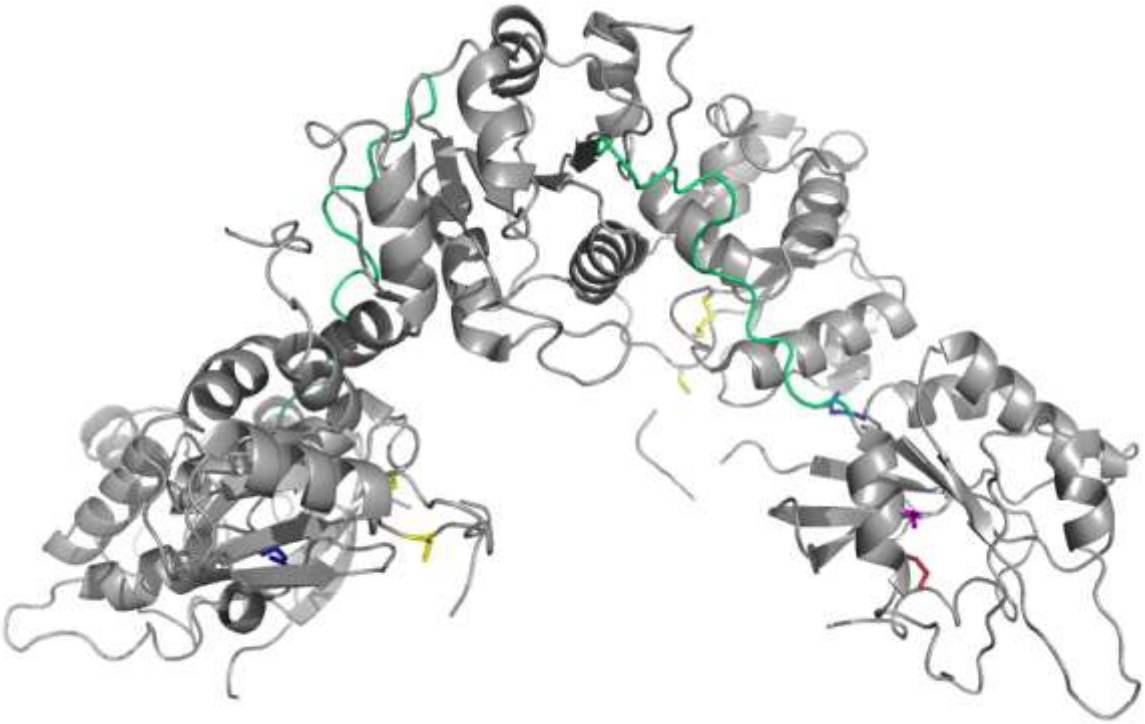

Figure 5

MANUSCRIPT UNDER REVISION IN: TOPICS IN CATALYSIS

Characterization of the [FeFe]-hydrogenase maturation protein HydF by EPR techniques: insights into the catalytic mechanism.

Marco Albertini[a], Laura Galazzo[a], Lorenzo Maso[b], Francesca Vallese[c], Paola Berto[c], Edith De Rosa[b], Marilena Di Valentin[a], Paola Costantini[b*] and Donatella Carbonera[c*]

[a] *Department of Chemical Sciences, University of Padova, Via F. Marzolo 1, 35131 Padova, Italy*

[b] *Department of Biology, University of Padova, Viale G. Colombo 3, 35131 Padova, Italy*

[c] *Department of Biomedical Sciences, University of Padova, Viale G. Colombo 3, 35131 Padova, Italy*

e-mail: donatella.carbonera@unipd.it; paola.costantini@unipd.it

Abstract

The catalytic site of [FeFe]-hydrogenase, the "H-cluster", composed by a [4Fe-4S] unit connected by a cysteinyl residue to a [2Fe] center coordinated by three CO, two CN^- and a bridging dithiolate, is assembled in a complex maturation pathway, at present not fully characterized, involving three conserved proteins, HydG, HydE and HydF. In this contribution we review our studies on HydF, a protein which acts as scaffold and carrier for the [2Fe] unit of the H-cluster. HydF is a complex enzyme which contains one [4Fe-4S] cluster binding site, with three conserved cysteine residues and a non-Cys ligand. We have exploited EPR, HYSCORE and PELDOR spectroscopies to get insight into the structure and chemical role of HydF. On the basis of the results we discuss the possibility that the non-Cys ligated Fe atom of the [4Fe-4S] cluster, is the site where the [2Fe] subcluster precursor is anchored and finally processed to be delivered to the hydrogenase (HydA). Our PELDOR experiments on the isolated GTPase domain of HydF, have also suggested that interactions with HydG and HydE proteins may be regulated by the binding of the nucleotide.

Keywords

HydF, hydrogenase, EPR, HYSCORE, PELDOR, [4Fe-4S] cluster

1. Introduction

[FeFe]-hydrogenases are enzymes occurring in several bacteria and eukaryotes [1], which are able to catalyze the reversible interconversion of protons to molecular hydrogen (H_2), at an active site called H-cluster. The H-cluster, composed by a [4Fe-4S] unit, connected by a cysteinyl residue to a 2Fe center coordinated by three CO, two CN^- and a bridging dithiolate, is assembled in a complex maturation pathway, at present not fully characterized, involving three conserved proteins called HydG, HydE and HydF [2].

HydE and HydG are enzymes belonging to the radical SAM (S-adenosyl methionine) family [3,4]. Both contain a [4Fe-4S] cluster (at the N-terminus of the protein) with an open binding site which can bind the SAM cofactor. HydE and HydG chemically modify a H-cluster precursor, while HydF is a GTPase with a suggested double role of scaffold, on which the H-cluster precursor is synthesized and/or modified, and of carrier, to transfer this precursor to the hydrogenase (HydA). Formation of the H-cluster within the cell remains still unclear and only a partial knowledge of the machinery driving its assembly *in vivo* is available. Different mechanisms have been proposed on the basis of a wide number of experiments. *In vitro* and/or cell-free experiments using purified recombinant proteins led to a two-step model (reviewed in [5] and [6]), in which HydE and HydG drive the chemical modifications of a H-cluster precursor working on HydF as a scaffold protein and, in a second step, HydF transfers this cluster to HydA, completing the maturation process [7-9]. This model has been further supported by independent experiments showing that a H-cluster synthetic mimic can be loaded on a recombinant HydF protein and then transferred to an apo-hydrogenase, confirming the key role of this scaffold protein [10, 11]. However, a different model has been recently proposed by Kuchenreuther *et al*. [12] who showed, in a combined Fourier-transform infrared and electron-nuclear double resonance spectroscopic work involving isotopic labelling, that the iron, carbon monoxide, and cyanide components of the H-cluster subsite in the active hydrogenase HydA, all originate from a chemistry that occurs at a [4Fe-4S] cubane center of HydG. A $Fe(CO)_2(CN)$ synthon is formed as an integral part of the modified [4Fe-4S] framework of HydG, as a $Fe_3S_4Fe(CO)_2(CN)$ cluster. The authors suggest that two of these complex synthons may assemble together with a dithiolate bridge to form the [2Fe] subcluster. The mechanism allowing the final assembly and the transfer of these moieties to apo-HydA (which contains the [4Fe-4S] component of the H-cluster but not the [2Fe] subsite) remains to be explained. Moreover, the specific role of HydE and HydF is not clear in this frame, although these proteins are known to have a function in the maturation process both *in vitro* and *in vivo*, since *Chlamydomonas reinhardtii* recombinant mutant strains, lacking single or combinations of maturases, are completely unable to express an active [FeFe]-hydrogenase [13, 2].

HydF has been suggested to be the transferase that shuttles the complete [2Fe] subcluster to the hydrogenase, but the exact molecular mechanism driving this translocation is still under investigation. HydF contains one [4Fe-4S] cluster binding site, with three conserved cysteine residues near the C-terminus, as well as a N-terminal GTPase domain, whose specific function is unknown [14]. Both these domains turn out to be essential for a correct HydA maturation [13]. Electron paramagnetic resonance (EPR) spectroscopy has been widely employed to get insights into structure and function of the maturation proteins [3,9,13,15-19]. In this paper we review the results obtained in our group with this technique on the study of HydF from *Thermotoga neapolitana* and *Clostridium acetobutilicum*. The X-ray structure of HydF from *T. neapolitana*, determined at 3 Å resolution, is the only structure of an HydF protein available, although obtained in the apo-form (PDB ID: 3QQ5) [20]. The protein monomer present in the asymmetric unit of the crystal comprises three domains: a GTP-binding domain, a dimerization domain, and a metal cluster-binding domain, all characterized by similar folding motifs. Two monomers dimerize, giving rise to a stable dimer, held together mainly by the formation of a continuous β-sheet comprising eight β-strands from two monomers. Based on the structural information available, we have designed several mutants of the whole HydF protein as well as of its isolated GTPase domain in order to get insight into the cluster structure and protein function. In this short review we will focus on the information derived from our EPR investigation and discuss the spectroscopic data on the light of the most recently proposed mechanisms of the [FeFe]-hydrogenase maturation pathway.

2. Experimental

2.1 Heterologous expression and purification of HydF proteins.

2.1.1 Full length HydF and GTPase HydF domain from T. neapolitana ($HydF_{T.n.}$).

The *hydF* gene (*$hydF_{T.n.}$*) was isolated from purified genomic DNA by PCR amplification and subcloned in frame with a 6His-tag sequence at the N-terminus in a pET-15b vector (from Novagen®) [17,18]. Site-directed mutagenesis of the *hydF* gene at selected sites was performed with the QuickChange® II Site-Directed Mutagenesis Kit (from Stratagene), using as template *pET-15b/$hydF_{T.n.}$* recombinant plasmid. *Escherichia coli* Rosetta (DE3) cells were transformed with the obtained *pET-15b/$hydF_{T.n.}$* plasmids and positive clones were selected by antibiotic resistance. The wild type and mutant 6His-tagged $HydF_{T.n.}$ proteins were expressed in anaerobic conditions, using 1 to 2 L cultures, purified by affinity chromatography and gel filtration, under anaerobic conditions. Briefly, cells were harvested by centrifugation, resuspended in lysis buffer (25 mM Tris-HCl pH 8, 200 mM KCl, and protease inhibitors 1µg/ml pepstatin A, 1 µg/ml leupeptin, 1 µg/ml antipain, 1

mM PMSF) and lysed by French press. The supernatant fractions were isolated from cell debris by centrifugation and the proteins purified to homogeneity by combining a nickel affinity chromatography (HIS-Select® Nickel Affinity Gel, from Sigma-Aldrich) and a gel filtration chromatography using a Superose 12 10/300 GL column (from GE Healthcare, Italy), equilibrated in lysis buffer. The proteins were finally concentrated to a final concentration ranging from 100 μM to 300 μM. All purification steps were performed under anaerobic conditions in a glove box with O_2-free solutions [20].

GTPase domain. The sequence coding for the GTPase N-terminal domain (domain I, residues 1 to 185) was PCR amplified using as template the vector containing the $hydF_{T.n.}$ gene and primers were designed to contain unique restriction sites allowing the directional subcloning of the amplified sequence in frame with a 6His-tag sequence at the 5'-terminus in a pET-28b vector (from Novagen®) suitable for T7 driven expression in *E. coli* [21]. Site-directed mutagenesis of the $hydF_{T.n.}$ gene at specific protein sites was performed using as template the $pET\text{-}28b/hydF_{T.n.}I$ recombinant plasmid. *E. coli* Rosetta (DE3) cells were transformed with the $pET\text{-}28b/hydF_{T.n.}I$ plasmid, and positive clones were selected by antibiotic resistance. The over-expressed proteins were purified in aerobiosis starting from 1 L cultures, as described above. Samples were concentrated giving rise to a final concentration ranging from 800 μM to 3 mM.

2.1.2 HydF proteins from Clostridium acetobutylicum ($HydF_{C.a.}$).

The $pCDFDuet\text{-}1/hydF_{C.a.}$ plasmid, carrying the HydF coding sequence from *C. acetobutylicum* in frame with a StrepII-tag at the 3' terminus, was kindly provided by M. C. Posewitz (from the Department of Chemistry and Geochemistry, Colorado School of Mine, Golden, Colorado). The $pCDFDuet\text{-}1/hydF_{C.a.}$ recombinant plasmid was used as template to introduce different mutations in the wild type *hydF* coding sequence. *E. coli* Rosetta BL21(DE3) cells were transformed with $pCDFDuet\text{-}1/hydF_{C.a.}$ recombinant plasmid, and positive clones were selected by antibiotic resistance [17]. Site-directed mutagenesis of the *hydF* genes from *C. acetobutilycum* was performed with the QuickChange® II Site-Directed Mutagenesis Kit (from Stratagene), using as template the $pCDFDuet\text{-}1/hydF_{C.a.}$ plasmid. The StrepII-tagged $HydF_{C.a.}$ proteins, either wild type or mutant, were expressed in anaerobic conditions and purified by a StrepTactin affinity chromatography (IBA, Göttingen, Germany), starting from 2 L cultures. For each purification, the eluted fractions were pooled together and concentrated by centrifugal filters (Vivaspin® Centrifugal Concentrators, 10,000 MWCO, from Sartorius Stedim Biotech) to a volume suitable for EPR giving rise to a final concentration ranging from 50 μM to 250 μM. All purification steps were performed under anaerobic conditions in a glove box (MBRAUN MB 200B) with O_2-free solutions. Purified proteins

were analyzed by 12% SDS-PAGE and electroblotted onto a poly(vinyldifluoridene) membrane. For immunoblotting analysis, the membrane was probed with an anti-StrepII-tag monoclonal antibody (from IBA, Göttingen, Germany) and with a horseradish peroxidase-conjugated goat anti-mouse IgG (from Kirkegaard & Perry Laboratories). Labeled proteins were then visualized with an ECL Western blotting detection kit (from Thermo Scientific Pierce Protein Research).

2.2 EPR spectroscopy

2.2.1 Full length HydF proteins. EPR tubes of as-isolated wild type and mutant of $HydF_{T.n.}$ and $HydF_{C.a.}$ proteins were prepared in the anaerobic box and frozen in liquid nitrogen. Reduced wild type and mutant HydF samples were made by adding 20 mM sodium dithionite. Low temperature continuous-wave EPR (CW-EPR) spectra were recorded using a Bruker Elexsys E580-X-band spectrometer equipped with a ER4102ST cavity and a helium flow cryostat (ESR 900 Oxford Instruments). Acquisition parameters were the following: temperature = 10–50 K; microwave frequency = 9.38 GHz; modulation = 1.0 mT, microwave power = 2.0 mW; time constant = 163.84 ms; conversion time = 81.92 ms; number of data points = 4096 (scan range = 700 mT) or 1024 (scan range = 100 mT). Simulations of the CW-EPR spectra, aimed to obtain the *g*-tensor principal components, were performed using Easyspin routine in Matlab® [22]; *g* values were estimated by calibration with a strong-pitch sample.

Hyperfine sublevel correlation spectroscopy (HYSCORE) experiments were carried out at a temperature of 10 K, using the same spectrometer equipped with a dielectric ring resonator (ER4118X-MD5) and a helium flow cryostat (Oxford CF935). A conventional two-dimensional (2D) four-pulse sequence ($\pi/2$-τ-$\pi/2$-t_1-π-t_2-$\pi/2$-τ-echo) was applied with a τ delay varied around 256 ns and a 8 ns detector gate, centered at the maximum of the echo signal. The nominal duration of both the $\pi/2$ and π pulses was 16 ns. The echo intensity was measured as a function of t_1 and t_2, incremented in steps of 8 ns from the initial value of 20 ns. HYSCORE data were collected as a 256 x 256 matrix at a repetition rate of 1200 Hz. A 4-step phase cycling procedure was used to remove unwanted echoes. Spectral processing was performed using a home-written Matlab® routine. The 2D time domain data were corrected by a third-order polynomial background in both dimensions. Traces were apodized using a Hamming window function, zero-filled to 1024 points and Fourier transformed in both dimensions. Frequency map was symmetrized before plotting as contour plot in logarithmic scale of intensity.

2.2.2 GTPase domain. Labelled samples were obtained by adding to the purified $HydF_{T.n.}$ GTPase domain a fivefold molar excess of S-(1-oxyl-2,2,5,5-tetramethyl-2,5-dihydro-1H-pyrrol-3-yl)methyl methanesulfonothioate) (MTSSL), dissolved in DMSO, and incubating the protein at 4 °C overnight in the dark. Samples for pulsed electron-electron double resonance (PELDOR) experiments were

concentrated (300 μM) and exchanged with deuterated buffer. Deuterated glycerol (40% w/v) was also added to the samples before freezing. In the nucleotide binding experiments, 50 mM GTPγS and 10 mM $MgCl_2$ were added to the samples and incubated for 30 minutes at 37 °C before freezing. Samples were loaded into quartz capillaries with 2.0 mm ID and 3.0 mm OD. PELDOR was performed on the same spectrometer described above equipped with a ER4118X-MS3 split-ring resonator (microwave frequency = 9.55 GHz) and helium flow cryostat (Oxford CF935). Measurements were carried out at 50 K. A standard four pulse sequence was applied; the microwave power was adjusted to obtain an observer sequence of 16/32/32 ns and a pump pulse of 16 ns. The difference between the pump and observer frequency was set to 70 MHz. A two-step phase cycle was applied for base-line correction while deuterium nuclear modulations were suppressed using an 8 step τ cycle, from a 180 ns starting value with 56 ns increment steps. Data on each sample were collected for about 15 hours. Distance distributions were extracted from PELDOR traces by using DeerAnalysis2013 [23].

3. Results and Discussion

3.1 The [4Fe-4S] cluster

The presence of a [4Fe–4S] cluster in HydF proteins, initially suggested by the presence of three conserved cysteine residues as putative ligands of an iron–sulfur cluster in different organisms, was confirmed by the observation of almost axial EPR signals (S = ½, $g_{\parallel}$ = 2.05 and $g_{\perp}$ = 1.90) following chemical reduction [9, 14-16]. These signals have microwave power and temperature saturation properties characteristic of reduced [4Fe–4S] centers. The role of this cluster was suggested to be accessory to the assembly of a [2Fe] subcluster, since HydF, isolated following heterologous co-expression with HydE and HydG, revealed Fe–CO and Fe–CN vibrational modes indicative of the ability of this protein to coordinate an iron center which resembles the [2Fe] subcluster of HydA [16]. When expressing HydF from *C. acetobutylicum* in the absence of HydE and HydG, Broderick and co-workers identified two paramagnetic S =1/2 species associated with photo-reduction of HydF [16]. One was assigned to the $[4Fe–4S]^+$ cluster, and the second was assigned to a $[2Fe–2S]^+$ cluster, suggested to be the [FeS] framework onto which HydE and HydG synthesize the H-cluster precursor. However, this assignment is still under discussion since Fontecave and co-workers found that HydF from *T. maritima,* when reduced with dithionite (DTH), coordinates only a $[4Fe–4S]^+$ cluster while the $[2Fe–2S]^+$ cluster is not present [14]. Moreover, Kuchenreuther et al. have shown, in a cell free system, that as-isolated HydF, heterologously expressed in a genetic background devoid of the HydE and HydG proteins, already exhibits an EPR

spectrum which in the lineshape resembles the signal that Broderick and co-workers characterized as the $[2Fe–2S]^+$ cluster [15]. The signal disappears upon reduction with DTH, which indicates that it cannot be due to a $[2Fe–2S]^+$ center. The conclusion drawn was that HydF neither coordinates a [2Fe–2S] cluster when anaerobically produced in the absence of HydE and HydG, nor does HydF supply an [FeS] cluster framework onto which the H-cluster non protein ligands are assembled. Kuchenreuther *et al*. suggest that the as-isolated HydF paramagnetic species observed, which appears to be the same signal assigned by Broderick and co-workers to a $[2Fe–2S]^+$ cluster [16], represents instead either a protein-associated radical or a $[3Fe–4S]^+$ cluster.

Afterwards, Kuchenreuther *et al*. [12] found that a $Fe(CO)_2(CN)$ synthon is formed as an integral part of a modified [4Fe-4S] framework (*i.e.* $Fe_3S_4Fe(CO)_2(CN)$) of HydG. This strongly indicates that the first step in the assembly of the [2Fe]-subsite occurs on one of the two [4Fe-4S] clusters of HydG. On the other hand, FTIR, EPR, and EXAFS experiments on HydF from *C. acetobutylicum,* which has been expressed in its native background with HydE and HydG, demonstrate that a binuclear iron species similar to the H-cluster is present also in fully "assembled" HydF [9, 26]. Thus it may be possible that a pre-synthesized binuclear model of the [2Fe] cofactor is introduced into HydF. According to this hypothesis, the [4Fe-4S] cluster of HydF would coordinate the $2[Fe]_H$-precursor before the transfer to HydA. Therefore, a detailed spectroscopic characterization of the [4Fe-4S] cluster of HydF is important to get insight into the chemistry taking place at that site.

All HydF proteins identified to date share an iron-sulfur cluster-binding motif ($CxHx_{46-53}HCxxC$) in the C-terminal end [14], with three highly conserved cysteine residues which are supposed to bind the FeS cluster. Indeed, site-specific mutagenesis experiments on the HydF protein from *C. acetobutylicum* confirmed that two of these conserved cysteines, *i.e.* Cys 353 and Cys 356, are essential to drive the assembly of a functional H-cluster [13]. On the basis of the three-dimensional crystal structure of HydF from *T. neapolitana* (PDB ID code 3QQ5) we described the domain containing the three conserved cysteine residues (*i.e.* Cys 302, Cys 353, Cys 356), which likely bind the FeS cluster [20]. Close to these residues, we have identified the position of the two conserved histidines (*i.e.* His 304 and His 352) which may be part of the cluster coordination sphere but their role is still controversial. In a work on the HydF from *T. maritima*, HYSCORE experiments excluded the presence of nitrogen atoms in the cluster coordination sphere, ruling out the role of histidine residues as ligands [14]. On the other hand, the same kind of experiments performed on the HydF protein from *C. acetobutylicum* showed the presence of nitrogen in the coordination of the [4Fe-4S] cluster [24], leading Czech et al. to interpret the HYSCORE data as due to a histidine ligation to the [4Fe-4S] unit.

In this panorama, we have used CW-EPR and HYSCORE, combined with a site-specific mutagenesis approach to investigate the role of cysteine and histidine residues, from the $CxHx_{46-53}HCxxC$ consensus sequence, as putative ligands of the [4Fe-4S] cluster of HydF proteins from *T. neapolitana* and *C. acetobutylicum*, and their influence on the characteristics of the cluster itself [17]. As shown in Fig 1, we found that the mutants $HydF_{T.n.}$C302S, $HydF_{T.n.}$C353S and $HydF_{T.n.}$C356S do not show the presence of an assembled [4Fe-4S] cluster, suggesting that none of the three conserved cysteines can be replaced by an isosteric serine residue. Instead, in both $HydF_{T.n.}$H304A and $HydF_{T.n.}$H352A proteins an EPR signal has been detected, although in the case of $HydF_{T.n.}$H352A the signal exhibited a shift of the principal g-values (1.840, 1.875, 2.055). These results indicate that while the three cysteines of the cluster binding consensus sequence of HydF from *T. neapolitana* are all essential for the assembly of a functional [4Fe-4S] center, the two conserved histidines are not decisive for metal coordination. Further investigation by HYSCORE was performed to evaluate the potential histidine ligation of the [4Fe-4S] cluster of $HydF_{T.n.}$[17]. The spectra reported in Fig 2, panel A, collected in correspondence of the g_y = 1.90 field position, clearly show the presence of a nitrogen ligand coupled to the spin system, in the (+ -) and (+ +) quadrants, in the low frequency region around the Larmor frequency of the ^{14}N nucleus. However, this signal is likely due to the presence of imidazole used in the column elution buffer since, if the sample is subjected to gel filtration, to remove the excess of imidazole, the spectral signatures of the nitrogen ligand disappear and only the peaks around 15 MHz, due to the weak interactions with surrounding protons, are clearly visible in the (+ +) quadrant. Thus, the HYSCORE results show that a His coordination is not present in the wild type $HydF_{T.n.}$ protein and that the native forth ligand can be easily exchanged with imidazole, as previously found for the HydF protein from *T. maritima* [14]. Different results were obtained for HydF protein from *C. acetobutylicum*. In fact, the HYSCORE experiments performed to evaluate the ligation of the [4Fe-4S] cluster of $HydF_{C.a.}$ reveal the presence of a nitrogen atom coupled to the spin system in the wild type protein as well as in the mutant $HydF_{C.a.}$H306A (Fig 2, panel B). The parameters of hyperfine and quadrupolar interactions (double-quantum frequencies, dq = [± 2.6 MHz ; ± 6.6 MHz]; hyperfine coupling constant, a = 4.2 ± 0.2 MHz; quadrupolar term, $K^2(3+\eta^2)$ = 0.71 MHz^2), derived according to the formula reported in reference [25], are in the range of those reported before for histidine ligands of iron-sulfur clusters [26-28]. The $HydF_{C.a.}$H352A HYSCORE spectrum lacks all the cross peaks due to strong N-coupling (Fig 2, panel B), clearly suggesting that His 352 is the fourth ligand of the [4Fe-4S] cluster in $HydF_{C.a.}$, differently from what observed in the $HydF_{T.n.}$ protein. Interestingly, a [4Fe-4S] cluster can be assembled also in the $HydF_{C.a.}$H352A mutant protein, as supported by the presence of the EPR signal of the reduced protein. This evidence suggests that also in *C.*

acetobutylicum the His 352 residue, which coordinates the iron atom of the [4Fe-4S] cluster in the native protein, can be at least partially substituted, upon deletion, by another undefined ligand. Moreover, very recently, Berggren et al. [19] have shown that His-tag may be responsible for unnatural coordination to the cluster in *T. maritima*. These authors suggest that also preparation containing a Strep-tag II (an eight amino acid oligopeptide featuring a histidine residue) could give an adventitious histidinyl ligation. Thus, at present it cannot be excluded that also the [4Fe-4S] cluster of the wild type HydF from *C. acetobutylicum* presents, in its native form, a non histidinyl fourth ligand.

Although the two histidines in the [4Fe-4S] binding pocket are not necessary for binding the cubane cluster, at least in *T. neapolitana* and *T. maritima*, we have proven that they are essential for a correct maturation of HydA [17]. Indeed, all the introduced mutations, including those not affecting the $HydF_{C.a.}$ EPR and HYSCORE spectra, resulted in a severe impairment of the $HydA_{C.a.}$ activation under anaerobic inducing conditions, as assessed by hydrogen gas evolution activities measured in whole-cell extracts. Thus, the two histidines are likely to play an active role in the stabilization of the [2Fe] precursor in HydF (*e.g.*, through hydrogen bonding) [19].

In conclusion, taken all together, the reported results on the HydF proteins from different microorganisms indicate that only the three cysteines are strictly required for the binding of the [4Fe-4S] cluster, whereas the fourth ligand of the coordination sphere can vary depending on the molecular environment created by local residues and/or experimental conditions. In the experiments carried out in both *T. neapolitana* and *T. maritima*, a [4Fe-4S] cluster-imidazole complex is detectable in the presence of an excess of imidazole, suggesting that the fourth metal coordination site is easily accessible and readily exchangeable. This may have important implications for the synthesis of a complete H-cluster precursor. Non-cysteinyl ligation to a cubane-type FeS cluster is known to occur in several enzymes and in each case the anomalous cluster coordination has a functional significance [29]. An accessible iron coordination site could be relevant in substrate binding and transfer. According to this evidence, as remarked before [19], HydF is able to bind a diiron synthetic complex, mimicking the active site of HydA, via a bridging cyanide ligand, and to eventually use it to activate apo-HydA [10].

The [4Fe-4S] cluster coordination in HydF proteins is evocative of the members of radical SAM superfamily including HydG and HydE, in which three cysteine residues coordinate three of the four irons of the [4Fe-4S] cluster at the active site of the enzyme, while the remaining ligand to the fourth iron, in the absence of SAM, is likely a small-molecule (such as thiol) from the buffer and not a protein ligand [30]. The coordination of this fourth iron makes it labile, explaining why in many cases these proteins are found to contain $[3Fe\text{-}4S]^{+}$ clusters in their as-isolated or air-exposed

states, as also observed for HydF (see Fig 1, orange trace). Upon reduction with a reducing agent, such as DTH or photoreduced 5-deazariboflavin, the $[3Fe\text{-}4S]^{+}$ clusters can usually be reconverted to the $[4Fe\text{–}4S]^{+}$ clusters, by scavenging of adventitious iron or by cannibalization of a fraction of the clusters [31]. Protein-bound [3Fe-4S] clusters are generally derived from $[Fe_4S_4(S\text{-}Cys)_3L]$ centers with $L = H_2O/OH^-$, a side chain carboxylate, or some other non-cysteinate ligand [32]. It has been suggested that, under oxidizing conditions, the reaction $[Fe_4S_4]^{3+} \rightarrow [Fe_3S_4]^{+} + Fe^{2+}$ may occur, the removal of ferrous ion being assisted by complexation with an exogenous ligand [33].

To further investigate this crucial problem of the cluster ligation characteristics, we focused on the iron-sulfur cluster environment of HydF from *T. neapolitana*, by analyzing the low temperature CW-EPR spectra of a series of significant site-directed mutants (D310A, D337A, E300A and Y380A), corresponding to residues which are in close proximity to the [4Fe-4S] cluster binding site, according to the crystal structure of apo-$HydF_{T.n.}$ [18]. These residues represent putative Fe cluster ligands. HYSCORE spectra of the mutants were also detected and compared to those of the wild type protein [18]. The results are reported in Fig 3. Comparison of the *g* principal values of the mutants with those of the wild type shows that the [4Fe-4S] cluster is only slightly affected by the substitution of Glu300, Asp310, Asp337 and Tyr380 with alanine, meaning that the assembly of the cluster is not compromised or altered by the removal of these residues. Thus, it seems likely that either the residues are not directly involved in the ligation of the [4Fe-4S] cluster or they can be easily substituted by other residues. This is also confirmed by the analysis of the HYSCORE spectra in the proton coupling frequency region. Three different protons contributions have been recognized in the spectra of the WT: i) weakly coupled protons (hyperfine couplings between 2.5-3.5 MHz) assigned to distant nuclei, likely belonging to protein residues or backbone, located at long distance from the cluster; ii) protons characterized by a strong coupling (hyperfine couplings between 14-16 MHz) (ridges III) tentatively assigned to the β-cysteinyl protons; iii) protons corresponding to ridges II, showing isotropic hyperfine couplings with intermediate values (7-9 MHz), which reflect a close distance to the spin carrying cluster. Since no significant changes of the hyperfine interactions are found in the mutants compared to the wild type, an involvement of the selected residues in either direct bonding or specific interactions, such as H-bonding of coordinated water, in close proximity of the FeS cluster, can be excluded. Therefore, the most likely non-Cys ligand of the cluster is an exogenous molecule such as a hydroxyl or water. This is also in agreement with the observed easy exchangeability of the forth ligand. Further HYSCORE experiments based on $^{2}H_2O$ exchange, to determine the exchangeable protons, and $H_2{}^{17}O$ exchange, to eventually measure the direct oxygen coordination to the iron, are in progress in our laboratory to support this hypothesis.

3.2 The GTPase domain

As suggested by Lubitz et al. [33], since in the living cell the concentration of free cofactors is small, transferases are needed to move a pre-assembled 2Fe-subcluster precursor to HydA. The role of HydF is likely to be crucial at this stage. However, both the mechanisms of ligand transfer to HydF and delivery of the 2Fe-subcluster precursor from HydF to HydA are still unknown. At present, it is not clear whether the CO and CN ligands are delivered as free to a FeS cluster bound to HydF, or mononuclear Fe species with bound ligands are delivered to HydF, or the whole 2Fe subcluster is synthesized on HydG before being transferred to HydF.

The GTPase activity of HydF is likely involved in the interaction with HydE and HydG rather than with HydA. In fact, Vallese et al. have shown that GTP addition to either the HydF–HydE or HydF–HydG complexes results in an increase in the rates of dissociation, suggesting that the dissociation of HydE and HydG from HydF may be driven by the GTPase activity of HydF [34]. It has also been reported that the presence of GTP significantly affects the EPR spectral properties of the HydF cluster, showing that a communication between the GTP and the iron-sulfur cluster binding domains of the protein may be present [16].

In order to investigate possible conformational changes induced by the GTP binding in the N-terminal domain of HydF, we have expressed in *E. coli*, a recombinant HydF protein from *T. neapolitana* including only the GTP-binding domain [21]. The isolated domain I can be indeed purified to homogeneity as a single monomeric species, keeping its capability of GTP hydrolysis. Site-directed mutants have been designed for PELDOR measurements, in which the native residues have been substituted by cysteines and subsequently spin-labeled with the methanethiosulfonate nitroxide. The wild type domain contains a single cysteine (*i.e.* C91), buried in the protein core, which, as proven by preliminary experiments, gives a low labeling yield. For this reason, it was substituted by serine (C91S) while three other sites were selected to introduce the cysteine residues in the construction of double labeled species for PELDOR experiments. They are the following: residue M26, close to the GTP-binding site; residue R88, located at the interface of domain I and III; residue T164, which belongs to the terminal part of an α-helix connecting domain I and II via a long loop (see Fig 4). Triple mutants (R88C-C91S-M26C and R88C-C91S-T164C) were produced and, after reaction with the spin label MTSSL, double spin labeled samples were obtained. The corresponding PELDOR spectra are shown in Fig 4. Tikhonov-derived distance distributions analysis of the PELDOR traces for the M26C-R88C-C91S and R88C-C91S-T164C mutants give main values which correspond, roughly, to those expected on the basis of the α-carbon distances derived from the X-ray structure of the apo-HydF protein (19 and 20 Å, respectively).

The PELDOR results show that the distance between residues 26 and 88, belonging to the protein region close to the GTP binding site and to the interface with the domain III, remains substantially unaffected upon binding of the nucleotide. A more significant effect is found for the spin labels at the 88 and 164 sites. In this case, the binding of the nucleotide induces an average increase of the distance with a change also in the distance distribution. Since the labeled position 88 is common to both the double mutants investigated, it is likely that the protein rearrangement takes place mainly in the region close to T164, rather than to R88. Interestingly, T164 belongs to an α-helix element connecting a loop close to the GTP binding site with a long protein loop which connects domain I with the dimerization domain (II). Although the nucleotide binding does not induce dramatic effects on the conformation within the GTP domain, at the level of the diagnostic positions investigated in our work, the observed changes may reflect a diffuse effect in the dimer conformation of HydF, which is the main form of the whole protein in solution. This in turn could be the origin of the change of interactions of HydF with HydE and/or HydG.

These preliminary experiments show that the PELDOR might be a powerful technique to investigate the mechanism of the maturation process, at the level of the nucleotide binding and/or hydrolysis. Design of new site-directed mutants of residues belonging to the above mentioned long loop and to an unstructured region reported in the X-ray structure (residues 32-44), together with spin-labeling of the GTPase domain in the full-length protein, will be performed to get a detailed map of the conformational changes.

4. Conclusions

HydF is a complex enzyme which contains one [4Fe-4S] cluster binding site with three conserved cysteine residues near the C-terminus and a N-terminal GTPase domain, whose specific function is unknown. It has been increasingly observed that, in many enzymes, the ligands of [4Fe-4S] clusters can be other than Cys and that the presence of the non-Cys ligands can strongly influence the physical properties of the clusters in terms of reduction potential, stability, and reactivity [35]. Therefore, it is likely that also in HydF the non-Cys ligated Fe atom of the cluster, whose ligand is easily exchangeable and variable depending on the organism, as we have shown, carries out the relevant chemistry.

HydF has been suggested to be the transferase that shuttles the complete [2Fe] subcluster to the hydrogenase, but the exact molecular mechanism driving this translocation is still under investigation. It seems likely that the [4Fe-4S] cluster of HydF is the site where the [2Fe] subcluster

precursor is anchored and finally processed to be delivered to HydA. The dimeric form of HydF in solution probably allows the interactions with HydG and HydE proteins for the transfer of the synthons. These interactions may be regulated by the GTPase domain of HydF, as revealed by our preliminary PELDOR experiments. In order to obtain more significant data in this regard, further investigation is needed.

5. Acknowledgements

This work has been supported by the CARIPARO Foundation (M3PC project) by the MIUR (PRIN2010-2011 prot. 2010FM38P_004).

6. References

1. Vignais PM, Billoud B (2007) Chem Rev 107:4206-4272

2. Posewitz MC, King PW, Smolinski SL, Zhang L, Seibert M, Ghirardi ML (2004) J Biol Chem 279:25711-25720

3. Rubach JK, Brazzolotto X, Gaillard J, Fontecave M (2005) FEBS Lett 579:5055-5060

4. Sofia HJ, Chen G, Hetzler BG, Reyes-Spindola JF, Miller NE (2001) Nucleic Acids Res 29: 1097-1106

5. Shepard EM, Mus F, Betz JN, Byer AS, Duffus BR, Peters JW, Broderick JB (2014) Biochemistry 53:4090-4104

6. Peters JW, Broderick JB (2012) Annu Rev Biochem 81:429-450

7. McGlynn SE, Shepard EM, Winslow MA, Naumov AV, Duschene KS, Posewitz MC, Broderick WE, Broderick JB, Peters JW (2008) FEBS Lett 582:2183-2187

8. Mulder DW, Boyd ES, Sarma R, Lange RK, Endrizzi JA, Broderick JB, Peters JW (2010) Nature 465:248-251

9. Czech I, Stripp S, Sanganas O, Leidel N, Happe T, Haumann M, (2011) FEBS Lett 585:225-230

10. Berggren G, Adamska A, Lambertz C, Simmons TR, Esselborn J, Atta M, Gambarelli S, Mouesca JM, Reijerse E, Lubitz W, Happe T, Artero V, Fontecave M, Nature (2013) 499:66-69

11. Esselborn J, Lambertz C, Adamska-Venkatesh A, Simmons T, Berggren G, Noth J, Siebel J, Hemschemeier A, Artero V, Reijerse E, Fontecave M, Lubitz W, Happe T (2013) Nat Chem Biol 9:607-609

12. Kuchenreuther JM, Myers WK, Suess DLM, Stich TA, Pelmenschikov V, Shiigi SA, Cramer SP, Swartz JR, Britt RD, George SJ (2014) Science 343:424-427

13. King PW, Posewitz MC, Ghirardi ML, Seibert M J (2006) Bacteriol 188:2163-2172

14. Brazzolotto X, Rubach JK, Gaillard J, Gambarelli S, Atta M, Fontecave M (2006) J Biol Chem 281:769-774.

15. Kuchenreuther JM, Britt RD, Swartz JR (2012) PLoS ONE 7:e45850 DOI:10.1371/journal.pone.0045850.

16. Shepard EM, McGlynn SE, Bueling AL, Grady-Smith CS, George SJ, Winslow MA, Cramer SP, Peters JW, Broderick JB (2010) Proc Natl Acad Sci U. S. A. 107:10448-10453

17. Berto P, Di Valentin M, Cendron L, Vallese F, Albertini M, Salvadori E, Giacometti M, Carbonera D, Costantini P, (2012) Biochim Biophys Acta 1817:2149-2157

18. Albertini M, Vallese F, Di Valentin M, Berto P, Giacometti M, , Costantini P, Carbonera D (2014) J Hydr Int 39:18574–18582

19. Berggren G, Garcia-Serres R, Brazzolotto X, Clemancey M, Gambarelli S, Atta M, LatourJM,. Hernandez HL, Subramanian S, Johnson MK, Fontecave M (2014) J Biol Inorg Chem 19:75–84

20. Cendron L, Berto P, D'Adamo S, Vallese F, Govoni C, Posewitz MC, Giacometti GM, Costantini P, Zanotti G (2011) J Biol Chem. 286:43944-43950

21. Maso L, Galazzo L, Vallese F, Di Valentin M, Albertini M, De Rosa E, Giacometti GM, Costantini P, Carbonera D (2015) Appl Magn Res *In press* DOI: 10.1007/s00723-015-0641-z

22. Stoll S, Schweiger A (2006) J Magn Reson 178:42e55.

23. Jeschke G, Chechik V, Ionita P, Godt A, Zimmermann H, Banham J, Timmel CR, Hilger D, Jung H (2006) Appl Magn Res 30:473–498

24. Czech I, Silakov A, Lubitz W, Happe T (2010) FEBS Lett 584:638-642

25. Moulis JM, Davasse V, Golinelli MP, Meyer J, Quinkal I (1996) J Biol Inorg Chem 1:2-14

26. Dikanov SA, Xun L, Karpiel AB, Tyryshkin AM, Bowman MK (1996) J Am Chem Soc 118:8048-8416.

27. Foerster S, van Gastel M, Brecht M, Lubitz W (2005) J Biol Inorg Chem 10:51-62

28. Chatterjee R, Milikisiyants S, Coates CS, Lakshmi KV (2011) Biochemistry 50:491-501

29. Jiang F, McCracken J, Peisach J (1990) J Am Chem Soc 112:9035-9044

30. Hinckley GT, Frey PA (2006) Biochemistry 45:3219-3225

31. Broderick JB, Duffus BR, Duschene KS, and Shepard EM (2014) Chem Rev 114:4229–4317

32. Holm RH, Kennepohl P, Solomon EI, (1996) Chem Rev 96:2239–2314

33. Lubitz W, Ogata H, Rüdiger O, Reijerse E (2014) Chem Rev 114:4081–4148

34. Vallese F, Berto P, Ruzzene M, Cendron L, Sarno S, De Rosa E, Giacometti GM, Costantini P (2012) J Biol Chem 287:36544-36555
35. Bak DW, Elliott SJ (2014) Curr Opin Chem Biol 19:50–58.

7. Figure captions

Fig 1

Panel A: cartoon tube representation of monomeric $HydF_{T.n.}$ (PDB entry code: 3QQ5). The three recognized domains are highlighted in different colours: GTPase domain in orange, dimerization domain in olive green and [4Fe-4S] cluster binding domain in brown. Residues of the iron-sulfur cluster-binding motif (**C**x**H**x_{46-53}**HC**xx**C**) are shown as sticks. Panel B: X-band EPR spectra of as-isolated $HydF_{T.n.}$ and anaerobically reduced (20 mM sodium dithionite) wild type and mutant $HydF_{T.n.}$ and $HydF_{C.a.}$ proteins. The inset shows the EPR signal of the as-isolated sample of $HydF_{T.n.}$ in the g = 4 region where nonspecifically bound Fe^{3+} contributes. Colour code: as-isolated $HydF_{T.n.}$ in orange, reduced $HydF_{T.n.}$ in black, reduced $HydF_{C.a.}$ in brown. Experimental conditions are reported in the Materials and methods section. The figure has been created starting from the EPR spectra reported in [17].

Fig 2

Panel A: X-Band HYSCORE spectra of reduced wild-type $HydF_{T.n.}$ before (left) and after (right) imidazole removal. Panel B: X-Band HYSCORE spectra of reduced wild-type and mutant $HydF_{C.a}$ proteins. Experimental conditions are described in the Materials and Methods. Spectra are recorded at 10 K and at the field position corresponding to the g_y value (1.90). The figure has been created starting from the spectra reported in [17].

Fig 3

Panel A: cartoon tube representation of the FeS cluster binding domain of $HydF_{T.n.}$ (PDB entry code: 3QQ5). Putative residues involved in the cluster binding are shown as sticks (colour code: carbon in black, nitrogen in blue, oxygen in red, sulfur in yellow). Panel B: low temperature X-band EPR spectra of anaerobically reduced (20 mM sodium dithionite) wild type and mutants of $HydF_{T.n.}$. Panel C: HYSCORE spectra of reduced $HydF_{T.n.}$ proteins. A comparison between wild type and mutant proteins is reported. Spectra are recorded at 10 K, at the field position corresponding to the g_y value (1.90). Experimental conditions are described in the Material and Methods. The figure is based on the data reported in [18].

Fig 4

Structure of $HydF_{T.n.}$ (PDB entry code: 3QQ5) showing the mutated residues in the GTPase domain (panel A). Background-corrected PELDOR traces for the M26C-R88C-C91S (panels B, C, D) and R88C-T164C-C91S (panels E, F, G). Samples in the absence (black, panels B, E) and after the addition (black, panels C, D) of 50 mM GTPγS. Tikhonov-derived distance distributions (panels D, G) for samples in the absence (black) and in the presence (red) of the nucleotide analogous. The figure has been modified starting from [21].

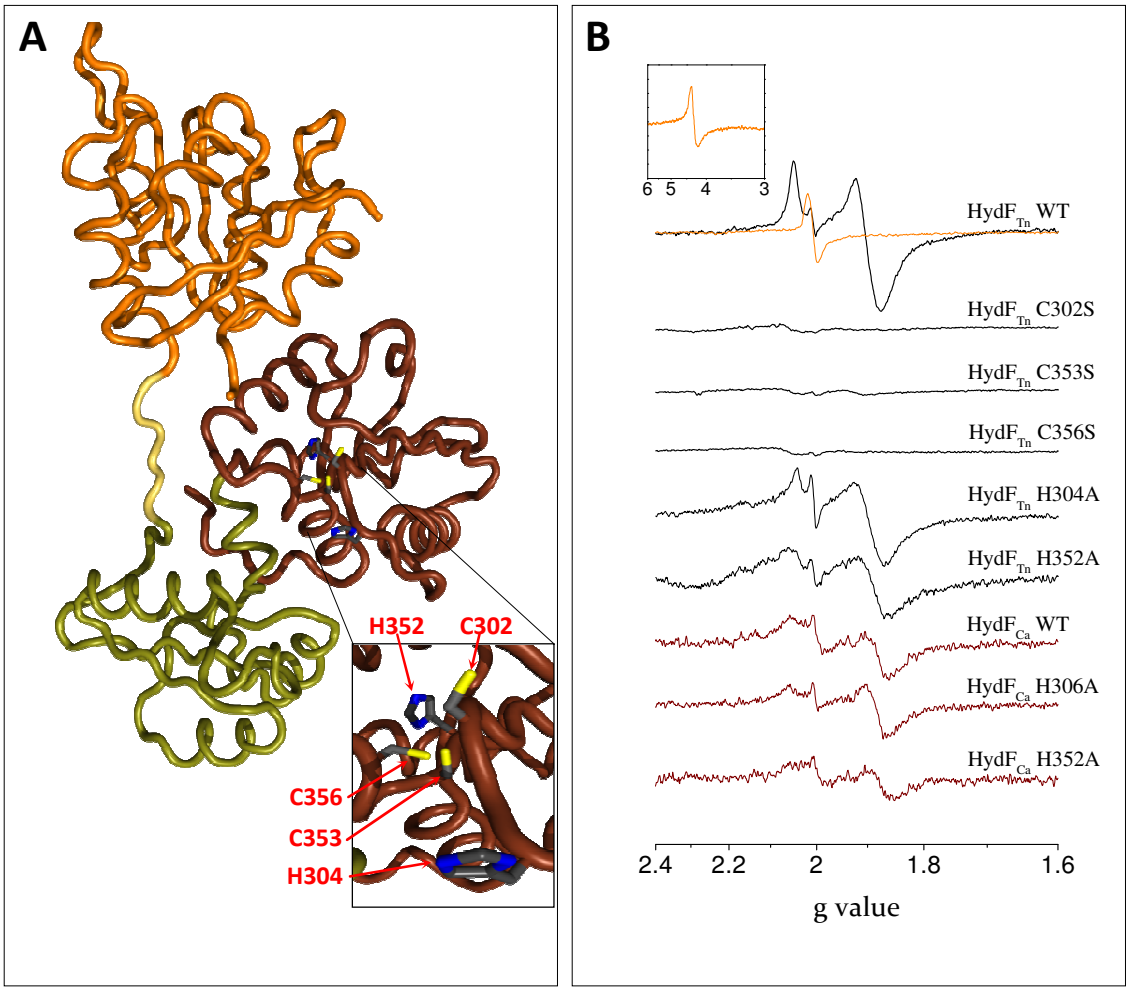
A
H352
C302
C356
C353
H304
B
6 5 4 3
HydF$_{Tn}$ WT
HydF$_{Tn}$ C302S
HydF$_{Tn}$ C353S
HydF$_{Tn}$ C356S
HydF$_{Tn}$ H304A
HydF$_{Tn}$ H352A
HydF$_{Ca}$ WT
HydF$_{Ca}$ H306A
HydF$_{Ca}$ H352A
2.4 2.2 2 1.8 1.6
g value

Fig 1

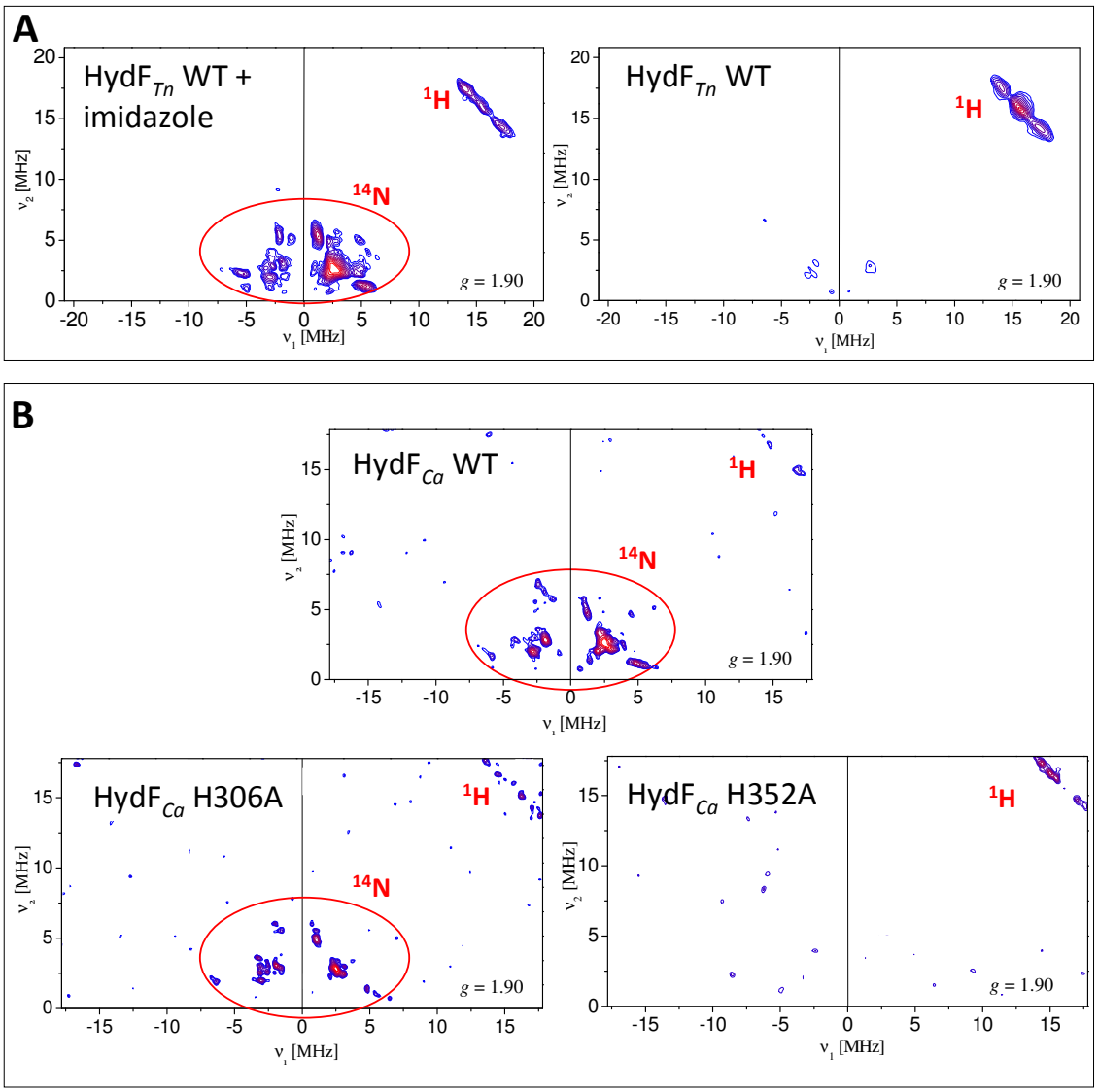
A
HydF$_{Tn}$ WT + imidazole
^{1}H
^{14}N
g = 1.90
HydF$_{Tn}$ WT
^{1}H
g = 1.90
ν$_2$ [MHz]
ν$_1$ [MHz]
B
HydF$_{Ca}$ WT
^{1}H
^{14}N
g = 1.90
HydF$_{Ca}$ H306A
^{1}H
^{14}N
g = 1.90
HydF$_{Ca}$ H352A
^{1}H
g = 1.90

Fig 2

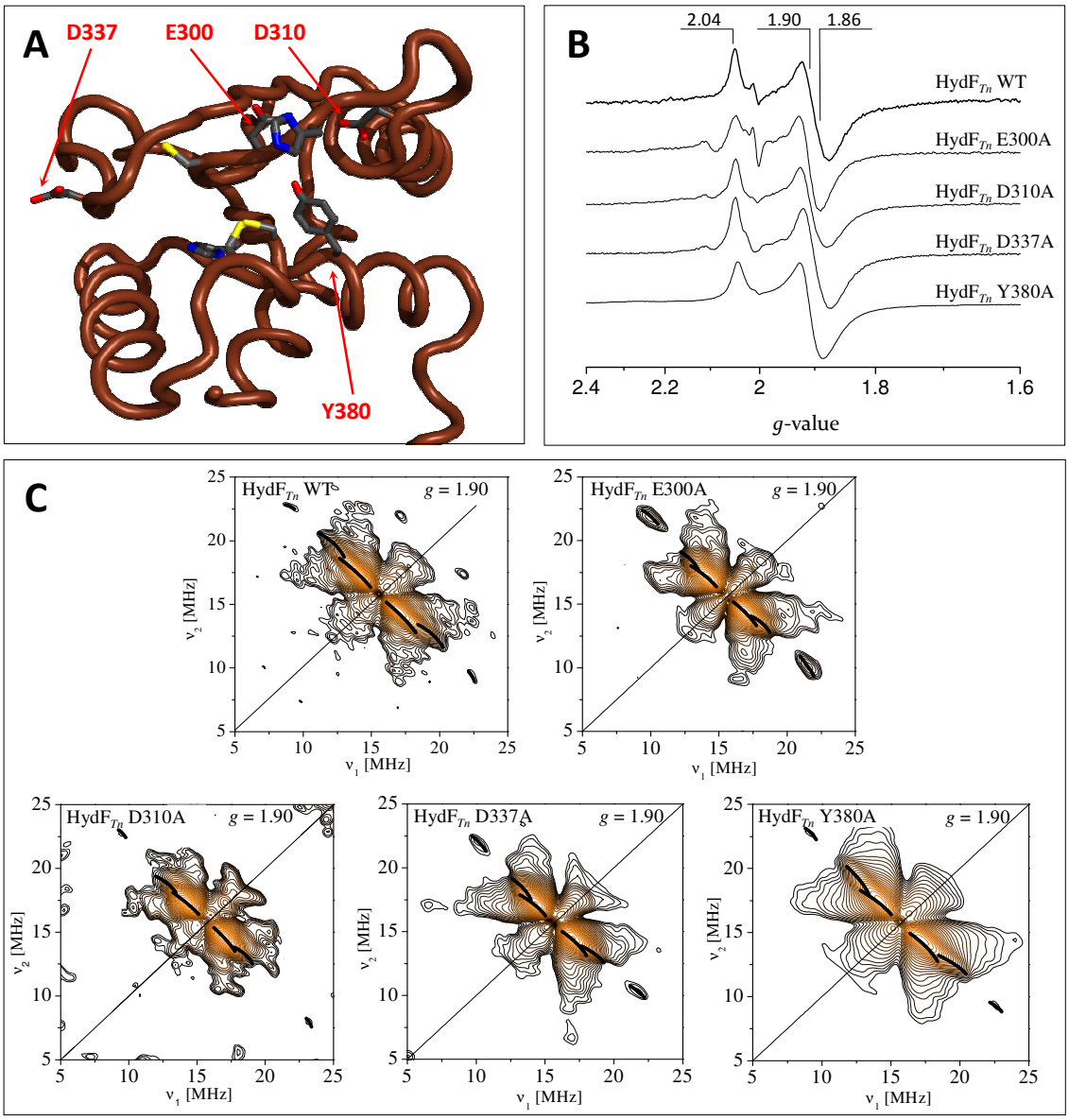
A
D337
E300
D310
Y380
B
2.04
1.90
1.86
HydF$_{Tn}$ WT
HydF$_{Tn}$ E300A
HydF$_{Tn}$ D310A
HydF$_{Tn}$ D337A
HydF$_{Tn}$ Y380A
2.4
2.2
2
1.8
1.6
g-value
C
HydF$_{Tn}$ WT
HydF$_{Tn}$ E300A
HydF$_{Tn}$ D310A
HydF$_{Tn}$ D337A
HydF$_{Tn}$ Y380A
g = 1.90
ν$_1$ [MHz]
ν$_2$ [MHz]

Fig 3

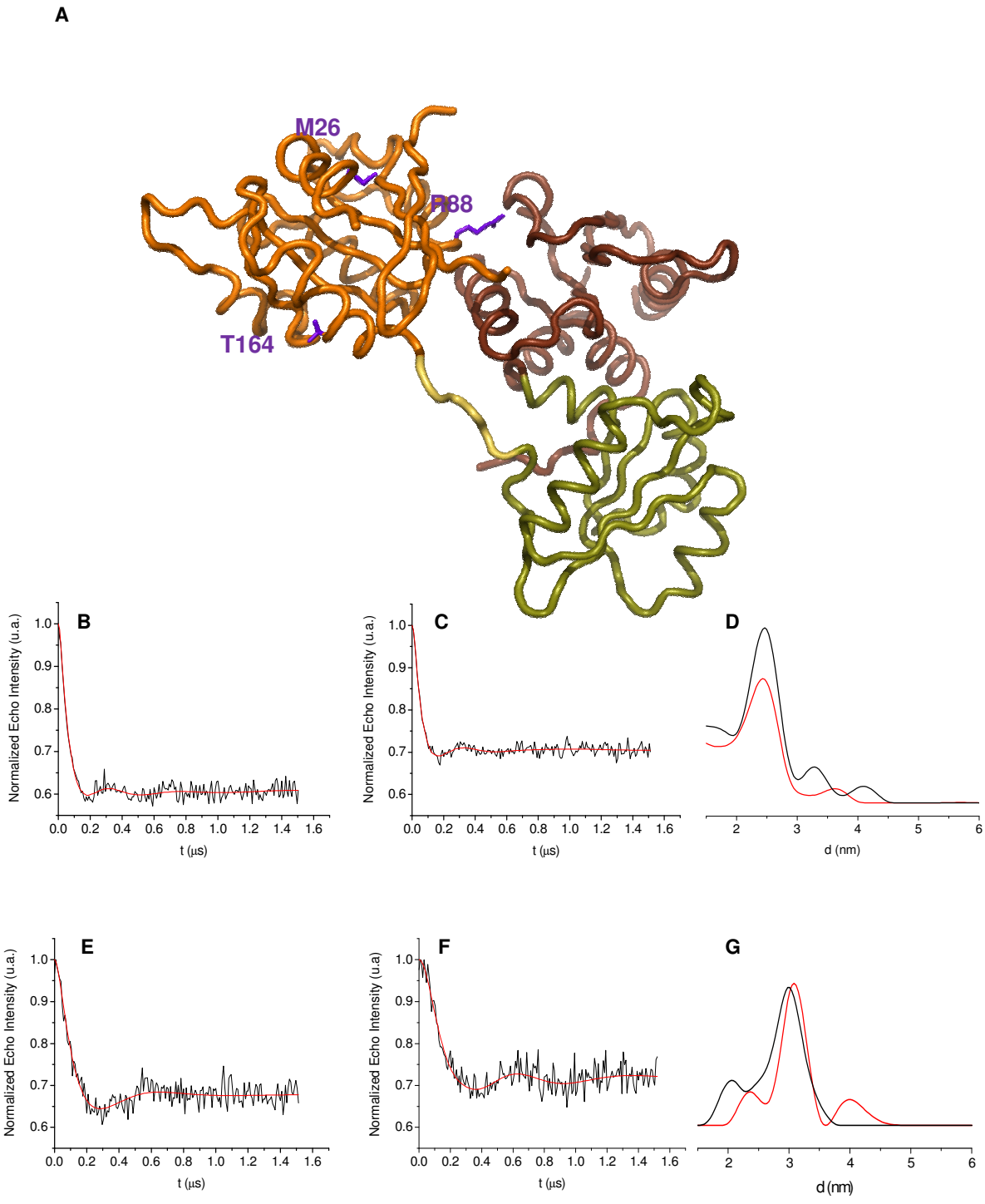

Fig 4

THE JOURNAL OF BIOLOGICAL CHEMISTRY VOL. 287, NO. 43, pp. 36544–36555, October 19, 2012

Biochemical Analysis of the Interactions between the Proteins Involved in the [FeFe]-Hydrogenase Maturation Process*

Received for publication, June 7, 2012, and in revised form, August 29, 2012 Published, JBC Papers in Press, August 29, 2012, DOI 10.1074/jbc.M112.388900

Francesca Vallese[‡1], Paola Berto[§], Maria Ruzzene[§], Laura Cendron[‡], Stefania Sarno[§], Edith De Rosa[§], Giorgio M. Giacometti[‡], and Paola Costantini[‡2]

From the [‡]Department of Biology, University of Padova, Viale G. Colombo 3, 35131 Padua, Italy and the [§]Department of Biomedical Sciences, University of Padova, Viale G. Colombo 3, 35131 Padua, Italy

Background: Activation of [FeFe]-hydrogenases requires coordinated interactions between the maturases HydE, HydF, and HydG.
Results: We characterized the interactions of HydF with HydE, HydG, and the hydrogenase that occur independently of the HydF GTPase activity, related to the dissociation step.
Conclusion: Additional insights into the [FeFe]-hydrogenases maturation process are provided.
Significance: This study contributes to a more detailed picture of how [FeFe]-hydrogenases are assembled.

[FeFe]-hydrogenases are iron-sulfur proteins characterized by a complex active site, the H-cluster, whose assembly requires three conserved maturases. HydE and HydG are radical *S*-adenosylmethionine enzymes that chemically modify a H-cluster precursor on HydF, a GTPase with a dual role of scaffold on which this precursor is synthesized, and carrier to transfer it to the hydrogenase. Coordinate structural and functional relationships between HydF and the two other maturases are crucial for the H-cluster assembly. However, to date only qualitative analysis of this protein network have been provided. In this work we showed that the interactions of HydE and HydG with HydF are distinct events, likely occurring in a precise functional order driven by different kinetic properties, independently of the HydF GTPase activity, which is instead involved in the dissociation of the maturases from the scaffold. We also found that HydF is able to interact with the hydrogenase only when co-expressed with the two other maturases, indicating that under these conditions it harbors *per se* all the structural elements needed to transfer the H-cluster precursor, thus completing the maturation process. These results open new working perspectives aimed at improving the knowledge of how these complex metalloenzymes are biosynthesized.

Iron-sulfur clusters are essential in several major biochemical processes in prokaryotic and eukaryotic organisms, including catalysis, electron transfer, determining of protein structure, and regulation of gene expression (1–3). Different FeS centers may exist in nature, ranging from the simplest [2Fe-2S] and [4Fe-4S] units, found in plant and bacterial ferredoxins, as well as in respiratory complexes I–III of bacteria and mitochondria, to more complex polymetallic clusters characterized in metalloproteins such as nitrogenase and hydrogenase (4), involved in nitrogen fixation and hydrogen metabolism, respectively. The biosynthesis of FeS clusters is a highly complex and strictly coordinated process driven by different, phylogenetically unrelated molecular systems, all sharing common biosynthetic principles (2, 5, 6). These pathways are key events in the overall cellular physiology, and according to their crucial role an increasing number of diseases are related to an impaired biogenesis of iron-sulfur proteins (2).

The paradigm of this complexity is represented by the biosynthesis and maturation machinery of the [FeFe]-hydrogenases, in which the active site (the so-called H-cluster) is composed by a [4Fe-4S] unit connected by a cysteinyl residue to a [2Fe-2S] center coordinated by three CO, two CN^-, and a bridging dithiolate (see Ref. 7 for a comprehensive review on this topic). This unique organometallic cluster serves as a catalytic site for the reversible reduction of protons to molecular hydrogen, which is central for both hydrogen metabolism in several prokaryotic and eukaryotic microorganisms and potential bioenergy applications exploiting this class of metalloenzymes. Because of the complexity of the H-cluster and the presence of species that are toxic in their free form, such as iron, CO and CN^-, a highly controlled and coordinated process is needed for its assembly (see Refs. 5, 6, and 8 for the most recent reviews on this topic). Three conserved proteins drive this maturation pathway, *i.e.*, HydE and HydG, two radical *S*-adenosylmethionine (SAM)[3] FeS enzymes (5, 9–13), and HydF, a GTPase containing the Walker A P-loop and Walker B Mg^{2+}-binding motifs, as well as a FeS cluster-binding sequence (14, 15). Site-specific mutagenesis analysis revealed that the con-

* This work was supported by Ministero delle Politiche Agricole e Forestali Grant (to G. M. G.).
[1] Recipient of a Ph.D. fellowship from the Fondazione Cassa di Risparmio di Padova e Rovigo.
[2] To whom correspondence should be addressed: Dept. of Biology, University of Padova, Viale G. Colombo 3, 35131 Padova, Italy. Tel.: 39-49-8276323; Fax: 39-49-8276300; E-mail: paola.costantini@unipd.it.

[3] The abbreviations used are: SAM, *S*-adenosylmethionine; HydA1, [FeFe]-hydrogenase 1; $HydF^{\Delta EG}$, HydF expressed in the absence of HydE and HydG; $HydF^{EG}$, HydF co-expressed with HydE and HydG; $HydF^{E}$, HydF co-expressed with HydE; $HydF^{G}$, HydF co-expressed with HydG; $HydA^{\Delta EFG}$, [FeFe]-hydrogenase expressed in the absence of HydE, HydF, and HydG; MCS, multiple cloning site; SPR, surface plasmon resonance.

TABLE 1
Plasmid constructs for T7 promoter driven expression of [FeFe]-hydrogenase structural and maturation genes in *E. coli*

Plasmid	
pCDFDuet-1/*hydF-StrepII*	Expression of wild type and mutant HydF proteins with a N-terminal StrepII tag or 6His tag
pCDFDuet-1/*hydF-StrepII*_G24A/K25A	
pCDFDuet-1/*hydF-StrepII*_D67A	
pCDFDuet-1/*hydF-6His*_C304S	
pCDFDuet-1/*hydF-6His*_G24A/K25A	
pCDFDuet-1/*hydF-6His*	
pACYCDuet-1/*hydE*	Expression of untagged HydE protein
pACYCDuet-1/*hydE-6His*	Expression of a HydE protein with a N-terminal 6His tag
pRSFDuet-1/*hydG*	Expression of untagged HydG protein
pRSFDuet-1/*hydG-6His*	Expression of a HydG protein with a N-terminal 6His tag
pETDuet-1/*hydA1-StrepII*	Expression of a HydA1 protein with a C-terminal StrepII tag
pETDuet-1/*hydA1-StrepII/hydE*	Co-expression of untagged HydE and a HydA1 proteins with a C-terminal StrepII tag
pRSFDuet-1/*hydF/hydG*	Co-expression of untagged HydF and HydG proteins

served radical SAM and GTPase consensus motifs are all essential for the [FeFe]-hydrogenase maturation and activation (16). According to several recent *in vitro* studies, this process occurs in a multistep pathway, in which the [4Fe-4S] unit is synthesized by the Isc/Suf FeS general cell machinery, whereas the biosynthesis and insertion of the 2Fe subcluster, together with its ligands, is driven by HydE, HydG, and HydF maturases (5–8, 17). Current data indicate that the addition of the CO/CN^-/dithiolate ligands to the 2Fe subcluster is accomplished through the action of the HydE/HydG radical SAM chemistry coupled to the presence of HydF, which would have a double involvement as scaffold and carrier to build and insert the modified 2Fe subcluster into a hydrogenase containing a preformed [4Fe-4S] unit (17–21).

Because of the multistep nature of the molecular pathway leading to the [FeFe]-hydrogenase maturation, a network of protein interactions between the players of this process must be established to accomplish and coordinate the H-cluster assembly. The dynamic behavior of HydF as scaffold and carrier assigns to this protein a key role along the entire maturation process and indicates its capability to interact with both HydE and HydG in the first step, when the 2Fe subcluster is processed and modified, and finally with the hydrogenase, when the complete 2Fe unit is ready to be transferred to the latter. The interactions of HydF with the other accessory proteins have been previously inferred from the co-purification of HydE and HydG with HydF (19), and recent data suggest that the GTP binding and/or hydrolysis could be associated with the interactions between the maturases, because both HydE and HydG increase by 50% the rate of GTP hydrolysis catalyzed by HydF (15). This led the authors to suggest that GTP binding and/or hydrolysis may induce structural changes in HydF, which would in turn influence the interactions between the three maturases. However, the molecular details of HydF GTPase activity during [FeFe]-hydrogenase maturation and its precise role in this process are still unknown.

We recently solved the crystal structure of a recombinant HydF from *Thermotoga neapolitana* (22). HydF is organized in three distinct domains, *i.e.*, (i) domain I, which carries all the conserved amino acids considered important for GTP binding and hydrolysis; (ii) domain II, responsible for HydF dimerization; and (iii) domain III, the FeS cluster-binding domain, which may be in principle involved in the interprotein interactions of this maturase with its potential partners.

In this work we address and characterize the protein-protein interactions of HydF with the two other maturases and the hydrogenase, which are expected to be pivotal in all steps of [FeFe]-hydrogenase maturation pathway, with the aim of gaining further insights into this complex molecular process.

EXPERIMENTAL PROCEDURES

All of the chemicals were of the highest purity commercially available.

Heterologous Expression of Hyd Maturation and Structural Proteins from Clostridium acetobutylicum—The *C. acetobutylicum hydE*, *hydF*, *hydG*, and *hydA1* coding sequences were cloned in the pCDFDuet-1, pACYCDuet-1, pRSFDuet-1, and pETDuet-1 vectors (Novagen®) suitable for T7 driven (co)expression in *Escherichia coli*, either as such or in frame with a tag sequence (6His or StrepII tag, depending on the experiment; see "Results" and "Discussion"), thus obtaining the recombinant plasmids listed in Table 1. The pCDFDuet-1/*hydF-StrepII*, pETDuet-1/*hydA1-StrepII*, pETDuet-1/*hydA1-StrepII*/*hydE*, and pRSFDuet-1/*hydF/hydG* plasmids were kindly provided by Dr. Matthew C. Posewitz (Department of Chemistry and Geochemistry, Colorado School of Mine, Golden, CO) and obtained as described previously (16). Some of these vectors were used as templates for PCR amplification with specific oligonucleotides designed with 5′ and 3′ end restriction sites for directional subcloning into the dual multiple cloning site (MCS 1 and MCS 2) of plasmids pACYCDuet-1 (*hydE*), pCDFDuet-1 (*hydF*), or pRSFDuet-1 (*hydG*). When required, the restriction sites were selected to clone the gene of interest in frame with a 6His tag coding sequence localized immediately downstream the BamHI restriction site of MCS 1. *hydE* and *hydG* were cloned either in MCS 1 between the BamHI and NotI restriction sites (forming the pACYCDuet-1/*hydE-6His* and pRSFDuet-1/*hydG-6His* plasmid, respectively) or in MCS 2 between the NdeI and BglII restriction sites (forming the pACYCDuet-1/*hydE* and pRSFDuet-1/*hydG* plasmid, respectively). *hydF* was cloned in MCS 1 between the BamHI and NotI restriction sites (forming the pCDFDuet-1/*hydF-6His* plasmid). The PCRs were performed using the high fidelity Phusion DNA polymerase (Finnzymes). The sequence and reading frame of each gene were confirmed by DNA sequencing (BMR Genomics, University of Padova). *E. coli* BL21(DE3) cells were transformed with the recombinant plasmid(s), and positive clones were selected by antibiotic resistance. The protein(s), either wild type or

mutant (see below), were expressed as described previously (16) by adding 1 mM isopropyl β-thiogalactopyranoside, in aerobiosis or anaerobiosis depending on the experiment, and purified.

Co-purification of HydF with Potential Interaction Partners—To evaluate the interactions of HydF-StrepII with HydE-6His and HydG-6His and of HydF-6His with HydA1-StrepII, *E. coli* cells (100 ml of culture) co-expressing the proteins of interest were collected by centrifugation at 4,000 × *g* for 10 min at 4 °C. The cell pellet was resuspended in lysis buffer (100 mM Tris-HCl, pH 8, 150 mM NaCl, 2 mM DTT, 2 mM Na_2S, 2 mM $(NH_4)_2Fe(SO_4)_2{\cdot}6H_2O$, and protease inhibitors 1 μg/ml pepstatin A, 1 μg/ml leupeptin, 1 μg/ml antipain, 1 mM PMSF) and broken in a French press (at 1.35 kbar; One Shot Constant System Cell Disrupter, from Constant Systems Ltd). A clarified crude extract was then obtained by centrifugation and incubated 1 h at 4 °C under mild shaking either with 200 μl of a StrepTactin-Sepharose suspension (IBA, Göttingen, Germany) or with 200 μl of a nickel affinity gel (HIS-Select® nickel affinity gel; Sigma-Aldrich), both pre-equilibrated with lysis buffer. At the end of this incubation, the mix was transferred into a chromatography column. The column was then washed with 5 volumes of lysis buffer, and the tagged proteins were eluted with 5 volumes of lysis buffer containing 2.5 mM desthiobiotin or 200 mM imidazole. The elution fractions were pooled together, analyzed by 12% SDS-PAGE, and electroblotted onto a nitrocellulose membrane. For immunoblotting analysis, the membrane was probed with a monoclonal anti-6His tag (Sigma-Aldrich) or anti-StrepII tag (IBA) antibody and with a horseradish peroxidase-conjugated goat anti-mouse IgG (Kirkegaard & Perry Laboratories). Labeled proteins were then visualized with an ECL Western blotting detection kit (Thermo Scientific Pierce Protein Research).

Analysis of the Stoichiometry of HydF-StrepII·HydE-6His and HydF-StrepII·HydG-6His Interactions—Recombinant HydF-StrepII (also as mutant HydF-StrepII_G24A/K25A and HydF-StrepII_D67A proteins) and HydE-6His or HydG-6His were co-expressed in *E. coli* as described previously, and the complexes between these proteins purified by a double affinity chromatography approach, by exploiting first the HydF StrepII epitope and in a second step the HydE or HydG 6His tag. Briefly, in both cases the Strep-Tactin elution fractions containing HydF-StrepII and HydE-6His or HydG-6His were pooled and subjected to a nickel-nitrilotriacetic acid affinity chromatography to retain HydE-6His or HydG-6His. The imidazole eluted fractions were pooled together and resolved on 12% SDS-PAGE with known amounts of BSA, ranging from 0.5 to 2 μg. The proteins were visualized with Coomassie Brilliant Blue stain, and their amount was estimated by densitometry on a Image Station 4000 MM PRO instrument (Kodak). The data were analyzed with Carestream molecular imaging software.

Purification of HydE-6His and HydG-6His Proteins to Homogeneity for Biacore Analysis—HydE-6His and HydG-6His were purified to homogeneity by subjecting affinity-purified proteins to gel filtration chromatography performed with a Superdex 200 HR 10/30 (GE Healthcare), equilibrated in 25 mM Tris-HCl, pH 8, 200 mM NaCl elution buffer. Each run was performed by injecting the appropriate sample volume at a flow rate of 0.75 ml/min and monitoring the UV absorbance at 280 nm, by a fixed wavelength detector. To estimate the molecular weight of the analyzed samples, the column was equilibrated in the same buffer and calibrated with the standards thyroglobulin (669,000 Da), ferritin (440,000 Da), catalase (232,000 Da), aldolase (158,000 Da), bovine serum albumin (67,000 Da), ovalbumin (43,000 Da), and ribonuclease (13,700 Da). Purified proteins were quantified by using a Micro BCA Protein Assay kit (Thermo Scientific Pierce Protein Research). The presence of monomeric HydE-6His and HydG-6His proteins in the selected peaks was confirmed by Western blotting analysis using a monoclonal anti-6His tag antibody.

Site-directed Mutagenesis of hydF-StrepII Coding Sequence—Site-directed mutagenesis of the *hydF-StrepII* was performed with QuikChange® II site-directed mutagenesis kit (Stratagene) using as template the pCDFDuet-1/*hydF-StrepII* or the pCDFDuet-1/*hydF-6His* plasmids. Oligonucleotides were designed according to the manufacturer's guidelines, and the mutant constructs were analyzed by DNA sequencing. The oligonucleotide sequences (with the modified bases underlined) were: mutWalkerAfor, 5′-GGAAAAACTAATGTTGCAGCATCCAGTGTAATAAATG-3′; mutWalkerArev, 5′-CATTTATTACACTGGATGCTGCAACATTAGTTTTTCC-3′; mutWalkerBfor, 5′-ACCAGTTATGCTTATAGCTACTGCTGGTCTTGATC-3′; mutWalkerBrev, 5′-GATCAAGACCAGCAGTAGCTATAAGCATAACTGGT-3′; mutCys304for, 5′-TTAATAGCAGAAGCCAGCACCCACCACCGTC-3′; and mutCys304rev, 5′-GACGGTGGTGGGTGCTGGCTTCTGCTATTAA-3′.

Surface Plasmon Resonance Analysis—For the surface plasmon resonance analysis, a BIAcore™ T100 system (GE Healthcare) was used. HydF-StrepII and HydF-StrepII_G24A/K25A proteins were covalently coupled to a CM5 (series S) sensor chip (carboxymethylated dextran surface) by amine-coupling chemistry to a final density of 6000 resonance units, as described (23); a 10 mM acetate pH 5.0 buffer was used for the immobilization. A flow cell with no immobilized protein was used as a control. Binding analysis was carried out in a running buffer consisting of 10 mM Hepes, pH 7.6, 150 mM NaCl, 2 mM $MgCl_2$, applying a flow rate of 30 μl/min. The absence of mass transport limitation was assessed by checking that signals observed at different flow rates (10–30 μl/min) were superimposable. Each sensorgram (time course of the surface plasmon resonance signal) was corrected for the response obtained in the control flow cell and normalized to baseline. After each injection, the surface was regenerated by a double injection of 2 M $MgCl_2$ for 1 min; this treatment restored the base line to the initial resonance unit value. For kinetics experiments, a Biacore method program was used that included a series of three start-up injections (running buffer), zero control (running buffer), and six different concentrations of the analytes (HydE-6His or HydG-6His), one of which was duplicated. Serial dilutions of the analytes were performed in running buffer from a 2 μM top concentration. High performance injection parameters were used; the contact time was of 120 s followed by a 120-s dissociation phase. The kinetic data were analyzed using the 2.0.3 BIAevaluation software (GE Healthcare). The curves (both association and dissociation phases) were fitted with the classical Langmuir 1:1 model or with a two-state binding model; the quality of the fits was assessed by visual inspection of the

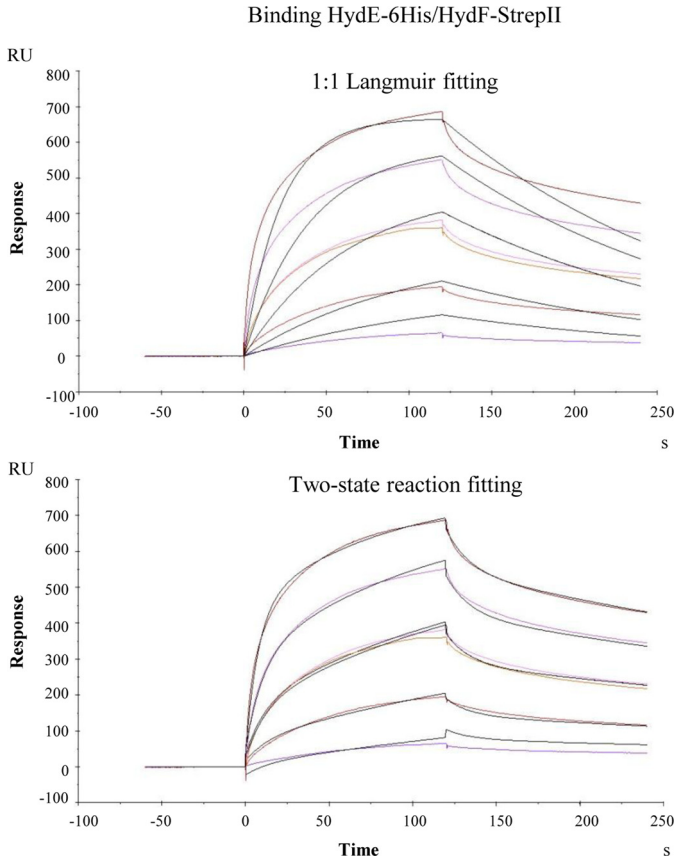

FIGURE 1. **Comparison between the 1:1 Langmuir and the two-state reaction fitting models for the binding HydE-6His·HydF-StrepII analyzed by means of SPR signal detection.** The kinetics shown are the same as those in Fig. 3*A*. For more details, see the legend of Fig. 3. The *color curves* are real sensorgrams, and *black curves* correspond to the fitting.

fitted data and their residual, and by chi-squared values. Although the K_D values calculated with the two models were very similar, better fits were generated by the two-state reaction model (as an example see Fig. 1, which reports the fits referring to the complex HydE-6His·HydF-StrepII), according to which 1:1 binding is followed by a conformational change that stabilizes the complex (24). Two independent experiments were performed.

GTP Hydrolysis Assay—Under aerobic conditions, HydF-StrepII, HydF-StrepII_G24A/K25A, and HydF-StrepII_D67A proteins were assayed for their ability to hydrolyze GTP using the protocol optimized by Shepard *et al.* (15), with slight modifications. Briefly, 40 μM of affinity-purified proteins were incubated at 30 °C with 2 mM GTP and 2 mM $MgCl_2$ in 20 mM Tris-HCl buffer, pH 8.0, containing 200 mM KCl. At time intervals, aliquots of the reaction mixture were collected and assayed for production of GDP. Assay aliquots were incubated at 95 °C for 3 min and centrifuged at 14,000 rpm at 4 °C in a benchtop microcentrifuge, and the supernatants were analyzed by reverse phase HPLC on a Synergi MAX-RP 80A (150 × 4.6 mm, 4 μm; Phenomenex). The samples were eluted with an isocratic mobile phase of 50 mM sodium phosphate buffer, pH 7.0, 10 mM tetrabutylammonium bromide, 10% CH_3CN. The guanosine nucleotides were detected by their absorbance at 254 nm. Under these conditions, GDP and GTP eluted after ~8.1 and ~18.6 min, respectively. Integration of peak areas (using the software Agilent Chemstation) of the samples taken at identical time points allowed the quantification of the μmoles of GDP produced liter^{-1} min^{-1}, from which the ratio between the k_{cat} were finally determined.

Hydrogen Evolution Assay—Hydrogenase activity of whole extracts obtained from cells co-expressing HydA1-StrepII with HydE, HydG, and HydF-StrepII or HydF-6His (also as HydF-StrepII_G24A/K25A, HydF-StrepII_D67A, and HydF-6His_C304S mutant proteins) were measured *in vitro*, as described previously (16). Briefly, 1 ml of 2× enzyme reaction buffer was added to 1 ml of *E. coli* cell cultures giving exactly the same absorbance at 600 nm, and the evolution of H_2 gas from reduced methyl viologen was measured using nitrogen-flushed 13.5-ml sealed serum vials and a gas chromatograph Perkin-Elmer Clarus GC500, fitted with a Restek 5 Å Molecular Sieve 80/100 6′ 1/8″ column and a thermal conductivity detector. All of the steps were performed in an anaerobic chamber (MBRAUN).

UV-visible Absorption—The UV-visible absorption spectra of HydF-6His and HydF-6His_C304S proteins were acquired as described previously (22) using a Lambda Bio 40 UV-visible spectrometer (PerkinElmer Life Sciences).

RESULTS AND DISCUSSION

To gain new biochemical insights into the dynamic roles of HydF, we analyzed the interactions of this protein with both HydE and HydG, as well as with the hydrogenase (HydA1). These interactions are central for the entire maturation process and are supposed to be associated with its scaffold and carrier activities, respectively.

Biochemical Analysis of Protein-Protein Interactions of HydF Scaffold with HydE and HydG Maturases—It has been previously shown that the recombinant HydE, HydF, and HydG proteins co-elute from an affinity chromatography column when co-expressed in *E. coli* (19), thus suggesting an interaction between the three maturases. The setup of a coordinated and regulated network of protein interactions between HydE, HydF, and HydG is the first crucial step in the HydA maturation pathway. According to all recent literature data concerning the H-cluster assembly, this complex multistep process requires the ability of the HydF scaffold to interact with both HydG and HydE, but the molecular and biochemical details of this key event are still not completely understood. Based on this, we first evaluated whether HydE and HydG are both able to directly and individually interact with HydF using recombinant proteins from *C. acetobutylicum* fused to different tags to be exploited for affinity chromatography purification and Western blotting analysis. To this end, we co-transformed the *E. coli* strain BL21(DE3) either with the plasmids *pCDFDuet/hydF-StrepII* and *pACYCDuet/HydE-6His* or with the plasmids *pCDFDuet/hydF-StrepII* and *pRSFDuet/hydG-6His*, which allowed the isopropyl β-thiogalactopyranoside-inducible T7 co-expression of the corresponding recombinant proteins (Fig. 2, *A–D*, *lanes 1*). The HydF-StrepII tag protein was then purified from the soluble fraction of the two cultures by Strep-Tactin affinity chromatography (Fig. 2, *A* and *B*, *lanes 3*), as described under "Experimental Procedures," and the presence of HydE-6His or HydG-6His in the eluted fractions was verified by Western blotting analysis using an anti-6His tag monoclonal antibody.

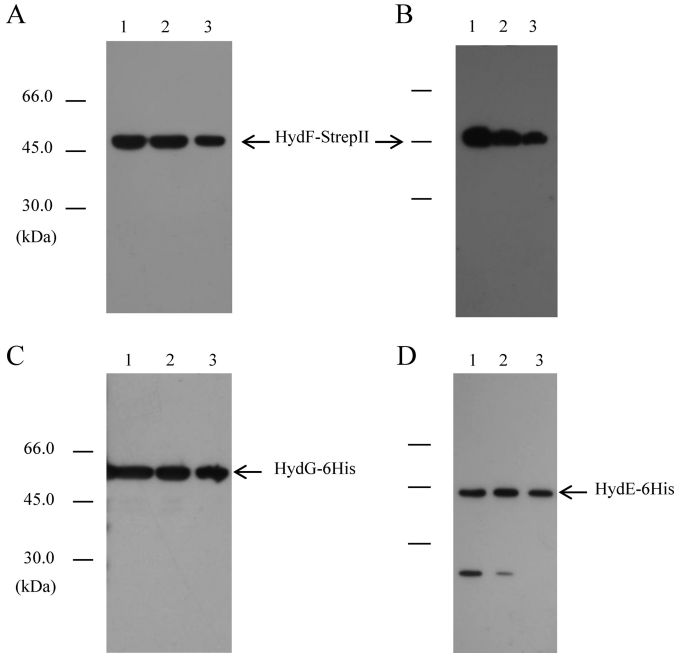

FIGURE 2. **Binary interactions of HydF-StrepII scaffold with the HydE-6His and HydG-6His maturases.** Western blotting analysis shows the StrepTactin purification of HydF-StrepII co-expressed with HydG-6His (*A* and *C*) or with HydE-6His (*B* and *D*). *Lanes 1*, total *E. coli* cell extract; *lanes 2*, soluble fraction of cell extract; *lanes 3*, total pool of desthiobiotin eluted fractions. 25 μl of each sample were loaded on a 12% gel for SDS-PAGE. *A* and *B*, Western blotting with anti-StrepII tag monoclonal antibody; *C* and *D*, Western blotting with anti-6His tag monoclonal antibody.

Fig. 2 (*C* and *D*, *lanes 3*) clearly shows that both HydE-6His and HydG-6His co-purify with HydF-StrepII, indicating that the interactions between HydF scaffold and the two other maturases can be envisaged as distinct, independent, and possibly unrelated events (*i.e.*, $HydF^{\Delta EG}$ may interact both with $HydE^{\Delta G}$ and $HydG^{\Delta E}$).

To quantify these protein interactions, we determined the stoichiometry of the HydF-StrepII·HydE-6His and HydF-StrepII·HydG-6His heterocomplexes. To exclude from this analysis the free HydF-StrepII protein (*i.e.*, the purified HydF-StrepII, which did not interact with the maturation partner), we isolated the HydF-StrepII·HydE-6His and the HydF-StrepII·HydG-6His complexes by a double affinity chromatography, exploiting first the HydF StrepII epitope and in a second step the HydE-6His or HydG-6His tag, as described under "Experimental Procedures." The Strep-Tactin elution fractions, containing HydF-StrepII and HydE-6His or HydG-6His, were pooled and subjected to a nickel-nitrilotriacetic acid affinity chromatography to retain HydE-6His or HydG-6His, still associated with HydF-StrepII. In both cases, the imidazole eluted fractions were pooled together and subjected to SDS-PAGE. The gel was then stained with Coomassie Brilliant Blue, and the amount of maturases estimated by densitometry as described under "Experimental Procedures." Based on this analysis, we found a stoichiometric ratio of roughly 1:4 for the HydE-6His·HydF-StrepII complex and of 1:1 for the HydG-6His·HydF-StrepII complex. The observed stoichiometries could be due to the presence of multiple oligomeric species of HydF-StrepII protein (dimers and tetramers) (22), as well as to the amount of HydE-6His, which is invariably lower when compared with HydG-6His in co-expression experiments (not shown).

To date, only qualitative evidence for protein-protein interaction between Hyd maturases has been reported (19). To obtain further quantitative data for the binding properties of the HydF scaffold protein and to provide the kinetic constants of the HydF·HydE and HydF·HydG interactions, we performed a surface plasmon resonance (SPR) analysis by means of a Biacore T100 instrument. An affinity-purified HydF-StrepII tag protein was covalently immobilized on a chip surface, and solutions at different concentrations of HydG-6His or HydE-6His, previously purified to homogeneity by a combination of affinity and gel filtration chromatography, were individually passed over the chip, as described in detailed under "Experimental Procedures." As shown in Fig. 3, which reports the curves corresponding to a two-state reaction fitting (see "Experimental Procedures" and Fig. 1), both HydE-6His (Fig. 3*A*) and HydG-6His (Fig. 3*B*) give a SPR signal, which is concentration-dependent and clearly indicates the expected binding to HydF-StrepII. However, as immediately evident from the figure, HydE-6His produces a much higher signal when compared with HydG-6His. We performed a quantitative analysis for the kinetics constants with the BIAevaluation software, and the values, reported in Table 2, show that the K_D of HydE-6His is 1 order of magnitude lower than that of HydG-6His, indicating a higher affinity for the interaction HydF-StrepII·HydE-6His.

Because HydE and HydG act on the same [2Fe2S]-cluster prior to its transfer from the scaffold to the [FeFe]-hydrogenase, they likely share the same interaction site within HydF domain III, which, based on the HydF three-dimensional structure recently solved, harbors the cluster-binding pocket (22). To strengthen the Biacore analysis results and to confirm the existence of a possible stepwise mechanism in which the HydF scaffold interacts only with a maturation partner at a time, we first injected the HydE-6His protein near the saturation level on the chip containing the immobilized HydF-StrepII, and in a second step we applied in the same chip a HydG-6His solution; the result was then compared with the one obtained with a similar protocol, in which in the first step the same volume of buffer has been added instead of HydE-6His. Fig. 4*A* shows that HydG-6His, which as expected interacts with a free HydF-StrepII (*line b*), is unable to produce any significant signal when injected after HydE-6His (*line a*), indicating that the occupancy of the HydE-6His sites on HydF-StrepII prevents the binding of HydG-6His. This result also suggests that HydG-6His does not interact with HydE-6His. Moreover, we can also conclude that HydG-6His is not able to displace HydE-6His already bound to the scaffold. Unfortunately, because of the low affinity of HydG-6His for HydF-StrepII, we were not able to perform the opposite protocol (*i.e.*, presaturation of HydF-StrepII with HydG-6His, followed by injection of HydE-6His); thus, we cannot assess whether the presence of HydG-6His prevents the binding of HydE-6His as well, using this Biacore approach. To better address this issue, we co-expressed in *E. coli* the recombinant HydF-StrepII and HydG-6His proteins and isolated the HydF-StrepII·HydG-6His complex by the same double affinity chromatography approach described above. Fig. 4 shows that the nickel-nitrilotriacetic acid elution fractions contain both

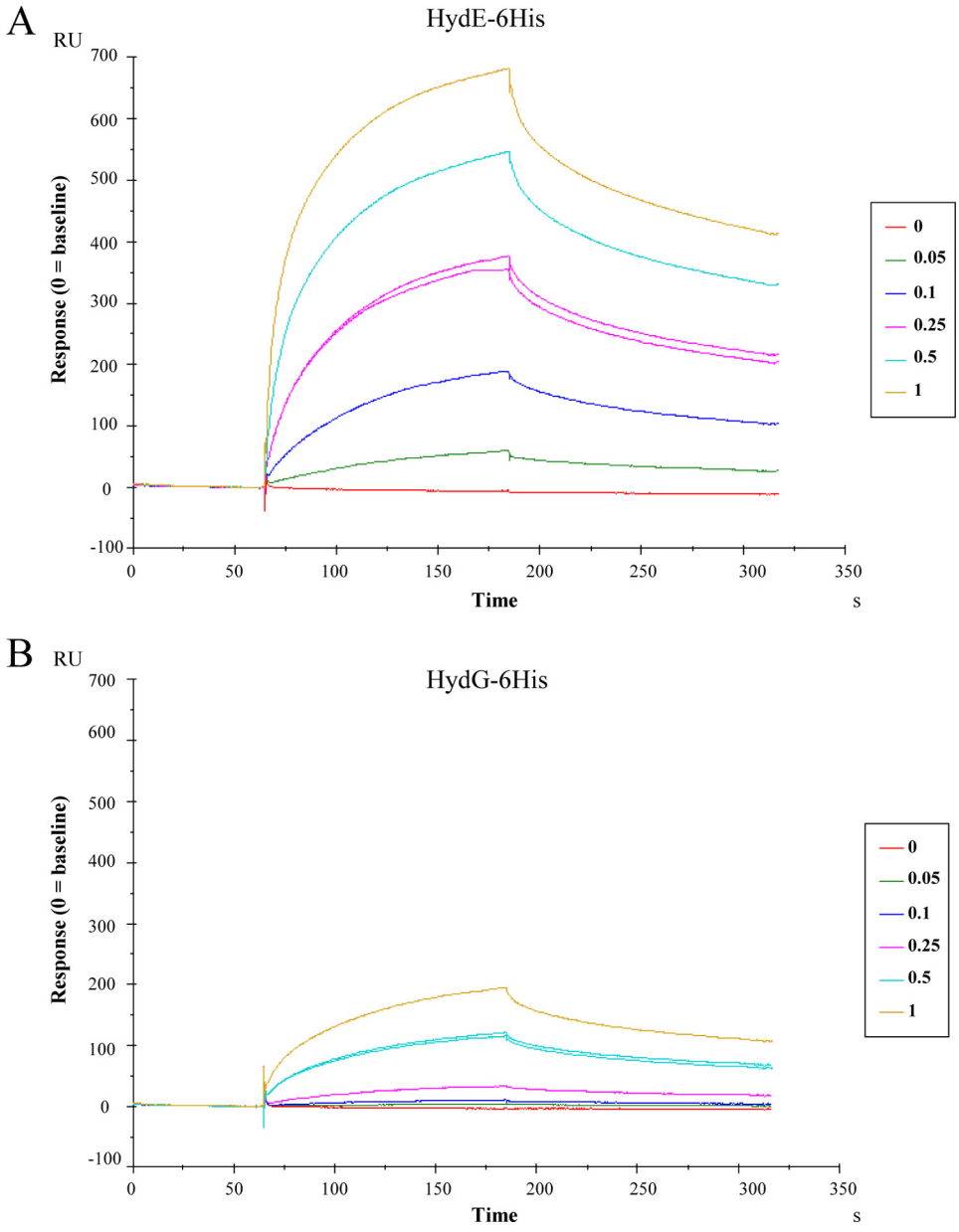

FIGURE 3. **Kinetics of the HydE-6His·HydF-StrepII and HydG-6His·HydF-StrepII interactions by means of SPR signal detection.** HydE-6His (*panel A*) or HydG-6His (*panel B*) solutions (analytes) at the concentrations (μM) indicated in the *boxes* were injected over a sensor chip where HydF-StrepII (ligand) was previously covalently immobilized in a Biacore T100 instrument (see the "Experimental Procedures" for details). SPR signal is shown as sensorgram, and the time course of the surface plasmon resonance response reported in resonance units (*RU*). Each sensorgram has been subtracted of the corresponding signal produced on a control surface and normalized to baseline. One solution of each analyte was injected twice at the same concentration (0.25 μM HydE-6His and 1 μM HydG-6His), as further control. 0 concentrations corresponded to dilution buffer.

TABLE 2

Kinetics values of the HydE-6His/HydF-StrepII and HydG-6His/HydF-StrepII interactions calculated from Biacore experiments

The constants ± S.E. are calculated from the kinetics shown in Fig. 3, with BIAevaluation software 2.0.3. Only two decimal digits are shown. A two-state reaction model was applied (see "Experimental Procedures" and Fig. 1).

	$k_{on,1}$	$k_{off,1}$	$k_{on,2}$	$k_{off,2}$	K_D
	$M^{-1} \times s^{-1} \times 10^4$	$s^{-1} \times 10^{-2}$	$s^{-1} \times 10^{-2}$	$s^{-1} \times 10^{-3}$	M
HydF-StrepII					
HydE-6His	7.27 ± 0.04	5.29 ± 0.05	1.83 ± 0.01	2.65 ± 0.02	9.19×10^{-8}
HydG-6His	0.65 ± 0.002	7.34 ± 0.25	1.90 ± 0.03	2.52 ± 0.06	1.31×10^{-6}
HydF-StrepII_G24A/K25A					
HydE-6His	9.96 ± 0.06	5.92 ± 0.05	1.72 ± 0.01	2.75 ± 0.02	8.20×10^{-8}
HydG-6His	1.02 ± 0.02	8.07 ± 0.23	1.88 ± 0.02	2.58 ± 0.05	9.47×10^{-7}

HydG-6His (Fig. 4*C*, *lane 2*) and HydF-StrepII (Fig. 4*B*, *lane 2*). The complex was then incubated for 30 min with the soluble fraction of a cell extract obtained by a HydE-6His overexpressing *E. coli* culture, and the mixture was subjected to a Strep-Tactin affinity chromatography. The presence of HydE-6His and HydG-6His, together with HydF-StrepII, in the eluted frac-

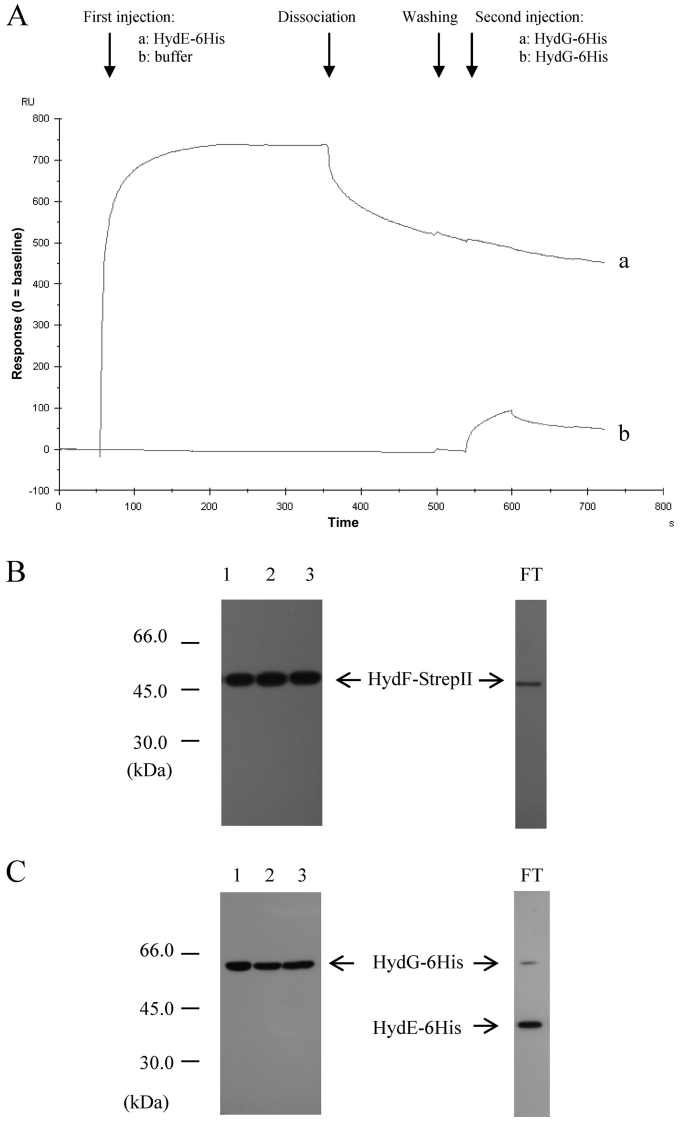

FIGURE 4. **Analysis of the interactions between HydG-6His and the HydF-StrepII·HydE-6His complex and between HydE-6His and the HydF-StrepII·HydG-6His complex.** *A*, Biacore analysis. Injection of 2 μM HydE-6His solution (*sensorgram a*) or running buffer (*sensorgram b*) was performed in a Biacore T100 system over a sensorchip with immobilized HydF-StrepII, at a flow rate of 30 μl/min for 5 min. After further 2 min of buffer flowing (dissociation phase) and washing, a 2 μM HydG-6His solution was injected (1 min of association, 1 min of dissociation). The shown sensorgrams are subtracted from the signal in control flow cell and normalized to a base-line value of 0. *B* and *C*, Western blotting analysis. *Lane 1*, pool of desthiobiotin eluted fractions from the first affinity chromatography; *lane 2*, pool of imidazole eluted fractions from the second affinity chromatography; *lane 3*, pool of desthiobiotin eluted fractions from the third affinity chromatography. *FT*, flow-through of the third affinity chromatography. 25 μl of each sample were loaded on a 12% gel for SDS-PAGE. *B*, Western blotting with anti-StrepII tag monoclonal antibody. *C*, Western blotting with anti-6His tag monoclonal antibody.

tions was finally evaluated by Western blotting analysis. Fig. 4 shows that HydG-6His still co-elutes with HydF-StrepII in this third chromatographic step (*lanes 3* of *C* and *B*, respectively), whereas HydE-6His is exclusively present in the flow-through fraction (*C*, *lane 3*, and FT), indicating that a HydF-StrepII·HydG-6His complex is not able to interact with a second maturation partner, exactly as previously observed in the Biacore experiments with the HydF-StrepII·HydE-6His complex.

The sequence of events leading to the synthesis of the complete [2Fe-2S]-cluster on the HydF scaffold is still undefined. Based on several independent compelling studies, a model has been recently proposed (5, 6) in which HydE synthesizes the dithiolate ligand of the H-cluster, thus generating an intermediate that would be then further modified by the addition of CO and CN^- catalyzed by HydG (11, 12, 25), leading to a complete H-cluster precursor, to be finally transferred to the [FeFe]-hydrogenase. The chemical rationale of this order is based on the hypothesis that HydE probably modifies the [2Fe-2S]-cluster via a BioB (biotin synthase) type sulfur insertion chemistry (6), even if substrates and products of HydE catalysis are still unidentified. Thus, the reaction catalyzed by HydE would be expected to take place first to protect the sulfide groups and move the reactivity toward the iron ions of the FeS cluster, making them susceptible to the addition of CO and CN^- in a second step (21). In this scenario, if HydE and HydG are simultaneously co-expressed *in vivo*, the higher affinity of HydE for the HydF scaffold, when compared with HydG, would allow the [2Fe-2S]-cluster modification sequence described above to occur. Because HydG is not able to interact with the complex HydF·HydE, nor to displace HydE (Fig. 4), a further step is required to allow the interaction of HydG with the scaffold to complete the FeS cluster chemical modification (see below). Structural analysis of the HydF-StrepII·HydE-6His and HydF-StrepII·HydG-6His heterocomplexes are currently underway in our laboratory to explore the modifications introduced in HydF by the other two maturases and to map the regions lying at the interface between the interacting proteins.

Investigating the Potential Involvement of GTP Binding/Hydrolysis in the Interactions of HydF with HydE and HydG—NTPases are commonly involved in the assembly of metal cofactors of FeS proteins and mediate either the metal delivery to the active site or the cluster transfer to the target protein. Experimental evidences against a role of HydF GTPase activity in FeS cluster precursor transfer to the [FeFe]-hydrogenase have been previously provided (15), and the role of GTP binding/hydrolysis in H-cluster assembly is elusive. As assessed in the Introduction, it has been shown that the HydF-dependent GTP hydrolysis *in vitro* increases in the presence of HydE or HydG (15), suggesting the existence of a HydF GTPase domain function/structure relationship driving the interactions of this scaffold with the two other maturases. To address this point and to test the requirement of intact HydF GTP hydrolysis properties for the protein-protein interactions described above, we generated two new recombinant HydF-StrepII proteins, carrying (i) two point-mutations in the Walker A P-loop sequence ((G/A)*XXXX*GK(S/T)), localized at residues 19–26 in HydF from *C. acetobutylicum* (GKTNVGKS) and responsible for the proper position of the triphosphate moiety of the bound nucleotide, and (ii) a single point-mutation in the Walker B-loop sequence (D*XX*G), localized at residues 67–70 in HydF from *C. acetobutylicum* (DTAG) and involved in the interaction with the nucleotide γ-phosphate and Mg^{2+}. We expressed in *E. coli* the mutant HydF-StrepII_G24A/K25A and HydF-StrepII_D67A proteins (i) alone, to measure their GTPase activity *in vitro*, (ii) in combination with HydE, HydG, and HydA1-StrepII, to evaluate their capability to activate the

[FeFe]-hydrogenase, and (iii) in combination with HydE-6His and HydG-6His, to test their ability to interact with the two other maturases. As expected, the introduced mutations impair the HydF-StrepII GTP hydrolysis and completely abolished the capability of HydF-StrepII to activate HydA1-StrepII (Table 3), confirming the crucial role of the HydF GTPase activity in the maturation process. On the other hand, both mutant proteins retain the ability to interact with HydE and HydG, as assessed by co-purification experiments performed exactly as described above (Fig. 5, *A* and *B*, *lanes 2*), suggesting that the HydF GTP hydrolysis does not introduce in the scaffold structural changes affecting its interactions with the two other accessory proteins. Moreover, the complexes between the mutant HydF-StrepII proteins and the two other 6His-tagged maturases have been purified by double affinity chromatography, exactly as described above, and the stoichiometry of these interactions has been determined by densitometry. We obtained the same ratios estimated with the HydF-StrepII protein, thus further proving that the point mutations introduced in the Walker A and Walker B sequences do not affect the capability of HydF-StrepII to interact with both HydE-6His and HydG-6His. This was also independently confirmed by a Biacore analysis, which showed that the kinetic constants of both proteins for HydF-StrepII_G24A/K25A mutant are similar to those calculated for the interaction with the wild type protein (Table 2).

We also addressed the question whether the nucleotide binding to HydF may influence *per se* the interaction of the scaffold with HydE and HydG, independently of the GTP hydrolysis. To this end, exactly as described for the experiment reported in Fig. 3, HydE-6His and HydG-6His were individually passed over the BIAcore chip carrying a HydF-StrepII in the presence of the nonhydrolyzable analog GTPγC at concentrations ranging from 0.1 to 5 mM. The results were very similar to those obtained in the absence of GTPγC (see Fig. 6, which refers, as an example, to the experiment with 2 mM GTPγC). The quantitative analysis of the experiment performed with 2 mM GTPγC, reported in Table 4, shows that the K_D for HydF-StrepII·HydE-6His and HydF-StrepII·HydG-6His interactions are not significantly different from those obtained in the absence of GTPγC (Table 2), ruling out an effect of the nucleotide binding on the interactions between the maturases. These data indicate that neither the GTP binding to HydF nor the nucleotide hydrolysis are directly involved in the protein interactions between the scaffold and the two other maturases, both in whole cell and in *in vitro* assays with purified proteins.

As reported in the Introduction, we recently solved the three-dimensional crystal structure of a nucleotide-free HydF protein (22) and showed that the GTP-binding domain includes a flexible loop that is expected to undergo a structural rearrangement upon nucleotide binding and/or hydrolysis that could in turn influence the interaction of the scaffold with the maturation partners. This prompted us to further investigate the role of this domain in the functional and structural network of the [FeFe]-hydrogenase maturation proteins. Interestingly, as shown in Fig. 7, in Biacore experiments when GTP is injected over HydE-6His (Fig. 7*A*) or HydG-6His (Fig. 7*B*) during their dissociation phase from HydF-StrepII, a concentration-dependent change of the curve slope can be observed, indicating an increased dissociation rate. Similar results have been obtained using the nonhydrolyzable analog GTPγC. This suggests that the binding of GTP to HydF can be related to the mechanism by which the displacement of an interaction partner from the scaffold occurs, allowing subsequent association of a different protein.

Analysis of Protein Interaction of HydF Carrier with the [FeFe]-Hydrogenase—The role of HydF as a carrier to transfer a complete [2Fe-2S]-subcluster to the [FeFe]-hydrogenase involves the interaction of these two proteins. Interestingly, it has been clearly shown that only a HydF co-expressed with HydE and HydG (*i.e.*, $HydF^{EG}$) is able to activate a hydrogenase produced in a genetic background completely devoid of maturases (*i.e.*, $HydA^{\Delta EFG}$) (15, 18, 19). Instead, the hydrogenase activity was not observed when the three accessory proteins were expressed separately or in varying combinations and

TABLE 3

Effects of point mutations of Walker A P-loop and Walker B conserved sequences on purified HydF-StrepII GTPase activity and HydA1-StrepII^{EFG} hydrogen evolution in whole cell extracts

The values reported for both GTPase and hydrogen evolution activities are the means of three independent experiments ± S.E.

Protein	GTPase, k_{cat}	Hydrogenase
	min^{-1}	$nmol\ H_2 \cdot ml^{-1} \cdot min^{-1}$
HydF-StrepII	4.84 ± 0.46	72.33 ± 3.83
HydF-StrepII_G24A/K25A	0.35 ± 0.05	0.58 ± 0.11
HydF-StrepII_D67A	0.08 ± 0.02	0.87 ± 0.12

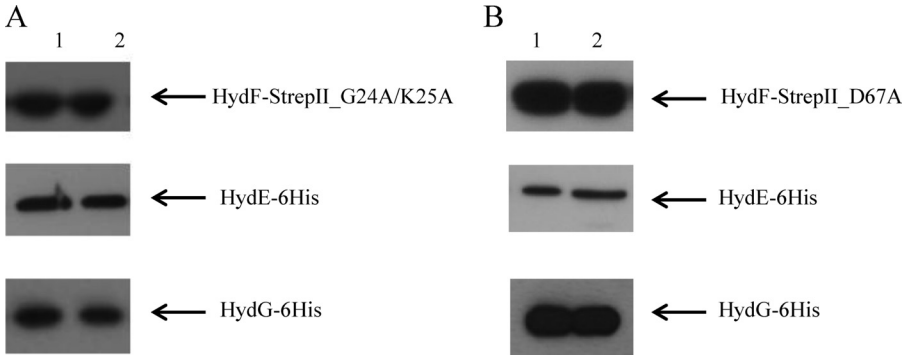

FIGURE 5. **Involvement of HydF GTPase domain in the interactions with HydE and HydG maturation partners.** Western blotting analysis showing the StrepTactin purification of HydF-StrepII_G24A/K25A (*A*) and HydF-StrepII_D67A (*B*) co-expressed either with HydE-6His or HydG-6His. *Lanes 1*, soluble fraction of *E. coli* cell extract; *lanes 2*, pool of desthiobiotin eluted fractions. 25 μl of each sample were loaded on a 12% gel for SDS-PAGE. Western blotting with anti-StrepII tag and anti-6His tag monoclonal antibodies is shown.

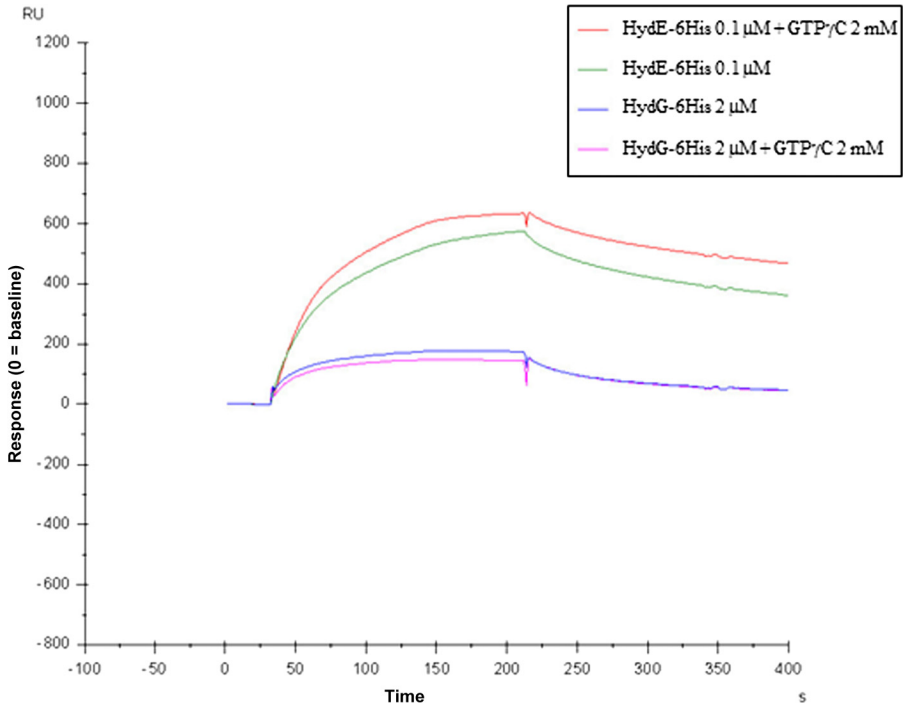

FIGURE 6. **Kinetics of the HydE-6His·HydF-StrepII and HydG-6His·HydF-StrepII interactions in the absence or in the presence of GTPγC 2 mM.** For more details, see the legend of Fig. 3.

TABLE 4

Kinetics values of the HydE-6His/HydF-StrepII and HydG-6His/HydF-Strep II interactions in the presence of 2 mM GTPγC, calculated from Biacore experiments

The constants ± S.E. are calculated from Biacore kinetics (not shown), with BIAevaluation software 2.0.3. Only two decimal digits are shown. A two-state reaction model was applied.

	$k_{on,1}$	$k_{off,1}$	$k_{on,2}$	$k_{off,2}$	K_D
	$M^{-1} \times s^{-1} \times 10^4$	$s^{-1} \times 10^{-2}$	$s^{-1} \times 10^{-2}$	$s^{-1} \times 10^{-3}$	M
HydF-StrepII					
HydE-6His	20.02 ± 0.17	4.30 ± 0.06	1.10 ± 0.01	1.29 ± 0.06	2.26×10^{-8}
HydG-6His	2.70 ± 0.007	9.21 ± 0.26	1.00 ± 0.01	1.42 ± 0.09	4.21×10^{-7}

added *in vitro* to $HydA^{\Delta EFG}$ (18). Based on this, we investigated the protein-protein interactions of HydA1 with both functional $HydF^{EG}$ and nonfunctional HydF proteins produced in different backgrounds. To this end, we co-expressed in *E. coli* a recombinant HydA1-StrepII protein in combination with (i) HydF-6His; (ii) HydF-6His, HydE, and HydG; (iii) HydF-6His and HydE; and (iv) HydF-6His and HydG. HydE and HydG were expressed without tags, to visualize only HydF-6His in the Western blotting analysis following the purification step. The HydA1-StrepII protein was purified by Strep-Tactin affinity chromatography (Fig. 8, *A–D*, *lanes 2*), and the presence of $HydF^{\Delta EG}$-6His, $HydF^{EG}$-6His, $HydF^{E}$-6His, and $HydF^{G}$-6His in the eluted fractions was evaluated by Western blotting. Interestingly, Fig. 8 shows that the StrepTactin elution fractions are completely devoid of $HydF^{\Delta EG}$-6His (Fig. 8*E*, *lane 2*) and that HydF-6His co-purifies with HydA1-StrepII not only when co-expressed with both HydE and HydG (Fig. 8*F*, *lane 2*) but also in combination either with only HydE (Fig. 8*G*, *lane 2*) or with only HydG (Fig. 8*H*, *lane 2*). Taken together, these results indicate that HydE and HydG could independently introduce in HydF structural changes or modulate the HydF scaffold properties, allowing its interaction with HydA. On the other hand, only $HydF^{EG}$ harbors a complete 2Fe subcluster carrying the CO, CN^-, and dithiolate ligands, separately added by HydE and HydG, and is able to activate the [FeFe]-hydrogenase.

We also investigated whether the presence of a FeS cluster precursor on the $HydF^{EG}$ scaffold is required for its interaction with the hydrogenase. To this end, we obtained a new recombinant HydF-6His protein in which one of the three highly conserved cysteine residues belonging to the FeS cluster-binding consensus sequence (*i.e.*, Cys-304 of the motif $CXHX_{45}HCXXC$ of HydF from *C. acetobutylicum*) has been mutated. We expressed in *E. coli* the HydF-6His_C304S protein (i) alone, to evaluate its capability to bind a FeS cluster and (ii) in combination with HydE, HydG and HydA1-StrepII to test both its maturation activity and the capability to interact with the hydrogenase. As reported in Fig. 9*A*, the UV-visible absorption spectra in the 320–550-nm range of the HydF-6His_C304S mutant protein shows a limited capability to bind iron (*gray line*) when compared with the HydF-6His protein (*black line*), confirming the key role of this residue in the binding of the FeS cluster precursor to the scaffold. Accordingly, the same mutation results in a severe impairment of the [FeFe]-hydrogenase maturation (Fig. 9*A*, *inset*). On the other hand, the $HydF^{EG}$-6His_C304S mutant protein co-elutes with HydA1-StrepII (Fig. 9*B*, *lanes 3*), as assessed by co-purification experiments performed as described in

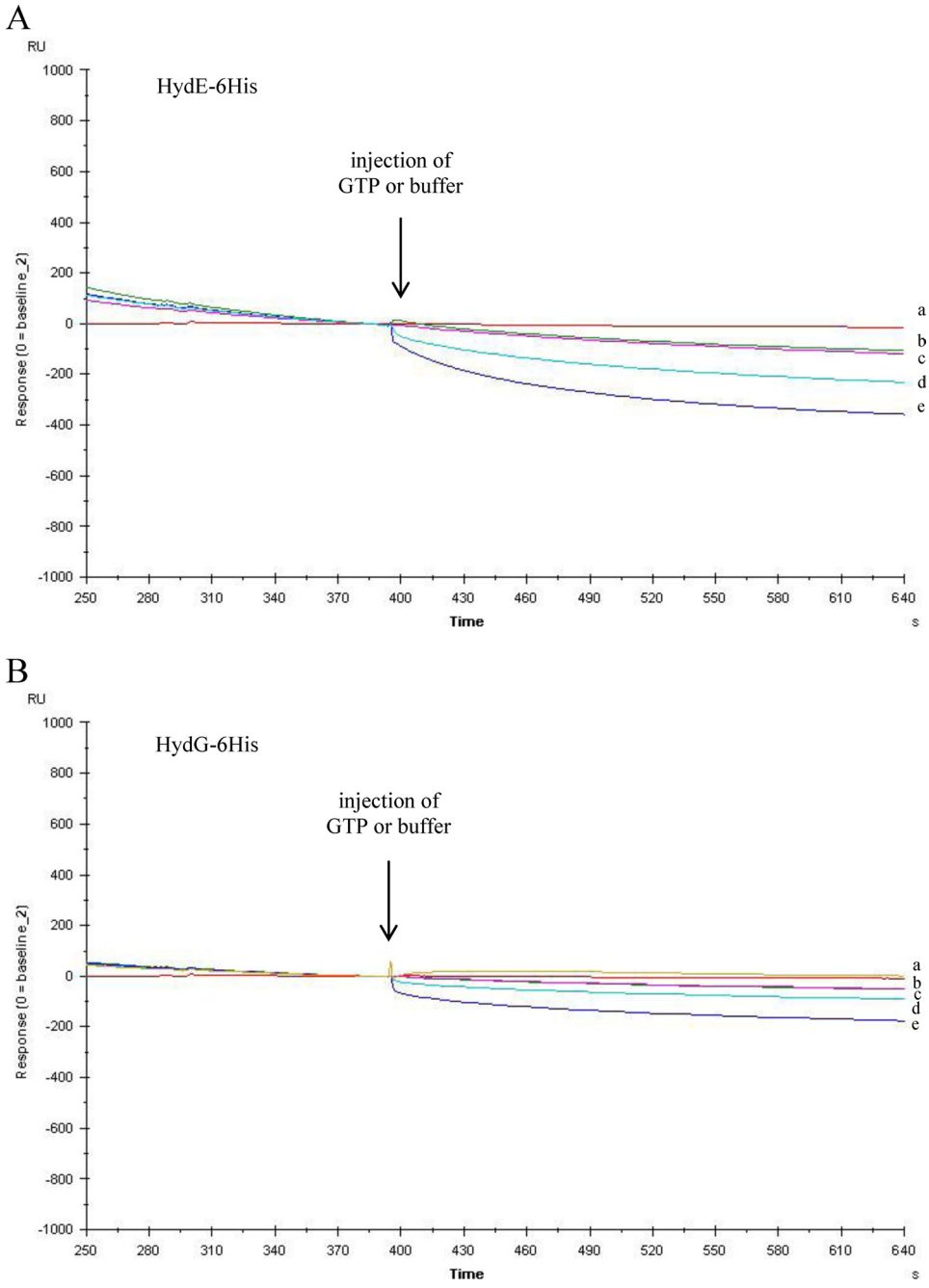

FIGURE 7. **GTP-induced dissociation of HydE-6His and HydG-6His from the HydF-StrepII scaffold as assessed by Biacore analysis.** 2 μM HydE-6His (*A*) or HydG-6His (*B*) was injected for 2 min over the immobilized HydF-StrepII, and then, during the dissociation phase, after 4 min of buffer flowing, a second injection was applied of 0.5 mM GTP (*sensorgram d*), 2 mM GTP (*sensorgrams e*), or buffer (*sensorgrams b* and *c*). The flow rate was 30 μl/min. The effect of 2 mM GTP directly injected, without previous binding of HydE or HydG, is shown by *sensorgram a*. The sensorgrams are shown for the second injection, after subtraction of the signal in control flow cell and normalization (value of 0) to the baseline at the moment of the second injection (GTP or buffer).

the previous paragraphs, indicating that the interaction between these proteins occurs independently of the presence of the FeS cluster on the scaffold. Also in this case, the ongoing structural analysis of the HydF-StrepII·HydE-6His and HydF-StrepII·HydG-6His heterocomplexes would add new molecular insights useful to define the protein environment driving the process of the 2Fe subcluster assembly/transfer.

It was previously shown that the GTPase activity of $HydF^{EG}$ is unrelated to its capability to activate an nonfunctional $HydA^{\Delta EFG}$ (15), suggesting that the nucleotide binding and/or hydrolysis are not essential for the transfer of the cluster precursor from the scaffold to the hydrogenase. To further address this point, we evaluated whether the HydF GTPase properties are involved in its interaction with the [FeFe]-hydrogenase. To this end, we co-expressed in *E. coli* HydA1-StrepII in combination with HydE, HydG, and the HydF-6His_G24A/K25A protein. The purification profile of the Strep-Tactin affinity chromatography, performed exactly as described above, clearly indicates that the mutant HydF-6His_G24A/K25A protein retains the capability to interact with the hydrogenase (Fig. 10),

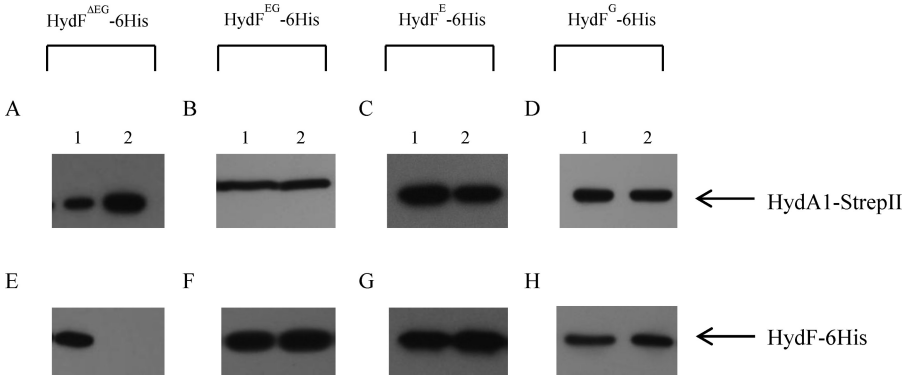

FIGURE 8. **Co-purification of HydA1-StrepII and HydF^{EG}-6His, HydF^{E}-6His and HydF^{G}-6His.** Western blotting analysis shows the StrepTactin purification of HydA1-StrepII expressed in the presence of HydF-6His without HydE-6His and HydG-6His (*A* and *E*), with HydG-6His and HydE-6His (*B* and *F*), with HydE-6His (*C* and *G*), and with HydG-6His (*D* and *H*). *Lanes 1*, soluble fraction of *E. coli* cell extract; *lanes 2*, pool of desthiobiotin eluted fractions. 25 μl of each sample were loaded on a 12% gel for SDS-PAGE. Western blotting with anti-6His tag monoclonal and anti-StrepII tag antibodies is shown.

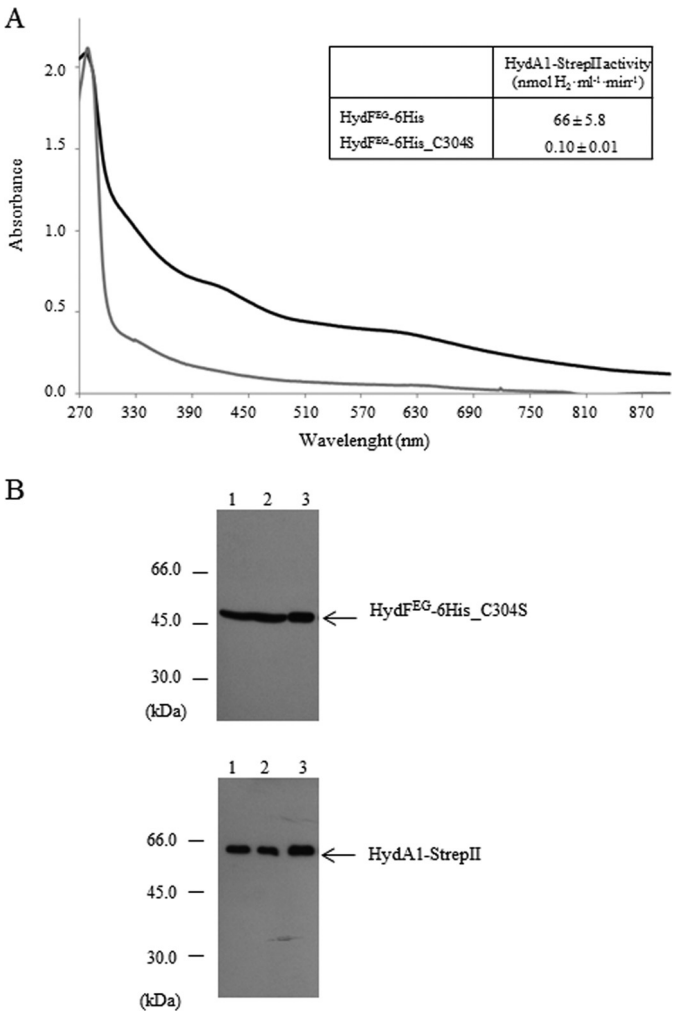

FIGURE 9. **Co-purification of HydA1-StrepII and HydF^{EG}-6His_C304S.** *A*, UV-visible spectroscopy of HydF-6His and HydF-6His_C304S proteins. *Black line*, HydF-6His; *gray line*, mutant HydF-6His_C304S protein. The same amount of affinity-purified protein (150 μM) was analyzed for each sample. *Inset*, H_2 evolution activity of HydA1-StrepII anaerobically co-expressed in *E. coli* with HydE, HydG and HydF-6His, or HydF-6His_C304S. The reported values are the means of three independent experiments ± S.E. *B*, Western blotting analysis showing the StrepTactin purification of HydA1-StrepII and HydF^{EG}-6His_C304S. *Lanes 1*, total *E. coli* cell extract; *lanes 2*, soluble fraction of cell extract; *lanes 3*, pool of desthiobiotin eluted fractions. 25 μl of each sample were loaded on a 12% gel for SDS-PAGE. Western blotting with anti-StrepII tag and anti-6His tag monoclonal antibodies is shown.

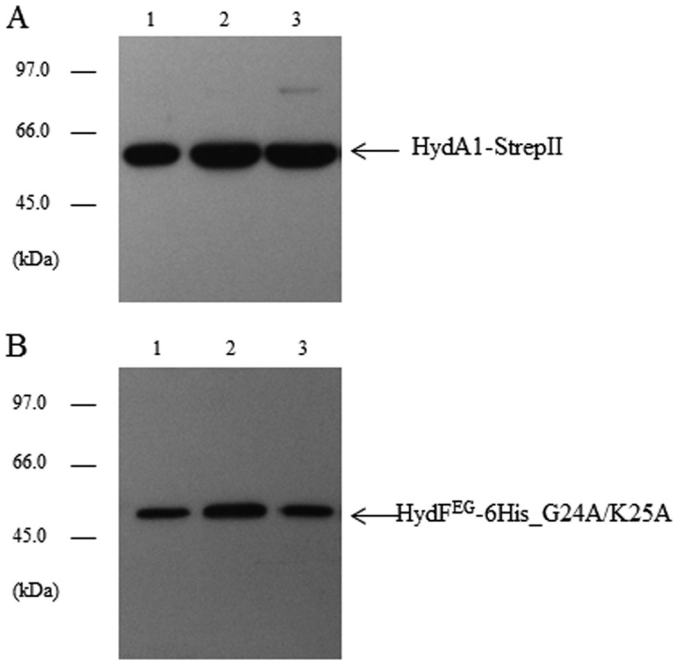

FIGURE 10. **Analysis of the interaction between the mutant HydF^{EG}-6His_G24A/K25A and HydA1-StrepII.** Western blotting analysis showing the StrepTactin purification of HydA1-StrepII (*A*) and HydF^{EG}-6His_G24A/K25A (*B*). *Lanes 1*, total *E. coli* cell extract; *lanes 2*, soluble fraction of cell extract; *lane 3*, pool of desthiobiotin eluted fractions. 25 μl of each sample were loaded on a 12% gel for SDS-PAGE. Western blotting with anti-StrepII tag and anti-6His tag monoclonal antibodies is shown.

ruling out a role of GTP hydrolysis in the binding of the [FeFe]-hydrogenase to the scaffold. Taken together, these data indicate that the [2Fe-2S]-subcluster biosynthesis/modification and delivery represent two functionally related but distinct steps, both involving dynamic HydF scaffold/carrier interactions with the two other accessory proteins as well as with the hydrogenase.

Conclusions—During recent years remarkable advances have been made in the knowledge of the molecular mechanisms driving the [FeFe]-hydrogenases maturation pathway. Nevertheless, significant gaps remain in the understanding of how this process occurs, and the precise contribution of some of the players involved has still to be assigned. In this work, the interactions between the Hyd structural and functional proteins

have been investigated in detail, and a quantitative analysis of these binding events has been provided for the first time. Our kinetic data suggest that the HydE and HydG radical-SAM proteins separately participate in modifying the H-cluster precursor on HydF. We also showed that HydF is able to interact with the two other maturases, as well as with the hydrogenase independently of its GTPase properties, which are otherwise involved in the dissociation of the HydE and HydG maturases from the scaffold. This would allow the coordinate stepwise process needed for the synthesis and chemical modification of the H-cluster precursor. Finally, our data suggest that HydE and HydG separately introduce in the HydF scaffold structural changes enabling its interaction with the hydrogenase, which nevertheless results in activation only when a complete 2Fe subcluster is transferred. The structural features of these intermediates of the hydrogenase maturation process are currently under investigation in our laboratory. These results provide new insights that may improve our understanding of the highly complex molecular pathway leading to the activation of the [FeFe]-hydrogenases, which requires further studies to be completely defined.

REFERENCES

1. Beinert, H., Holm, R. H., and Münck, E. (1997) Iron-sulfur cluster. Nature's modular, multipurpose structure. *Science* **277,** 653–659
2. Lill, R. (2009) Function and biogenesis of iron-sulphur proteins. *Nature* **460,** 831–838
3. Meyer, J. (2008) Iron-sulfur protein folds, iron-sulfur chemistry, and evolution. *J. Biol. Inorg. Chem.* **13,** 157–170
4. Fontecilla-Camps, J. C., Amara, P., Cavazza, C., Nicolet, Y., and Volbeda, A. (2009) Structure-function relationships of anaerobic gas-processing metalloenzymes. *Nature* **460,** 814–822
5. Duffus, B. R., Hamilton, T. L., Shepard, E. M., Boyd, E. S., Peters, J. W., and Broderick, J. B. (2012) Radical AdoMet enzymes in complex metal cluster biosynthesis. *Biochim. Biophys. Acta.* **1824,** 1254–1263
6. Peters, J. W., and Broderick, J. B. (2012) Emerging paradigms for complex iron-sulfur cofactor assembly and insertion. *Annu. Rev. Biochem.* **81,** 429–450
7. Mulder, D. W., Shepard, E. M., Meuser, J. E., Joshi, N., King, P. W., Posewitz, M. C., Broderick, J. B., and Peters, J. W. (2011) Insights into [FeFe]-hydrogenase structure, mechanism, and maturation. *Structure* **19,** 1038–1052
8. Nicolet, Y., and Fontecilla-Camps, J. C. (2012) Structure-function relationships in [FeFe]-hydrogenase active site maturation. *J. Biol. Chem.* **287,** 13532–13540
9. Posewitz, M. C., King, P. W., Smolinski, S. L., Zhang, L., Seibert, M., and Ghirardi, M. L. (2004) Discovery of two novel radical *S*-adenosylmethionine proteins required for the assembly of an active [Fe] hydrogenase. *J. Biol. Chem.* **279,** 25711–25720
10. Rubach, J. K., Brazzolotto, X., Gaillard, J., and Fontecave, M. (2005) Biochemical characterization of the HydE and HydG iron-only hydrogenase maturation enzymes from *Thermotoga maritima*. *FEBS Lett.* **579,** 5055–5060
11. Pilet, E., Nicolet, Y., Mathevon, C., Douki, T., Fontecilla-Camps, J. C., and Fontecave, M. (2009) The role of the maturase HydG in [FeFe]-hydrogenase active site synthesis and assembly. *FEBS Lett.* **583,** 506–511
12. Shepard, E. M., Duffus, B. R., George, S. J., McGlynn, S. E., Challand, M. R., Swanson, K. D., Roach, P. L., Cramer, S. P., Peters, J. W., and Broderick, J. B. (2010) [FeFe]-hydrogenase maturation. HydG-catalyzed synthesis of carbon monoxide. *J. Am. Chem. Soc.* **132,** 9247–9249
13. Nicolet, Y., Rubach, J. K., Posewitz, M. C., Amara, P., Mathevon, C., Atta, M., Fontecave, M., and Fontecilla-Camps, J. C. (2008) X-ray structure of the [FeFe]-hydrogenase maturase HydE from *Thermotoga maritima*. *J. Biol. Chem.* **283,** 18861–18872
14. Brazzolotto, X., Rubach, J. K., Gaillard, J., Gambarelli, S., Atta, M., and Fontecave, M. (2006) The [FeFe]-hydrogenase maturation protein HydF from *Thermotoga maritima* is a GTPase with an iron-sulfur cluster. *J. Biol. Chem.* **281,** 769–774
15. Shepard, E. M., McGlynn, S. E., Bueling, A. L., Grady-Smith, C. S., George, S. J., Winslow, M. A., Cramer, S. P., Peters, J. W., and Broderick, J. B. (2010) Synthesis of the 2Fe subcluster of the [FeFe]-hydrogenase H cluster on the HydF scaffold. *Proc. Natl. Acad. Sci. U.S.A.* **107,** 10448–10453
16. King, P. W., Posewitz, M. C., Ghirardi, M. L., and Seibert, M. (2006) Functional studies of [FeFe]-hydrogenase maturation in an *Escherichia coli* biosynthetic system. *J. Bacteriol.* **188,** 2163–2172
17. Mulder, D. W., Boyd, E. S., Sarma, R., Lange, R. K., Endrizzi, J. A., Broderick, J. B., and Peters, J. W. (2010) Stepwise [FeFe]-hydrogenase H-cluster assembly revealed in the structure of HydA(Δ^{EFG}). *Nature* **465,** 248–251
18. McGlynn, S. E., Ruebush, S. S., Naumov, A., Nagy, L. E., Dubini, A., King, P. W., Broderick, J. B., Posewitz, M. C., and Peters, J. W. (2007) *In vitro* activation of [FeFe]hydrogenase. New insights into hydrogenase maturation. *J. Biol. Inorg. Chem.* **12,** 443–447
19. McGlynn, S. E., Shepard, E. M., Winslow, M. A., Naumov, A. V., Duschene, K. S., Posewitz, M. C., Broderick, W. E., Broderick, J. B., and Peters, J. W. (2008) HydF as a scaffold protein in [FeFe] hydrogenase H-cluster biosynthesis. *FEBS Lett.* **582,** 2183–2187
20. Mulder, D. W., Ortillo, D. O., Gardenghi, D. J., Naumov, A. V., Ruebush, S. S., Szilagyi, R. K., Huynh, B., Broderick, J. B., and Peters, J. W. (2009) Activation of HydA($^{\Delta EFG}$) requires a preformed [4Fe-4S] cluster. *Biochemistry* **48,** 6240–6248
21. Peters, J. W., Szilagyi, R. K., Naumov, A., and Douglas, T. (2006) A radical solution for the biosynthesis of the H-cluster of hydrogenase. *FEBS Lett.* **580,** 363–367
22. Cendron, L., Berto, P., D'Adamo, S., Vallese, F., Govoni, C., Posewitz, M. C., Giacometti, G. M., Costantini, P., and Zanotti, G. (2011) Crystal structure of HydF scaffold protein provides insights into [FeFe]-hydrogenase maturation. *J. Biol. Chem.* **286,** 43944–43950
23. Ruzzene, M., Brunati, A. M., Sarno, S., Donella-Deana, A., and Pinna, L. A. (1999) Hematopoietic lineage cell specific protein 1 associates with and down-regulates protein kinase CK2. *FEBS Lett.* **461,** 32–36
24. Karlsson, R., and Fält, A. (1997) Experimental design for kinetic analysis of protein-protein interactions with surface plasmon resonance biosensor. *J. Immunol. Methods* **200,** 121–133
25. Driesener, R. C., Challand, M. R., McGlynn, S. E., Shepard, E. M., Boyd, E. S., Broderick, J. B., Peters, J. W., and Roach, P. L. (2010) [FeFe]-hydrogenase cyanide ligands derived from *S*-adenosylmethionine-dependent cleavage of tyrosine. *Angew. Chem. Int. Ed. Engl.* **49,** 1687–1690